Book of Extended Abstracts

ESCC 2019

16th European Symposium on Comminution & Classification

Edited by
Mojtaba Ghadiri, Sadegh Nadimi, Mehrdad Pasha

EFCE
European Federation of Chemical Engineering
Europäische Föderation für Chemie-Ingenieur-Wesen
Fédération Européenne de Génie Chimique

EFCE Event No. 761

2 - 4 September 2019
Leeds, UK

UNIVERSITY OF LEEDS

16th European Symposium on Comminution and Classification (ESCC2019)

2-4 September 2019
University of Leeds
Leeds, UK

Book of

Extended Abstracts

Edited by

Mojtaba Ghadiri, Sadegh Nadimi, Mehrdad Pasha

Contact Information:
Prof. Mojtaba Ghadiri, *Conference Chair*
m.ghadiri@leeds.ac.uk

How to Cite:
Ghadiri, M., Nadimi, S. and Pasha, M. (Eds.) 16th European Symposium on Comminution and Classification: book of extended abstracts, Leeds, UK, 2-4 September, 2019. Leeds: University of Leeds. DOI: https://doi.org/10.5518/100/17

Welcome to the 16th European Symposium on Comminution and Classification, ESCC 2019

ESCC started over 55 years ago, held mainly in Germany with the past two Symposia held in Sweden and Turkey, and now for the very first time in UK. The Organisng Committee is very proud to have had the opportunity to organise this important conference, which is the European Federation of Chemical Engineering Event Number 761, and to welcome the worldwide community in this field to Leeds. We acknowledge and are grateful for sponsorship support from DEM Solutions, ESSS, Freeman Technology, Hosokawa Micron, IFPRI,MEI, Quadro, Retsch, Surface Measurement Systems, WAB and Ytron.

Milling is one of the oldest technologies developed by the early civilisations. Remnants of roller mills for cereal milling can be seen in the Roman archaeological sites of Pompeii and Herculaneum in southern Italy. Yet milling still poses great challenges, as it is not only the most energy intensive and inefficient particulate solids process but is also the least understood. The physics of damage and fracture is highly complex and dependent on material structure, properties and interactions with machine dynamics. From a process engineering view point, the interest is in energy utilisation and scale-up of various mill types, classification to desirable particle size distribution with little/no out of specification product, issues which have forever besetted the industry. The materials-related aspects of interest pose even greater challenges, such as (i) the smallest possible particle size, which can be produced by comminution for a number of applications, such as the highly sought-after 'top-down' approach to nano-particle manufacturing; (ii) the most desirable, yet challenging issue of being able to predict the size distribution of comminuted materials based on fracture pattern; (iii) the most appropriate methods of application of stresses for a given set of materials properties; (iv) solid state transformations and instabilities due to milling, etc. So there is plenty of opportunities for the next generation scientists and enginers to make impactful contributions.

We received around 80 extended abstracts which have been scheduled for two parallel oral presentation sessions and two evening poster sessions along with exhibitions by the symposium sponsors. ESCC 2019 symposium promises to be a highly informative and engaging forum in which leading-edge engineering science and technology of particle size reduction and classification are presented and discussed. There are three plenary and six keynote lectures from leaders in the field, outlining the recent progress in the field, relevant to chemical and allied, food, mineral and pharmaceutical industries. Based on the abstracts received, the symposium is structured in the following themes: fundamentals of size reduction, innovations in milling and classification, nanomilling, mechano-chemistry and solid state transformations, pharmaceuticals and foods, attrition and wear, and related modelling. The notable number of abstracts received on modelling made it possible to divide them in sub-themes: mechanistic, population balance, discrete element and coupling with computational fluid dynamics.

The extended abstracts are collated in a pdf file, which are uploaded onto a memory stick and handed out at the symposium venue, and also downloadable from the symposium website. We are devising plans to make them searchable and available for future reference via the University of Leeds website. Moreover Powder Technology Journal have agreed to publish a selection of the contributions in extended full manuscript.

Finally, I wish the participants a great time for technical exchanges, networking, renewing old and making new acquitances and having memorable visit to Leeds.

Mojtaba Ghadiri, ESCC 2019 Organising Committee Chair

Organising Committee

Professor Mojtaba Ghadiri,
University of Leeds, Conference Chair

Dr Lian Liu,
University of Surrey, UK

Mr Iain Crosley,
Hosokawa Micron, UK

Dr Sadegh Nadimi,
Newcastle University, UK

Dr Ali Hassanpour,
University of Leeds, PTSIG

Professor Raffaella Ocone,
Heriot-Watt University, PTSIG Chair, IChemE

Professor Arno Kwade,
University of Braunschweig, WP Chair, EFCE

Dr Mehrdad Pasha,
University of Leeds, UK

International Technical Commitee

Dr Tim Addison
Centre for Process Innovation

Professor Sergiy Antonyuk
Technical University of Kaiserslautern

Professor Peter Baláž
Slovak Academy of Sciences

Professor Hakan Benzer
Hacettepe University

Professor Ecevit Bilgili
New Jersey Institute of Technology

Professor Alain Chamayou
École des mines d'Albi-Carmaux

Professor Magnus Evertsson
Chalmers University of Technology

Professor Jozsef Faitli
University of Miskolc

Professor Christine Frances
INP-ENSIACET

Dr Colin Hare
University of Surrey

Dr Willie Hendrickson
AVEKA & International Fine Particle Research Institute

Dr Jerry Heng
Imperial College London

Dr Michael Juhnke
Novartis Pharma AG

Professor Haim Kalman
Ben Gurion University of the Negev

Professor Junya Kano
University of Tohoku

Professor Arno Kwade
Technical University of Braunschweig

Professor Aubrey Mainza
University of Cape Town

Professor Vadim Mizonov
Ivanovo State Power Engineering University

Dr Martin Murtagh
Corning

Dr Frank Müller
BASF SE

Professor Jin Ooi
University of Edinburgh

Dr Massih Pasha
The Chemours Company

Professor Wolfgang Peukert
University of Erlangen

Professor Malcolm Powell
University of Queensland

Professor Pavol Rajniak
Slovak Technical University & Process Systems Enterprise

Dr Mehdi Safari
University of Cape Town

Professor Agba Salman
University of Sheffield

Professor Tomáš Sverák
Brno University of Technology

Professor Luis Marcelo Tavares
Federal University of Rio de Janeiro

Professor Cino Viggiani
University of Grenoble

Professor Yanmin Wang
South China University of Technology

Professor Satoru Watano
Osaka Prefecture University

Professor Karl-Ernst Wirth
University of Erlangen

Dr Mohsen Yahyaei
University of Queensland

Acknowledgements

We acknowledge the support of MEETinLEEDS in particular Mr Corin Nanton for the organisation of this conference in Leeds. We also gratefully acknowledge sponseship for the conference by the following organisations:

MEI

Hosokawa Micron

ESSS Rocky DEM

IFPRI (Aveka)

Freemantech

Netzsch

Retsch

Surface Measurement Systems

YTRON-QUADRO (UK) LIMITED

EDEMSimulation

Rhewum

WAB Group

Gold Sponsors

HOSOKAWA MICRON LTD

IFPRI International Fine Particle Research Institute

Silver Sponsors

ROCKY

freemantechnology a micromeritics company

NETZSCH Proven Excellence.

Bronze Sponsors

Surface Measurement Systems World Leader in Sorption Science

YTRON QUADRO

EDEM® Simulate material. Deliver results.

WAB

RHEWUM® Enjoy the Difference

Retsch® MILLING SIEVING ASSISTING

Reception Sponsor

IFPRI International Fine Particle Research Institute

Presentation Prize Sponsor

EDEM® Simulate material. Deliver results.

Media Partner

MEI

Plenary Speakers

Prof. Arno Kwade

Prof. Kwade is the Head of the Institute for Particle Technology of the Technical University of Brunswick. His research activities are on production, tailoring, formulation of nano and micro sized particles and their use for the design of structured products like battery electrodes, pharmaceutical active ingredients and nano-composites. He is the Chairman of the EFCE Working Party on Comminution and Classification and has extensive collaborations worldwide.

Milling within Energy Storage Industry

Dr Michael Juhnke

Dr Juhnke is process engineer graduated in 1997 from Cologne University of Applied Sciences (BSc) and 2000 from Clausthal University of Technology (MSc). He continued with a PhD in particle technology and graduated in 2006 from Clausthal University of Technology. He then joined Novartis Pharma AG, Basel, Switzerland, in the Technical R&D department. He is currently Senior Fellow and responsible for the process development of engineered drug particles for oral, parenteral and respiratory applications from pre-clinical to production scale.

Size reduction of active pharmaceutical ingredients – Overview, challenges and advancements

Prof. Malcolm Powell

From a physics background, Prof. Powell worked at Mintek, then established the comminution research and consulting groups at the University of Cape Town. He took up the Chair in sustainable comminution in the University of Queensland in 2007. He has founded the Anglo American Centre for Sustainable Comminution and formed the Global Comminution Collaborative (GCC) of six University world-leading groups providing a comprehensive worldwide process optimisation team. He aims to link fundamental research into applied outputs through the development of mechanistically correct but practical and robust process models. Interests cover liner design, SAG mill modelling and control, the unified comminution model (UCM), ore characterisation, flexible circuits and application of novel processes to reducing the environmental impact of mining.

Applying primary rock properties of strength and mineral association to a new suite of mechanistic comminution models

Keynote Speakers

Prof. Aubrey Mainza

Prof. Mainza is the Head of Department of Chemical Engineering, University of Cape Town (UCT). He graduated from UCT with a PhD in 2006. He has 18 years of collective experience in academia, research and industry. He is the Deputy Director and Head of Comminution and Classification Research in the Centre for Minerals Research, which is a large multi-disciplinary research centre. His research areas include comminution and classification and uses Discrete Element Method (DEM), Computational Fluid Dynamics (CFD), and Positron Emission Particle Tracking (PEPT) as tools in his modelling methods. He has participated in many local and international research projects and has worked on numerous comminution circuit design and optimisation projects.

Integrating classification in circuit during design and equipment selection –an important aspect in developing robust comminution circuit

Dr Lian Liu

Dr Liu joined the University of Surrey in May 2016 as the research centre manager at the Department of Chemical and Process Engineering. Dr Liu obtained her PhD from the University of Queensland in Australia in 1991 and worked in Carrier Transicold in Singapore for three years after her PhD. She then moved back to the University of Queensland and spent most of her academic career in the same University before moving to the University of Surrey. Dr Liu's research expertise is in particle technology, ranging from comminution (particle breakage process) to granulation process (particle size enlargement process) as well as bulk powder flow and compaction. She has worked with a wide range of industries such as minerals, agricultural and pharmaceutical industries.

Modelling of milling process in the minerals and pharmaceutical industry

Dr.-Ing. Steffen Sander

Steffen Sander studied process engineering/mineral processing at the Freiberg University of Mining and Technology. He continued to do research on the comminution of metals and received his Dr.-Ing. in 2002. After 10 years in different R&D related functions in the paper industry, during which his main focus was on paper making and paper coating technology, he joined HOSOKAWA ALPINE Aktiengesellschaft in February 2012. He is currently Head of R&D of the Powder and Particle Processing business segment of HOSOKAWA ALPINE Aktiengesellschaft with a strong focus on size reduction and classification for all kind of applications.

Current trends in air classification of fine powders

Dr.-Ing. Steffen Sander

The research interests of Wolfgang Peukert focus on key aspects of particle science and technology with special emphasis on formulation of functional particle systems. He is seeking for unifying principles in the design of particulate products in combination with modelling and optimization strategies. He uses methods from interface science and engineering for tailoring particle interactions, colloidal stabilization and ultimately particle properties. His activities include comprehensive particle characterization for size, shape, surface and functional properties. Recent progress in micro- and nanomechanical particle characterization coupled to size reduction at the nanoscale opens new pathways for scalable production of 2D materials such as graphene, particle shape control in mills and the formulation of pharmaceuticals,. He likes to work in interdisciplinary teams, his motto is: Innovation occurs at the interfaces.

Milling at the Nanoscale

Prof. Marcelo Luis Tavares

Prof. Tavares holds a bachelor's degree in mining engineering from the Federal University of Rio Grande do Sul (1988), a Master´s degree in Mining, Metallurgical and Materials Engineering from the Federal University of Rio Grande do Sul (1991) and a PhD in Metallurgical Engineering from the University of Utah (1997). He is Professor of the Federal University of Rio de Janeiro and Head of the Laboratory of Mineral Technology of the Graduate School of Engineering (COPPE). He has experience in Mining, Metallurgical and Materials Engineering, with emphasis on Mineral Processing, working mainly in the topics of modelling and simulation of comminution and mineral concentration processes and fundamentals of particle breakage. He is a founding member of the Global Comminution Collaborative, has been a member of the editorial board of several scientific journals, including International Journal of Mineral Processing, Minerals, Heliyon and KONA Powder and Particle. He has presented invited keynote lectures in twelve countries and has been the principal investigators in more than 100 projects.

Adapting a breakage model to discrete elements using polyhedral particles and applying to industrial comminution

Dr Jerry Heng

Dr Heng is Reader in Particle Technology, Department of Chemical Engineering, Imperial College London and currently an EPSRC Manufacturing the Future Fellow. He received his PhD from Imperial College (2006) and his BEng from Universiti Teknologi Malaysia (2002). His research interests are in developing approaches to control nucleation and crystallisation of small molecule organic organic solids (polymorphism), studying the role of surface properties in processability and manufacturability of powders, including the effect of processing on powder properties, and developing methods to experimentally measure powder surface energy heterogeneity and models to determine surface energy distributions.

Milling induced surface property changes in crystalline pharmaceutical solids

List of Extended Abstracts

ID01-Milling within Energy Storage Industry

Arno Kwade[1,*], *Markus* Noeske[1], *Michael* Grube[2], *Jutta* Hesselbach and *Sabrina* Zellmer[2]

[1]Institute of Particle Technology, Technische Universität Braunschweig, Braunschweig, Germany
[2]Fraunhofer Institute for Surface Engineering and Thin Films IST, Braunschweig, Germany

Summary. The most used energy storage system today is the lithium-ion battery. This paper reveals the use of mills for particle breakage and particle dispersing within the long process chain from the raw material to the final lithium-ion battery cell and its recycling at end of life. First of all the raw materials for the electrochemical active materials synthesis have to be produced by typical mining processes which are not addressed further. For the synthesis of the cathode material the precursors eventually have to be wet milled. Moreover, after calcination the aggregates are typically dry milled to achieve the final product size distributions. On the other side, the natural graphite increasingly used as anode material has to be broken, rounded and classified to achieve the appropriate product properties like packing density, pore size distribution and electrochemical capacity. Beside graphite today nanosized silicon gets more and more important as anode material. One way to produce these silicon nanoparticles is nanomilling in stirred media mills. In order to produce the electrodes for the lithium-ion battery cell the different components, especially the conductive additives like carbon black have to be dispersed in a solvent. For this task machines like planetary mixers, extruders and occasionally also stirred media mills are applied. The resulting structure of the carbon black aggregates and agglomerates is very decisive for the later electrochemical performance of the battery cells. Finally, at the end of the cells life the battery cells have to be crushed and milled to get back the very valuable components like cobalt, nickel and lithium.

1 Introduction

Today energy storage is a very important theme in science, industry and people´s live. The most used energy storage system today is the lithium-ion battery. However, usually it is not known which process steps are required to produce at the end a high performance lithium-ion battery cell. The composition and function of a lithium-ion battery cell is shown in Figure 1.

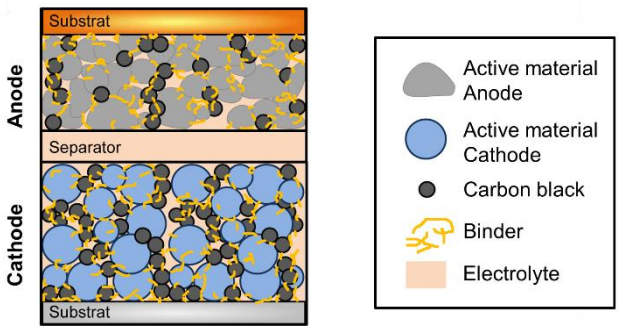

Fig. 1: Schematic drawing of a compartment of a lithium-ion battery cell

A compartment of a lithium-ion battery cell is composed out of the anode, the cathode and the separator in between. Both, anode and cathode are made out of active material particles which are coated on a substrate foil (aluminium for cathode, cupper for anode) and fixated by a binder (cathode usually PVDF, anode a combination of CMC and SDS). Moreover, small amounts of conductive additive are added to secure a sufficient electric conductivity. Today on the anode side usually graphite is employed as active material, increasingly supplemented by silicon. Within the cathode lithium metal oxide particles with different contents of Nickel, Cobalt, Manganese and Aluminum (usually $LiNiCoMnO_2$, $LiNiCoAlO_2$).[1,

Within this plenary paper an overview of the milling and classification processes used to produce the active materials and the lithium-ion battery cells as well as within the recycling of lithium-ion battery systems.

2 Material and methods

Within this plenary paper beside results published by other groups also results from own investigations are presented. In current research projects we are focusing on the increase in energy density on the anode side of the lithium-ion battery. One promising approach is the usage of silicon nanoparticles as an active material. Therefore, we are investigating the impact of particle size of ball milled silicon and the structure of the electrode carbon matrix, where the silicon particles are embedded, on the electrochemical anode performance. Within the anode

* Corresponding author: a.kwade@tu-braunschweig.de

production process, we are investigating especially the dispersing process to form silicon-carbon black composites. In order to study the impact of mixing intensity on the carbon black dispersion and the resulting electrode performance we separated the dispersion process into two steps. In the first step, the ball milled silicon and the carbon black particles were dispersed together with varying intensities in a dissolver or a stirred media mill. The anode slurry was completed in a second dispersing step where the graphite and the binder were added in a second dissolver (see figure 2).

For the variation of the dispersing intensity we varied the first pre-dispersing step three times while the second step was kept constant. For the reference electrode (strategy 1) the carbon black is dispersed in the silicon-ethanol suspension in the dissolver. For the first variation (strategy 1a) the stabilizing additive was added in this step. The second dispersing strategy (strategy 2) was performed in the stirred media mill. The carbon black and the stabilizing additive were inserted to the mill after the silicon comminution. In strategy 3 the carbon black and the stabilizing additive were added together with the silicon feed into the comminution process in the stirred media mill. The total specific energy for all strategies was kept constant.

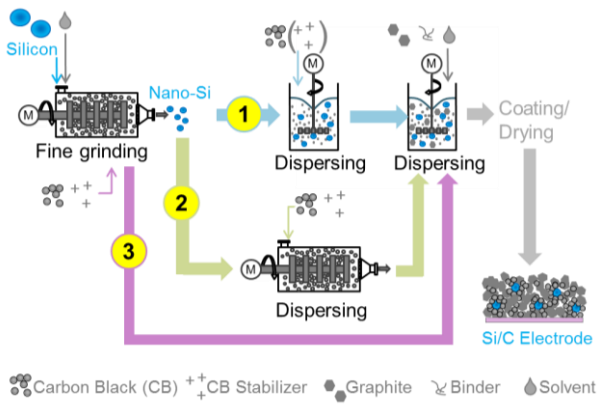

Fig. 2: Scheme of the three dispersing strategies for formation of silicon-carbon black composites

3 Results and discussion

Along the life cycle of a battery comminution (milling, dispersing) and classification equipment is applied for the battery material formation, the production of battery electrodes and the recycling of spent batteries. This overview paper will address these three areas of application. However, as well known for the mining and mineral processing of the substances like cobalt, nickel, lithium and cupper milling operations are extremely important, but they are not battery specific and will not be covered here.

3.1 Active material production

Mills are used in different areas of active material production: Cathode material synthesis, tailoring of graphite particles, especially natural graphite, and production of silicon as new anode material.

One key factor to address this challenge is to improve the quality/performance of nickel and cobalt containing cathode active materials (CAM) like NMC with optimized and application-tailored production processes. Recent studies regarding the production of resources for energy storage report that by 2025 the demand for battery grade nickel will reach 540 kt (demand 2017: approx. 30 kt) and up to 166 kt for cobalt (demand 2017: approx. 38 kt), if the share of electro mobility increases further. This increased demand for battery materials in the year 2025 will lead to exceeding the global supply of these elements by approx. 220 kt for nickel and by approx. 20 kt for cobalt. [3-5]

Such processes for CAM need to define morphology, particle size and particle size distribution as crucial properties for a good performance and applicability in lithium-ion batteries. Established production processes for CAM are usually based on precipitation in batch reactors, continuously stirred tank reactors (CSTR) or the taylor vortex reactor (TVR), which uses a controlled taylor flow for continuous mixing of educts. However, the particle size and aggregation state of the produced precursors are not always sufficient so that the precursors are milled within a stirred media mill before granulation and calcination [6-8]. After calcination the resulting aggregates have to be further milled and classified which is usually done within jet mills.

The normal anode material for lithium ion batteries is graphite. Especially in case of natural graphite the graphite particles have to be tailored regarding their size distribution and their shape/morphology. For this process usually a cascade of pin mills in combination with classifiers and/or classifier mills is applied. Within this process a high amount of the original product mass is lost.

The use of silicon is a promising approach to increase the energy density on the anode side. However, the integration of this new material into the conventional lithium-ion battery technology is still challenging. This is due to volume expansion of the silicon particles during charging and discharging of the cell, which leads to mechanical tension and degradation on silicon particle and coating side. On the other hand, silicon particles exhibit an enormous surficial reactivity, which leads to degradation reactions on the particle surface. Thus the particles tend to form an electrochemical passivated shell. To overcome all these challenges, the silicon particle needs to be small enough to withstand volume contractions and well dispersed into a conductive and flexible carbon matrix to cause only small local stresses on the electrode level during battery cyclization. Therefore, stirred media milling of silicon particles provides a wide range of advantages like controllable and efficient adjustment of suitable particle sizes, flexible adaptability of a wide range of formulations and scale ability of this production process [2]. Figure 3 presents the dependency of primary particle size of ball

milled silicon on the anode performance in a half-cell setup. The use of the smallest silicon particles with 118 nm results in the best cycle ability of the anodes compared to the other anodes with bigger particle sizes. However, the starting capacity is already slightly lowered compared to the 160 nm particles which could be caused by a greater amount of inactivated particle surface.

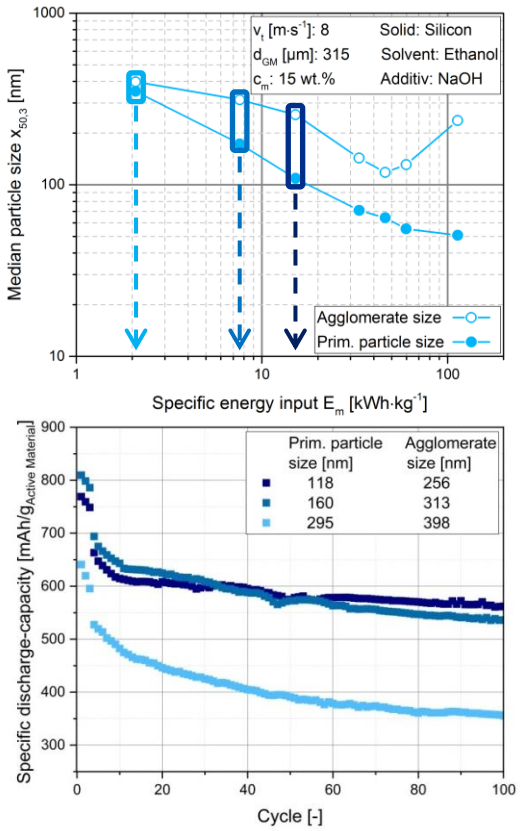

Fig. 3: Specific discharge-capacity of silicon reach anodes dependent on the cycle number and for three different primary silicon particle sizes

Alongside the influence of the silicon particle size the specific adjustment of a particulate composite structure can also help to overcome the challenges of the large volume expansion. Therefore, an additional granulation step can be integrated after grinding and before electrode slurry preparation. The granulation step enables a specific design of the particle structure such as a uniform silicon distribution, a defined porosity and also the usage of conductive additives to overcome the poor electric conductivity of silicon. Therefore, a fluidized bed granulation process using the ground silicon and larger graphite particles was established. As shown in Figure 4 the silicon nanoparticles adhere on the surface of the graphite particles and form a continuous layer.

3.2 Lithium-ion battery cell production

For the production of battery electrodes the active material particles have to be dispersed within a solvent together with the conductive additives (especially carbon

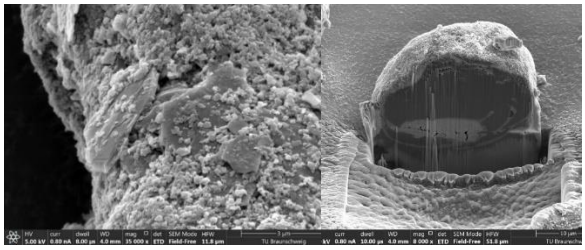

Fig. 4: SEM pictures of silicon-graphite composite particles prepared by fluidized bed granulation; top: cross section of a composite particle; bottom: silicon nanoparticles and graphene sheets

black, increasingly also carbon nano tubes) and binder (few percent of active material mass each). Especially the dispersing of the conducting additive carbon black plays a major role for the electrode structure and thus its electrochemical performance. Usually planetary mixers are used for this process. Besides first applications of using extrusion machines as well as stirred media mills for the dispersing and mixing processes are reported. As an example in Figure 4 the specific resistance of silicon anodes without stabilizing additive for the carbon black particles (strategy 1) and with (strategy 1a/ 2/ 3), but apart from that with the same formulation are shown. The use of a stabilizer and different dispersing strategies (see Fig. 1) results in greater extent of carbon black dispersing with higher dispersing intensity. The increase in electrode resistance prepared by strategy 2 and 3 are due to the stabilizing effect of the used additive. Smaller agglomerates exhibit a larger surface area, which leads to a greater amount of stabilizer present on the carbon black surface and the forming a passivation layer.

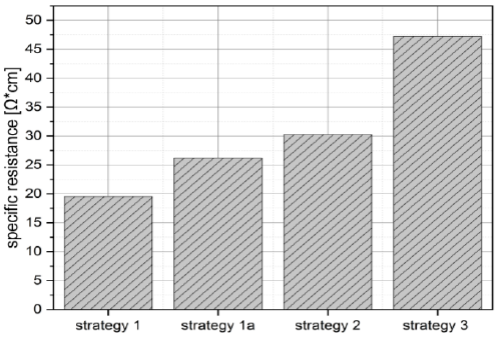

Fig. 5: Specific resistance of silicon anodes with variation of carbon black dispersing strategy

3.2 Lithium-ion battery recycling

After reaching their end of life lithium ion battery systems have to be discharged and dismantled. For the further processing in principle mechanical, hydrometallurgical and pyrometallurgical processes can be used. Very often at first the achieved battery modules or cells are shredded in a closed shredder, usually under inert gas atmosphere (or under water) [9,10]. In some cases before shredding the cells are heated up so that all

organic components are burned. If the solvent is not removed, the remaining solvent can be extracted by drying. Now the different particulate components (metals, active material particles, plastic parts) with different size, density and shape can be separated using a zigzag-classifiers and tumbler screening machines.

References

[1] Kwade, A., Haselrieder, W., Leithoff, R., Modlinger, A., Dietrich, F., Droeder, K. (2018) *Current status and challenges for automotive battery production technologies*, Nature Energy 3 (4), 290-300

[2] Noeske, M., Breitung-Faes, S., Kwade, A. (2019) *Electrostatic Stabilization and Characterization of Fine Ground Silicon Particles in Ethanol*, Silicon

[3] Reuter, B., Hendrich, A., Hengstler, J., Kupferschmid, S., Schwenk, M. (2019) *Rohstoffe für innovative Fahrzeugtechnologien* : *Herausforderungen und Lösungsansätze*. Stuttgart, 2019

[4] McKinsey (2017) *The future of nickel: A class act*. Basic Materials November 2017

[5] McKinsey (2018) *Lithium and Cobalt - A tale of two commodities*. Metals and Mining June 2018

[6] Kim, J.-M. ; Chang, S.-M. ; Chang, J. H. ; Kim, W.-S. (2011) *Agglomeration of nickel/cobalt/manganese hydroxide crystals in Couette–Taylor crystallizer*. In: *Colloids and Surfaces A: Physicochemical and Engineering Aspects* 384, 1-3, 31–39

[7] Kim, J.-E. ; Kim, W.-S. (2017) *Synthesis of Core–Shell Particles of Nickel–Manganese–Cobalt Hydroxides in a Continuous Couette-Taylor Crystallizer*. in: Crystal Growth & Design 17, 7, 3677–3686

[8] Cheralathan, K. K. ; Kang, N. Y. ; Park, H. S.; Lee, Y. J. ; Choi, W. C. ; Ko, Y. S. ; Park, Y.-K. (2010) *Preparation of spherical LiNi0.80Co0.15Mn0.05O2 lithium-ion cathode material by continuous co-precipitation*. In: *Journal of Power Sources* 195, 5, 1486–1494

[9] Kwade, A., Diekmann, J. (2017) *Recycling of Lithium-Ion Batteries: The LithoRec Way*, Springer

[10] Diekmann, J., Hanisch, C., Froboese, L., Schaelicke, G., Loellhoeffel, T., Folster, A.-S., Kwade, A. (2017) *Ecological recycling of lithium-ion batteries from electric vehicles with focus on mechanical processes*. Journal of the Electrochemical Society 164(1), A6184-A6191

ID02-Size reduction of active pharmaceutical ingredients – Overview, challenges and advancements

Michael Juhnke*

Novartis Pharma AG, Technical R&D, Basel, Switzerland

Summary. A general overview is provided on the process development and production of engineered drug particles by size reduction techniques. Scientific and business driven challenges are introduced considering process development and drug product characteristics. Advancements are presented to facilitate the development of engineered drug particles by size reduction techniques at early development stage using small equipment scales as well as the transition to late development stage and commercial manufacturing. Case studies are provided for commercialized products where size reduction techniques could provide an essential element to enable key drug product features.

* Corresponding author: michael.juhnke@novartis.com

ID03-Applying primary rock properties of strength and mineral association to a new suite of mechanistic comminution models

Malcolm S. Powell

JKMRC, Sustainable Minerals Institute, University of Queensland, Australia

Summary. It is high time to dramatically upgrade historic empirical comminution models, that are based on back-fitted breakage rates, to mechanistic models. This work presents an approach to embracing the available computational power and the progress in understanding of comminution systems to rewrite models to be predictive and reliable with respect to the range of conditions to be encountered in the current and future devices we use in industry. Underpinning such an approach is the need for appropriate measurement of breakage properties, that include mineral association, that respond to the range of conditions encountered in comminution equipment. For mineral processing.

1 The Need for a Paradigm Shift

A significant drawback of empirical models currently employed in the mineral processing industry for design and optimisation, is not just accuracy, but that they by definition lock our operating effectiveness at 50-year old inefficiencies, when the mining industry is driven by a need to dramatically improve production efficiencies.

It is the author's objective to embrace the available computational power and the progress in understanding of comminution systems to rewrite models to be predictive and reliable with respect to the range of conditions to be encountered in the current and future devices we use in industry (Powell, 2006; Powell, Govender & McBride, 2008b; Bonfils & Powell, 2018). A limited number of researchers also propound this approach, such as Beinert, Fragnière, Schilde & Kwade (2017) and de Carvalho & Tavares (2013).

Mechanistic modelling requires appropriate measurement of breakage properties that respond to the range of conditions encountered in comminution equipment. Correlating a laboratory test to operating equipment via scaling relationships or rates functions is woefully inadequate, in fact misleading. The correlations only apply for the range of ore types and equipment conditions they are fitted to. For mineral processing, the ore description needs to include mineral association, to enable prediction of the underlying driver of all mineral processing – the separation of valuable minerals from waste. The correct understanding and measure of breakage properties was found to be lacking, preventing the application of mechanistic models, as discussed in Powell & McBride (2006) and Powell, Govender & McBride (2008a,b).

Motivated by the inadequate input to modelling, a course of work was embarked upon to link primary rock properties to mechanistic models in order to enable predictive modelling of comminution processes in the mining industry.

2 Primary Rock Properties

Primary rock properties are measurable rock responses that are conserved over time and along the process chain. Force to fracture, loading force and applied energy to abrade the rock surface, fracture frequency, mineral association, are such properties. They do not depend upon the local environment or test equipment, and are not a function of a specific set of conditions.

Conventional comminution tests are all condition specific. For example, the famous Bond Work index is a function of a specific mill size, test routine etc. this makes it a robust fairly reproducible test, but it is the response of the material to a specific test condition that is being measured, not the rock strength. The JK Drop-weight test applies a controlled range of input energies to rocks, but is actually a mini-comminution device applying progressive stages of breakage with varying degrees of rebreakage dependent on the stiffness of the rock (Saeidi, Yahyaei, Powell & Tavares, 2016).

Primary properties can be applied to all comminution devices, then used to calculate the response of equipment and the ore as it is processed along the production chain. In this manner, different units in the mining and mineral processing chain can communicate mathematically via models and integrated process simulation. For example, the loading force required to induce first fracture is a measure of rock strength that can be used by mining engineers, in blast design, rock handling, crushing and milling and to define the properties of the waste material. Likewise, the natural fracture structure of the rock controls the processes from pit wall strength to blast size, though to primary milling, and possibly to final product if the fine fracture structure is known. Grade distribution

* Corresponding author: malcolm.powell@uq.edu.au

is controlled by mineral association in the rock formation, which also dictates the required fragmentation size for mineral recovery – potentially at multiple progressive recovery stages along the processing route.

3 Breakage Characterisation

Mass-specific energy, expressed in kWh/t, is not the underlying driver of particle breakage, but rather applied strain is. However, the prediction of applied strain rates between colliding particles in mills and other comminution devices is still an area of research development, so not yet a reliable input to mill models. Energy has proven to provide a robust input parameter to understanding and modelling breakage in ore comminution processes, and is readily accurately measured as an input to these processes. Although the amount of energy absorbed or utilised may be considered a consequence of breakage, the consistency of the relationship between energy input and degree of breakage retains this as a useful input parameter in comminution models.

The consumption of energy is a critical design parameter of comminution devices and the reduction of energy consumption a major objective of equipment optimisation and development of novel processes. Thus, having an accurate output of energy consumption is a critical capability of all comminution models.

The principal understood modes of mechanical rock breakage are:

1. Body breakage under normal loading applied by an impact or compressive force
2. Surface breakage through abrasive sliding or low energy impacts that do not cause body breakage
3. Bed breakage – interparticle loading with combined shear and normal forces (a complex combination of breakage under normal loads and shear).

Based on the hypothesis that any comminution device will apply some combination of these three principal modes, then these are the only three tests required.

The outputs of characterisation should include:

1. Absorbed energy
2. Progeny size distribution arising from the specific breakage mode and loading
3. Mineral association of the progeny
4. Distribution of all parameters, not a single average
5. The outputs should provide a probability distribution of the breakage occurring

3.1 Rock Strength

Rock strength is a measure of the resistance of the rock to body breakage. In measuring rock strength, the breakage probability and resulting progeny should be measured as a function of applied strain and the applied and absorbed energy should be measured. A split Hopkinson bar is ideal for this (Bbosa, Powell & Cloete, 2006), but the impact load cell has proven more usable with natural rock shapes, such as the short impact load cell (SILC) used at the JKMRC, which was developed by Bourgeois & Banini (2002).

The response of a rock to applied strain can be divided into three regimes:

- Single impact breakage
- Incremental breakage
- Surface damage

Although transition specific energies have been used to define these regimes in the past, the reality is that there is a broad response of particles to a given input force, so it is more useful to model breakage as a probability distribution rather than to define artificial boundaries between the three regimes. The work of Bonfils, Ballantyne & Powell (2016) takes this approach. This was further developed by Ballantyne, Bonfils & Powell (2017) to provide a continuum of breakage size (appearance function) and probability of breakage in a single relationship. Although the current relationship contains empirically fitted parameters, ongoing work will seek to draw out the physical significance of these over-arching relationships – to provide the basis of more predictive descriptions of impact breakage.

An impact load cell or compressive breakage with precision load-displacement measure, both deliver the required outputs. If the input energy of the impact is adjusted to be sufficient to break the rock but avoid secondary breakage, or the compression test is halted as the rock fractures, then the primary breakage function can be measured (Saeidi et al, 2016). As noted earlier, the standard drop weight test applies significant rebreakage.

In order to measure incremental damage leading to breakage, low input energies or forces are required, with repeat tests until each particle breaks. This is difficult to implement due to the small input energies requiring light weight and small drop heights, leading to inaccuracy of tests, plus tedious repeats for many particles. This becomes exacerbated for small particles, leading to infeasibly small input energies. This has led to the development of carefully conducted mono-layer breakage of many small particles (Barrios, Carvalho & Tavares, 2011). Rotary breakage testing, which flings particles at an anvil, is suited to dealing with low energies and with small particles if run under vacuum, as applied by Ballantyne, Peukert & Powell (2014). However, this too is tedious and does not provide the distribution of strengths or absorbed energy, plus the low mass of tested material renders the measure of the appearance function difficult.

The problem of measuring body breakage under low energies (below 0.1 J/g) and for small particles (under 3 mm) using a commercially viable technique has not been resolved. To this end, tests are being trialled at the JKMRC to provide a combination of particle strength distribution, breakage energy and sufficient progeny to measure the appearance function arising from primary breakage.

3.2 Surface breakage

Abrasion is the surface damage induced by shearing or sliding of particles across another surface. But surface, or surficial, breakage is also caused by low energy

loading events fracturing off grains and chips from the surface of a particle. These independent sub-modes are difficult to separate in practice. This has been investigated by Yahyaei, Weerasekara & Powell (2015). Useful pragmatic measures have been obtained but sample size is far too large for routine testing in the full-scale test. A small-scale equivalent test, with controllable loading environment is being investigated in ongoing student work at the JKMRC.

What is particularly difficult to capture in shear is the loading force. The degree of shear damage is not a function of input energy, it is dependent on normal loading force and the distance it is applied over. This relationship flattens above a saturation force, where after the rate of wear does not increase with increased normal force.

Another aspect of surficial damage is the contribution of surface roughness – angular projections are chipped off by relatively low forces, but once smoothed out, the shear rate is dramatically lower, demonstrated in the work of Yahyaei, Weerasekara & Powell (2015).

Thus, surficial breakage requires the following variables as input:

- A range of loading force up to the saturation force
- Fresh broken surface
- Abraded smooth surface

3.3 Bed breakage

Theoretically, it should be possible to calculate the response of rocks to bed breakage from the strength and surface breakage relationships. However, the complexity of the interactions makes it more feasible to directly characterise bed breakage. The Piston and Dye test is the most common, with some range in how the bed is packed in and then loaded, and what measures are used. An interesting application was provided by Liu & Powell (2016), which accounts for multicomponent ores, i.e. a mixture of different ore types and competencies. The approach models the breakage of each component as a function of reduction in voidage – that is equivalent to reduction ratio in the compression test.

3.4 Mineral association

As the purpose of comminution in mineral processing it to expose minerals for recovery, this should be an integral part of modelling, and thus of ore characterisation. Driven by this need and that it was not delivered in even the best prior work, such as by King (2001), a new approach was sought that could use the considerable computational power at our disposal. Hilden (2014) and Hilden & Powell (2017) developed a model to mathematically represent the textural association of a mineral structure in a tractable mathematical form. This modelling approach describes each mineral type in terms of size distribution, association with each of the other minerals and bias to spatial distribution. This approach allows many minerals (up to 5 plus the gangue host have been modelled) with minerals within minerals and banding distribution structures to be modelled with four physically meaningful parameters per mineral. The parameters are back-fitted to match mineral liberation data – such as MLA, QEMSCAN, density distribution, magnetic susceptibility etc. from the progeny of breakage tests. The model can be run with breakage models at any stage of the comminution process, taking less than 10 seconds to reproduce a full mineral association distribution based on the modelled progeny size distribution.

The Hilden mineral association model is thus well suited to be fitted to the progeny of breakage tests that represent the primary modes of breakage. In principle the mineral association resulting from quite different modes can each be calculated and passed on to the total progeny description based on the amount of material and particle types that have each mode applied to them.

4 Application to Mechanistic models

Only the energy / force transmission is discussed in this abstract. All comminution devices must have a feed, transport, and discharge mechanism, the application of which is described in Bonfils & Powell (2018).

The basis of a mechanistic model is the distribution of collision events, the forces and energies of these and the rate of these events. The collision energy applied to particles is calculated from the probability of impact of each particle size class; the total energy imparted to that size class; and the distribution of that imparted energy. These are considered to be the key factors to capture in the impact breakage part of the model. For the surficial breakage the loading force and sliding distance or period are required. For bed breakage the loading force and displacement are required per loading event.

For each mode of breakage and the distributions of load intensities, it should be possible to calculate the resultant mineral associations, based on the parameters fitted for that particular ore.

It is extremely challenging to calculate or simulate the distribution of these collision events in a real comminution device. The discrete element method offers the most useful input at this stage, as presented in the overview of Weerasekara et al (2013). The work of de Carvalho & Tavares (2013) has explored this more deeply than others.

In essence the model is required to provide a probability distribution of collisions, that are allocated to the modes of breakage. In terms of applying the range of breakage modes, they can be sequenced according to loading force from highest to lowest with the breakage action being distributed by the modes and degree of breakage that each would apply. By using a probability distribution the total available energy will not be violated. Thus, the sum of the progeny from the distributed modes will conserve mass and energy.

If on the other hand empirical breakage relationships are used that embody a fixed relationship between a test and measured outputs from equipment, it is unlikely that energy will be conserved in the model, as the mechanistic approach demands a ‘correct’ input of energies / forces related to the breakage characteristics.

The equipment production cannot be hidden in back-fitted rates.

When expressing the modes of breakage over a time period (such as one mill rotation or 1 second) they become rate functions - number of collisions of energy/force X per particle per second. This is not to be confused with the rates functions fitted to population balance models, which absorb all unknowns in the empirical models.

If the relationships contained within the mechanistic model are exact, then this model is fully predictive with no fitting factors. However, this is unlikely in such a complex system as a mill. The approach is to apply a rate correction, called the 'fitting factor' that modifies the predicted rates to those back-fitted to experimental data. For a perfect model the fitting factor is 1, deviations from this should represent differences between the model prediction and measurement.

5 Conclusions

A brief overview is presented of the author's experience in applying breakage models to mechanistic modelling of comminution processes. Over many years of building the unified comminution model (UCM) since first published by Powell (2006), it has been held back as much by inadequate ore characterisation methods as the complexities of the model itself. Mechanistic breakage tests are a pre-requisite for mechanistic models. Although considerable progress has been made in addressing this, the process it not yet adequate, with greater joint effort being required to successfully populate mechanistic comminution models.

References

Ballantyne, G.R., Bonfils, B., and Powell, M.S., (2017). Evolution of impact breakage characterisation: re-defining t-family relationship. *International Journal of Mineral Processing*, 168, 126–135.

Ballantyne, G.R., Peukert, W. and Powell, M.S., (2014). Size Specific Energy (SSE) – Energy Required to Generate Minus 75 Micron Material. *International J. Mineral Processing*, 139, 2-6.

Barrios, G.K.P. Carvalho, R.M. and Tavares, L.M. (2011). Extending breakage characterisation to fine sizes by impact on particle beds, *Mineral Processing and Extractive Metallurgy*, 120, 37-44.

Bbosa, L., Powell, M.S., Cloete, T., (2006). An investigation of impact breakage of rocks using the Split Hopkinson pressure bar. *J. SAIMM* 106 (4), 291–296.

Beinert, S., Fragnière, G., Schilde, C. & Kwade, A. (2017). Multiscale simulation of fine grinding and dispersing processes: Stressing probability, stressing energy and resultant breakage rate. Advanced Powder Technology, https://doi.org/10.1016/j.apt.2017.11.034

Bonfils, B. and Powell, M.S. (2018). Initial application of a dynamic, mechanistic mill model. Proc. IMPC 2018, Moscow, Russia, Sept.

Bonfils, B., Ballantyne, G.R. and Powell, M.S. (2016). Developments in incremental rock breakage testing methodologies and modelling. *International Journal of Mineral Processing*, 152, 16-25.

Bourgeois, F.S. and Banini, G.A. (2002). A portable load cell for in-situ ore impact breakage testing. IJMP, 65, 31-54. https://doi.org/10.1016/S0301-7516(01)00057-6

de Carvalho, R. M. and L. M. Tavares (2013). Predicting the effect of operating and design variables on breakage rates using the mechanistic ball mill model. Minerals Engineering 43-44, 91-101

Hilden, M.M. & Powell, M.S. (2017). A geometrical texture model for multi-mineral liberation prediction. Minerals Engineering, 111, 25–35.

https://doi.org/10.1016/j.mineng.2017.04.020

Hilden, M.M. (2014). Simulating the effect of mineral association using a multi-mineral rock texture and liberation model. In Proceedings XXVII International Mineral Processing Congress - IMPC 2014, Santiago, Chile, (210-218). 20-24 October.

King, R.P. (2001). Modeling and simulation of mineral processing systems, Butterworth-Heinemann, Oxford, pp. 58–80.

Liu, L.X. and Powell, M.S. (2016). New approach on confined particle bed breakage as applied to multicomponent ore. Minerals Engineering, 85, 80-91.

Powell, M.S., Govender, I and McBride, A.T. (2008a). Challenges in applying the unified comminution model. In Proceedings of the XXIV IMPC. 23 - 27 Sep., Beijing, China. Ed. W.D. Zuo et al. Vol. 2, pp 367-376. ISBN 978-7-03-022711-9

Powell, M.S., Govender, I., and McBride, A.T. (2008b). Applying DEM outputs to the unified comminution model – the SAG mill. Minerals Engineering, Special edition - DEM07. Vol 21, pp. 744-750. DOI: 10.1016/j.mineng.2008.06.010

Powell, M.S., and McBride, A.T. (2006). What is required from DEM simulation to model breakage in mills? Minerals Engineering, Special issue – computation 05, Vol. 19, No. 10, pp. 1013-1021.

Powell, M.S. 2006. The Unified Comminution Model - a conceptually new model. Proceedings of the XXIII IMPC. 3 - 8 Sep. (2006). Istanbul, Turkey. ISBN 975-7946-27-3. pp. 1783-1788.

Saeidi, F., Yahyaei, M., Powell, M.S. and Tavares, L.M., 2016. A Phenomenological Model of Single Particle Breakage as a Multi-stage Process. Minerals Engineering vol.98, pp90-100 · November.

Weerasekara, N.S., Powell M.S., Cleary, P.W., Tavares, L.M., Evertsson, M., Morrison, R.D., Quist, J. & Carvalho, R.M. (2013). The contribution of DEM to the science of comminution. Powder Technology, 248, pp 3-24. DOI: 10.1016/j.powtec.2013.05.032

Yahyaei, M., Weerasekara, N.S. and Powell, M.S. (2015). Characterisation of superficial breakage using multi-size pilot mills. Minerals Engineering, 81, 71-78.

ID05-Modelling of milling process in the minerals and pharmaceutical industry

Lian X. Liu[1*]

[1]Department of Chemical and Process Engineering, Senate House, University of Surrey, Guildford, Surrey, GU2 7XH, UK

Summary. Comminution is one of the commonly used unit operations in industries such as mining, food, chemical, metal and pharmaceutics and it consumes a considerable amount of energy in the mining industry. Therefore, predictive modelling of comminution process is essential for improving the process design, process optimisation, quality control and reducing operational cost. In this talk, two examples of dynamic mill models based on the population balance model (PBM) will be presented. The first one is for tumbling mills such as ball and SAG/AG mills used in the mining industry. The mill models for tumbling mills was developed in a generic dynamic model structure which incorporates ore breakage characteristics, transport, classification along the mill, a discharge function, and energy consumption. The second example is the milling of pharmaceutical ribbon for downstream tableting in the pharmaceutics industry, where specific ribbon feed properties to the mill are taken into consideration. The key sub-model that determines the success of modelling in the PBM is the breakage function and the function based on the Weibull distribution was found to be able to predict both of milling processes well.

1 Introduction

Comminution consumes a considerable amount of energy in the mining industry and it is estimated (Ballantyne and Powell, 2014) that about 0.2% of global electricity is consumed by comminution of gold and copper ores alone. Therefore, predictive modelling of comminution process, especially the product size distribution is essential for improving the process design, application of control systems for varying feeds and sizing mills within the dynamics of a milling circuit. In minerals processing, the product size distribution from comminution process has direct impact on minerals liberation. Whereas in pharmaceutical tableting process, the quality of tablets largely depends on the size of granules from the dry milling process. In this work, models based on PBM are developed to predict the product size distribution from different milling environment.

2 Theoretical models based on PBM

The population balance model (PBM) for a perfect mixed mill can be written as follows (Fuerstenau, and Sullivan, Jr., 1962; Whiten, 1974):

$$\frac{dm_i(t)}{dt} = f_i(t) - p_i(t) + \sum_{j=1}^{i} b_{ij}\, s_j m_j(t) - s_i m_i \qquad (1)$$

$$p_i(t) = d_i m_i(t) \qquad (2)$$

Where $m_i(t)$ is mass of material in size class i at time t in the mill ; $f_i(t)$ is the mass flow rate of feed in size class i, p_i (t) is the mass flow rate of product in size class i ; s_i is the breakage rate of particles in size i, b_{ij} is the breakage function which describes the fraction of materials broken into size i from the breakage of size class j; d_i is the discharge rate from the mill for size class i. The breakage function is the most important sub-model that determines the success of PBM.

2.1. Model structure for tumbling mills in the minerals processing

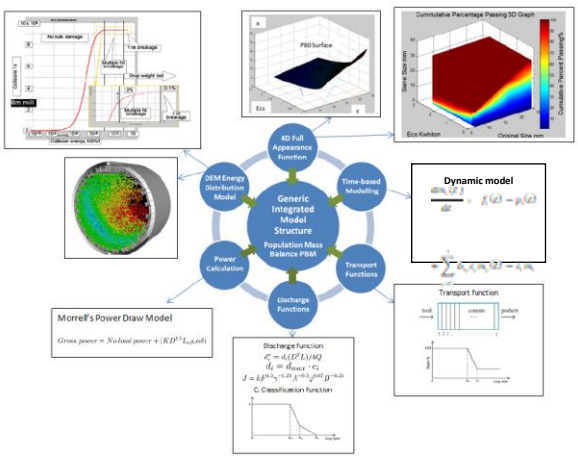

Fig.1. The generic mill model structure for tumbling mills

Yu et al (2018) have developed a generic model structure with different sub-models and one of them is shown in Fig. 1. The main characteristic of the model structure is that the breakage function b_{ij} is determined from independent impact breakage experiments and can be expressed by the Weibull distribution (Rosin-Rammler distribution) (Wills and Napier-Munn, 2006):

* Corresponding author: l.x.liu@surrey.ac.uk

$$passing = 100 * \left[1 - e^{\left(ln(0.2)\left(\frac{x}{P80}\right)^m\right)}\right] \quad (3)$$

Where *P80* and *m* are model parameters and x is particle size. DEM was used for modelling the mill energy environment and was used for the distribution of mill power to different particle size intervals.

2.2 Model structure for ribbon milling

The batch mass based population balance model with a fixed screen for ribbon milling is as follows:

$$\frac{dm_i(t)}{dt} = -s_i c_i m_i + \sum_{j=1}^{i-1} b_{ij}\, s_j m_j(t) \quad (4)$$

Where c_i is the classification function for size *i* and all the other symbols are the same as those in eq.(1). A breakage function similar to eq.(3) but to reflect the bi-modal distribution was developed:

$$B(x) = a\left(1 - e^{\ln(0.2)\left(\frac{x}{p_1}\right)^{m_1}}\right) + (1-a)\left(1 - e^{\ln(0.2)\left(\frac{x}{p_2}\right)^{m_2}}\right) \quad (5)$$

3 Results and discussion

3.1. Modelling results for tumbling mills

Fig. 2a shows an example of the size specific energy distribution for a case study and Fig.2b shows very good agreement between the model results and copper ore plant survey data.

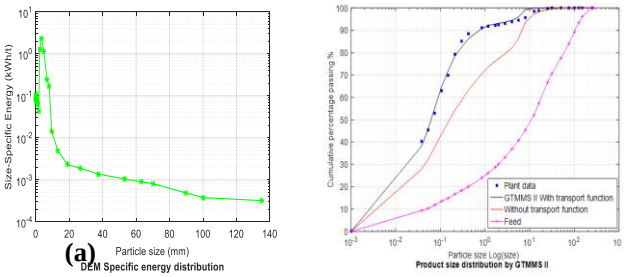

Fig. 2. (a). Example of DEM specific energy distribution **(b)**. Comparison of modelled product size distribution with plant data

3.2. Ribbon milling

A small semi-batch Retsch® cutting mill was used to mill microcrystalline cellulose (MCC) ribbons with defined ribbon porosity to granules. Figs. 3 shows comparisons between the modelled granule size distribution and the experimental data. Bimodal distribution is clearly observed and the proportion parameter **a** in eq.(5) that reflects the proportion of the two modes is clearly dependent on the ribbon strength /porosity and a linear relationship between **a** and ribbon porosity is observed (Fig. 4).

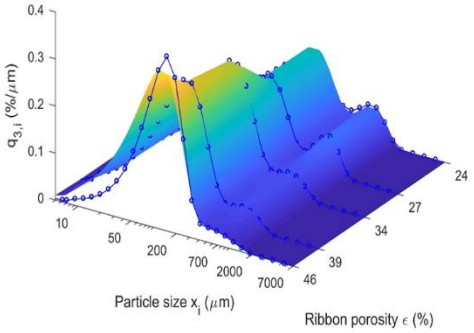

Fig. 3. Comparisons between modelled MCC granule size distribution (GSD) and experimental GSD at two ribbon porosity values.

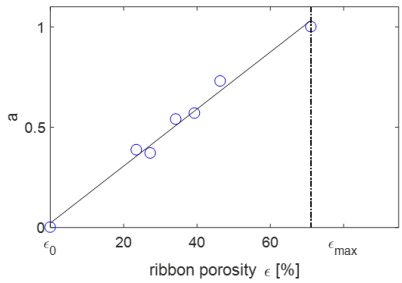

Fig. 4. Parameter **a** in eq.(5) vs. ribbon porosity

4 Conclusions

The breakage functions based on the Weibull distribution are developed and incorporated into the population balance model frame work for modelling both the industry scale tumbling mills and small scale cutting mill for ribbon milling. The models developed are able to match the plant data and experimental data with both single mode and bi-modal distribution very well and has great potential for dynamic modelling of mill circuit.

The author would like to thank her former colleagues at JKMRC UQ for their contribution on the work in mineral processing and her colleagues and students at Surrey University.

References

Ballantyne, G.R. and Powell, M.S. (2014), Benchmarking comminution energy consumption for the processing of copper and gold ores, Minerals Engineering, 65 109-114.

Fuerstenau, D.W. and Sullivan, Jr, D.A. Analysis of comminution of mixtures, Canadian Journal of Chemical Engineering, 40 (1962) 46-50.

Whiten, W.J., A matrix theory of comminution machines, Chem. Eng. Sci., (1974) 585-599.

Wills, B.A., Napier-Munn, T.J. (200. Wills' Mineral Processing Technology: An Introduction to the Practical Aspects of Ore Treatment and Mineral Recovery, seventhed. Elsevier, Great Britain.

Yu, P., Xie, W., Liu, L.X., Hilden, M. and Powell, M. (2018), Powder Technology, Vol 339, 396-407.

ID06-Current trends in air classification of fine powders

Steffen Sander*, and *Daniel* Droop

Hosokawa Alpine Aktiengesellschaft, Augsburg, Germany

Summary. Air classification utilising deflector wheel classifiers has been state of the art in powder processing for many decades. The micro processes taking place inside these machines are still not fully revealed and remain subject to further investigations. In practice, three main trends can be observed today: tendency to finer powders, powders with tailored particle size distributions, and focus on specific energy consumption. The presentation describes these trends more in detail and gives some examples of technical solutions to meet the requirements.

1 Introduction

The production of fine powders is a necessity in all kinds of applications. Deflector wheel classifiers are often used in powder processing to ensure product quality at different fineness levels, preferential for x_{97} of below 100 µm. In many cases these classifiers are operated in a closed circuit with a mill or are even part of the mills, such as in classifier mills.

Inside a deflector wheel classifier the gas flow with dispersed particle passes through the deflector wheel rotating at high speed. Due to the rotation, each particle entering the classifying zone is subject to two competing forces:

- the centrifugal force acts from the centre radially outwards:

$$F_c = \frac{\pi}{3} x^3 \cdot \rho_s \cdot \frac{v_t^2}{D} \quad (1)$$

- The drag force resulting from the air flow acts to the center of the deflector wheel:

$$F_d = c_d(Re) \cdot \frac{\pi}{4} x^2 \cdot \frac{\rho_g}{2} v_r^2 \quad (2)$$

The resulting settling velocity of an equivalent particle which is equal to the radial air velocity v_r can be described by

$$v_r = 1.63 \sqrt{\frac{\rho_s \cdot v_t^2 \cdot x_{eq}}{\rho_g \cdot c_d(Re) \cdot D}} \quad (3)$$

For a classification in the fine range a laminar flow can be presumed and c_d can be approximated by $c_d = 24/Re$. Thus, the classifier equation can be derived, indicating the main parameters on the equilibrium particle size x_{eq}:

$$x_{eq} = 3 \sqrt{\frac{v_r}{v_t^2} \cdot \frac{\eta_{gas}}{\rho_s} \cdot D} \quad (4)$$

Coarser particles will be deflected by the classifier wheel and discharged in the coarse fraction. Particles having a smaller diameter than x_{eq} will be drawn through the classifier wheel into the fines fraction.

By transforming equation (3) into the dimensionless form, a diagram can be plotted in which results of actual classifiers can be compared to the equation [1]. In **Fig. 1** it becomes obvious that by incorporating a fitting factor of 2 the x_{97} of the fines can be approximated over a wide range of parameters. This is still one of the handiest tools for the layout of classifiers or for determining suitable operating conditions.

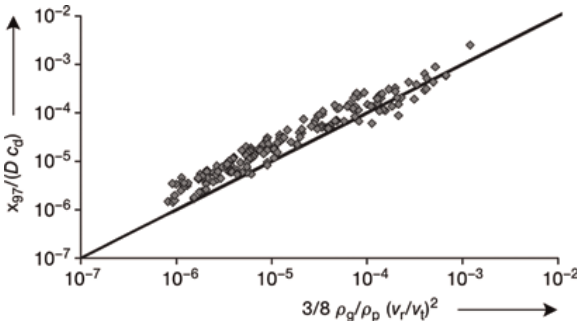

Fig. 1. Dimensionless particle size versus dimensionless operating parameters. wheel diameter: 200 – 500 mm; weight-to-diameter ratio: 0.13 – 0.6; radial air velocity: 5 – 50 m/s; Peripheral speed: 9 – 70 m/s; Fineness x_{97}: 5 – 200 µm [1]

More recent investigations focused on the description of the gas flow around and inside the deflector wheel by means of PIV measurements and CFD [2] or the motion of the particles inside the classification zone [3].

Besides the fineness x_{97} there are other characteristics to evaluate classifiers. The product yield, the throughput of the classifying system in relation to its investment costs and the operational costs are important for operators, to name just a few. The grade efficiency curve is often used to compare classifiers or operating conditions.

2 Current trends

Currently, three main trends can be observed in powder technology in different industries.

* Corresponding author: s.sander@alpine.hosokawa.com

2.1 Tendency to finer powders

For many applications, the fineness of the powders used as raw materials has an important influence on the properties of the final product. For fillers utilized in polymer parts, for instance, finer particles lead to improved strength properties. Thus, the percentage of mineral fillers can be increased resulting in reduced costs and improved optical properties. In silicate ceramics, finer raw materials result in improved material properties, such as in increased fracture toughness. In the case of active ingredients in pharmaceutical products finer particles result in faster dissolution of the drugs. Therefore, in many cases finer particle sizes increase the value of the products resulting in higher prices.
From equation (4) it becomes obvious, that high circumferential speed and low radial air velocity are beneficial for the production of finer products. For classification in the very fine range, classifiers are usually operated in a closed circuit with mills or form a part of classifier mills. This is due to the fact that the dispersion of particles with particle sizes in the range of a few µm becomes increasingly difficult. Moreover, the sharpness of the cut decreases and the bypass increases resulting in a lower fines yield. However, if using the right conditions very fine powders can be obtained. Using a 200 TTD classifier on top of a Pulvis PV 600 stirred media mill or a 400 TDG fluidized bed jet mill enabled the production of mineral powders with approx. x_{97} = 1 µm. One problem in investigating classifier mills is that there are no proven models of the material behaviour inside such mills.

2.2 Tailored particle size distributions

For many applications tailored particle size distributions are necessary to ensure the properties of the end product. The following examples might help to illustrate this trend:

- The production of breathable films for diapers requires GCC fillers of a defined steep particle size distribution to make sure that the pores have the required size. Moreover, the residues on a 20 µm wet sieve have to be as low as possible.
- Graphite powders for lithium ion batteries are ground to different fineness levels and undergo a subsequent periodization process. In order to improve electro-chemical properties, among other requirements the powders have to have a x_{90}/x_{10} ratio of 2…3.
- Metal powders for additive manufacturing are required to be dust free to improve the flowability and to reduce handling problems. On the other hand, the top cut of the powders is important to ensure an even bed formation during the manufacturing process, which is of vital importance for the quality of the manufactured parts.

Fig. 2 shows the PSD for a Ti64 powder produced using hot gas atomizing. The products were obtained using Argon as a process gas and a TTSP classifier which can be used to produce 3 fractions simultaneously in one machine. The resulting final product has a very steep PSD.

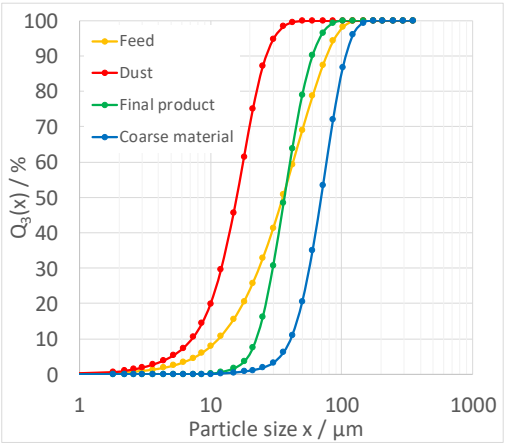

Fig. 2. Particle size distributions of the feed material and the three fractions produced using a 100 TTSP classifier (Ti64, Argon)

2.3 Focus on specific energy consumption

Especially for the producers of commodities, the specific energy consumption of a classifying system is important to tune the operational cost. Usually, the fan creating the gas stream is one of the biggest energy consumers in processing plants. Therefore, the pressure drop across the classifiers is an important value to focus on. This was one of the main intentions during the development of the new ACP classifier for the production of GCC and other mineral fillers [4]. With the 1250 ACP the production of 10 t/h of GCC with x_{98} = 8 µm is feasible creating a pressure drop of 64 mbar only [4].

3 Conclusions

Due to the big number of different applications resulting in manifold requirements, the design and the operation conditions of classifiers have to be tuned regularly. However, the micro processes taking place inside deflector wheel classifiers are still not fully revealed. Especially in the case of classifier mills, modelling needs to be further investigated to develop effective tools to support the engineering process in day-to-day business.

References

[1] Furchner, B. and Zampini, S. (2009). Air classifying. In : *Ullmann's Ecyclopedia of Industrial Chemistry*, Wiley-VCH Verlag GmbH & Co. KGaA, Weinheim, 10.1002/14356007.b02_17.pub2

[2] Toneva, P. I. (2010). Experimentelle und numerische Untersuchung zur Mehrphasenströmung in Sichtermühlen. Dissertation, Universität Erlangen-Nürnberg

[3] Spötter, C. (2018). Dynamik der Trenncharakteristik eines Abweiseradsichters, Dissertation, TU Clausthal

[4] Sander, S. and Droop, D. (2018). Runter mit dem Energieverbrauch, *Schüttgut 3/2018, p. 37*

ID07-Milling at the Nanoscale

Wolfgang Peukert* and *Stefan* Romeis

Institute of Particle Technology, Friedrich-Alexander University Erlangen-Nürnberg

Summary. Milling at the nanoscale is a fascinating field involving aspects of nanomechanics, internal defect formation and defect stability, colloid and formulation science as well as mechanochemistry. Inorganic and organic nanoparticles including drug particles, novel 2D materials such as graphene or boron nitride and even nanoemulsions can be produced this way. This contribution introduces basic concepts and highlights recent developments.

1 Introduction

Size reduction is discussed from a multiscale perspective ranging from the process level of grinding and classification down to defect formation and fracture at the lower nanoscale. Deformation and fracture of particles across all length scales are highly relevant for many applications including comminution, adhesion, friction and powder flow. This contribution reviews the current state-of-the-art in characterization and modelling of elastic and inelastic particle properties relevant for grinding processes and other powder processing unit operations. Nano-mechanical elastic and inelastic particle properties are measured systematically in a nanoindentation device installed within an electron microscope to obtain simultaneously force-displacement information and optical images of deformed and broken particles[1]. This information helps to understand phenomena during nanomilling. Nanoparticles down to 10 nm can be produced by top-down wet comminution in stirred media mills. Applications include oxide nanoparticles, pigments, drug nanoparticles, novel 2D materials and even nanoemulsions.

2 Apparent and true grinding limit

Nanoparticles can be produced by the top down method wet comminution in stirred media mills[1]. To prevent the nanoparticles from agglomeration in the suspension during the milling process, the interparticle interactions have to be controlled by the suspensions' properties: an equilibrium state between agglomeration and desagglomeration is formed. These competing phenomena often lead to a plateau in particle size above a certain energy input, the so called apparent grinding limit. The degree of agglomeration and therefore the final aggregate size can be controlled by the addition of stabilizers and by the applied shear forces. In contrast to the apparent grinding limit, the true grinding limit was identified during long-term milling experiments[2]: when the true grinding limit is reached, no further particle breakage takes place. By X-ray diffraction and the application of the Rietveld refinement method it is shown that defects are generated during mechanical stressing of the particles in the mill. These defects enhance the elastically stored energy in the crystalline lattice and weaken the material. Breakage occurs for ceramic particles even down to a size range of 10 nm. Below a critical size, defects cannot be stored or generated within the crystallites and the overall limit of grinding is reached. By comparison of the crystallite and particle sizes derived from gas sorption measurement, different grinding behaviors of nanoparticles are distinguished: fracture through nano-crystallites and fracture along grain boundaries[3]. Furthermore, it is shown that the grinding limit is strongly influenced by material properties, whereas process conditions analyzed in a practically relevant range hardly affected the limit. The breakage kinetics strongly depend on the process parameters and suspension conditions as long as the grinding limit is not reached: Proper choice of process parameters saves not only up to 90 % of the energy input to reach the grinding limit, it also leads to a higher product quality in terms of crystallinity and less milling bead wear.

3 Scalable production of 2D materials

In case of particles with highly anisotropic structures such as graphite or BN (2D materials), delamination can be induced by mild stressing conditions leading to free standing only nm-thin graphene-like platelets in dispersion. We introduce the underlying process technology in stirred media mills and high pressure homogenizers and show how the highly anisotropic nanoplatelets with

* Corresponding author: wolfgang.peukert@fau.de

lateral dimensions of up to 1 µm are characterized by novel methods based on analytical ultracentrifugation. Breakage of such sheets by liquid phase processing is an ideal way to generate also nano-sized sheets. However, until now it is unknown how functionalization influences the breakage behavior. We have chosen single layered oxo-functionalized graphene (oxo-G) derivatives with lattice defects < 1% to evaluate their size reduction rate upon ultrasonication and stirred media milling with respect to the type and degree of functionalization of the graphene sheets. The highest size reduction rate is observed for pristine oxo-G, which bears the highest degree of functionalization of around 60% and the negatively charged organosulfate group. Scaling laws are discussed which are surprisingly similar to other size reduction technologies (grinding, emulsification, spraying) and different materials[4].

2 Mechano-chemical effects

High energy input can induce phase transitions, radical formation at the particle surface and interactions of the solvent with the particles shedding new light on mechano-chemical reactions in liquid phase[5]. Despite the vast field of mechano-chemistry which encompasses an increase in reactivity due to the effect of mechanical energy input, there is still no clear picture of the involved mechanisms. In ultra-fine wet grinding the situation is further complicated due to the presence of the solvent: reactions of the stressed solid with the surrounding liquid phase can occur. Several aspects of mechano-chemistry can occur in stirred media mills. A key to the understanding of the underlying phenomena lies in the comprehensive product characterization and on the role of the liquid phase. It is shown that the liquid phase influences product properties like particle size, porosity, particle shape, structure, chemical composition and the molecular termination of the surface. An increase in the reactivity of glass particles is manifested by a significant increase in dissolution in the aqueous phase during processing in water. The liquid dispersion medium is considered as a relevant process parameter in stirred media milling and offers new prospects for innovative product design.

4 Shape control upon milling

Stressing of metal particles or glass particles below their brittle-to-ductile transition leads to irreversible plastic deformation. This effect is used in two directions: i.) model-based determination of stress energy and stress number distributions in mills[6] and ii.) production of functional platelets with interesting applications ranging from bioglass to battery materials.

During comminution particles are stressed in mills. The distributions of acting stress energy and number of stress events per product particle are governed by the used mill and its operational conditions. Mill functions link the stress energy and stress number distributions to the operating parameters and are widely unknown. We directly characterize the effective stress energy and effective stress number distributions within mills by using mechanically fully characterized spherical particles as particulate probes (e.g. made from Cu or Al beads). Finite element models describe the deformation behavior of the probes during uniaxial compression quantitatively on the single particle level. The respective changes of the particles' shapes are used to determine the stressing history of the particles and hence the stress energy and stress number distributions in the mill.

Stressing of glass particles below the brittle-to-ductile transition offers new options for shape controlled formation of functional glass platelets. These particles do not break anymore but are plastically deformed to platelets. The deformation can be related to the internal structure which is characterized by RAMAN and NMR spectroscopy, for instance. The shape evolution can be predicted by proper FEM modelling. These platelets with controlled thickness between a few 10 to 500 nm can be used as bioglass for bone replacements, pigments or battery materials.

References

[1] Paul J, Romeis S., Tomas J., Peukert W., A review of models for single particle compression and their application to silica microspheres, Advanced Powder Technology 25 (2014) 1, 136-153

[2] Knieke C., Sommer M., Peukert W., Identifying the apparent and true grinding limit, Powder Technology 195 (2009) 25-31

[3] Knieke C., Romeis S., Peukert W., Influence of process parameters on breakage kinetics and grinding limit at the nanoscale, AIChE J. 57 (2011) 7, 1751-1758

[4] Halbig C., Nacken T.N., Walter W., Damm C., Eigler S., Peukert W., Quantitative investigation of the fragmentation process and defect density evolution of oxo-functionalized graphene due to ultrasonication and milling, Carbon 96 (2016) 897-903

[5] Romeis S., Schmidt J. Peukert W., Mechanochemical aspects in wet stirred media milling, International Journal of Minerals Processing 156 (2016) 24-31

[6] Strobel A., Schwenger J. Wittpahl S., Schmidt J., Romeis S., Peukert W., Assessing the influence of viscosity and milling bead size on the stressing conditions in a stirred media mill by single particle

ID08-Adapting a breakage model to discrete elements using polyhedral particles and applying to industrial comminution

Luís Marcelo Tavares[1,*], *Flávio P.* André[1], *Alexander* Potapov[2], and *Clovis* Maliska Jr[2]

[1]Department of Metallurgical and Materials Engineering, COPPE-UFRJ, Universidade Federal do Rio de Janeiro, Rio de Janeiro, Brazil
[2]ESSS Rocky, Florianópolis, Brazil

Summary. The discrete element method (DEM) is a powerful tool to describe the behaviour of particulate flows. However, in some cases, breakage is not taken into account, leading to biased results. This becomes critical for simulations where particle flow and particle size reduction cannot be properly decoupled. The Tavares breakage model, implemented in the commercial platform Rocky DEM, takes in consideration important rock behaviour based on the energy dissipated in a contact to determine if a particle will break or not, specifying the progeny size distribution generated on a breakage event. The work presents the adaptation that was necessary for the model to discrete elements, its validation in coded form and application to size reduction in industrial size reduction by crushing.

1 Introduction

The discrete element method (DEM) is a numerical method that allows motion simulation of a large number of particles in a granular medium through the application of Newton's second law and contact models to predict the interaction between particles and between particles and boundaries (Cundall & Strack, 1979). The use of DEM allows the estimation of important data regarding particle flow, distribution of collision energies, rate of collisions, residence time and so on (Weerasekara *et al.*, 2013).

DEM faces several challenges and restrictions to represent breakage of particles (Jiménez-Herrera *et al.,* 2018). In most of the cases, breakage is often left to a post-processing stage using the information collected from the simulation or even altogether disregarded. However, breakage description is of key importance for the understanding of several types of crushers and mills in which particle flow and particle size reduction cannot be decoupled. Several approaches have been adopted on recent years to overcome this limitation, most of them by addressing particle as a cluster of spherical elements bonded together (Potyondy & Cundall, 2004) or by replacing the original particle by a set of progeny particles (Cleary, 2001). The approaches that have been adopted so far in commercial DEM packages present several limitations concerning the correct description of the breakage phenomena and the necessary computational power to perform it (Jiménez-Herrera *et al.,* 2018).

The Tavares breakage model consists of a series of equations proposed by Tavares (2004, 2009) and Tavares & King (1998, 2002) to address important characteristics of particle breakage based on the dissipated energy in each collision event, and therefore, decoupling dominant mechanisms involved in the comminution process. The model covers important rock behavior, such as the variation of particles' fracture energy within particles of same size and different sizes and rock weakening due to damage accumulation.

The present work validates the Tavares breakage model implemented in Rocky DEM, comparing results from experiments in particle beds stressed by a falling ball to simulations. Finally, simulations are then conducted of a vertical shaft impact crusher and compared to data.

2 Breakage modelling

The breakage model implemented in Rocky DEM is able to describe body breakage of polyhedric particles when subjected to stresses of varied magnitudes. This approach takes into account the energy dissipated in the contact between two elements to decide whether particles will break or not. The model also takes in consideration the damage sustained by a particle when subjected to stresses of insufficient magnitude to promote particle breakage.

The fracture energy distribution of particles, which corresponds to the cumulative breakage probability distribution $P_o(E)$ (Tavares & King, 1998), can be represented by an upper-truncated lognormal distribution represented by the following equations:

$$P_o(E) = \frac{1}{2}\left[1+erf\left(\frac{\ln E^* - \ln E_{50}}{\sqrt{2\sigma^2}}\right)\right] \quad (1)$$

* Corresponding author: tavares@metalmat.ufrj.br

$$E^* = \frac{E_{max}\, E}{E_{max} - E} \quad (2)$$

where E_{max} is the upper truncation value of the distribution, E_{50} and σ^2 are the median and the geometric variance of the distribution, respectively.

E_{50} is strongly related to the particle size. As particles become finer, the number of flaws in its composition decrease and, due to that, they become stronger. The relation between particle size and the median fracture energy is described by (Tavares, 2004):

$$E_{50} = E_{\infty}\left[1 + \left(\frac{d_0}{d_j}\right)^{\varphi}\right] \quad (3)$$

Whenever the dissipated energy of a collision is lower than the necessary energy to promote breakage, the particle will accumulate damage without breaking (Tavares & King 2002). Due to that, the particle will become more amenable to breakage on a subsequent contact. Damage sustained in the nth impact is given by

$$D_n^* = \left[\frac{2\gamma}{(2\gamma - 5D_n^* + 5)}\,\frac{E_{k,n}}{E_{n-1}}\right]^{\frac{2\gamma}{5}} \quad (3)$$

where γ is the damage accumulation coefficient, $E_{k,n}$, the contact specific energy and E_{n-1}, the particle fracture energy prior to the stressing event. The fracture energy of a particle is reduced after each collision, according to the expression:

$$E_n = E_{n-1}\,(1 - D_n^*) \quad (4)$$

where E_n is the particle fracture energy after damage.

Particle size distribution of the progeny will be related to the stressing energy based on the parameter t_{10}, which corresponds to the percentage in weight of the original particle that passes through a sieve with aperture equal to 1/10th of its original size. t_{10} is given by an expression in which the ratio between the stressing energy $E_{k,n}$ and the median fracture energy of the particle in question E_n (Tavares, 2009).

The complete particle size distribution is estimated using the incomplete beta function distribution, which depends on the t_{10} resulting from the breakage event.

The simulation of drop weight tests was performed in DEM to assess breakage probability and particle size distribution of the progeny. Copper ore and limestone particles were considered in the simulations. Calibration parameters of the material are presented elsewhere (Carvalho & Tavares, 2013). In addition, simulations of a vertical shaft impact crusher were also carried out of an aggregate rock.

3 Results

At first, results from the analytical model are compared to simulations in Rocky DEM for the case of particles in a drop weight. Fig. 1 presents the relation between the expected t_4 values of the model and the simulated values on Rocky DEM, showing good agreement for both materials studied.

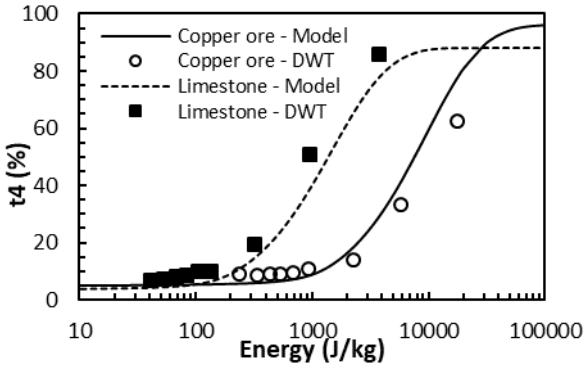

Fig 1. Comparison between the modelled and simulated t_4 values for drop weight tests of 5.5 mm particles for different impact energies

Results show generally good agreement between experiments and simulations for particle beds stressed with a range of impact energies. In particular, good agreement between predicted broken mass was observed, with reasonable agreement between the size distributions of the product.

Finally, simulations of an industrial BARMAC vertical shaft impact crusher were carried out for a range of operating conditions and results compared favourably with results from industrial surveys.

References

Carvalho, R.M. and Tavares, L.M. (2013). *Miner. Eng.* 43–44, 91–101.

Cleary, P.W. (2001). *Miner. Eng.* 14, 1295–1319.

Cundall, P.A. and Strack, O.D.L. (1979). *Géotechnique*, 29, 47–65.

Jiménez-Herrera, N., Barrios, G.K.P. and Tavares, L.M. (2018). *Adv. Powder Technol.* 29, 692–706.

Napier-Munn, T.J., Morrell, S., Morrison, R.D. and Kojovic, T. (1996). Mineral Comminution Circuits - Their Operation and Optimisation, JKMRC.

Potyondy, D.O. and Cundall, P.A. (2004). *Int. J. Rock Mech. Min. Sci.* 41, 1329–1364.

Tavares, L.M. (2004). *Powder Technol.* 142, 81–91.

Tavares, L.M. (2009). *Powder Technol.* 190, 327–339.

Tavares, L.M., King, R.P. (1998). *Int. J. Miner. Process.* 54, 1–28.

Tavares, L.M., King, R.P. (2002). *Powder Technol.* 123, 138–146.

ID09-Milling induced surface property changes in crystalline pharmaceutical solids

Jerry Y.Y. Heng* and *Vikram* Karde
Department of Chemical Engineering, Imperial College London
London SW7 2AZ, UK

Summary. Surface properties are critical for pharmaceutical manufacturing with an increasing trend towards the use of fine particles in pharmaceutical development where the surface will be increasingly important. Milling is often a unit operation of choice for size reduction in pharmaceutical processing although a range of surface changes can occur in crystalline solids subsequently affecting further processing, handling and performance. Here, we show that crystalline materials are anisotropic and milling results in the generation of new surfaces exposing different crystal facets varying in facet specific surface energy. Investigating the breakage behaviour of powders using finite dilution inverse gas chromatography (FD-IGC), it is demonstrated that crystals fracture along the weakest attachment energy planes, which are known to be the most hydrophobic. This work also highlights the importance of crystal habit and crystal anisotropy in milling and breakage behaviour. Furthermore, an approach to decouple the effect of contribution of milling induced increase in surface area and the powder cohesion was presented from silanisation studies.

1 Introduction

The surface properties of a crystalline solids could influence powder processing, particle handling and particle performance. A number of studies in literature describe the milling induced changes on particle interfacial or surface properties and correlate these to the performance (dissolution rates, DPI), processability (granulation) and powder handling (flow) (1).

2 Experimental methodology

Single macroscopic crystals (>1cm) of paracetamol, aspirin, mannitol are grown (Fig 1) by slow solvent evaporation. The facet specific surface wettability was determined by sessile drop contact angles on individual crystalline facets of macroscopic single crystals. Contact angles for water (Table 1) and diiodomethane were measured.

Milling studies were performed on different pharmaceutical materials such as paracetamol, D-mannitol and mefenamic acid (MA). The recrystallized powders were milled using ball mill and sieved to obtain different size fraction of powders. The milled MA was also silanised with different silane solutions. A new methodology based on finite dilution inverse gas chromatography (FD-IGC) for determination of surface energy distributions is employed (2). This technique was applied to study variations of surface energies due to milling and surface modification of crystalline solids.

3 Results and Discussion

3.1 Facet specific surface properties

The variability in contact angles for probe liquids tested confirms that crystalline organic solid is anisotropic in nature (3). Additionally, we report that the weakest attachment energy facets are the most hydrophobic facets, and have implications in powder processing such as milling, which may result in an increase in powder hydrophobicity (4). These variations are due to facet specific surface chemistry confirmed by XPS studies.

Table 1. Water contact angles on facets of macroscopic crystals

Sample	(001)	(010)	(011)	(110) (hkl)*
Paracetamol	15.9°	**67.7°**	29.8°	(110) 50.8°
Aspirin	**60.7°**	-	42.9°	(100) 52.9°
Mannitol	-	**56.2°**	12.8°	(120) 46.2 °

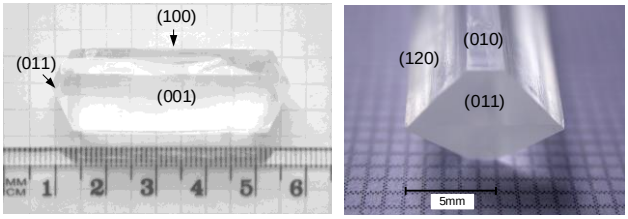

Figure 1. Macroscopic (>1cm) crystals.

3.2 Milling induced alterations

The FD-IGC approach was able to determine the effects of milling on powders (different crystal shapes/habits) (5), milling (exposure of different facets) (6).

3.2.1 Effect of crystal habit

The dispersive surface energy (γ^d) heterogeneity profiles for the milled D-Mannitol samples are shown in Fig. 2.

* Corresponding author: jerry.heng@imperial.ac.uk

As the aspect ratio increases, the dispersive surface energy profiles display a downward trend toward lower dispersive surface energy. This decrease in γ^d can be explained by the milling caused exposure of relatively higher hydrophobic crystal plane (011) of D-mannitol needles. This work emphasizes the importance crystal shape and exposed facets on surface properties.

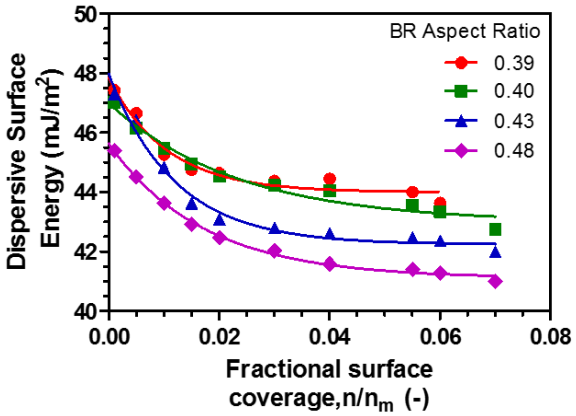

Figure 2. Dispersive surface energy profiles of milled D-mannitol sieve fractions as a function of aspect ratios.

3.2.2 Decoupling surface properties for powder cohesion

The γ^d profiles, before and after silanisation of MA, are presented in Fig.3. The γ^d values remained constant as a function of surface coverage for milled silanised samples of MA. On the other hand, the γ^d for unsilanized milled MA was observed to decrease and exhibiting surface energy heterogeneity. Therefore, it can be concluded that silanization results in energetically homogenous surfaces. The γ^d for silanised MA was observed in the ascending order from methyl, phenyl and vinyl functional end groups.

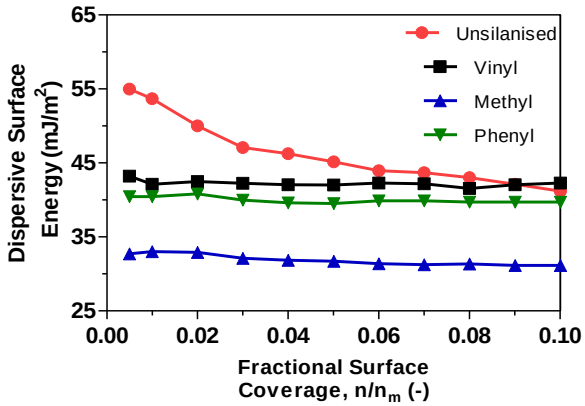

Figure 3. Surface energy heterogeneity profiles of milled MA powders.

Surface silanisation allowed normalisation of the surface energy and decouple its contribution on cohesion from the surface area. A linear correlation between the milled was observed, which increases in surface area and surface energy, and powder cohesion for surface modified and unmodified powders (Fig.4). This work presented an approach to decouple and quantify the effect of different surface attributes allows quantification of surface properties of pharmaceutical solids.

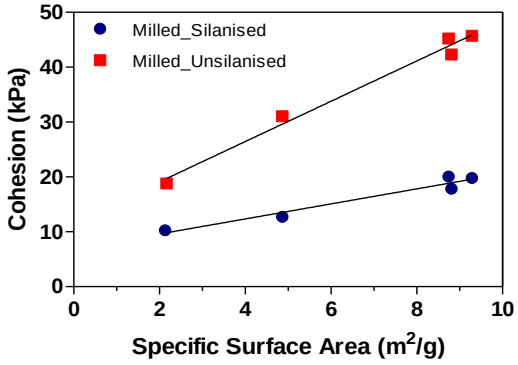

Figure 4. Cohesion as a function of surface area of silanised and unsilanised milled MA

4 Conclusions

In a series of studies, we showed that crystalline solids have variable (anisotropic) surface energetics. Results highlighting the influence of milling induced surface energy heterogeneity changes in several powders were reported. Milling of needle shaped D-Mannitol crystals indicated that crystal habit can also influence the breakage behaviour in crystalline materials, FD-IGC is useful in understanding the fracture behaviour of these solids during milling. Furthermore, an approach to decouple the effect of contribution of milling induced increase in surface area and the powder cohesion was presented from silanisation studies. In conclusion, it was showed FD-IGC is able to map differences in surface properties of processed particles.

The authors acknowledge the Engineering and Physical Science Research Council for funding (EP/N025261/1).

References

1. Shah, U.V., Karde, V., Ghoroi, C., and Heng, J.Y.Y. (2017) Influence of particle properties on powder bulk behaviour and processability. *Int. J. Pharm.* **518**, 138–154
2. Ho, R., and Heng, J. Y. Y. (2013) A review of inverse gas chromatography and its development as a tool to characterize anisotropic surface properties of pharmaceutical solids. *KONA J.* **30**, 164–180
3. Heng, J. Y. Y., Bismarck, A., Lee, A. F., Wilson, K., and Williams, D. R. (2006) Anisotropic surface energetics and wettability of macroscopic form I paracetamol crystals. *Langmuir*. **22**, 2760–2769
4. Heng, J.Y.Y., Thielmann, F., and Williams, D.R. (2006) The effects of milling on the surface properties of form I paracetamol crystals. *Pharm. Res.* **23**, 1918–27
5. Shah, U. V, Olusanmi, D., Narang, A. S., Hussain, M. A., Gamble, J. F., Tobyn, M. J., and Heng, J.Y.Y. (2014) Effect of crystal habits on the surface energy and cohesion of crystalline powders. *Int. J. Pharm.* **472**, 140–147
6. Ho, R., Naderi, M., Heng, J. Y. Y., Williams, D. R., Thielmann, F., Bouza, P., Keith, A., Thiele, G., and Burnett, D. (2012) Effect of milling on particle shape and surface energy heterogeneity of needle-shaped crystals. *Pharm. Res.* **29**, 2806–2816

ID10 - Influence of process properties on the comminution of lignocellulosic biomass

Moritz Eisenlauer[1,2,*], *Ulrich* Teipel[1,2,3]

[1] Technische Hochschule Nuremberg Georg Simon Ohm, Faculty Process Engineering, Wassertorstraße 10, 90489 Nuremberg, Germany

[2] Forschungsgruppe „ Partikeltechnologie und Rohstoffinnovation“ (FPR), Innere Cramer-Klett-Straße 4-8, 90403 Nuremberg, Germany

[3] Universität Ulm, Institut für Chemieingenieurwesen, Albert-Einstein-Allee 11, 89081 Ulm, Germany

Summary. Comminution of lignocellulosic biomass is a highly energy consuming process. Energy efficiency of the comminution process is of utmost importance to make renewable resources more competitive with petrochemical products. This work, therefore, focuses on the comminution of lignocellulosic biomass in a cutting mill and a hammer mill and how the specific energy comminution and particulate properties are effected by the type of mill, the species of wood, the achieved comminution ratio as well as the moisture content. For this reason two spices of hardwood- common beech (*Fagus sylvatica L.*) and oak (*Quercus robur L.*)- one species of coniferous wood common spruce (*Picea abies L.*) where comminuted at three different states of moisture content. The specific comminution energies were determined and the comminution products were characterized by two different methods. For the characterisation of the comminution products the sieve analysis and dynamic image analysis where used. From the results of the experiments, functions were determined which can describe the influence of the type of mill, the moisture content, the type of wood and the comminution ratio on the specific comminution energy.

1 Introduction

As a result of the development of innovative technologies, renewable raw materials are progressively being used for the production of precursors and basic chemicals for the chemical industry. The key factors influencing the energy efficiency and the particulate properties of the comminution products are, besides the mill type and the mill operation factors, the species of the lignocellulosic resource, in terms of moisture content and the mechanical properties which are the dominant factors in biomass size reduction. A better understanding of these interdependencies can help improve the adjustment of particle size distribution and particle shape as well as the energy demand for the comminution process, which impacts the overall efficiency of the supply chain. This work, therefore, focuses on the comminution of lignocellulosic biomass in a cutting and hammer mill. As part of this work, three different types of wood were used. Therefore two spices of hardwood and one species of coniferous wood where comminuted at different states of moisture content. The study reports the effects of different influencing parameters on the comminution process, the energy consumption and the physical properties of the products regarding their particle size. Furthermore, functions were determined which can describe the relation between specific comminution energy and comminution ratio.

2 Materials and Methods

The wood samples came from one deciduous and two coniferous species: common beech (*Fagus sylvatica L.*), common spruce (*Picea abies L.*) and oak (*Quercus robur L.*). The comminution experiments were carried out on a cutting mill of the type *Retsch SM 2000*. Furthermore, comparative experiments, to study the influence of the kind of stress, were carried out selectively on a swing hammer mill of the type *CONDUX LHM 20/60*. The power consumption of the mills was measured with a *Fluke Power Quality and Energy Analyzer meter*. With the no load power consumption and the total power consumption during the comminution process, the specific comminution energy E_{spec} can be calculated.

3 Results and Discussion

Figure 1 shows the relation between specific comminution energy and comminution ratio for the experiments by setting the degree of comminution $Z_{50,3}$ in relation to the specific comminution energy $E_{spec.}$ required for it. The materials where comminuted at

three different moisture content levels, w= 1.5, 15 and 34 %.

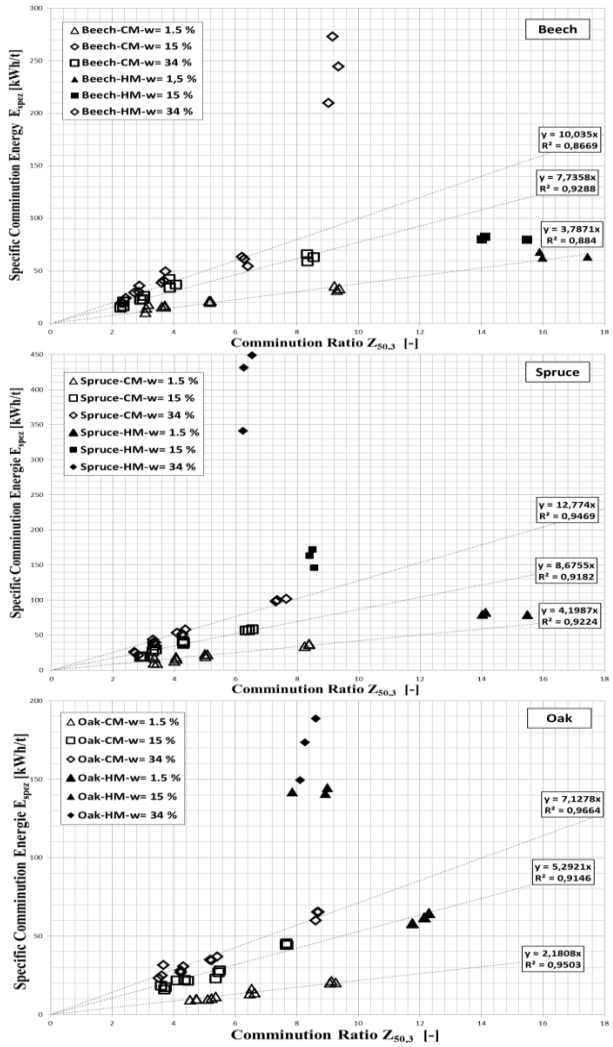

Fig. 3. Relationship between the specific comminution energy E_{spec} and the comminution ratio $Z_{50,3}$

Figure 1 comprises a linear correlation between the specific comminution energy and the comminution ratio with a high correlation coefficient of R^2 between 0.97 and 0.87 for all materials and moisture contents when comminuted in the cutting mill. At the low moisture content of w = 1.5 % the slope of the linear regression lines with all three materials is the lowest. With the increase of the moisture content the slope of the linear regression increases strongly. For spruce and oak wood the highest slope of the regression lines can be found with the highest moisture content w = 34 %. Beech wood is here an exception. The highest slope of the regression line is found with the moisture content w = 15 %. This behaviour clearly indicates that the specific properties of the material, that determine their stress resistance, are changing individually with the moisture content according to the type of species. Furthermore, it is remarkable, that in Figure 1 the results from the experiments with spruce at the low moisture content are located on the same linear regression line for the hammer mill and the cutting mill. A similar result is obtained with the experiments with beech at low moisture content. The two materials, exhibit specific comminution energy at the low moisture content, which is not dependent on the type of stress but on the comminution ratio. This behaviour is not observed in the experiments with oak. The results of the comminution of oak at the low moisture content with the hammer mill deviate strongly from the linear regression observed in the experiments with the cutting mill. At the higher moisture contents of w = 15 and 34 % for all materials the specific comminution energy from the hammer mill differ strongly from the linear regression lines of the cutting mill. In the hammer mill for all three materials, the comminution ratio decreases significantly at the high moisture content compared to the low moisture content, whereas the specific comminution energy increases dramatically. In Figure 1 it can be also obtained that the achieved comminution ratio $Z_{50,3}$ at the low moisture content is significantly higher in the hammer mill compared to the cutting mill. With the increase of the moisture content the achievable comminution ratio in the hammer mill decreases strongly.

4 Conclusions

The moisture content of the biomass influences the comminution energy consumption significantly. At the high moisture content, the specific comminution energy of the materials was up to three times higher as compared to the low moisture content. The moisture content also influences the particle size distribution of the comminution product. Especially in the hammer mill, the lower moisture content, leads to a finer product with a higher content of fines. Also, the type of material shows a distinct influence on the specific comminution energy. Spruce exhibits the highest specific comminution energy at all three moisture contents. The other two materials require lower specific comminution energy. The differences in the specific comminution energy of the three materials are more pronounced at the high moisture content. To what extent these relationships are caused by different structures of the materials and their different mechanical properties or due to the fact that the materials are different types of species - deciduous and coniferous wood – needs to be clarified in further studies. Regarding the type of mill, it can be concluded that the hammer mill is not appropriate for the comminution of the three materials with high moisture content in terms of energy consumption. However, the comminution ratio in the hammer mill at the low moisture content is remarkably higher compared to the cutting mill at the low moisture content. Furthermore, the products from the hammer mill have a wider volume density particle size distribution than the ones from the cutting mill. The relationship between the required specific comminution energy and the particle size distribution of the comminution product exhibits for all three materials a linear regression. The specific comminution energy increases linearly with the increase of the comminution ratio. The gradient of these linear regressions is dependent on the moisture content as well as the type of material.

ID11 - Energy-related materials: Mechanochemical synthesis via industrial milling

Peter Baláž[1*], *Oleksandr* Dobrozhan[1,2], and *Matej* Baláž[1]

[1]Institute of Geotechnics, Slovak Academy of Science, Košice, Slovakia
[2]Department of Electronics and Computer Technology, Sumy State University, Sumy, Ukraine

Summary. This work illustrates application of industrial milling to synthesize energy-related materials from non-toxic and earth-abundant components. Using eccentric vibratory mill for preparation of mohite Cu_2SnS_3 and mawsonite $Cu_6Fe_2SnS_8$ enables to scale-up the synthesis process from hundreds of gram to kilogram of product per batch.

1 Introduction

Energy is one of the most significant concers in the 21st century and is ultimately related to our daily life and global economy [1]. Development of sustainable, low-cost and clean energy sources represents one of the most important challenges for materials science. Optoelectronic and thermoelectric materials offer the viable way to convert solar and thermal energy directly to electrical energy without hazardous side products. However, their practical application remain limited because currently the best known materials are based on toxic, scarce, costly compounds with low chemical stability at operating conditions. Mechanochemical synthesis is selected as a simple, one-pot solid-state synthesis of complex materials with capability to reduce, or even eliminate solvents, enhance yields, improve crystallinity and provide access to new product libraries. Also, mechanochemistry allows simple up-scaling to the production of products in larger batches [2-3].

Several examples of using industrial milling for preparation of energy-related materials will be given in this work.

2 Mechanochemical synthesis via industrial milling

Vibration mills and their industrially successful alternative, eccentric vibration mills (ESM), represent a suitable option of high energy mills [4]. The ESM mills have modular tube design in which the exciter unit consisting of a bearing block and unballance masses are connected to the motor by means of the drive shaft. For the purpose of mass compensation, a counterweight is located on the opposite side to the exciter unit. The major technological advance is the fixed amplitude of vibration up to 20 mm (normally 12 mm maximum) and eliptical, circular, and linear vibrations in comparison with circular vibrations in conventional mills. Except for "traditional" applications in mineral processing, hydrometallurgy, soil rehabilitation, pharmaceutical industry, and agriculture, etc. where ESM were applied for mechanical activation of solids, they could be also used in "advanced" applications as mechanochemical reactors to produce new compounds. In this case, solid state reactions are executed directly in the mills.

In this work the application of high energy milling is illustrated for synthesis of energy-related materials. Mechanochemical solid state syntheses were performed in an industrial eccentric vibratory ball mill ESM 656-0.5 ks (Siebtechnik, Germany) working under the following conditions: a 5L steel satellite milling chamber attached to the main corpus of the mill, tungsten carbide balls with a diameter of 35 mm with a total mass of 30 kg, 80% ball filling, amplitude of the mill 20 mm, rotational speed of the eccenter 960 min^{-1}, argon atmosphere, 100 g of feed. The milling was performed at various times. The photographs of the mill with satellite are given in Figure 1.

2.1 Mohite Cu_2SnS_3: material for photovoltaics [6]

The mohite nanoparticles have been synthesized in an industrial eccentric vibration mill. The results of kinetic studies show that the reaction proceeds relatively fast yielding product with the stoichiometry close to that of Cu_2SnS_3. The powders composed of agglomerated nano- and microparticles morphology were obtained. The crystallite size around 15 nm is thought to be the consequence of used nanocrystalline precursors. Thermodynamical barrier of the reaction was also overcome by ''nano'' approach and the milling-time was

Fig.1. Eccentric vibratory mill with attached satellite milling chamber (top), the open satelite milling chamber filled with milling balls (bottom) [5].

significantly reduced compared to other studies. Samples include small amounts of impurity phases. Therefore, an annealinstep was is needed for higher purity and more accurate characterization of the samples. The calculated band-gap energy of 1.19 eV is in an optimum range for photovoltaic application.

2.2 Mawsonite $Cu_6Fe_2SnS_8$: material for thermoelectrics [5]

In this study we demonstrate the use of elemental precursors Cu, Fe, Sn, and S to obtain mawsonite $Cu_6Fe_2SnS_8$ by a solid-state process at ambient temperature. For the synthesis an industrial eccentric vibration mill was applied. The milling was performed up to 240 min in argon atmosphere. The transformation of elemental precursors to $Cu_6Fe_2SnS_8$ proceeds via several intermediate steps. The kinetics of this transformation is also in agreement with the results of non-consumed sulfur content in reaction mixtures and was well correlated with magnetization data measured. An average crystallite size of 58 nm was calculated using Rietveld refinement for mawsonite powder milled for 240 min. As for thermoelectric measurements, the properties of densified samples were measured using the standard methods needed to calculate zT values. Based on the measurements, the calculated figure-of-merit reached a value zT = 0.51@623K due to very low lattice thermal conductivity 0.29W/mK and a moderate power factor $3.3\mu W/cm^2K^2$. The obtained thermoelectric results for mawsonite $Cu_6Fe_2SnS_8$ synthesized in an industrial mill are comparable to the values obtained by milling in a laboratory ball-mill. Some parameters, e.g. electrical conductivity and power factor, are even improved compared to previous studies.

This work was supported by the projects of the Slovak Grant Agency VEGA (2/0044/18, 2/0065/18) and European project COST (OC-2015-1-19345).

References

1. Liu, Y., Li, Y., Kang, H., Jin, T., Jiao, L. (2016). Design, synthesis, and energy-related applications of metal sulfides. *Materials Horizonts*, 3, 402-421.

2. Baláž, P. (2008). *Mechanochemistry in Nanoscience and Minerals Engineering*. Springer-Verlag Berlin Heidelberg, 413 pp.

3. Baláž, P., Baláž, M., Achimovičová, M., Bujňáková, Z., Dutková, E. (2017). Chalcogenide mechanochemistry in materials science: insight into synthesis and applications (a review). *Journal of Materials Science*, 52, 11851-11890.

4. Gock, E., Kurrer, K. E. (1999). Eccentric vibratory mills - Theory and practice. *Powder Technology*, 105, 302-310.

5. Baláž, P., Hegedus, M., Reece, M., Zhang, R.-Y., Su, T., Škorvánek, I., Briančin, J., Baláž, M., Tešinský, M., Achimovičová, M. (2019). Mechanochemistry for thermoelectrics: Nanobulk mawsonite $Cu_6Fe_2SnS_8$ synthesized in an industrial mill. *Journal of Electronic Materials*, in press.

6. Hegedus, M., Baláž, M., Tešinský, M., Sayagues, M. J., Siffalovic, P., Kruľáková, M., Kaňuchová, M., Briančin, J., Fabian, M., Baláž, P. (2018). Scalable synthesis of potential solar cell absorber Cu_2SnS_3 (CTS) from nanoprercursors. *Journal of Alloys and Compounds*, 768, 1006-1015.

ID12 - Comparison of the impact breakage of synthetic rock samples using short impact load cell experiments and discrete element methods

Temitope Oladele[1,*], *Lawrence Bbosa*[1], and *Dion Weatherley*[2]

[1]Centre for Minerals Research, Department of Chemical Engineering, University of Cape Town, South Africa
[2]Sustainable Minerals Institute, Julius Kruttschnitt Mineral Research Centre, The University of Queensland, Australia

Summary. This paper presents a comparison of the impact breakage of synthetic rock samples using short impact load cell (SILC) experiments and discrete element method (DEM) numerical simulations. The findings show that the effect of particle shapes and size were consistent in both the SILC experiments and DEM numerical simulations. This finding suggests that DEM can further be used as an alternative tool to investigate effect of other material properties that might affect breakage behaviour with a reasonable degree of confidence.

1 Introduction

Comminution is one of the most energy intensive steps during mineral processing. Many breakage studies have been carried to gain fundamental understanding into the breakage process. Impact breakage studies of a single particle are often used as the initial basis to characterize comminution in terms of the energy-size reduction relationship and determine rock properties such as hardness and stiffness (Napier-Munn et al., 1996).

Several factors, including rock properties have been identified to affect breakage dynamics and the behaviour of particles during breakage tests. These have contributed to some of the unresolved fundamental challenges of breakage testing (Barbosa et al., 2019). Some of these factors include rock heterogeneity with pre-existing cracks, particle shape, mineralogical composition and particle orientation during loading. Therefore, attributing variations in breakage testing to a definite factor remains a challenge. However, an alternative approach to breakage testing using synthetic rock samples, such as 3D-printed sandstone, has emerged which provides controlled material properties akin to real rocks with minimal flaws and heterogeneity. The main advantages of using synthetic rock samples include fabrication of isotropic and homogenous samples with desired shape and size. The usage of synthetic rocks also enables many samples with the same mechanical properties to be produced for accurate repeatability of laboratory experiments (Barbosa et al., 2019).

Many laboratory-scale comminution devices that have been developed for particle characterization studies, however, the short impact load cell (SILC), modified from the drop weight tester and split-Hopkinson bar is noted for several benefits such as: (i) it is suited for testing both single particles and beds of particles (ii) appropriate for single impact and repeated/incremental breakage conditions (iii) can present the impact event in the form of a historical high resolution force-time chart/data set for further calculation of other standard breakage measures such as fracture energy and elastic stiffness. Computational tools such as DEM, a numerical means of calculating the motion and interaction of particles under applied force, have further emerged as a means of validating and complementing experimental measurements (Cundall and Strack, 1979).

This study investigates and explores the capacity of DEM to simulate the impact breakage of synthetic rock samples of different shapes (cylinders and spheres) and compares results against impact breakage SILC experiments of synthetic rock samples conducted by Barbosa et al. (2019).

2 Methodology

The numerical simulations were conducted using ESyS-particle 2.3.5, an open source package which uses Python based libraries to generate geometries and simulations. The DemGenGeo library version 1.2-1build4 was used for the construction of particle geometries (Weatherley et al., 2011). A volume filling algorithm was used to populate the DEM elements for the prescribed shape. Adjacent spheres were recognised via a neighbour search algorithm and connected via brittle-elastic bonds (Place and Mora, 2001).

3 Results and discussion

Figures 1a and b show the measured SILC experimental and DEM force to fracture for cylinder and spherical particles respectively. These figures also show the

sample size dependency measured from both experiments and simulations. In both cases, results were found to be consistent, evidenced with an increase in fracture force as the sample size increases. Furthermore, the fragments generated after the impact event for both particle shapes under study are shown in Figs 1c to f. Two major fragments were produced for cylinders indicated by experiment (Fig.1c) and DEM simulation (Fig. 1d) while three major fragments were produced for the spheres from experiment (Fig 1e) and also complemented by DEM simulations (Fig 1f)

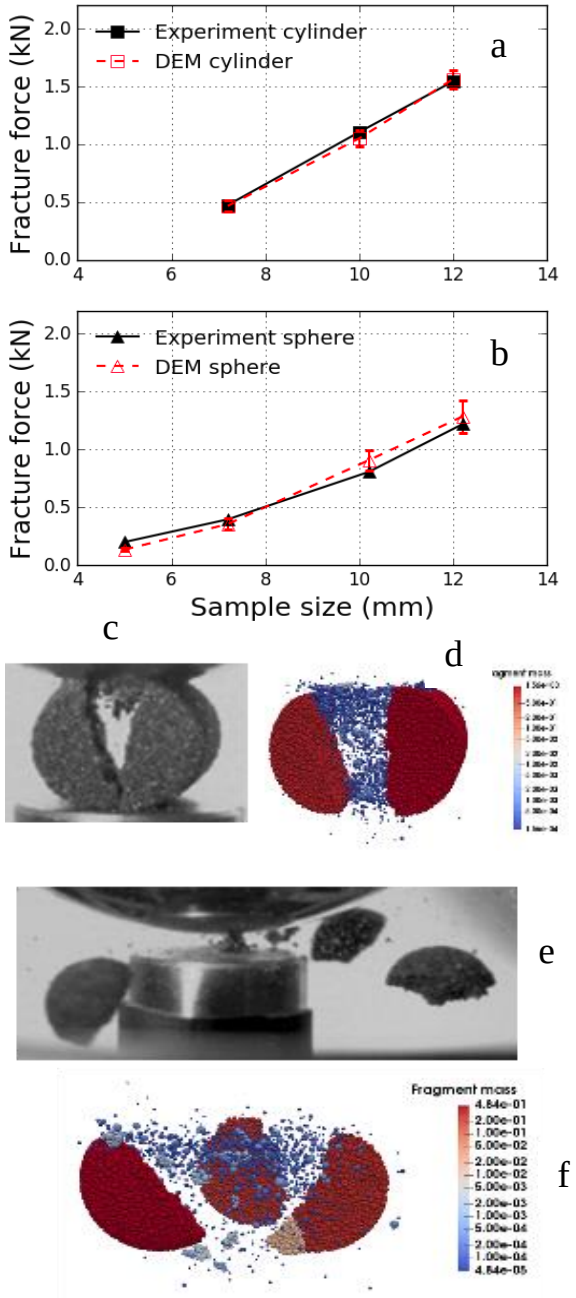

Figure 1 Measured fracture force for cylinder (a) and sphere (b).Fragments generated from cylinders (c and d) and spheres (e and f)

References

Barbosa K., Chalaturnyke R., Bonfils B., Esterle J., & Chenc Z., (2019). Testing Impact Load Cell calculations of material fracture toughness and strength using 3D-printed sandstone

Bourgeois, F. and Banini, G., (2002). A portable load cell for in-situ ore impact breakage testing. International Journal of Mineral Processing, 65 (1), 31-54

Cundall, P. & Strack, O. (1979) A discrete numerical model for granular assemblies. Goetechnique 29 (1), 47–65.

Napier-Munn, T., Morrell, S., Morrison, R., & Kojovic, T. (1996)..Mineral Comminution Circuits–Their Operation and Optimization, JKMRC Monograph Series in Mining and Mineral Processing, 2

Place, D. & Mora, P., (2001). A random lattice solid model for simulation of fault zone dynamics and fracture process. Bifurcation and Localisation Theory for Soils and Rocks' 99. 1.

Weatherley, D., Boros, V., & Hancock, W. (2011) ESyS-particle tutorial and user's guide Version 2.1. Earth Systems Science Computational Centre, The University of Queensland.

The primary funding of this work was provided by the South African Minerals to Metals Research Institute (SAMMRI). The authors would also like to thank the National Research Foundation of South Africa (NRF) for their continuing support of this research work. Furthermore, the author sincerely appreciates the technical support and guidance provided by the ESyS-particle development team. Computations were performed using facilities provided by the University of Cape Town's ICTS High Performance Computing team: (http://hpc.uct.ac.za)

ID13 - Assessing comminution energy efficiency with the Size Specific Energy (SSE) approach

Grant Ballantyne[1]

[1]University of Queensland, Sustainable Minerals Institute, Julius Kruttschnitt Mineral Research Centre

Summary. The high energy intensity and low energy efficiency of rock breakage processes provides great incentives for engineering optimisation. The optimisation process must begin with benchmarking energy efficiency by measuring the power, throughput and size reduction. However, the size reduction achieved by many modern comminution devices are not effectively described using traditional techniques that use the screen size through which 80% of the particles pass (P80). This is due to the difference in the shape of size distributions measured in modern comminution circuits that are significantly different to those seen at the time that P80 measurements were developed. A new methodology has been developed to fairly characterise the energy efficiency of modern comminution equipment, the Size Specific Energy (SSE) approach. This technique measures size reduction in relation to the generation of new fines, a much fairer approach that is less dependent on the shape of the size distribution and more closely related to the new surface area production.

1 Introduction

Benchmarking energy efficiency requires three measurements: comminution power, rock throughput and the resulting size reduction. The first two measurements are fairly objective, however, the third is subjective and could be measured in numerous different ways. Two of the most popular methods for estimating grinding energy requirements are the Bond operating work index (OWi) and the Morrell specific comminution energy method. Both relate the comminution energy to the reduction in the 80th percent passing size of the feed and product streams (F80 and P80). An important condition that needs to be met for using the Bond formula is that the distributions should have a similar slope, and correction factors (such as those introduced by Rowland (1982)) attempt to accommodate cases when slopes are different. Size Specific Energy (SSE) differs by relating the grinding energy to the quantity of new fines generated. For typical circuits that involve AG/SAG, HPGR or ball milling, the generation of -75 µm material (denoted as SSE75) is a suitable marker size with which to benchmark performance because it contains 80% of the surface area generation (Musa and Morrison, 2009) and energy is proportional to surface area generation (Rittinger, 1867). In one example, the OWi of the SAG mill was found to be 30% higher than the ball mill, thus suggesting that the SAG mill was less efficient than the ball mill. The apparent inefficiency of SAG mills when using Bond analysis is widely understood to be due to the difference in the slopes of the size distributions. In contrast, when the SSE75 was calculated, it showed the SAG mill consumed 20% less energy to produce final product material than the ball mill. Since the aim of a comminution circuit is to generate final product material, the SSE methodology gives a fairer indication of energy efficiency.

2 Operating work index vs size specific energy

To further explore the difference between the OWi and SSE, data from ten surveys of the same comminution circuit were compared using the two approaches. The OWi results differ significantly (factor of 3 times) whereas the SSE method results are more consistent and show that both mill types produce fine particles roughly in proportion to the energy input. In fact, in four of the surveys, the SAG mill was found to be more efficient at producing circuit product than the ball mill. Similar results have been seen consistently across all the surveys where this approach has been used, including circuits with AG mills, pebble mills, HPGR, stirred mills and ball mills with fine screens.

3 Simulation of ideal size distributions

Bond's method of quantifying size reduction by measuring the F80 and P80 relies on parallel particle size distributions in log-log space. The Gates-Gaudin-Schumann (GGS) ideal power law size distribution equation was used to test the difference between the three approaches (Bond, Morrell and SSE). Through this process the results from the SSE approach were found to provide the same result as both the Bond and

Morrell approaches depending on the gradient of the size distributions. When the gradient of the size distributions equalled 0.5, the SSE was mathematically equivalent to 1.44 times the OWi. This result is consistent with Bond's approach as he found that the GGS slope was "often about 0.5" (Bond, 1961). And SSE was proportional to the Morrell approach when the gradient of the size distribution equalled the Morrell exponent parameter (0.295 + P80/1000000) (Morrell, 2009). This result potentially shows that the Bond and Morrell approaches could actually be special cases, and SSE could have more general application.

4 Alternative marker sizes

As referred to earlier, the size specific energy calculation has typically been conducted at a marker size of 75 µm (Davis, 1919; Hukki and Allenius, 1968; Schönert, 1988) because of the size reduction range of the equipment being assessed. However, in order to apply the technique to fine grinding devices such as stirred mills requires the use of a finer marker size. For instance a marker size of 25 and 38 µm has been used to assess the performance of TowerMills and Vertimills (Palaniandy et al., 2018). However, no methodology is available to link the results from different marker sizes.

The ideal GGS size distribution investigation presented above was used to find a relationship between marker size and SSE. The SSE increased linearly (in log-log space) as the marker size decreased, and this ideal case where the size distribution followed a power law function, was found to be consistent with the measured data from many site surveys. This relationship between marker size and SSE can be used to link results from different marker sizes to apply SSE over a wider range of size distributions. Therefore, when fine grinding precludes the use of 75 µm as the marker size, an effective SSE75 can be extrapolated from the SSE at a finer marker size and the gradient of the relationship. Figure 1 shows one of the survey results from a SAG and ball mill. In the first survey the ball mill was underperforming due to the low density in the mill, which was rectified in the second survey. The ball mill was grinding to a P80 of 50 to 70 µm, therefore the traditional marker size (75 µm) was not applicable, and this can be seen by the increase in SSE for coarser sizes as the marker size approached P100. Using a finer marker size and the gradient of the relationship between log(SSE) and log(marker size), an equivalent SSE75 could be extrapolated. This approach allowed the data to be mapped on to the standard SSE intensity energy curve, which is based on a 75 µm marker size. These results show that the ball mill operated poorly at low densities, performing in the bottom 5% of mills in the database (95th percentile). By increasing the density of mill, it moved towards a more average operational regime, resulting in performance at the 65th percentile in the database.

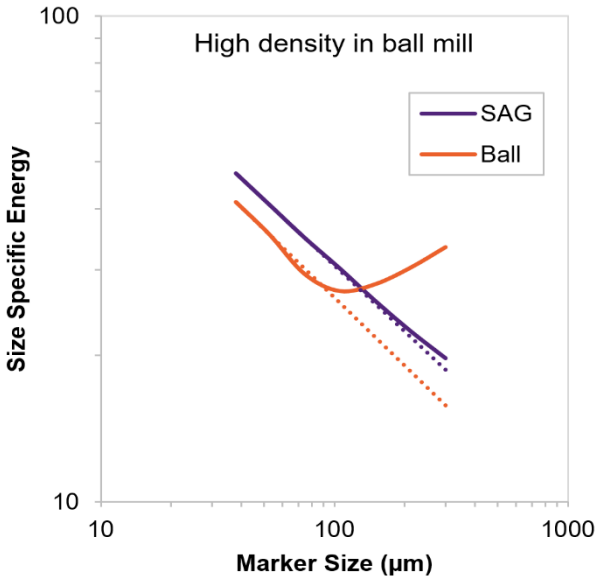

Figure 1 - Example of relationship between Size Specific Energy and marker size for one of the surveys.

5 Conclusion

The presented method provides a consistent measurement of comminution energy efficiency across the circuit, independent of the particle size gradient and fineness of grind.

References

Bond, F.C., 1961. Crushing and Grinding Calculations Parts 1 and 2. British Chemical Engineering 6, 378-385, 543-548.

Davis, E.W., 1919. Fine crushing in ball-mills. Transactions of the American Institute of Mining Engineers 61, 250-296.

Hukki, R.T., Allenius, H., 1968. A quantitative investigation of the closed grinding circuit. Society of Mining Engineers, AIME, Transactions 241, 482-488.

Morrell, S., 2009. Predicting the overall specific energy requirement of crushing, high pressure grinding roll and tumbling mill circuits. Minerals Engineering 22, 544-549.

Musa, F., Morrison, R., 2009. A more sustainable approach to assessing comminution efficiency. Minerals Engineering 22, 593-601.

Palaniandy, S., Halomoan, R., Ishikawa, H., 2018. Shifting the comminution workload from the primary ball mill to TowerMill Circuit, AusIMM Mill Operators' Conference, Brisbane, Australia.

Rittinger, P.R., 1867. Lehrbuch der Aufbereitungskunde. Ernst and Korn, Berlin.

Rowland, C.A., 1982. Selection of rod mills, ball mills, pebble mills and regrind mills, Design, installation of comminution circuits The American Institute of Mining, Metallurgical, and Petroleum Engineers.

Schönert, K., 1988. A first survey of grinding with high-compression roller mills. International Journal of Mineral Processing 22, 401-412.

ID14 - Investigation of the hydrocyclone classification of a two component particle mixture from the photovoltaic industry

Maximilian Beier[1,*], *Christian* Reimann[1], *Jochen* Friedrich[1], *Thomas* Leißner[2] and *Urs Alexander* Peuker[2]

[1]Fraunhofer IISB, Department Materials, Schottkystr. 10, 91058 Erlangen, Germany
[2]TU Bergakademie Freiberg, Institute of Mechanical Process Engineering and Mineral Processing, Agricolastraße 1, 09599 Freiberg, Germany

Summary. In the photovoltaic industry a total of 200,000 tons of silicon is lost as waste per year, mainly in the form of fine powder mixed with abrasive particles and cutting fluid. Among different approaches to recycle the silicon from this waste is the utilization of hydrocyclones, which can be used to separate or classify particles by weight and size. In this work the use of a hydrocyclone was evaluated to upgrade the silicon fraction from a typical sawing waste and the classification behaviour of a two component particle mixture, especially a potential interaction of the different particle species was investigated.

1 Introduction

In the photovoltaic industry a total of 200,000 tons of silicon is lost as a multi-component waste product per year [1]. This waste is mainly originating from the solar cell wafer production, resulting in used cutting suspensions containing fine silicon, cutting particles and metal abrasions. These sawing wastes can be further processed in an attempt to recover the silicon from it. Typically one would utilize classification and separation processes for fine particles, like hydro-classification [2], centrifugation [1], electro-kinetic-separation [3] or liquid-liquid-extraction [4].

2 Classification of silicon sawing waste

The goal of this work is to produce an upgraded silicon product with the highest possible silicon content by a fast and cheap classification method.

For this work a waste product containing only a mixture of oxidized silicon kerf particles and silicon carbide debris particles with a ratio of approximately 55 wt% to 45 wt% was used. The particle size range of the silicon carbide particles was measured by laser diffraction method to be 0.3 µm to 20 µm and for the silicon particles the particle size range could be calculated to be approximately 0.3 µm to 8 µm, thus overlapping in a wider range. The density difference of silicon to silicon carbide is roughly 0.9 g/cm³.

This two component particle mixture was classified in a single small diameter hydrocyclone, with varying orifices configurations to achieve cut sizes of around 3 µm to 5 µm. The resulting products from the hydrocyclone overflow and underflow are silicon enriched respectively silicon carbide enriched. The maximum achievable silicon content in an overflow product for a single hydrocyclone classification was found to be varying from 85 wt% to 75 wt%, depending on the total recovery of silicon in the overflow, which was 49% to 82% of the original silicon mass.

By accessing the individual material fractions in the products, the separation functions for the two dimensional particle mixture were determined for each material individually, showing significant different trends for silicon and silicon carbide during the same classification. While silicon carbide shows a highly developed fish-hook for particles smaller than 2 µm, silicon exhibits a higher misclassification for small particles in the separation functions and only a moderate fish-hook.

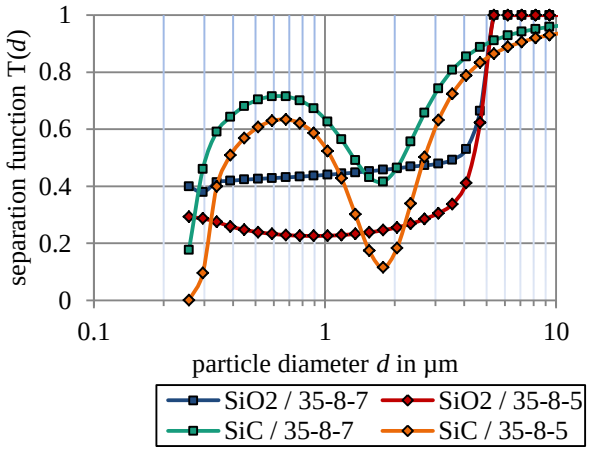

Fig. 1. Separation functions for pure silicon dioxide and silicon carbide classifications. 35-8-7 & 35-8-5 represent two different hydrocyclone configurations

To evaluate a possible interaction of the two particle species during the classification, experiments with only silicon carbide or silicon dioxide as replacement for the silicon were conducted. The resulting separation

functions showed a similar behaviour as in the two component experiments (see Fig 1).

The results show that an explicit interaction of silicon and silicon carbide particles could not be found, but rather the classification effect is based on other material properties. Further investigation of the fish-hook form and the classification behaviour in submicron range will be carried out to determine if interactions occur here or if other factors can explain the different classification behaviour.

These research and development activities are carried out within the REWASI project (0325938C) funded by the German Federal Ministry for Economic Affairs and Energy. Further thanks go to SiC Processing (Deutschland) GmbH for providing the sawing waste.

References

[1] Moen, M., Halvorsen, T., Mørk, K., Velken, S. (2017). Recycling of silicon metal powder from industrial powder waste streams. *Metal Powder Report*, 72, 182–187.

[2] Sergiienko, S. A., Pogorelov, B. V., Daniliuk, V. B. (2014). Silicon and silicon carbide powders recycling technology from wire-saw cutting waste in slicing process of silicon ingots. *Separation and Purification Technology*, 133, 16–21.

[3] Lin, Y.-C., Tai, C. Y. (2010). Recovery of silicon powder from kerfs loss slurry using phase-transfer separation method. *Separation and Purification Technology*, 74, 170–177.

[4] Tsai, T.-H. (2011). Modified sedimentation system for improving separation of silicon and silicon carbide in recycling of sawing waste. *Separation and Purification Technology*, 78, 16–20.

ID15 - Current approaches and future prospects for comminution process modelling based on population balance equation

Alain Liné[1], *and Christine* Frances[2,*]

[1]LISBP, University of Toulouse, Toulouse, France
[2]Laboratoire de Génie Chimique, University of Toulouse, Toulouse, France

Summary. Population balance equation applied to comminution processes is based on selection and breakage functions, which usually allows the description of the change over time of the particle size distribution. However, other properties, such as the particle resistance or shape, may also be of interest. An example of a bivariate PBE is presented, taking into account the particle size and the minimum energy needed to break the particles defined on the base of a fracture probability distribution. The changes of the bivariate distribution over time are well predicted using the Direct Quadrature Method of Moments approach, choosing a number of nodes equal to 3 associated with a smart selection of the moment set needed to solve the bivariate population balance equation.

1 Introduction

Particulate processes are currently modelled using population balance equations (PB) either in homogeneous or heterogeneous conditions combining computation fluid dynamics (CFD) modelling. In the framework of comminution processes, PBE usually tracks the change in the density distribution of the weight of particles distributed over defined size classes. Such an approach allows optimizing grinding processes and it has been intensively used in the past to model ball mills for instance or to determine kinetic parameters based on a back-calculation mode (Hennart et al., 2009). However, the particle size or volume is not the only important solid characteristics. Another important quantity for grinding processes is the energy consumed by the mill, a part of which is transmitted to the particles. The energy spectra depends on the mill geometry and process conditions. Concerning ball milling, it may be modelled by computing the collision energy via the discrete element method or simulating the hydrodynamics inside the grinding chamber using CFD codes or direct numerical simulation (Lane, 1999; Gers et al., 2010). From the solid point of view, the resistance of particles may be expressed by the minimum energy needed to break them, also called the breakage energy, which can be evaluated from fracture tests usually performed on individual particles. Other properties, in particular morphological ones, may also be of interest in grinding applications. In this context, the main objective of our work is to develop and solve multidimensional population balance modelling in order to improve the mill design or optimization.

2 Bidimensional population balance equation applied to a grinding process

A bivariate population balance equation may be developed considering two solid properties, for instance, the particle size, x, and the particle resistance or grindability, e, expressed here by the minimum energy needed to break the particles. Thus we introduce the population density or particle size-energy distribution $f(x,e,t)$ and the two-dimensional population balance equation is written as :

$$\frac{\partial f(x,e,t)}{\partial t} = -a(x,e)\,f(x,e,t) + \iint_{x}^{+\infty} a(x_0,e_0)\,b(x,e,x_0,e_0)\,f(x_0,e_0,t)\,dx_0\,de_0 \quad (1)$$

in which the birth and death terms of the right hand side of the equation contain the selection function $a(x,e)$ describing the rate at which particles of size x and resistance e are broken and the breakage function $b(x,e,x_0,e_0)$ representing the probability to obtain fragments of properties (x,e) after a breakage event of particles having initial properties (x_0,e_0).

In that example, the selection function $a(x,e,t)$ was considered as the product of two probabilities: the impact probability, which depends on the process conditions and the particle size, and commonly described by a power law, and the breakage probability, which depends on the particle strength. The breakage probability after a stress event was described by an exponential law. Similarly, the breakage function was assumed to be composed of two contributions, the first

one related to the mother and daughter particle size, for which the usual self-similar breakage distribution was chosen and the second one related to the energy spectrum. The energy needed for breakage is often evaluated on calibrated individual particles and the fracture probability is thus depending on particle size and translated using statistical tools. So, the fracture probability was expressed by a log-normal distribution. Finally, the breakage function was defined as:

$$b(x,e,x_0,e_0) = \frac{a_0}{x_0}\left(\frac{x}{x_0}\right)^{a_0-1} \frac{exp\left[-\frac{(ln(e/e_{50}))^2}{2\sigma_E^2}\right]}{e\sqrt{2\pi\sigma_E^2}} \quad (2)$$

in which e_{50} and σ_E are the median and geometric variance of the energy distribution, conditioned by the particle size. Other details concerning the experimental conditions and kinetics laws used in the model could be found in Frances and Liné (2014).

3 Results and discussion

The bivariate PBE was solved by the Direct Quadrature Method of Moments (DQMOM) (Marchisio and Fox, 2013). The mixed moments of the size-energy distribution are expressed by the quadrature form of the population density defined for a number of nodes (N) and incorporating the weights (w_i) and the abscissas defined for the two properties (x_i) and (e_i) :

$$f = \sum_{i=1}^{N} w_i(t)\delta\big(x(t) - x_i(t)\big)\,\delta\big(e(t) - e_i(t)\big) \quad (3)$$

The validation of the method was first done comparing the results with the solution of a discretized model considering one hundred classes on both properties. A vey significant reduction of the computational time was observed with the DQMOM method. The interest of the bivariate population balance compared to the monovariate case was also evaluated. An example is illustrated on Fig. 1 in which the Sauter diameter is reported over time in the monovariate case (size only) and two bivariate cases considering different energy breakage functions. The calculated d_{32} in the monovariate approach is similar to the bivariate case only when the breakage energy is assumed constant over time and independent of the particle size (noted as special case in the legend).

The effect of the number of nodes or order of the quadrature N and the selected set of the $3N$ moments needs to solve the system on the accuracy of the results was evaluated. It was shown that for a given order, the set of moments has an influence on the values of the calculated moments and their change over time, but only for high orders in relation with the respective range of the solid properties considered. To avoid such mathematical divergence, the choice of dimensionless variables for the solid properties is preferred. Problems of convergence also arise when the number of node is equal to 2. But a number of nodes equal to 3 is enough to calculate with a very good accuracy the first pure and mixed moments of the population density. Thus, the usual mean sizes as d_{32} or d_{43} are predicted with a good precision if the pure moments of order 2 and 3 (m_{20}, m_{30} in which the first index refers to the particle size), respectively 3 and 4 (such as m_{30} and m_{40}) are chosen in the selected set.

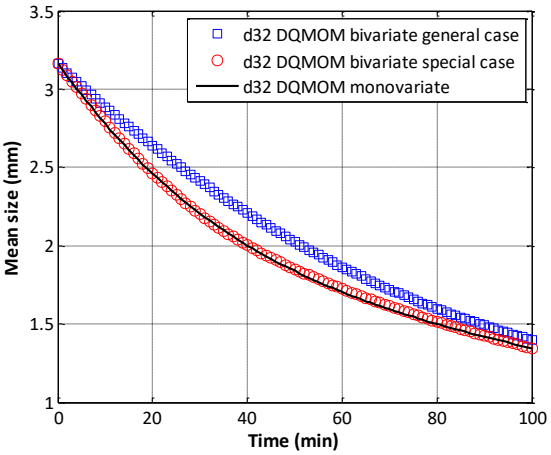

Fig. 1. Comparison of monovariate and bivariate solutions.

The bivariate approach can be interesting when the material grindability or the minimum energy for breakage is a complex function of the particle size or when it is not only governed by it in case of a fatigue phenomenon, a decrease of the particle resistance, a change of the fracture mechanism during the process or when heterogeneous materials are ground. Other examples of the use of a two-dimensional grinding modelling could be discussed, for instance when size and shape characteristics are simultaneously tracked.

References

Frances, C. & Liné, A. (2014). Comminution process modeling based on the monovariate and bivariate direct quadrature method of moments. *AIChE J.*, 60(5):1621-1631.

Gers, R., Climent, E., Legendre, D., Anne-Archard, D. & Frances, C. (2010). Numerical simulation of grinding in a stirred media mill: Hydrodynamics and collision characteristics, *Chem. Eng. Sci.*, 65, 2052-2064.

Hennart, S.L.A., Wildeboer, W. J., van Hee, P. & Meesters, G. M. H. (2009). Identification of the grinding mechanisms and their origin in a stirred ball mill using population balances. *Chem. Eng. Sci.*, 69(19), 4123-4130.

Lane, G.L. (1999). CFD modeling of a stirred bead mill for fine grinding. Second International Conference on CFD in the Minerals and Process Industries CSIRO, Melbourne, Australia.

Marchisio, D.L. & Fox R.O. (2013). Computational models for polydisperse particulate and multiphase systems, Cambridge University Press

ID16 - A microhydrodynamic analysis of the impact of stirrer speed and media loading on breakage kinetics during wet media milling

Ecevit Bilgili[1,*], *Nathaniel* Parker[1], and *Mahbubur* Rahman[1]

[1]Department of Chemical and Materials Engineering, New Jersey Institute of Technology, New Jersey, USA.

Summary. The aim of this study is to develop a fundamental understanding of the impact of stirrer speed and volumetric loading of crosslinked polystyrene (PS) beads on the breakage kinetics of griseofulvin (GF), a poorly water-soluble drug, during wet stirred media milling. To this end, GF nanosuspensions were prepared under various processing conditions in a wet stirred mill using hydroxypropyl cellulose and sodium dodecyl sulfate as stabilizers. Laser diffraction and viscometry were used to characterize the milled suspensions and explore the breakage kinetics. A microhydrodynamic model was used to explain the observed breakage kinetics in view of the bead–bead collisions inside the mill. Our experimental results and the model suggest that while granular temperature and maximum contact pressure slightly decreased, the dramatic increase in average frequency of drug particle compressions governed the faster breakage at higher bead loadings. On the other hand, all microhydrodynamic parameters increased at higher stirrer speed leading to faster breakage. Besides elucidating the impact of stirrer speed and beads loading, this study also rationalizes the use of zirconia beads over PS beads based on their impact on the microhydrodynamics.

1 Introduction

Production of nanoparticles via wet stirred media milling (WSMM) is one of the approaches for enhancing the dissolution rate and bioavailability of poorly water-soluble drugs [Li et al., 2016]. In WSMM, drug suspension is passed through a milling chamber and the mill stirrer is rotated at a high speed which induces turbulent motion in the suspension. Drug particles are captured between frequently colliding beads and broken down to smaller particles, eventually forming nanoparticles. Stabilizers are usually added to prevent the nanoparticles from aggregating and inhibit ripening during milling and storage [Li et al., 2016]. While being continuous, scalable, and solvent-free, WSMM is a time-consuming, costly, and energy-intensive process, which limits its potential use in pharmaceutical industry as a platform technology. Process parameters such as stirrer speed, beads loading, and suspension flow rate have significant effects on the breakage kinetics and milling time. Hence, the current study aims to gain fundamental insights into the impact of stirrer speed and loading of crosslinked polystyrene (PS) beads on the breakage kinetics of griseofulvin (GF) during WSMM using a microhydrodynamic model and compare PS beads with zirconia beads in terms of their milling effectiveness.

2 Materials and methods

Griseofulvin (GF) was selected as a model poorly water-soluble drug. A non-ionic cellulosic polymer, hydroxypropyl cellulose (HPC, SL grade), and an anionic surfactant, sodium dodecyl sulfate (SDS), were used as stabilizers. Crosslinked PS beads with a nominal size of 400 μm was used as the milling media and compared with Zirmil Y grade yttrium-stabilized zirconia (YSZ) with identical nominal size. Four different bead volume fractions/loadings (c), i.e., 0.198, 0.298, 0.397, and 0.594, with respect to the total volume (80 mL) of the mill chamber were used. About 230 g pre-suspensions were prepared by dispersing 10% GF particles in an aqueous solution of 5% HPC and 0.2% SDS, where all the percentages were w/w with respect to de-ionized water (200 g). The pre-suspensions were milled for 256 min in a Netzsch Microcer recirculation mill at the stirrer speeds of 2000, 3000, and 4000 rpm with the aforementioned bead loadings. Laser diffraction (Coulter Beckman LS 13 320) and viscometry (Brookfield R/S plus cylinder-in-cylinder rheometer) were used to characterize the particle size distribution and apparent shear viscosity, respectively.

To quantify the breakage kinetics, time for the 50 vol.% passing size (median, d_{50}) to reach 0.5 μm (t_{d50}) and time for 90 vol.% passing size (d_{90}) to reach 1 μm (t_{d90}) were calculated. Moreover, d_{50}–t data were fitted to

$$d_{50}(t) = d_{\lim} + [d_{50}(0) - d_{\lim}]\exp(-t/\tau_p) \qquad (1)$$

where t is time, $d_{50}(0)$ and $d_{\lim}$ are the initial d_{50} and the limiting (equilibrium or plateau) d_{50}, and τ_p is a characteristic time constant of the process. Along with viscosity and power consumption, a microhydrodynamic model [Eskin et al., 2005; Afolabi et al., 2014] was used to calculate granular temperature (θ), average frequency of drug particle compressions (a), and maximum contact pressure at the center of the contact circle formed between two colliding beads (σ_b^{max}).

3 Results and discussion

GF nanosuspensions with d_{50} < 200 nm were produced within 256 min using PS beads for all stirrer speed–

bead loadings (c) except for 2000 rpm and c < 0.4. Their sizes did not change after 7-day storage. This suggests that aggregation was effectively suppressed by the stabilizers. Fig. 1 illustrates that all three characteristic milling times t_{d50}, t_{d90}, and τ_p decreased with an increase in stirred speed and beads loading monotonically, indicating faster breakage. YTZ beads exhibited similar trends [Afolabi et al., 2014]; however, they achieved significantly faster breakage than PS beads of similar sizes (results not shown here for the sake of brevity).

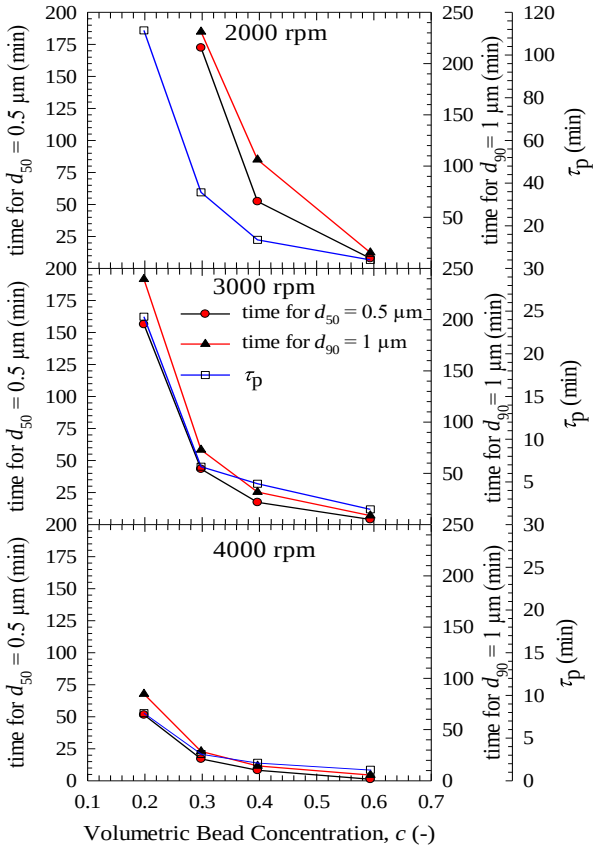

Fig. 1. Effects of volumetric PS bead loading c on the characteristic milling times t_{d50}, t_{d90}, and τ_p for stirrer speeds of 2000, 3000, and 4000 rpm. Note that d_{50} = 0.5 µm and d_{90} = 1 µm were not attained within 256 min for c = 0.198–2000 rpm.

Fig. 2 shows the impact of beads loading on θ, a, and σ_b^{max} at various stirrer speeds. Counteracting effects of beads loading were apparent for all speeds: an increase in beads loading led to higher frequency of drug particle compressions (a) despite less vigorous, energetic, and forceful collisions (lower θ and σ_b^{max}) due to higher viscous losses. The higher a appears to govern the faster breakage at higher beads loading. Higher stirrer speed led to an increase in all of θ, a, and σ_b^{max}, which explains the faster breakage at higher stirrer speed. Despite having a similar nominal size, the denser YTZ beads were associated with higher θ, a, and σ_b^{max} than the PS beads, which explains the faster breakage resulting from the use of YTZ beads (results not shown for brevity).

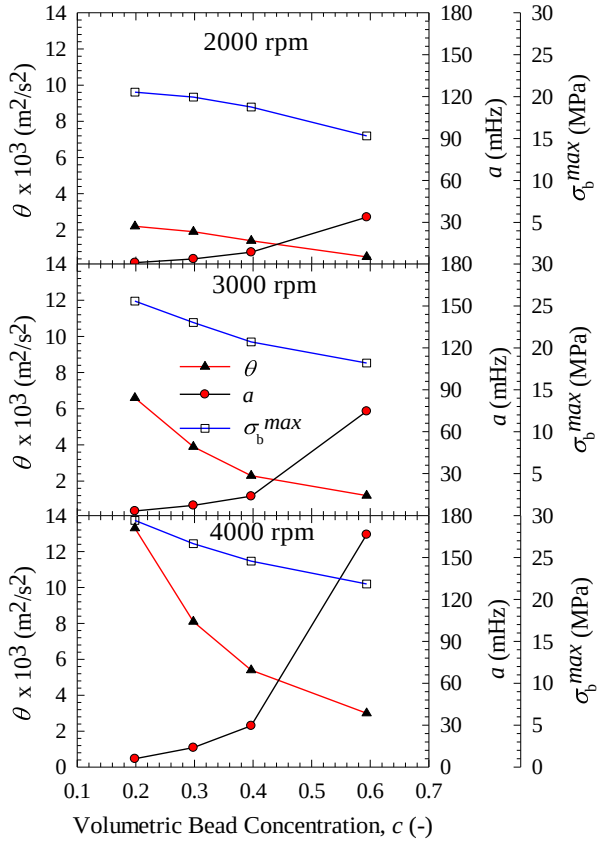

Fig. 2. Effects of volumetric PS bead loading c on the granular temperature θ, average frequency of drug particle compressions a, and maximum contact pressure σ_b^{max} for stirrer speeds of 2000, 3000, and 4000 rpm.

4 Conclusions

Stable griseofulvin (GF) nanosuspensions were prepared by WSMM under various stirrer speed–bead loading conditions. The microhydrodynamic analysis has provided significant insights into the faster breakage associated with higher stirrer speed and higher beads loading. This study has also rationalized the preference for the denser YTZ beads over PS beads of similar sizes for faster production of drug nanosuspensions.

References

Afolabi, A., Akinlabi, O., & Bilgili, E. (2014). Impact of process parameters on the brekage kinetics of poorly water-soluble drugs during wet stirred media milling : a microhydrodynamic view. *European Journal of Pharmaceutical Sciences*, 51, 75-86.

Eskin, D., Zhupanska, O., Hamey, R. Moudgil, B., & Scarlett, B. (2005). Microhydrodynamic analysis of nanogrinding in stirred media mills. *AIChE Journal*, 51, 1346-1358.

Li, M., Azad, M., Dave, R., & Bilgili, E. (2016). Nanomilling of drugs for bioavailibility enhancement : a holistic formulation–process perspective. *Pharmaceutics*, 8 (2), 17.

ID18 - Fracture Force variation in altered rocks associated with quantitative geological characterisation

Pia Lois-Morales[1], *Cathy* Evans[2], *Dion* Weatherley[1], *Benjamin* Bonfils[1]

[1] The University of Queensland, Sustainable Minerals Institute, Julius Kruttschnit Mineral Research Centre, Brisbane, Australia
[2] The University of Queensland, Sustainable Minerals Institute, W.H. Bryan Mining and Geology Research Centre, Brisbane, Australia

Summary. The relationship of geological properties of rocks such as mineralogical composition, mineral association, border complexity, porosity and grain size of rocks with the initiation and propagation of fractures has been previously described in the literature. Most of the existing approaches have qualitatively, or semi-quantitatively related measurements from rock mechanics tests with these geological properties. To date, it has not been possible to unravel which of these characteristics are more important in the fracture process to the point of building a model. A different approach was developed in the context of this work. Consistently quantitative measurements were obtained in samples of rock which were selected to show a variation in its degree of alteration. A standardised breakage procedure using the short impact load cell and regular shaped particles to reduce the experimental error was used to measure the fracture force variability associated with the variation of geological parameters. The results show that in this case, the increasing amount of phyllosilicates minerals and porosity contribute to reducing the force required to break the samples. Additional measurements of textural complexity help to explain slight differences in fracture force for samples with similar mineralogy. The results of this research show that the relationship of the geological properties of rocks with their fracture behaviour needs to be addressed through a multicomponent approach.

1 Introduction

Rocks inside a tumbling mill are subjected to stresses due to impact and abrasion phenomena. When this stress exceeds the strength of the rock, fracture occurs. The heterogeneity of rock composition and the geometric arrangements of minerals can change the strength for each rock type and even for each particle within one specific rock type. Consequently, the initiation point and how fractures propagate inside each rock is different. Knowing and possibly modelling the variation of rock strength associated with geological properties can contribute to understanding whether or not rocks will break when a specific breakage mechanism (i.e. device) with determined force is acting upon them.

A number of geological parameters have been identified as being important for breakage such as porosity, regularity of border of grains or size of mineral grains. Djordjevic (2013) modelled the propagation of fracture and found that when minerals with different elastic parameters are in contact, these contribute to the ease with which the fracture propagates.

Subsequently, this work aims to quantify the variation of the previously described parameters according to the variation of the strength of rocks to quantitatively assess their importance in force required to break a particle.

2 Methodology

2.1 Sample Selection

Four different rock types with increasing degree of hydrothermal-hydrolytic alteration were selected for this study, named as A, B, C and D, with the alteration increasing from A to D. Routine visual observations identified an increasing amount of soft minerals such as clays, increasing porosity due to leaching of sulphides and decreasing grain size as the alteration progressed. These characteristics were confirmed with imaging procedures.

2.2 Breakage Methodology

All samples were subjected to the same breakage methodology using the Short Impact Load Cell (SILC). This equipment is a hybrid machine between the Drop Weight Tester, and the Split Hopkinson Pressure Bar. The SILC allows impact breakage tests under two points of loading to be performed relatively quickly and precisely. The signal received through the long steel rod equipped with strain gauges can be deconvoluted and transformed into the time-history of the force of each particle (King & Bourgeois, 1993; Tavares & King, 1998).

In this research, cylindrical particles were used in the breakage experiment, which reduces the variation in the results due to shape effects (Bonfils, 2017; Chandramohan, 2013). Fifty particles were drilled from

each rock type, for each cylinder size. Five cylinder sizes were tested ranging from 3 to 17 mm in diameter. In all cases, the diameter to length ratio was 1:1.

2.3 Image Analysis Methods

A multisource image analysis method was developed to capture the relevant rock characteristics. Each sample was imaged using a Digital Optical Microscope (LEICA DM6000). Likewise, thin-sections were measured with the Mineral Liberation Analyser to obtain mineralogy in 2D dimensions. Also, some cores of each sample were imaged with an X-ray Micro-tomography system to assess their 3D structure.

A process of image cleaning and information extraction was developed using eCognition Developer v.9 for 2D images and Avizo Lite v. 9.7 for 3D images.

3 Results and Discussion

The Fracture Force results show a difference, statistically tested, between A-B and C-D rocks (See Fig. 1). The results show that the force required to generate the first fracture changes significantly at a certain point of the alteration progression. Median strength values for A and B are close to 17 MPa while for C and D they are close to 10 MPa.

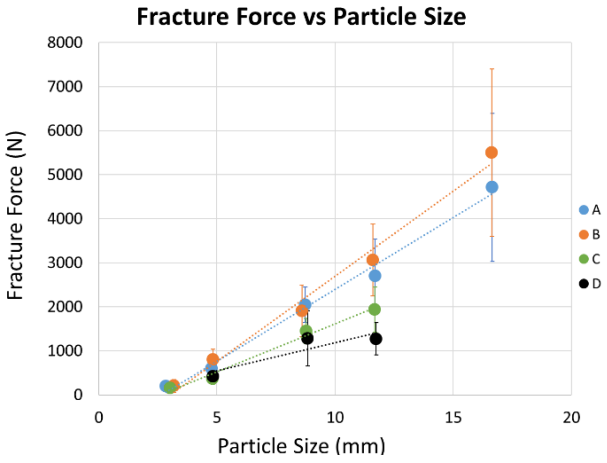

Fig. 1. Fracture Force vs Particle Size dependency for four rock types

Considering that these samples have the same original rock with increasing degrees of alteration, it is interesting to investigate what type of textural and mineralogical characteristics have changed in the rock that may cause a change in strength. The image analysis procedure was carried out to analyse five different parameters described in Table 1. The Border Complexity Index equals to 1 refers straight borders between minerals and increases to ∞^{+} when the borders become more crenulated.

Table 1. Results from image analysis

	Grain Size Mode (µm)			Porosity	Micas-Clays	Main Mineral Associations (%)			Border
	Pop n 1	Pop n 2	Pop n 3	(%) Mean	Weigth (%) Mean	plg+qz	plg+clays	qz+clays	Index Complexity
A	1200	-	-	0.99	19.96	23.66	21.94		2.17
B	120	1800		1.70	16.26	37.72	32.92	3.28	1.41
C	60	500	2200	2.62	21.3	24.35	36.12	7.12	1.28
D	1500	-	-	3.13	43.13	3.41	4.43	69.07	1.96

The results show that rock types B and C present multimodal grain size distributions. In the case of rock D, the grain size measurement represents the size of patches of ultrafine clays intercalated with quartz mineral grains. In this case, the clay grain sizes were below the resolution limit of the images (3 µm), so their aggregates were considered in the grain size measurements.

Interestingly, the number of populations of different grain sizes increases in medium-high pervasive alterations (B-C), but also the complexity of the borders decreases to finally form a very fine-grained sample distributed in patches with a high border complexity (D). When a hydrothermal fluid alters the host rock, this injects more energy into the system which makes the crystals migrate to a new state of textural equilibrium (Higgins, 2006). However, it is very hard to reach the final state which tends to result in coarser grains with straight borders. Intermediate states consider recrystallisation of irregular grain borders and straightening borders as is observed in the data (B-C). According to several authors (Ali, Guang, & Ibrahim, 2014; Ozturk, Nasuf, & Kahraman, 2014) reducing the size of grains should strengthen the rock, as should more complex borders.

On the other hand, chemical imbalances associated with the injection of new chemical elements during alteration changes the mineralogy. In this case, the amount of clays and micas increases as the alteration progresses, as does the number of boundaries shared between minerals with different elastic moduli, such as clays, quartz and plagioclases, which should contribute to weakening the rock.

Also, the increasing porosity, associated with the changing mineralogy and texture should decrease the strength of rocks according to Bourgeois, Lippiatt, and Powell (2015).

Consequently, the total strength of the rock is controlled by the interaction of mineralogical and textural changes which are reflected in the captured data. In this particular alteration progression case, the amount of clays and pores seems to have a greater impact on the strength of the rock as the alteration progress (A → D). However, these parameters are not enough to explain slight differences in the results of A and B, where for example in B the porosity is higher, but the rock requires a higher force to be broken. Alternatively, C and D, where in D, the amount of clays is considerably higher than C, but the required force is not much different. In these situations, it is likely that the grain sizes and boundary complexities observed contribute to differentiating rocks' fracture properties.

References

Ali, E., Guang, W., & Ibrahim, A. (2014). Empirical relations between compressive strength and microfabric properties of amphibolites using multivariate regression, fuzzy inference and neural networks: A comparative study. Engineering Geology, 183(Supplement C), 230-240. doi:https://doi.org/10.1016/j.enggeo.2014.08.026

Bonfils, B. (2017). Quantifying of impact breakage of cylindrical rock particles on an impact load cell. International Journal of Mineral Processing, 161(Supplement C), 1-6. doi:https://doi.org/10.1016/j.minpro.2017.02.005

Bourgeois, F., Lippiatt, N., & Powell, M. (2015). Introducing the concept of mechanical texture in comminution: The case of concrete recycling. International Journal of Mineral Processing, 136, 7-14. doi:http://dx.doi.org/10.1016/j.minpro.2014.09.012

Chandramohan, R. (2013). Effect of rock shapes in comminution. Thesis(Ph.D.) - University of Queensland, 2013.
St. Lucia, Qld.,

Djordjevic, N. (2013). Image based modeling of rock fragmentation. Minerals Engineering, 46-47(Supplement C), 68-75. doi:https://doi.org/10.1016/j.mineng.2013.03.002

Higgins, M. D. (2006). Quantitative Textural Measurements in Igneous and Metamorphic Petrology (Vol. 9780521847827): Cambridge : Cambridge University Press.

King, R. P., & Bourgeois, F. (1993). Measurement of fracture energy during single-particle fracture. Minerals Engineering, 6(4), 353-367. doi:https://doi.org/10.1016/0892-6875(93)90015-F

Ozturk, C. A., Nasuf, E., & Kahraman, S. (2014). Estimation of rock strength from quantitative assessment of rock texture. Journal of the Southern African Institute of Mining and Metallurgy, 114, 471-480.

Tavares, & King. (1998). Single-particle fracture under impact loading. International Journal of Mineral Processing, 54(1), 1-28. doi:10.1016/S0301-7516(98)00005-2

ID19 - Fragments spawning and growth as part of a new parallelized coarse grain DEM particle breakage model

Stefanie Bußmann[1,*], and *Harald* Kruggel-Emden[1]

[1]Mechanical Process Engineering and Solids Processing (MVTA), Technische Universität Berlin, Berlin, Germany

Summary. Comminution causes a reduction in the sizes of solid particles. In this way, particular properties of the material are altered as desired for processing and application. The particle-based discrete element method (DEM) can be applied to model and study particle breakage processes thereby assuming particles for simplicity as spherical. After a breakage event has occurred, the crushed parent particle is replaced by spherical fragments. To avoid large overlaps when the fragments are placed within the volume of the parent particle, the fragments are shrunken before their placement. The fragments reach their desired diameters by a growing process in the following time steps. The initial mass loss is counterbalanced. Predefined maximal overlaps with adjacent particles and walls are allowed and even required. Due to the large number of particles in comminution processes, the proposed breakage model is realized as part of a parallelized DEM code. Furthermore, a coarse grain DEM model has been used to reduce the number of particles to be modelled. The results show that the breakage model but in particular the algorithm realizing the fragment growth is suitable to model particle breakage as part of comminution processes. The fragments reach their desired sizes and multiple fracture can occur.
.

1 Introduction

In order to change the properties of solid particles for processing and application, it is often necessary to reduce particle sizes referred to as comminution. As a result of its fundamental importance, comminution processes are widespread and of relevance in many industrial sectors.

In order to investigate particle breakage in detail without the need for expensive and time-consuming experiments, simulations are performed. The particle-based discrete element method (DEM), which has been introduced by Cundall and Strack [1], is a commonly used approach to model comminution processes often assuming spherical particles.

An important aspect in modeling breakage events as part of a comminution process is the mass conservation. Achieving this is particularly challenging if the parent particles as well as the fragments are assumed to be spherical and the fragments may only be placed within the volume of the broken parent particle. One approach is the placement of the fragments with overlaps between them [2,3]. These overlaps cause artificially increased contact forces, which might result in high velocities of the fragments in successive time steps. To avoid this, the fragment sizes can be reduced before the fragments are placed within the volume of the parent particle. The resulting mass loss can be counterbalanced by fragment growth to its desired diameter after the fragment has been placed [4,5].

2 Numerical method

The DEM is suitable for tracking the motion and interactions of particles in different systems. For the translational and the rotational movement the Newton's and the Euler's equation are integrated [6]. The contact forces consist of a normal and a tangential component [7].

Due to the normally very large number of particles, realistic simulations of comminution processes are computationally intensive. To reduce the resulting high computational time a spatial domain decomposition for parallelization can be used. Thereby the computational domain is divided into several smaller subdomains. One processor core calculates the forces and movements in one subdomain only [8]. Information on the particles at the subdomain boundaries has to be exchanged in regular intervals between processor cores leading to some additional computational overhead.

Another approach to reduce the computational time is using coarse grain DEM models. Thereby, several particles at a fine scale are represented by one particle at a coarser scale. The particle scale-up has to be considered in the calculation of the contact forces and further other forces when relevant [9]. The particle strength also has to be scaled for the simulation of particle breakage from the fine to the coarse scale [10], which has only been addressed very sparsely in literature so far.

3 Breakage model

The breakage criterion used is based on the average stress tensor. It is assumed that particle breakage does not occur under hydrostatic loading. The used definition of the octahedral shear stress q reflects this:

$$q = \frac{1}{3}\left[(\sigma_1 - \sigma_2)^2 + (\sigma_1 - \sigma_3)^2 + (\sigma_3 - \sigma_2)^2\right]^{1/2}. \quad (1)$$

The principal stresses σ_1, σ_2 and σ_3 are the eigenvalues of the stress tensor [11]. A breakage event occurs, if q exceeds a critical value [12].

In the present study, an approach for fragments spawning is used to avoid artificially increased forces. The fragments diameters are reduced before the fragments are placed. After a particle has fulfilled the breakage criterion, the size-reduced fragments are placed within the volume of the broken parent particle. To counterbalance the resulting mass loss, the fragments grow to their desired diameters after their placement in the computational domain in successive time steps. An overlap threshold limits the fragment growth. In this way, the overlaps with adjacent particles and walls are limited so that excessive overlaps and increased forces are avoided. The overlap threshold has to depend on the particle size because larger overlaps are more critical for small particles. The breakage model has been realized in a parallelized DEM code with a coarse grain model.

4 Results and discussion

It is important that the shrunken particles reach their desired final diameters as quickly as possible so that multiple fracture of particles can occur because only fragments with their final sizes are allowed to break. Fig. 1 shows the experimentally and numerically obtained cumulative mass-based particle size distribution of particulate material attributed to a comminution process involving a vertical roller mill.

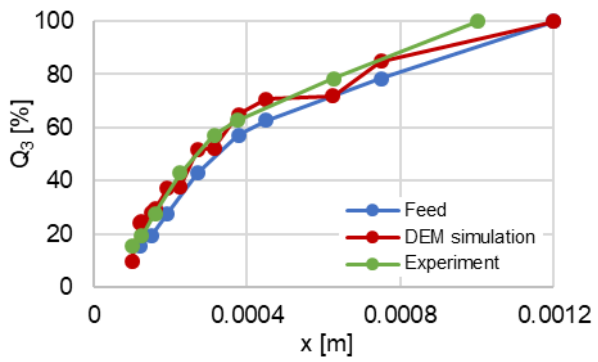

Fig. 1. Cumulative particle size distribution. Permitted overlap for fragment growth: 6 %

The size distribution of the feed in the simulations is based on the feed in the experiments. The simulation has been performed with a permitted overlap for fragment growth of 6 %. The simulation results for the overall size distribution show a good agreement with the experimental data. Based on this the implemented breakage model and the assumptions, which were made, seem suitable to model comminution processes. Multiple fracture of particles was observed, which indicates that the fragments grow fast enough.

The original form of the DEM-code "DEM-Calc" applied is based on a development of LEAT, Ruhr-Universität Bochum, Germany. The code "DEM-Calc" has then been continuously extended both at Ruhr-Universität Bochum and Technische Universität Berlin, Germany. We thank all who have contributed. We gratefully acknowledge Loesche GmbH for partly funding this work.

References

[1] Cundall, P.A. and Strack, O.D.L., (1979). A discrete numerical model for granular assemblies. *Géotechnique*, 29, 47–65.

[2] Li, H., McDowell, G. & Lowndes, I., (2014). Discrete element modelling of a rock cone crusher. *Powder Technology.*, 263, 151–158.

[3] Jiménez-Herrera, N., Barrios, G.K.P. & Tavares, L.M., (2018). Comparison of breakage models in DEM in simulating impact on particle beds. *Adv. Powder Technol.*, 29, 692–706.

[4] Brosh, T., Kalman, H. & Levy, A., (2011). Fragments spawning and interaction models for DEM breakage simulation. *Granul. Matter*, 13, 765–776.

[5] Chaudry, M.A. and Wriggers, P., (2017). On the computational aspects of comminution in discrete element method. *Comput. Part. Mech.*, 5, 175–189.

[6] Kruggel-Emden, H., Rickelt, S., Wirtz, S. & Scherer, V., (2008). A study on the validity of the multi-sphere Discrete Element Method. *Powder Technol.*, 188, 153–165.

[7] Kruggel-Emden, H., Simsek, E., Rickelt, S., Wirtz, S. & Scherer, V., (2007). Review and extension of normal force models for the Discrete Element Method. *Powder Technol.*, 171, 157–173.

[8] Maknickas, A., et al., (2006). Parallel DEM Software for Simulation of Granular Media. *Informatica*, 17, 207–224.

[9] Hilton, J.E. and Cleary, P.W., (2014). Comparison of non-cohesive resolved and coarse grain DEM models for gas flow through particle beds. *Appl. Math. Model*, 38, 4197–4214.

[10] Ciantia, M.O., Arroyo, M., Calvetti, F. & Gens, A., (2015). An approach to enhance efficiency of DEM modelling of soils with crushable grains. *Géotechnique*, 65, 91–110.

[11] Esnault, V.P.B. and Roux, J.-N., (2013). 3D numerical simulation study of quasistatic grinding process on a model granular material. *Mech. Mater.*, 66, 88–109.

[12] Wang, P. and Arson, C., (2016). Discrete element modeling of shielding and size effects during single particle crushing. *Comput. Geotech.*, 78, 227–236.

ID22 - Assessing the Influence of Viscosity on Stress Energy and Stressing Probability in Stirred Media Mills using Particle Probes

Stefan Romeis, *Alexander* Strobel, *Jan* Schwenger and *Wolfgang* Peukert*

Institute of Particle Technology (LFG), Friedrich-Alexander-Universität Erlangen-Nürnberg, Cauerstraße 4, 91058 Erlangen, Germany

Summary. Milling in stirred media mills is described by the collision bead frequency (stress number SN) distribution and the transferred stress energy (SE) distribution. These distributions are widely unknown. Recently, we have established an experimental protocol to determine SE and SN by well-characterized metal particle probes: The plastic deformation of the particles is assessed by electron microscopy. The deformation is described by an experimentally informed finite element model. Here we focus on the grinding media size and fluid viscosities for a small-scale horizontal stirred media mill which is operated in open-loop mode. The influences of viscosity on bead dampening and particle capture are discussed.

1 Introduction

Comminution, as part of interconnected process chains, is an extensively used unit operation in chemical engineering and particle technology. Various designs of mills exist and all mills are designed to stress the product particles by compression (two-sided contact) or impact (one-sided contact). In wet operated stirred media milling an externally driven stirrer agitates milling beads which in turn stress the product particles by compression. Stirred media mills are characterized by the transmitted energy per stress event (stress energy SE) and the number of stress events (stress number SN). The dependency of the SE and SN distributions on the operating parameters is known as mill function. The response of the product material to the externally applied stresses is known as material function. The combination of mill and material function describes the whole process. The overall performance of a wet grinding process is influenced by the probability of stressing the product particles: i.) Product particles need to be trapped between approaching grinding beads. ii.) The grinding beads need to transfer sufficient energy to introduce breakage. Despite their importance the SE and SN distributions are still widely unknown. Detailed experimental studies are not available and the few existing works rely mainly on CFD-DEM simulations. Within this work we present results on the characterization of stirred media milling by single particle probes [1,2]. Our experiments provide access to the stress energy, give an indication for the stress number and reveal that viscosity has significant influences on the stress number and the stress energy.

2 Experimental

2.1 Particle probes

Aluminium spheres (TLS Technik & Spezialpulver, Germany) were used as probe particles. The particles show elastic-plastic deformation behaviour, i.e. the particle deform permanently by stressing. Hence, the stressing history can be accessed by counting the number of contacts (SN) and measuring the size of the formed contact areas (SE).

2.2 Stirred media milling and sampling

Comminution experiments were performed in the horizontal mill Labstar LS1 MiniCer (Netzsch Feinmahltechnik, Germany) in open circuit mode. Yttrium stabilized zirconia grinding beads (Tosho Inc.) were used. Milling medium was deionized water. Sucrose (Südzucker, Germany) was added to increase the viscosity. A mass of 6.5 g aluminium powder (corresponds to a volume concentration of 0.01 V/V) was used. The stressed probes were collected, washed and dried prior to analysis by scanning electron microscopy (SEM).

2.3 Single particle compression testing

Compression was performed in a custom-made scanning electron microscope (SEM) supported particle tester. Finite element modelling (FEM) provided the link between deformation and the corresponding energy. SE distributions are obtained from the contact areas and the waist diameters of the deformed probe particles: The ratio of contact diameter x_c to waist diameter x links the strain and volume specific energy. About 100 particles were evaluated for each sample.

3 Results

Inspection of the probe particles by SEM showed spherical contacts, which were arranged in pairs on opposed sides of the probes. Hence, the probe particles are thus mainly deformed by normal stressing. Figure 1A shows the stress energy distributions obtained for the milling bead sizes 3 mm (blue), 2 mm (red) and 0.5 mm (black). The influence of viscosity was investigated for the 2 mm beads: 1 mPas (solid), 16 mPas (long dashes) and 179 mPas (short dashes) are given. As expected SE increases with the milling bead size. For the increased viscosities a slight shift of SE to overall lower values is observed: Mean SE values are shifted to 0.52 µJ (16 mPas) or 0.15 µJ (179 mPas). The decrease of SE is attributed to viscous dampening.

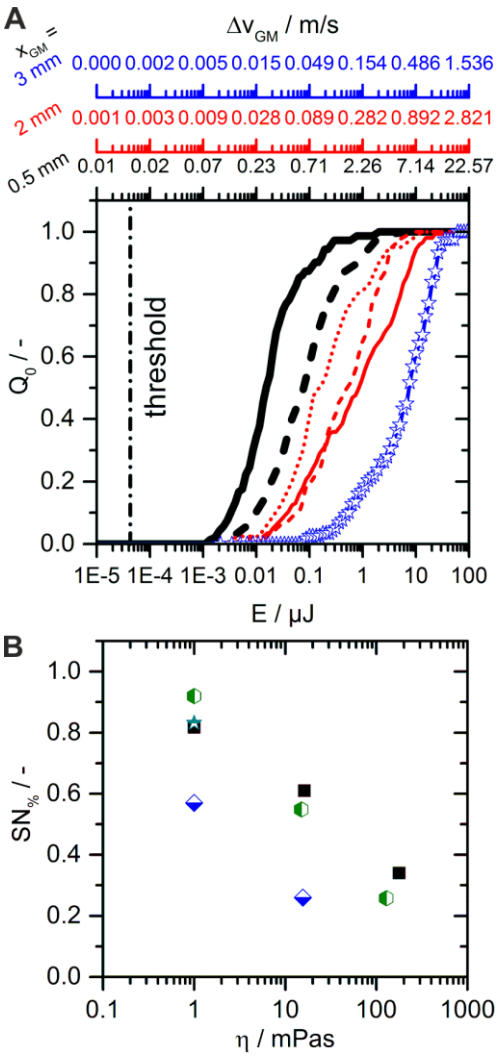

Fig. 1. A: Stress energy distributions measured for the laboratory mill LS1. Milling bead sizes are 3 mm (blue), 2 mm (red) and 0.5 mm (black). For 2 mm beads the viscosities 1 mPas (solid), 16 mPas (long dashes) and 179 mPas (short dashes) are given. Stirrer tip speed was 3.1 m/s for all experiments (exception: black dashed line, 0.5 mm, 6.2 m/s). B: Overall amount of stressed particles $SN_{\%}$. Black filled square: x_{GM} = 2 mm, v_t = 3.1 m/s; blue semi-filled diamonds: x_{GM} = 0.5 mm, v_t = 3.1 m/s; green semi-filled hexagon: x_{GM} = 0.5 mm, v_t = 6.2 m/s; light blue semi-filled star: x_{GM} = 3 mm, v_t = 3.1 m/s [2].

Analysis of the contact pairs per probe particle showed that the overall amount of stressed particles ($SN_{\%}$, see Figure 1B) and the average number of contact pairs per particle (SN_{eff}) decrease with viscosity. This is attributed to changes of particle capturing probability due to emerging viscous squeezing flows and the inertia of the probe particles [2].

The German Research Foundation is acknowledged for funding the DFG priority program 1679 “Dynamic Simulation of Interconnected Solids Processes”.

References

[1] Strobel, A., Romeis, S., Wittpahl, S., Herre, P., Schmidt, J. & Peukert, W. (2017). Characterization of stressing conditions in mills – A comprehensive research strategy based on well-characterized model particles. *Powder Technology*, 305, 652–661.

[2] Strobel, A., Schwenger, J., Wittpahl, S., Schmidt, J., Romeis, S & Peukert, W. (2018). Assessing the influence of viscosity and milling bead size on the stressing conditions n a stirred media mill by single particle probes. *Chemical Engineering Research and Design*, 136, 859–869.

ID23 - Single particle compression testing of oxide microparticles

Stefan Romeis, *Jan* Schwenger, *Patrick* Herre, *Julian D.* Esper and *Wolfgang* Peukert*

Institute of Particle Technology (LFG), Friedrich-Alexander-Universität Erlangen-Nürnberg, Cauerstraße 4, 91058 Erlangen, Germany

Summary. The mechanical behaviour of microparticles differs significantly from bulk material. Generally speaking the strength of particles increases as their size is being reduced. So far, however, only little work has been reported on the mechanical behaviour and the fracture of individual particles. Within this account, we present results on *in-situ* single particle compression testing of crystalline oxides and silica-based glasses in a scanning electron microscope. The influences of composition, crystallinity, grain size and phase content on the deformation and fracture behaviour are discussed. Furthermore, advanced *ex-situ* characterization methods, which include e.g. focused ion beam machining and electron diffraction in a transmission electron microscope, reveal a rich variety of pressure induced microstructural features.

1 Introduction

A detailed knowledge of the mechanical properties and the breakage behaviour is fundamental for many particle related processes. Especially in the particle size range relevant to fine- and ultrafine grinding only very limited work has been performed also it is well-known that smaller particles become harder to crush. In all, the correlations between microstructure and mechanical properties are widely unknown. Oxides are perceived as brittle materials on the macroscale, i.e. at room temperature particle fracture occurs with only little deformation. At the micro- and nanoscale, however, this behaviour changes remarkably [1]. Despite the recent advances of *in-situ* compression devices in electron microscopes the mechanical characterization of (sub) micro- particles as free standing structures has so far been widely omitted [2].

Within this account we present results on the single particle compression testing of various oxide particles (including SiO_2 [3-4], TiO_2 [5], ZrO_2 [6]) in the size range of about 200 nm to 5 µm [3-6]. The influences of particle size, crystalline phase, grain size and internal cross-linking are discussed. To this end the internal structures of the particles were systematically varied by thermal treatments. Our findings reveal a huge variety of different effects which can be attributed to the particle size.

2 Experimental

2.2 Single particle compression testing

Experiments were performed in a custom-made scanning electron microscope (SEM) supported single particle compression device [2]. In brief the device consists of a piezoelectric tripod scanner with an attached and interchangeable boron doped flat punch (typical plateau diameter 2 µm) and a spring system. The tripod scanner performs all tip movements and the spring system supports the sample. During compression the spring system is deflected, i.e. acting forces can be calculated. The corresponding deformation is obtained from the difference between spring deflection and piezo elongation.

3 Results

The influence of the internal cross-linking was studied for sol-gel derived submicron SiO_2: The internal degree of cross-linking was varied by thermal treatments and with increasing cross-linking the stiffness, the Young's modulus and the hardness of the particles increased. In the fully densified state the vitreous silica particles exhibited a strength which exceeded bulk silica glass [3]. With increasing particle size a clear brittle-to-ductile transition was observed at about 700 nm, i.e. with increasing particle size the plasticity of the particles decreased and brittle fracture becomes predominant. By single particle Raman spectroscopy the plasticity was attributed to a local densification of the silica particles [4]. Plastic deformation and densification of silica glasses is also

observed during wet milling under carefully controlled conditions [1].

For sol-gel derived TiO_2 and ZrO_2 microparticles the influences of crystallite size and phase were studied [5,6]. For amorphous and nc particles a significant plasticity and a crack initiation at high deformations were observed. The stable cracks followed grain boundaries. With increasing grain size cracking occurred at smaller strains and crack growth became unstable. Plastic deformation by activation of dislocations is restricted to the asperities directly at the contacts.

Figure 1A shows the stress strain behaviour for the TiO_2 microparticles [5]. The amorphous particles (blue) show a ductile deformation. For the nc anatase particles (black) and the rutile particles (red) the strain at cracking (marked by arrows) is significantly reduced. Figure 1B shows the Weibull strength distributions at the onset of cracking. For nc anatase the highest Weibull modulus is found. The modulus of the rutile particles is reduced significantly. By focused ion beam (FIB) machining of a single particle the pressure induced changes of the internal structure could be revealed. The plasticity of nc anatase is accommodated by a local densification of the particles at the contacts (Figure 1C, left reference, right compressed nc particle).

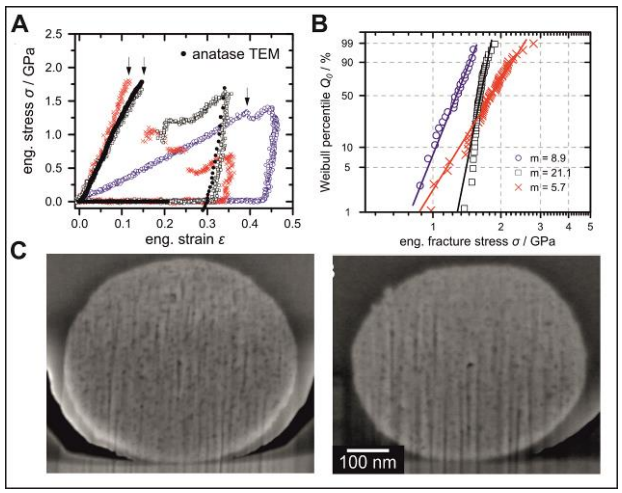

Fig. 1. A) Force-deformation data of amorphous (blue), nc anatase (black) and rutile TiO_2 (red) particles. B) Corresponding Weibull plots for the fracture stresses of the different TiO_2 particles. C) SEM images of focused ion beam (FIB) prepared cross-sections of a reference (left) and compressed (right) mesoporous nc-anatase TiO_2 particle. Structural densification of the particle is seen at the top [5].

In addition to grain and crystal structure the influences of a pressure induced martensitic phase transformation were revealed for zirconia microparticles by electron diffraction performed for a FIB cross section [6]. The texture of the transformed grains and their amount are explained by FEM calculations: Phase transformation occurs for grains which are preferentially oriented with respect to the deviatoric stresses.

The German Research Foundation is acknowledged for funding the DFG priority program 1679 “Dynamic Simulation of Interconnected Solids Processes” and the research training group 1896 “In situ microscopy with electrons, X-rays and scanning probes”.

References

[1] Romeis S., Schmidt J. & Peukert W. (2016). Mechanochemical aspects in wet stirred media milling. *International Journal of Mineral Processing*, 156, 24–31, 2016.

[2] Romeis S., Paul J., Ziener M. & Peukert W. (2012). A novel apparatus for in situ compression of submicron structures and particles in a high resolution SEM. *Review of Scientific Instruments*, 83, 95105.

[3] Romeis S., Paul J., Hanisch M., Marthala V.R.R., Hartmann M., Klupp Taylor R.N., Schmidt J. & Peukert W. (2014). Correlation of enhanced strength and internal structure for heat-treated submicron Stöber silica particles. *Particle and Particle Systems Characterization*, 31, 664–674, 2014.

[4] Romeis S., Paul J., Herre P., Ligny D. de, Schmidt J., Peukert W., Ligny D. de & Peukert W. (2015). Local densification of a single micron sized silica sphere by uniaxial compression. *Scripta Materialia*, 108, 84–87.

[5] Herre P., Romeis S., Mačković M., Przybilla T., Paul J., Schwenger J., Torun B., Grundmeier G., Spiecker E. & Peukert W. (2017). Deformation behavior of nanocrystalline titania particles accessed by complementary in situ electron microscopy techniques. *Journal of the American Ceramic Society*, 100, 5709-5722.

[6] Schwenger J., Romeis S., Herre P., Yokosawa T., Finsel M., Leib E.W., Weller H., Vossmeyer T., Spiecker E. & Peukert W. (2019). Pressure induced local phase transformation in nanocrystalline tetragonal zirconia microparticles. *Scripta Materialia*, 163, 86–90.

ID24 - Investigation of the Wet Classification of Fine Particles Using Crossflow Filtration

Philipp Lösch*, and *Sergiy* Antonyuk

Institute of Particle Process Engineering, Technische Universität Kaiserslautern, Kaiserslautern, Germany

Summary. A novel wet classification process based on the crossflow microfiltration was successfully developed. In this batch-mode process, particles smaller than 5 µm can be classified out of a broad particle size distribution. After a layer of the small fraction on the membrane is formed, the classified particles can achieved by backflushing the membranes. In this contribution, different models of the hydrodynamic forces in the boundary layer are compared to predict a cut size for the developed process.

1 Introduction

Due to the increasing need for particulate products with a fine and narrow particle size distribution, processes are needed to generate such particle systems. Particles below 10 µm are used for pigments, polishing compounds or pharmaceutics. Especially for these products, it is necessary that not a single coarse particle occurred. Conventional production processes like precipitation, crystallisation or comminution of coarse particles cannot guarantee, that all particles are smaller than a few µm or have a narrow particle size distribution at a small size. Additionally, conventional wet classification processes like hydro-sieves or centrifuges cannot separate fine particles in highly concentrated suspensions with a high selectivity. The disadvantage of these processes are the limits of the concentration of the suspension or a high energy consumption.

In this work, the cross-flow classification is investigated as a method to classify particles in a particle size range down to 1 µm. Meier et al. [1] suggest a new method of wet classification with the cross-flow filtration. They recognized a selective deposition of fine particles. Altmann and Ripperger [2] developed a model on the particle deposition, which is based on a hydrodynamic model.

2 Theory

The cross-flow classification utilizes the principles of the crossflow filtration. A suspension flows tangentially across a membrane. Due to a higher pressure on the concentrate side, pure liquid permeates through the membrane (permeate flux). The permeate flux creates a drag force on the suspended particles which transports them towards the membrane surface. For small particles in a Stokes flow, the force on the particle can be calculated as:

$$F_D = 3 \cdot \pi \cdot \eta \cdot x \cdot v_F \tag{1}$$

The velocity gradient in the boundary layer of the crossflow creates a lift force on the suspended particles which transports them back into the bulk flow. In the present work, the model of the lift force of Rubin [3], Saffman [4] and Leighton [5] are compared.

Rubin: $$F_L = (0.761 \cdot x^3 \cdot \tau_w^{1,5} \cdot \rho^{0,5})/\eta \tag{2}$$
Saffman: $$F_L = (0.807 \cdot x^3 \cdot \tau_w^{1,5} \cdot \rho^{0,5})/\eta \tag{3}$$
Leighton: $$F_L = (0.576 \cdot x^4 \cdot \tau_w^2 \cdot \rho)/\eta^2 \tag{4}$$

Where τ_w is the wall shear stress, calculated with the roughness of the wall λ and the overflow velocity w.

$$\tau_w = (\lambda/8) \cdot \rho \cdot w^2 \tag{5}$$

Both forces depend on the particle size x. By regulating the crossflow rate and permeate flux, a separation size can be adjusted. The particles smaller than the separation size are deposited on the membrane, while the larger particles remain in the bulk flow. After rinsing of the system with pure liquid the particles deposited on the membrane can be resuspended by backwashing and discharged from the system. To find an optimal operating point, investigation of the influence of the velocities and the concentration have to be carried out.

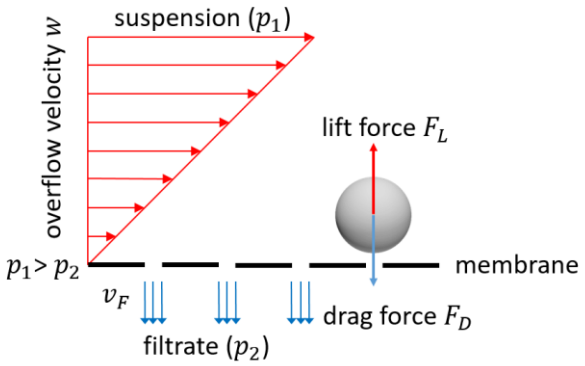

Fig. 1. Forces on a single particle in the boundary layer

3 Experimental Setup

For the experiments, a lab-scale experimental plant is constructed. It contains a pipe module with tubular membranes, which have a good resistance against back flushing. The polypropylene (PP) membranes have a nominal pore size of 0.2 µm. The effective membrane area can be adjusted with different modules between 0.008 and 0.086 m^2. An automatic regulated pump produces a defined constant overflow. The filtrate flux can be adjusted with a membrane valve. The overflow velocity and the filtrate flux are detected by an inductive flow meter.

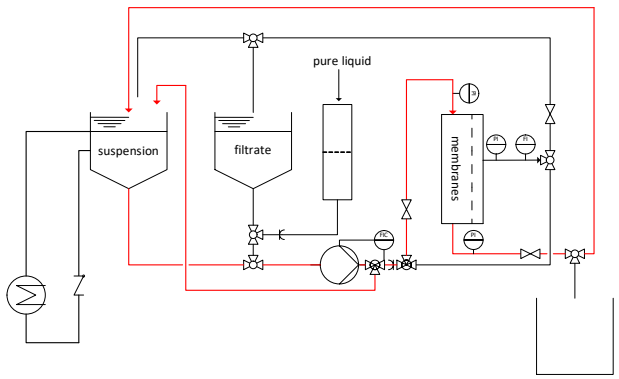

Fig. 2. Experimental setup

4 Experiments

With the developed setup, a parameter study for the influence of the mean velocity of the cross-flow on the separation size and the selectivity is performed. An overflow velocity between 0.1 and 2.5 m/s is varied. The models for the lift and drag forces will be adjusted for the influence of the particle concentration and are validated by experiments with different particle systems and concentrations. The influence of the flow velocities inside the membranes of a bundle is investigated. The resuspension and discharging of the deposited fine particles are optimized. The stabilization of the suspension of the resuspended particles is investigated to inhibit re-agglomeration of the particles after the classification. Therefore, the charge of the particle system is investigated.

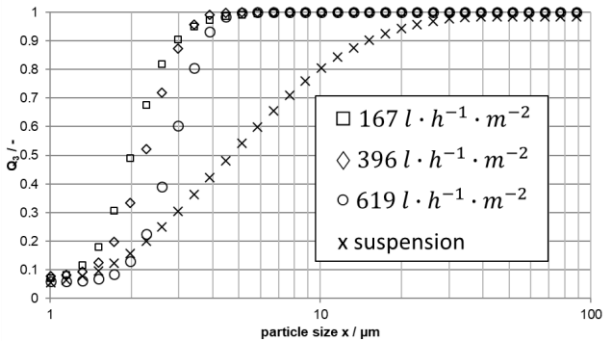

Fig. 3. Successful classification of particles smaller than 5 µm ($CaCO_3$)

5 Results

The experiments have shown a successfully classification of particles smaller than 5 µm. The separation size was compared with different models of the hydrodynamic forces. By consideration of the concentration in the models of the particle deposition, the experimental data can get closer to the requested separation size.

References

[1] J. Meier, G.-M. Klein, Volker Kottke, Crossflow filtration as a new method of wet classification of ultrafine particles, Separation and Purification Technology 26 (2002) pp.43-50

[2] J. Altmann, S. Ripperger, Particle deposition and layer formation at the crossflow microfiltration, Journal of Membrane Sciense 124 (1997) 119-128

[3] G. Rubin, Widerstands- und Auftriebsbeiwerte von ruhenden, kugelförmigen Partikeln in stationären, wandnahen laminaren Grenzschichten, University of Karlsruhe, 1977

[4] Philip Geoffrey Saffman, The lift on a small sphere in a slow shear flow, Journal of fluid mechanics (1965) 385–400.

[5] D. Leighton, A. Acrivos, The lift on a small sphere touching a plane in the presence of a simple shear flow, Z. angew. Math. Phys. 36 (1985) 174–178.

ID25 - Simplified model for particle attrition in pneumatic conveying

Dmitry Portnikov[1,*], *Nir* Santo[1], and *Haim* Kalman[1,2]

[1]Mechanical Engineering, Ben-Gurion University of the Negev, Beer Sheva, Israel.
[2]Aaron Fish Chair in Mechanical Engineering – Fracture Mechanics.

Summary. The current work presents a simple method to predict particle attrition during pneumatic conveying. The proposed model calculates a change in particle size using empirical correlations for both, machine and material functions and does not require usage of complicated simulations such as: DEM-CFD. The machine functions include particle velocity distribution function, collision angle function and concentration function. The material functions include five empirical comminution functions, namely: strength distribution function, selection function, breakage function, fatigue function and equivalence function. The results of the calculations show a fair agreement with experimental ones. The results correctness should be improved in the future. The computation time is a few seconds.

1 Introduction

Nowadays, it is common to use complicated numerical simulations such as DEM-CFD in order to predict the final size distribution of the conveyed material. The computational breakage algorithm is usually based on the concept of two groups of comminution functions, i.e. the process function and material function [1]. The process function, also known as the machine function is determined by the stress conditions that the particles are subjected to during comminution. The material function comprises the effect of material properties on the comminution result. In 2009, Kalman et al. [2] suggested, for the first time, a method to combine the machine and material functions in a computational algorithm. Brosh et al. [3] applied this algorithm in a full CFD-DEM two-way coupling simulation in dilute phase pneumatic conveying where both, the machine functions and the breakage algorithm were calculated in the simulation. The results showed a good agreement with the experiments. However, the computation time was significantly high. It took weeks to get the results for a certain case of initial particle size, a certain flow rate conditions and a pipeline route. In this situation, it is difficult to perform a design.

In the current study, we suggest a simplified method to account particle attrition during pneumatic conveying. The proposed model calculates a change in particle size using empirical correlations for both, machine and material functions and does not require usage of DEM-CFD simulation at all. Since most of the damage occurs in bends, the model calculates the breakage as a result of collisions between the particles and the bend walls only. The material functions are defined based on previous empirical studies. They include five empirical comminution functions, namely: strength distribution function, selection function, breakage function, fatigue function and equivalence function. The machine functions include three empirical and geometry based functions. The first one is the particle steady state velocity distribution function. Santo et al. [4] recently developed this function empirically for various materials and particle sizes. Two other functions are the impact angle distribution function and particle location distribution function. These functions will be introduced in this paper.

2 The machine functions

2.1 Impact angle distribution function

The collision angle between the particle and the bend wall is predicted by the impact angle distribution function. Assuming that the particles moves horizontally in a pipe until the collision, the impact angle can be calculated based on bend geometry. If x and y denote the location of the particle in a pipe cross section, R_b is the bend radius and D is the internal pipe diameter, the impact angle (θ) can be calculated by the following expression:

$$\theta = cos^{-1}\left(\frac{R_b - y}{R_b + \sqrt{(D/2)^2 - x^2}}\right) \quad (1)$$

Impact angle defined as acute angle between the particle trajectory line and tangent line at the collision point of the bend wall. It follows that as the bend radius is increasing, the impact angles are decreasing, resulting in less damage to the material.

2.2 Location distribution function

In practice, the particles are not always homogeneously distributed in a pipe cross section. It depends mostly on the particle size, the density of the material and fluid velocity. To check the location distribution of the particles, we conducted an experiment where we

measured the location of the particles in a transparent pipe section using high speed camera. The experiments were performed with salt particles of $2-2.36\,mm$ in size. The cumulative distribution of the measured particle location in a pipe cross section for various gas velocities between 13.4 and $29.2\,m/s$ is shown in **Fig. 2**. The results show that the gas velocities within the measured range do not affect the distribution of the particle location and the distribution has a linear trend up to about 70% of the pipe internal diameter. Hence, the particles are randomly distributed in a pipe cross section up to this limit. These measurements will be extended in further studies for various materials, particle sizes and wider range of gas velocities to find a general correlation of the particle location distribution.

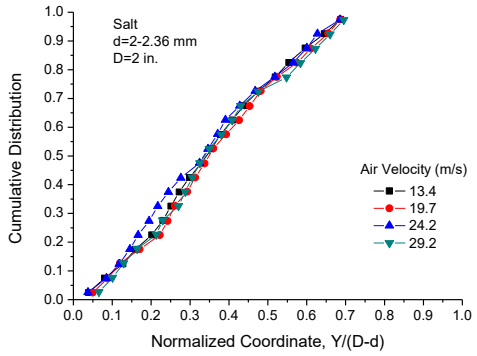

Fig. 2. Cumulative distribution of the measured particle location in a pipe cross section. Y is the vertical coordinate of the particle location measured from the bottom of the pipe. D and d are the pipe internal diameter and particle size respectively.

3 Results

At this stage, the model predicts the final size distribution of the particles as a result of a single impact between the particles and the bend walls. The computational algorithm initialized by randomly defining size and strength for each particle based on empirical initial size distribution and strength distribution functions. The gas average velocity is also chosen as input parameter. Then, by using the velocity distribution function, a specific velocity is chosen randomly for each particle. Each particle is randomly located in the pipe at the bend entrance up to height of 70% of the pipe diameter. Assuming the particles move in the bend at straight lines, the impact angle is predicted by Eq. (1). The impact velocity and angle define the required stress conditions for comparison with the particle strength to check whether the particle breaks or not. Then, the size distribution of the broken particles are predicted based on the breakage function.

To validate the results obtained by the model we conducted an experiment in a pneumatic conveying system. The system consists of a straight horizontal 2 in. pipe and examined bend. A sample of at least 50 g of salt particles with narrow size fraction of $2.36-2.8\,mm$ was fed into the pipeline by gravity feeder with various gas velocities between 15 and $30\,m/s$. The particles were accelerated in the pipe towards the examined bend and collected after the bend to measure the size distribution of particles by weight.

A comparison between the experimental and predicted by model results for various air velocities are shown in **Fig. 3**. The results are for salt particles with a narrow size interval of $+2.36-2.8\,mm$ and bend ratio of $R_b/D=4.5$. Evidently, the predicted by model results show a fair agreement with the experimental ones.

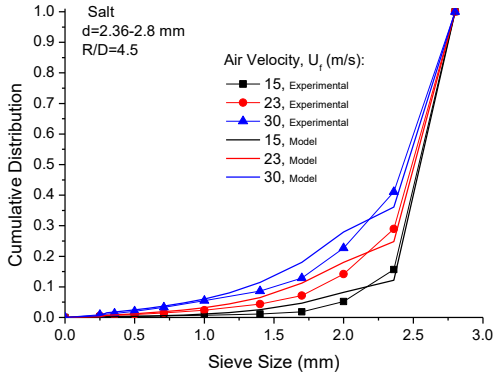

Fig. 3. Size distribution of examined salt particles. Experimental results compared with the results predicted by model for various air velocities.

4. Conclusions

In this study, an easy to use breakage algorithm has been developed. The model does not require the use of CFD-DEM simulations since the machine functions are defined based on empirical correlations and bend geometry. The distribution of broken particles predicted by the model during pneumatic conveying show a fair agreement with experimental results. The computation time is few seconds. In further analysis, we attempt to add a fatigue function to account for repeated collisions with additional bends along entire pipeline. Eventually, this model provides powerful and simple design tool to predict the breakage of particles during pneumatic conveying.

References

[1] Frye, L. and Peukert, W. (2002). Attrition of bulk solids in pneumatic conveying: mechanisms and material properties. *Particulate Science and Technology*, 20, 267-282.

[2] Kalman, H., Rodnianski, V. and Haim, M. (2009). A new method to implement comminution functions into DEM simulation of a size reduaction system due to particle-wall collisions. *Granular Matter*, 11, 253-256.

[3] Brosh, T., Kalman, H. and Levy, A. (2011). DEM simulation of particle attrition in dilute-phase pneumatic conveying. *Granular Matter*, 13, 175-181.

[4] Santo, N., Portnikov, D., Eshel, I., Taranto, R. and Kalman, H. (2018). Experimental study on particle steady state velocity distribution in horizontal dilute phase pneumatic conveying. *Chemical Engineering Science*, 187, 354-366.

ID27 - Comminution of single waste particles in hammer shredder and axial gap rotary shear

Ádám Rácz [1,*] *and Barnabás* Csőke[1]

[1]Institute of Raw Material Preparation and Environmental Processing, University of Miskolc, Miskolc, HU

Summary. The comminution of real waste particles – PET bottle, cardboard, textile, bevarage can, detergent bottle- was carried out in hammer shredder and axial gap rotary shear. During the comminution process the breakage probability of the waste particle was measured. The particle underwent a single stress event in the mill and then was classified at a certain size, later the oversize was feed to the mill again. The experiments were carried out at different rotor velocity in both machines. As a result of the experimental work the different behaviour of the waste particles under different stress type was revealed and the optimal rotor velocity for each waste type was determined. The results also provide the opportunity to lay the foundation for a new dimensioning method.

1 Introduction

The majority of wastes (metals, plastics, rubber, wood, paper and other biomass), excluding construction waste belong to the group of non-brittle materials, which are most preferred stressed by shearing, cutting, pulling, tensile stresses ans bending. The classification of comminution machines used for coarse and intermediate size reduction of materials of non-brittle behaviour according to the dominating types of loading was carried out by (Schubert and Bernotat, 2004). Based on this classification rotary shears, rotary cutters, rotary shredders and translation shears can be used for the comminution of non-brittle waste particles. The comminution process in axial-gap rotary shears takes place both in the axial and the radial gaps. A proportional shearing stress in the narrow axial gaps of the overlapping rotors (multi-rotor design) is significant for these machines (Woldt et al., 2004). In the swing-type hammer shredder the particle is stressed by shear, tearing, impact, bending and twisting loads. A speed of 40 to 60 m/s of hammers, there is a very complex load which leads to a high degree of liberation of structural materials that build up waste particles (Csőke, B., Schubert, 2013). Single-particle comminution experiments of five polymers, limestone and glass spheres of different sizes were carried out by Vogel and Peukert, 2003, however so far real waste particles was not investigated with this view.

2 Experimental

The experimental work was carried out partly in an axial gap rotary shear. There are two rotary rotors at the machine with small circumferential speeds (v = 0.58 m / s; f = 50 Hz). The rotary shear has the following dimensions: Rotor diameter: D = 230 mm, length: L = 500 mm, rotor speed: 48 1 / min. Thickness of the discs: b = 20 mm. Drive motor power: P = 2x11 kW. The applied hammer schredder is a schredder obtained by the conversion of a mineral hammer crusher AGJ UKM 40/20 (D = 400 mm, L = 200 mm, P = 15 kW). An anvil was built in the original crusher, as well as new grinding tracks and massive sieve was built in, and the weight of the hammers was increased as well. Experiments were carried out on samples from a selective waste sorting plant. During the laboratory experiments the following types of materials were used: Plastic: Pet bottle, detergent bottles (HDPE), Paper: Paper, newspaper, cardboard, Metal: aluminum bevarage, textile. During the single-particle comminution experiments, one waste particle was fed to the shredder and rotary shear. The particles were exposed to a single stress in the machine, and then a 30 mm sieve was used to classify the material. The mass of >30 mm and 0-30 mm fractions were measured. The > 30 mm fraction was re-fed to the machine and the above method was repeated until a significant amount of particle was under 30 mm. At the end of the fracture, the particle size distribution of the resulting <30 mm product was determined by sieving.

3 Results

From the measurements, the probability of breakage (S) can be directly determined as the sum of the weight percentages of the <30 mm product produced during each feed. The number of stresses (SN) is the same as the number of feed to the shredder, as the particles were subjected to one stress during each feed. Fig 1 shows the breakage probability as a function of the stress number in case of cardboard comminution in hammer shredder at different rotor circumferential velocities.

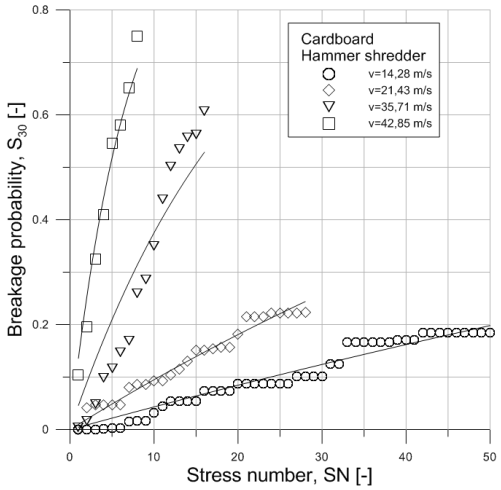

Fig. 1. Breakage probability as a function of the stress number in case of cardboard comminution in hammer shredder

The higher the rotor velocity, the lower stress number required to reach a certain breakage probability. From the results of hammer schredder, it can be seen that in this equipment a higher stress number was needed to fracture the particles compared to the axial gap rotary shear. The different behavior of the materials for high-speed shear - impact stresses is clearly seen from the experiments. PET and HDPE are very difficult to fracture as a result of this stress, while cardboard is easily broken. From the hammer schredder experiments carried out at different circumferential speeds, it can be concluded that the rotor velocity in all three materials (HDPE, PET, cardboard) is greatly influences the requiered stress number for a certain breakage probability. This effect is most evident in the case of cardboard (Fig 1), where there is a clear separation of the breakage probability curves at different rotor velocity.

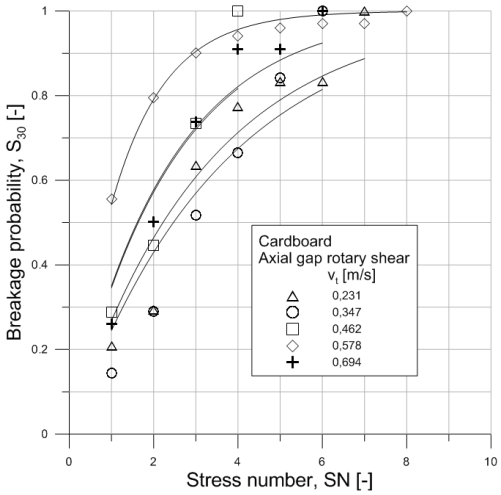

Fig. 2. Breakage probability as a function of the stress number in case of cardboard comminution in axial gap rotary shear

The breakage probability as a function of the stress number in case of cardboard comminution in axial gap rotary shear at different rotor circumferential velocities can be seen in Fig 2. The results in the rotary shear show the probability of breakage by different types of material, mainly by shearing. It can be stated that the highest number of stresses (about 50) was required for textiles, while the easiest case was the aluminum box, where 5 stresses were sufficient to fracture the particles below 30 mm.

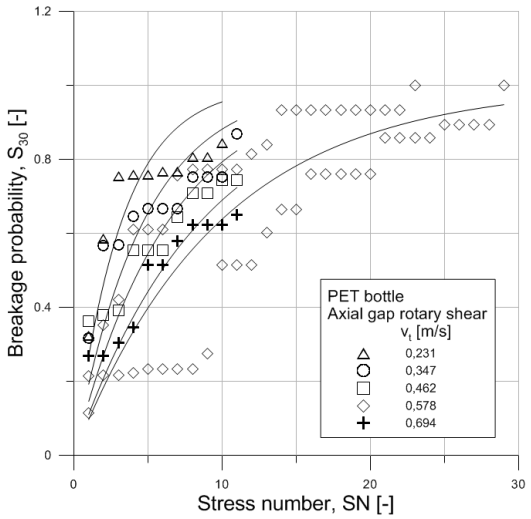

Fig. 2. Breakage probability as a function of the stress number in case of PET bottle comminution in axial gap rotary shear

Cardboard and newspaper and HDPE are easy to fracture, since typically less than 12 stress were required for these materials, while PET is much more difficult to comminute, around 30 stress was necessary. In the case of rotary shear, there is no clear correlation between the circumferential speed of the rotor and the probability of breakage for any material.

Acknowledgements

The described work was supported by the projects GINOP-2.1.1-15-2016-00904 “Development of new equipment production for the low and medium capacity RMSW processing technologies” and the “Sustainable Raw Material Management Thematic Network – RING 2017”, EFOP-3.6.2-16-2017-00010. The realization of these projects is supported by the Hungarian Government and the European Union in the framework of the Széchenyi 2020 program supported by the European Structural and Investment Fund.

References

Csőke, B., Schubert, G., 2013. Nemrideg hulladékok aprítóberendezései. Bányászati és Kohászati Lapok - Bányászat 1.

Schubert, G., Bernotat, S., 2004. Comminution of non-brittle materials. Int. J. Miner. Process. 74, 19–30. doi:10.1016/j.minpro.2004.08.004

Vogel, L., Peukert, W., 2003. Breakage behaviour of different materials—construction of a mastercurve for the breakage probability. Powder Technol. 129, 101–110. doi:10.1016/S0032-5910(02)00217-6

Woldt, D., Schubert, G., Jäckel, H.G., 2004. Size reduction by means of low-speed rotary shears. Int. J. Miner. Process. 74, 405–415. doi:10.1016/j.minpro.2004.07.008

ID28 - Calibration and simulation of breakage by using DEM

Marina Sousani[1,*], *Anderson* Chagas[2], *Carles* Bosch Padros[1], *Amit* Saxena[3] and *Youqing* Yang[3]

[1]DEM Solutions Ltd, Edinburgh, UK
[2]Institute for Particle Technology, Braunschweig, Germany
[3] ME Elecmetal, Minneapolis, USA

Summary. This work presents a methodology to simulate a pilot-scale milling application with the use of an advanced breakage model and the calibration of its Discrete Element Methodology (DEM) parameters. The presented model is based on the DEM and the previous work from Tavares (2009), Tavares and King (2002). It focuses on demonstrating the capabilities of the model in capturing the different breakage mechanisms of a brittle material and is validated using data from Drop Weight Tests (DWT) performed by ME Elecmetal laboratories.

1 Introduction

Particle breakage and subsequent size reduction is a perpetual problem across a wide range of industries including the food, chemical, mineral and pharmaceutical sectors which encompass an even wider range of processed materials. Specifically, research has shown that particles are often loaded using insufficient energy to cause breakage inside comminution equipment, being fractured only after repeated low-energy stressing. This has been particularly well-known for autogenous and semi-autogenous mills, where rock lumps are broken by a combination of attrition and self-induced impact-fracture [4].
This work describes a suitable calibration process and analyses the simulation of an industrial pilot-scale milling application in order to assess the performance of the equipment and the product material. The material used is copper-ore which was processed through ball-mill (AG) and semi-autogenous (SAG) tests. The presented breakage model is based on previous work of Tavares (2009) and is further developed to reflect the latest advances in research. It provides some novel analysis and provides information on the product size distribution, mass loss of the particles due to abrasion, grinding rate, fracture energy per particle type and average power mill.

2 Materials and methods

The virtual material is described by DEM parameters obtained from Drop Weight Tests (DWT), while the size distribution of the fragments is defined by using a combination of a t10 parameter and a clever algorithm that provides realistic representation of real-life scenarios.

2.1 Pilot-scale test program

This pilot-scale test program was conducted by ME Elecmetal including test design, execution and data analysis. The copper-ore sample was 408kg in total and after crushed and screened, it provided a size distribution ranking from 125 to 13mm diameter. This was used as the input feed material for the DEM simulations.

2.2 Calibration of DEM parameters

Calibration involves tuning the mechanical DEM parameters (particle density, Young's modulus, friction coefficients, etc) and the parameters used by the contact model that describes the physical problem. For this project simulations of DWTs were performed to determine suitable DEM parameters. The described DWT was performed by dropping a steel ball from a specified height onto a bed of copper-ore material.
Figure 1 demonstrates the comparison between the DEM results and the DWT results. It can be observed that the model provides results in very good agreement with the experimental ones but also captures the uniqueness of the material by reproducing the two peaks of the breakage behaviour of this material.

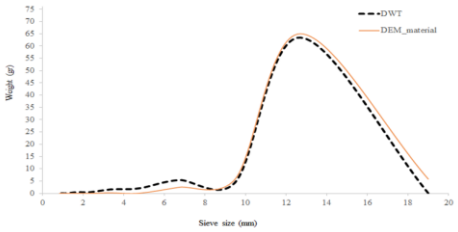

Fig. 1. Comparison between the results from the DWT and the DEM simulation

3 Results and Discussion

Figure 2 demonstrates the comparison between the DEM results and the experimental data for the AG test. It can be observed that the DEM results are in very good agreement with the experimental data and that the simulation has captured the breakage behaviour of the material. Also, it highlights the region of breakage, demonstrating that the area towards the perimeter of the mill (the toe of the charge flow profile) is the most aggressive environment for the material. The toe of the charge profile is the area where the highest energies are observed, hence the flow profile shows that the broken particles tend to concentrate round the perimeter of the charge.

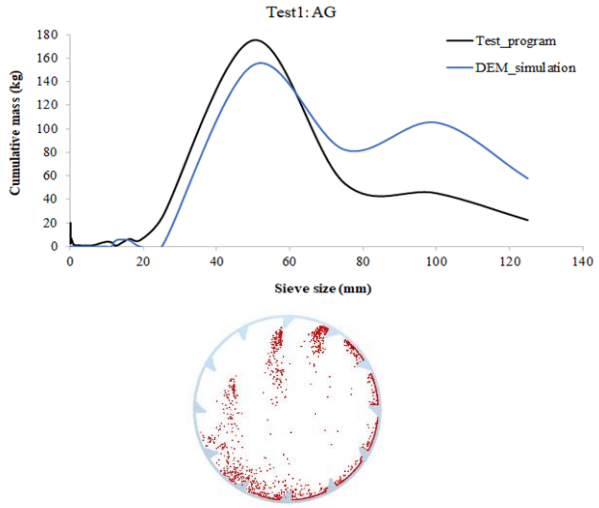

Fig. 2. Comparison between experimental data from the AG test (black line) and the DEM results. Illustration demonstrates the broken particles in the perimeter of the mill.

Similarly, Figure 3 demonstrates the DEM results from the SAG test and the comparison with the experimental data. The model clearly captures the trends of the breakage behaviour, while showing size reduction around 13% (from 125mm to around 14mm diameter), including fines up to 1.30mm diameter.

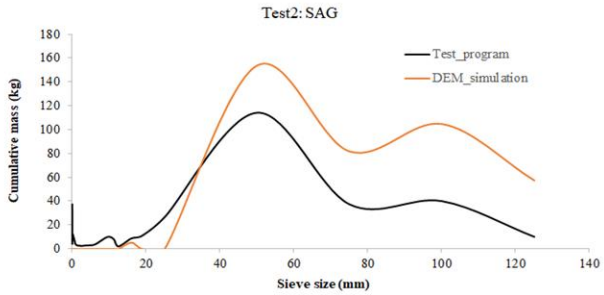

Fig. 3. Comparison between experimental data from the SAG test (black line) and the DEM results.

The deviation can be attributed to the limited simulation time compared to the real test refers to the 1/15th of real physical time, which is not a like-for-like comparison. Figure 4 demonstrates analysis relative to the total mass loss of the system. It can be observed that after 2mins of simulation the system is losing around 0.30% of the total mass. In addition, the results showed that the presence of steel balls (SAG test) has increased the abrasion breakage by 3.5%. The average mill power from the DEM simulations after 2mins was 2.60kW and 4.20kW, respectively, which was in good agreement with the experimental data.

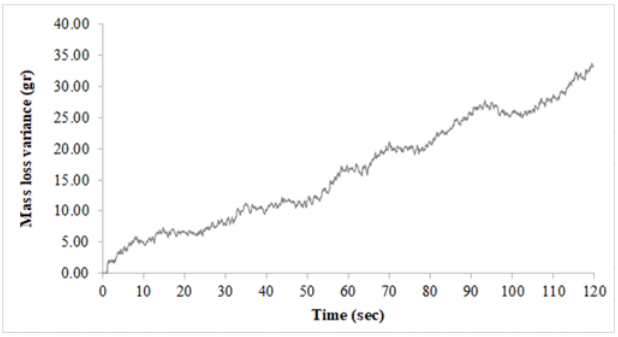

Fig. 4. Mass loss variance between the AG and SAG tests.

An important measurement that is used typically in plant optimisation is the rate of size reduction of the material, referred as grinding rate. Figure 5 demonstrates the grinding rate for the two tests providing novel information on the material behaviour in time intervals of the process.

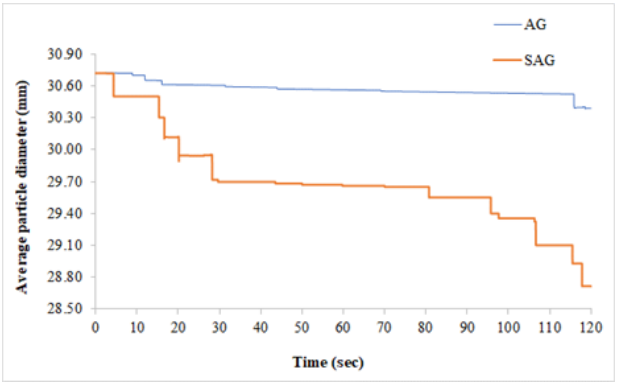

Fig. 5. Average particle diameter versus time for the AG and the SAG tests.

This type of analysis is novel and highlights the importance of such modelling techniques as they provide key insights in areas of interest that would be impossible to gain otherwise.

References

Tavares L.M. (2009) Analysis of particle fracture by repeated stressing as damage accumulation. Powder Technology, 190(3): p. 327-339. https://doi.org/10.1016/j.powtec.2008.08.011

Tavares L. and King R. (2002) Modeling of particle fracture by repeated impacts using continuum damage mechanics. Powder Technology, 123(2-3): p. 138-146.

ID29 - Application of newly developed hammer shredders for used oil filters and residual municipal solid wastes preparation

Barnabás Csőke[1], *Ádám* Rácz[1], *György* Posán[2], *Szabolcs* Német[3] *and József* Faitli[1*]

[1]Institute of Raw Material Preparation and Environmental Processing, University of Miskolc, Miskolc, HU

[2]Terra Center Ltd, Debrecen, HU

[3]3B Hungária Ltd, Zalaegerszeg, HU

Summary. Comminution of non-brittle materials can be effectively carried out in hammer shredders. In the present work two application examples of such machines is presented. Used oil filters from vehicles are hazardous waste, containing iron, aluminium, oil and paper. For the effective recycling of this material stream the liberation of the components by comminution is necessary. In Debrecen (Hungary) a new plant was built for the recycling of oil filters, where a newly developed industrial size hammer shredder for the purpose has been installed. In Zalaegerszeg – Búslakpuszta (Hungary) a new plant was inaugurated at 13th July, 2018 for the mechanical preparation of the residual municipal solid wastes (RMSW) of the region. A new hammer shredder was designed, constructed and installed in the plant for the comminution of the drum sieve oversize (+200 mm) fraction. Paper reports about the design and construction of the shredders as well as about the process engineering results of the first industrial tests.

1 Introduction

Shredders have found very widespread application for the comminution of scrap and waste (Timmel et al., 2000). Swing-hammer type shredders machines with the tearing type of stress are able to handle a broad variety of materials, from paper and card board or metal chips to old cars, aluminium scrap, preparation of waste for incineration plants, lead-batteries, electronic scrap including small motors or fridges (Schubert and Bernotat, 2004). Used oil filters from vehicles are hazardous waste, containing iron, aluminium, oil and paper. For the effective recycling of this material stream the liberation of the components by comminution is necessary which can be done by swing-hammer type shredders. The aim of the mechanical preparation of the municipal solid waste (MSW) in Zalaegerszeg now is the RDF production. In such technologies the comminution of the drum sieve oversize (+200 mm) fraction can be effectively done by swing-hammer type shredders.

2 Applications

2.1. Hammer shredder for RMSW preparation

The municipality of Zalaegerszeg decided on the improvement of the MSW management of the region. A consortium comprising a machine and technology producer (3B Hungary Ltd.), a scientific partner (the Institute of Raw Materials Preparation and Environmental Processing, University of Miskolc), and a public waste managing service company (Zala-Müllex Ltd.) has started the development and construction of an RMSW processing technology targeting no-landfilling for this waste stream. The development and construction of the mechanical-physical processing plant as the first stage is supported by an EU-funded grant. This plant is Hungary's first in the respect that almost all key machines (comminution machines, separators and sorters) are Hungarian made. Generally a rotary pre-shredder is applied as the first technological element for RMSW processing; however it has a serious disadvantage, namely this machine makes the Fe and plastic particles to be intergrown and that is a huge problem for the downstream separation. The energy need of a rotary pre-shredder is also significant. A bag opener machine was developed. The big rotor with teeth of the bag opener rotates opposite compared to the moving floor conveyor; therefore the bags are lifted and teared into the hydraulically supported standing teeth. The afterward machine is an industry standard drum sieve. It has two drum shaped screens, one with 60 mm and the other with 200 mm circular openings. The separated bio-fraction (< 60 mm) will be still landfilled after this first stage of development (Faitli et al., 2018). The drum sieve oversize fraction (+200 mm) goes into the newly developed hammer shredder. Figure 1 shows the hammer shredder.

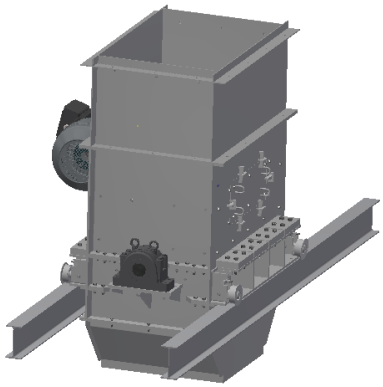

Figure 1. Swing-hammer type pre-shredder in the MSW processing technology

The capacity of the shredder is 3 - 5 t/h, the diameter of the rotor is 860 mm, length 1500 mm. The number of the hammers is 44 (4x 11). The weight of each hammer is 7.1 kg. The power of the electric motor is 135 kW. The shredder equipped with a comb anvil for the effective textile comminution. A large free space has been created over the rotor to provide space for loosening the bulky heterogene material during operation. The shredder is eqipped with a 200 mm internal sieve.

2.2. Hammer shredder for oil filter recycling

In the oil filter recycling technology (Enviszam Ltd, Debrecen, Hungary) the used oil filters are fed into a bunker with a loader belt, from which the shredder is fed with a rubber belt.

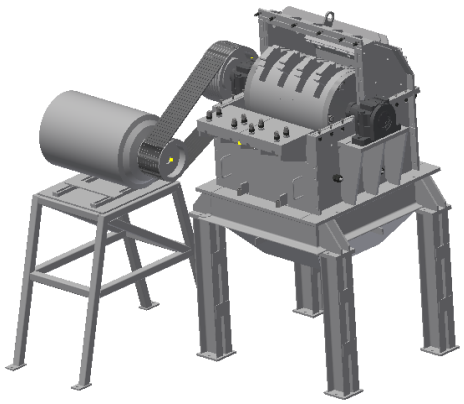

Figure 2. Swing-hammer type shredder for waste oil filters

The technology includes comminution with a swing-type hammer shredder with mild water spray cooling to avoid warming and ignition during shredding. The main objective of the comminution is the liberation of the iron/aluminium outer casing, paper oil filter and plastic pieces. After the comminution a coarse oil removal with drum screen and magnetic separation with a top belt magnetic separator is carried out. Later paper-Al or plastic-Al separation with an air flow separator can be done. The parameters of the shredder are as follows: capacity 500 kg/h, rotor diameter: 800 mm, rotor length: 820 mm. Number of hammers: 12 pieces (3x 4 pieces), hammer weight 9.3 kg, and power 75 kW. The shredder is equipped with a moderate hammer number to reduce wear. The distance between the anvil and the hammers can be varied. The shredder is equipped with a 60x80 mm internal sieve.

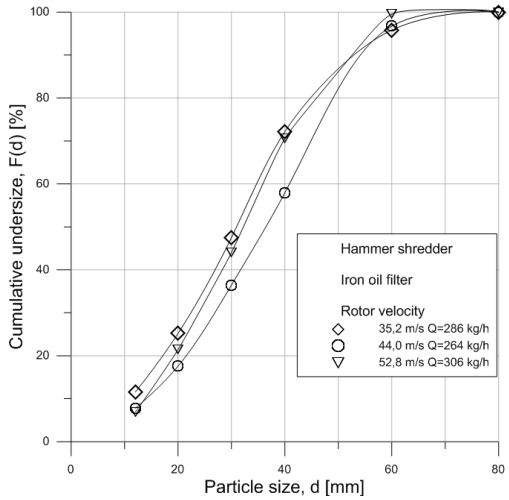

Figure 3. Cumulative undersize of the swing-hammer type shredder's product in oil filter comminution

The cumulative undersize curve of the hammer shredder's product in the case of iron oil filters can be seen in Fig 3 at different rotor velocities.

Acknowledgements

The described work was supported by the projects GINOP-2.1.1-15-2016-00904 "Development of new equipment production for the low and medium capacity RMSW processing technologies" and the "Sustainable Raw Material Management Thematic Network – RING 2017", EFOP-3.6.2-16-2017-00010. The realization of these projects is supported by the Hungarian Government and the European Union in the framework of the Széchenyi 2020 program supported by the European Structural and Investment Fund.

References

Faitli, J., Csőke, B., Romenda, R., Nagy, Z. and Németh, S., (2018): Developing the combined magnetic, electric and air flow (KLME) separator for RMSW processing. Waste Management & Research, doi.org/10.1177/0734242X18770251

Schubert, G., Bernotat, S., 2004. Comminution of non-brittle materials. Int. J. Miner. Process. 74, 19–30. doi:10.1016/j.minpro.2004.08.004

Timmel, G., Sander, S., Schubert, G., 2000. Comminution of scrap and metals in shredders with horizontally and vertically mounted rotor. Dev. Miner. Process. 13, 274–281. doi:10.1016/S0167-4528(00)80091-5

ID32 - HPGR modeling of iron ore pellet feed

Túlio Moreira Campos[1], *Gilvandro* Bueno[1,2], *Luís Marcelo* Tavares[1,*]

[1]Department of Metallurgical and Materials Engineering, Universidade Federal do Rio de Janeiro, Rio de Janeiro, BR

[1]Vale S.A., Complexo de Tubarão, Vitória, Espírito Santo, BR

Summary. Roller pressing has been successfully used for over 25 years in iron ore pellet feed preparation, given its several advantages. However, there have been not systematic studies that demonstrate the validity of any of the published models in predicting this operation. The work validates changes that have been proposed by the authors to the model by Torres and Casali to predict roller press throughput, power and product size distribution, taking into account the by-pass along the cheek-plates, extrusion, saturation, as well as the non-normalizable breakage response of such ores. Predictions of the improved model have compared favourably to data from surveys at both pilot and industrial plants.

1 Introduction

Since the introduction of the roller press in the cement industry, the design and engineering of the equipment has undergone a considerable development, culminating in the great acceptance of the technology in different applications in the industrial mineral (Kellerwessel, 1990). In the early 1990s, Vale SA implemented the iron ore pellet feed pressing with a HPGR combined with ball mill grinding to produce pellet feed fines at the Complexo Tubarão pelletizing plants, whether in pre-milling or in regrinding (Van der Meer, 1997).

Parallel to the technology application in the mineral industry, several authors (Schönert, 1988, Fuerstenau, 1991, Austin, 1993, Morrell, 1998 and Torres and Casali, 2009; Dundar et al., 2013) have been responsible for studying and modelling the phenomenology that describes the HPGR performance. Basically, the models are able to predict, from the operating conditions, machine configurations and material characteristics, the performance of the equipment. Although the models describe reasonably well the HPGR performance variables, there have been identified a series of physical phenomena not yet described in these models, which have resulted in limitations of their application (Lim et al., 1998; Lim and Weller, 1999; Campos et al., 2019).

The present work proposes a series of modifications in the Torres and Casali model to predict the HPGR performance in a specific case of iron ore pellet feed pressing in pilot and industrial scale.

2 Background

Torres and Casali (2009) used a phenomenological approach capable of predicting the HPGR throughput, the power consumption and the product size distribution.

Using a throughput model based on the piston flow model (Schönert, 1988; Morrell et al., 1998), a power consumption model that describes the energy consumption of the equipment from the torque required to move the rolls, Torres and Casali (2009) proposed a different approach in predicting particle breakage in the HPGR operation. Based on the population balance model, the authors discretized the roll in N blocks along the axial roll position and proposing a parabolic power profile along the same roll position (Torres and Casali, 2009). Along with this, the authors proposed using the specific selection function, developing a powerful model for predicting HPGR performance that allows discriminating between centre and edge products. However, recent studies by the authors (Campos et al., 2018; Campos et al., 2019) have demonstrated that the model has significant limitations when applied to iron ore pellet feed pressing.

3 Material and Methodology

The iron ore from the Iron Quadrangle from Minas Gerais (Brazil) has been selected for the study. The material was selected in the Complexo de Tubarão plants and used in several pilot and industrial HPGR tests. Table 1 show the key variables, material characteristics and the principal details of the tests.

Table 1 – Operating conditions of HPGR tests

	Pilot scale	Industrial scale
Op. pressure (bar)	8 - 60	40 - 100
Op. gap (mm)	7 – 20	10 - 25
Roll speed (m/s)	0.2 – 0.9	0.5 – 2.5
Feed moisture (%)	1 – 7	7 - 11
Throughput (t/h)	20 – 60	400 - 1200
Power draw (kW)	15 – 170	500 - 2500
Product BSA (cm²/g)	600 - 1000	1800 - 2000

4 Results and Discussion

Several reasons have been identified for limitations identified in Torres and Casali (2009) model in predicting throughput in iron ore pellet feed pressing. As already observed by other authors (Lim et al., 1998; Lim and Weller, 1999) the extrusion of the material by the side of the rolls and the material acceleration on the compression zone are critical to determine the HPGR throughput. Campos et al. (2019) proposed an empirical equation to calculate the percentage of the material which is extruded by the roll side in a pellet feed pressing using a pilot scale HPGR and a dry iron ore pellet feed.

However, for pressing with high moisture contents, it was observed that there is an acceleration of the material in the compressing zone, leaving the particle bed with a greater speed than the rollers. The present work proposes another equation to calculate the material acceleration and is given by

$$U_g = \frac{U x_c}{x_g} \frac{\rho_a}{\rho_g} \quad (1)$$

where U_g is the material speed, U is the roll speed, ρ_a is the bulk density, ρ_g is the flake density, x_c is the critical gap and x_g is the operating gap.

Now to improve the power consumption prediction of the Torres and Casali model, Campos et al. (2019) suggested an introduce a correction factor for the calculated nip angle, back-calculated from selected data. In fact, the feed moisture and feed particle size, although not explicitly present in the model, are crucial for determining the nip angle and, therefore, the HPGR power consumption.

Figures 1 and 2 compare the experimental and calculated HPGR performance variables using the modified model. Results showed that the modified models were able to describe with fidelity the capacity and power consumption roller pressing operations both in pilot and industrial scale.

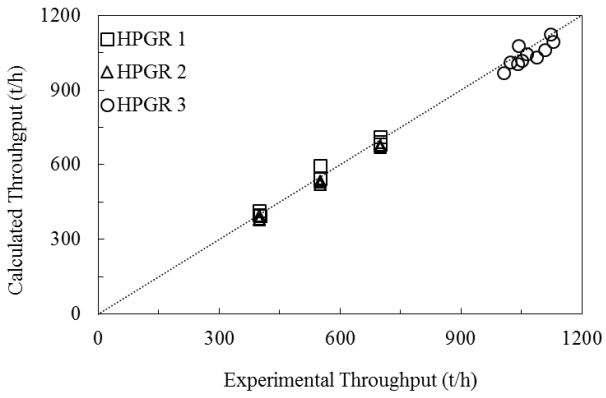

Figure 4 – Comparison between experimental and calculated throughput using the modified model

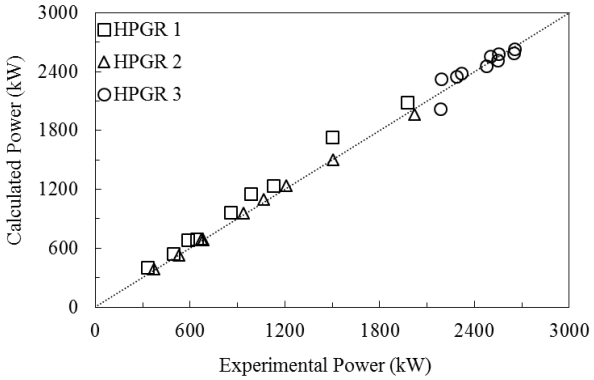

Figure 2 – Comparison between experimental and calculated power consumption using the modified model

Figure 3 presents then a comparison between the simulated and experimental values for percentage passing in 10 µm along the axial rolls in an industrial scale pressing test. It is worth mentioning that the precision of the model to predict the particle size distribution at the fine part of the distribution is extremely important, since it will directly influence the product Blaine specific surface area.

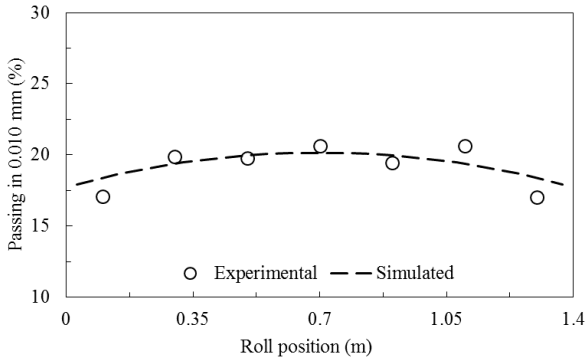

Figure 3 – Comparison between experimental and simulated percentage passing in 0.010 mm along the axial roll position

5 Conclusions

Improvements in the Torres and Casali model allowed reaching very good agreement between experiments and simulations for throughput and power. Challenges still remain for predicting product size for very high specific powers, given bed saturation, which has only been dealt with at a preliminary level.

6 Acknowledgments

The authors would like to thank Vale for financial support to the investigation, as well as the Brazilian Agencies CNPq, FAPERJ and CAPES.

References

Austin, G., Weller, R., Lim, I.L., XVIII Int. Miner. Process. Congr., May, p. 87–96, 1993.

Campos, T.M., Barrios, G.K.P., Bueno, G.B., Tavares, L.M. 6º Seminário de Aglomeração, 2018, São Paulo. p. 737.
Campos, T.M., Bueno, G.B., Barrios, G.K.P., Tavares, L.M. *In preparation*, 2019
Dundar, H., Benzer, H., Aydogan, N., Miner. Eng.**,** v. 50-51, p. 114–120, 2013.
Fuerstenau, D.W., Shukla, A., Kapur, P.C., Int. J. Miner. Process., v. 32, p. 59–79, 1991.
Kellerwessel, H., Zement-Kalk-Gips 2, 57–64, 1990.
Lim, W.I.L., Campbell, J.J.; Tondo, L.A., Miner. Eng., v. 10, n. 4, p. 401–419, 1997.
Lim, W.I.L., Weller, K.R., Miner. Eng., v. 12, n. 2, p. 187–203, 1999.
Morrell, S., Lim, W, Shi, F, Tondo, L, Comminution Practices, p. 117–126, 1998.
Schönert, K., Int. J. Miner. Process., v. 22, p. 401–412, 1988a.
Torres, M., Casali, A., Miner. Eng**,** v. 22, n. 13, p. 1137–1146, 2009.

ID33 - Population balance modelling of ribbon milling with a new mass-based breakage function

Pozza Filippo[1], *Busayo* Olaleye[2], *Chuan-Yu* Wu[2] *and L.X.* Liu[2]

[1]Department of Chemical and Industrial Engineering, University of Padova, via Marzolo 9, 35131 Padova, IT

[2]Department of Chemical and Process Engineering, University of Surrey, Guildford, Surrey GU2 7XH, UK

In pharmaceutical tableting process, powders that are sensitive to heat and moisture are often compacted into ribbons. This is followed by a milling step, where ribbons are broken into granules and then the production of tablets via die compaction process. The quality of tablets therefore largely depends on granules from the milling process and compaction conditions. Currently, ribbons are produced and milled at pre-defined process conditions. Therefore any slight change in the properties of the feed powder (e.g. moisture content) and process condition (e.g. compaction pressure) will directly affect the ribbon strength, which will in turn affect granule size distribution and thus tablet quality. In addition, the production of weak ribbons will result in a broad granule size distribution and high amount of fines, which are detrimental to die filling process and will further lead to high tablet weight variation and lower tablet strength. The aim of this study therefore is to develop a mechanistic population balance model (PBM) for predicting the granule size distribution from ribbon milling process.

In this study, MCC, Avicel® PH-102 (FMC, Biopolymer, USA) was used as the feed powder. 1g of powder mass was added to a 32mm die an Instron® press. The press was set to a fixed compaction speed of 5 mm/min and round ribbons with precisely controlled porosities (from 24 up to 46 %) were produced at five compression forces, varying from 15 to 60 kN. The ribbons were milled using a SM 100 Retsch cutting mill at a fixed speed of 1500 rpm. Granules were collected after 1 minute and characterised using QICPIC ® (SYMPATEC, Germany).

The granule size distribution for each porosity was found to be bi-modal. For a batch milling process, equipped with a mesh screen, the PBM for ribbon milling is given as:

$$\frac{dM_i}{dt} = -S_i c_i M_i + \sum_{j=1}^{i-1} b_{ij} S_j M_j c_j \qquad (1)$$

where M_i and M_j are the mass in size class i and j respectively, S_i is the selection function or rate function, and c_j is the classification function for size j. b_{ij} is the breakage function which represents the progeny distribution from the breakage of size j.

A new breakage function in cumulative form, which reflects the bi-modal distribution curve was developed based on the Weibull distribution below (Yu et al.):

$$B(x) = a\left(1 - e^{\ln(0.2)\left(\frac{x}{p_1}\right)^{m_1}}\right) + (1-a)\left(1 - e^{\ln(0.2)\left(\frac{x}{p_2}\right)^{m_2}}\right) \qquad (2)$$

where $B(x)$ is the cumulative passing percentage after breakage. p_1, m_1, p_2 m_2 are model parameters that reflect the two modes in the granule, whereas the parameter a characterises the proportion of the two modes. For a single mode size distribution, either p_1 or p_2 is the particle size at which 80% of the total mass passes through and is also denoted as p_{80}. Parameters m_1 and m_2 represent the spread of the distribution for each of the mode. The discrete breakage function b_{ij} can be calculated from:

$$b_{ij} = B(x_j) - B(x_i) \qquad (3)$$

Eight PBM parameters were obtained for each ribbon porosity, and good agreement was obtained between the model and experimental results (Figure 1). Sensitivity analysis was then performed on the model parameters thereby reducing the number of model parameters that changed with ribbon porosity in the breakage function to two. These two parameters are the proportionality constant (a) which reflects the two modes and the spread of the second mode (m_2) in the distribution (Figure 2). The relationship between these two parameters and ribbon porosity was established, and used to predict granule size distribution both within and outside the experimental ribbon porosity boundaries.

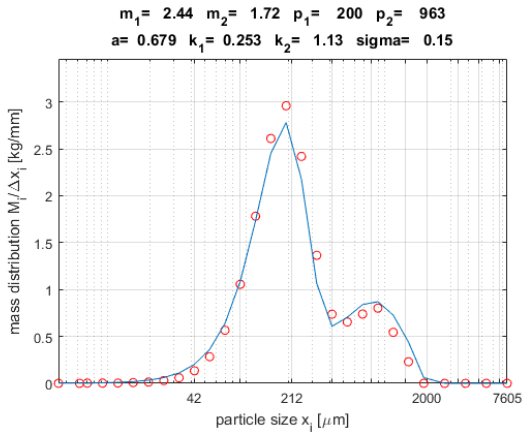

Figure 1. Granule size distribution from experiment (red) and model (blue) at ribbon porosity of 46%

In conclusion, the refined mechanistic model is capable of predicting granule size distribution both within and outside the experimental boundaries. One of the benefits of the model developed in this study is that the optimum feed ribbon porosities for achieving a desired granule size distribution with the SM 100 Retsch mill has been identified. Further work will look into linking process conditions from other mills with the model parameters, thereby paving way for optimising the design space for Quality by Design in the manufacture of pharmaceutical tablets.

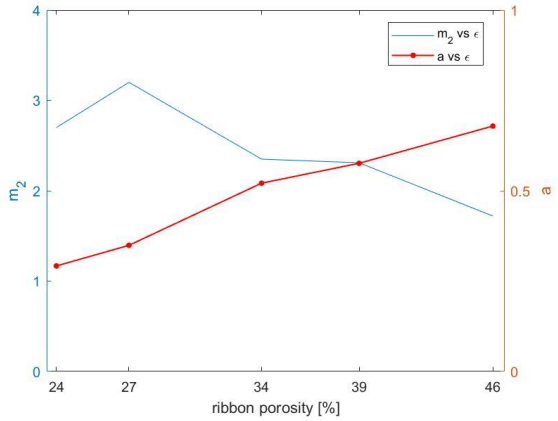

Figure 2. Variation in model parameters m_2 and a with ribbon porosity

References

P. Yu, W. Xie, L. Liu, and M. Powell. The development of the wide-range 4d appearance function for breakage characterisation in grinding mills. *Minerals Engineering*, 110:1-11, 2017.

ID34 - Impact Classifier Mill ICX - Superfine and Efficient Comminution

Marc Giersemehl*, *Fabian* Mertens, and *Daniel-Christian* Karhoff

NEUMAN & ESSER Process Technology GmbH, Übach-Palenberg, Germany

Summary. A new design for an impact classifier mill is introduced. Using a high intensity grinding zone, advanced routing, and new classifying technology, a fineness below 5 µm has been achieved. Several mills of this new type are recently in operation, confirming the precalculated performance. A comparison to conventional impact classifier mills illustrates higher throughputs, finer particle size distributions, and lower specific energy consumptions.

1 Introduction

The objective was to create a new Impact Classifier Mill for superfine comminution (see Figure 5).

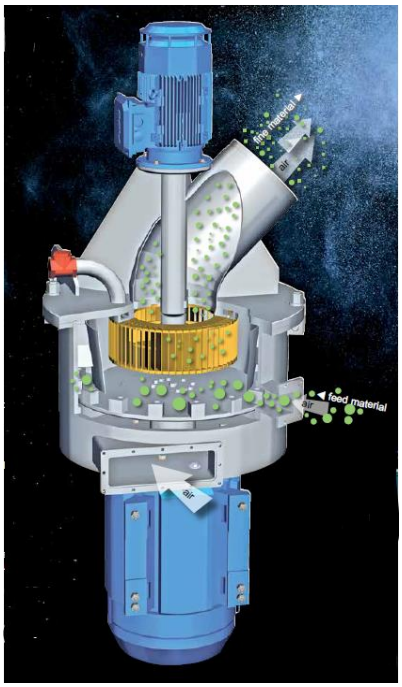

Figure 3 : Impact Classifier Mill Extra ICX

The new impact classifier mill had to be suitable for top cuts between 5 µm and 50 µm, and for applications as food, chemicals, minerals, etc. This mill has been designed by NEUMAN & ESSER Process Technology GmbH, it is called Impact Classifier Mill Extra (ICX).

The ICX is displayed in Figure 5: The feed material is transported pneumatically by a part of the process gas into the ICX's housing. Once the gas and the feed material enter the grinding zone, the material is accelerated by the hammers and comminuted in the grooves of the liner. The ground product is transported towards the classifier wheel. The product is then classified at the classifier wheel into the coarse and the fine fraction. The coarse fraction falls onto the grinding disc and will be reground. The fine fraction is being conveyed through the classifier outlet.

2 Design Approach

Superfine comminution requires increased grinding intensity; therefore the grinding zone geometry was designed accordingly. The size of the final product is determined by both the intensity and the frequency of the stress during the grinding process. These factors are both strongly influenced by the fluid dynamics in the mill [1] [2] [3].

At least of the same importance is the routing of the particles from the grinding zone towards the classifier wheel: The ground material must be distributed homogenously to the classifier wheel flow cross-section.

For good classification results, both the radial and tangential velocity component of the process gas have to correspond to the desired cut condition at the outer circumference of the classifier wheel. The classification efficiency strongly depends on the inflow conditions of the dynamic classifier wheel [4] [5] [6] [7] [8]. The guide ring design takes this requirement into account. Furthermore, the classifier wheel was designed for superfine cuts. The design principle of both the classifier wheel and the guide ring correspond to the design of the NEA PMX [9], and the NEA GRC [10].

3 Results, Conclusion, and Outlook

Preliminary tests with different materials have been performed and their results verify the prior calculations.

A production-size ICX with a classifier wheel diameter of 600 mm is in operation for more than two years, achieving at top cut size (d_{97}) of 6 µm and a median size (d_{50}) of 2.5 µm at a specific energy consumption of approx. 50 kWh/t. Feed material is Calcium Carbonate. The feed material's particle size distribution was measured using two sieves, resulting in 13% residue on a 32 µm sieve, and 79 % residue on a 20 µm sieve. The corresponding particle size distribution is depicted in Figure 4 (green curve). In the same figure, two more particle size distributions for a NEA ICX are shown (red and blue curves). The only differences between the three tests were the circumferential velocity of the classifier wheel.

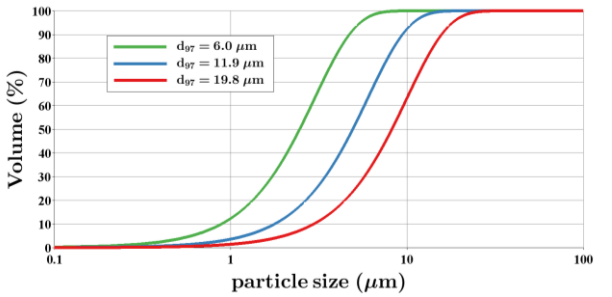

Figure 4: ICX particle size distribution

The presentation will show the development as well as test scores and operational outcome. The comparison to conventional impact classifier mills validates higher throughputs, finer PSDs, and increased energy efficiency. It will be illustrated that the ICX represents an alternative to current superfine comminution machines. An outlook for further similar developments will be given.

References

[1] P. Toneva, K.-E. Wirth and W. Peukert, "Grinding in an air classifier mill — Part II: Characterisation of the two-phase flow," *Powder Technology*, vol. 211, no. 1, pp. 28-37, 2011.

[2] J. Galk, "New Comminution Plant for the Production of Narrow Particle Size Distributions – The Link between Laboratory Mill and Production Plant," *Powder Handling & Processing*, vol. 12, no. 2, pp. 204-205, 2000.

[3] M. Giersemehl and G. Plihal, "Fine Grinding System with Impact Classifier Mill and Cyclone Classifier," *Powder Handling & Processing*, vol. 11, no. 3, pp. 269-279, 1999.

[4] J. Galk, Feinsttrennung in Abweiseradsichtern, Köln: Botermann und Botermann, 1996.

[5] J. Galk, W. Peukert and J. Krahnen, "Industrial classification in a new impeller wheel classifier," *Powder Technology*, vol. 105, no. 1-3, pp. 189-189, 1999.

[6] K. Leschonski, "Classification of particles in gases," IFPRI-Report, Clausthal, 1981.

[7] K. Leschonski, "Das Klassieren disperser Feststoffe in gasförmigen Medien," *Chemie Ingenieur Technik 49 (9)*, vol. 49, no. 9, pp. 708-719, 1977.

[8] H. Rumpf and K. Leschonski, "Prinzipien und neuere Verfahren der Windsichtung," *Chemie-Ingenieur-Technik 39*, vol. 39, no. 21, p. 1231–1241, 1967.

[9] D.-C. Karhoff, F. Mertens and M. Giersemehl, "Feinmahlung und –klassierung in einer Pendelrollenmühle," in *Jahrestreffen der ProcessNet-Fachgruppen Zerkleinern und Klassieren, Kristallisation und Grenzflächenbestimmte Systeme und Prozesse*, Bamberg, 2019.

[10] D.-C. Karhoff, F. Mertens and M. Giersemehl, "Entwicklung eines Leitringsichters," in *Freiberger Symposium für Aufbereitungstechnik*, Freiberg, 2019.

ID35 - In-/online particle sizing during wet media milling of colloidal drug suspensions

Michael Juhnke*, *Andreas* Welle and *Edgar* John

Novartis Pharma AG, Technical R&D, Basel, Switzerland

Summary. Ultrasonic extinction spectroscopy (UES) was evaluated for the in-/online particle sizing during wet media milling of a colloidal drug suspension to support process capability improvements, transfer and scale-up activities. The developed UES method could be successfully applied during a proof-of-concept experiment to monitor the evolution of drug particle size from the beginning of the process until the major size reduction has taken place. Good sensitivity of the UES method was identified down to about 0.2 µm.

1 Introduction

Tailoring poorly water-soluble drugs into products with colloidal particle size is a proven formulation approach to tackle general issues in drug delivery. The increase in specific surface area and corresponding dissolution rate is considered to be the main implication for the improvement of the pharmacokinetic performance. Drugs with colloidal particle size are typically manufactured by wet-media milling technology, due to the availability from pre-clinical to commercial scale and regulatory acceptance for oral and parenteral administered drug products, Li, M., et al., (2016), Merisko-Liversidge, E., and Liversidge, G. G., (2011).

The timely determination of particle size during wet media milling is of interest to support process capability improvements, transfer and scale-up activities during development, and to strengthen the control strategy and efficiency during commercial manufacturing. Ultrasonic extinction spectroscopy is a proven in- and online measuring technique for the determination of particle size during size reduction for ore, mineral, inorganic pigment and ceramic suspensions, Hess, W. F., et al., (2003), Pankewitz, A., et al., (2010), Scott D. M., (2006). Interestingly, applications of ultrasonic extinction spectroscopy are rare in the pharmaceutical field, especially for in- and online measuring tasks, Bonacucina, G., et al., (2016).

In this paper, an in-/online particle sizing equipment based on ultrasonic extinction spectrometry was assessed and investigated for the inline particle size determination during wet-media milling of a colloidal drug suspension.

2 Materials and methods

Aqueous Naproxen suspension of 20% w/w drug load containing 3% w/w Copovidone and 0.05% w/w Sodium Laurylsulfate was selected for the investigations. Ultrasonic extinction spectroscopy (UES) equipment Opus, Sympatec GmbH, Clausthal-Zellerfeld, Germany, suitable for in-/online particle sizing was evaluated in this study, Geers, H., and Witt, W., (2003). Complementary offline particle sizing was performed by laser light diffraction (LLD), model Helos, Sympatec GmbH, Clausthal-Zellerfeld, Germany, dynamic light scattering (DLS), model Zetasizer Nano, Malvern Ltd., Malvern, UK, and by analytical centrifugation (AC), model Lumisizer, LUM GmbH, Berlin, Germany. Naproxen suspensions were manufactured by using wet media milling technology, model Labstar, Netzsch Feinmahltechnik GmbH, Selb, Germany. Method development of the ultrasonic extinction spectroscopy (UES) equipment was performed with an experimental set-up at controlled temperature and flow rate using Naproxen suspensions of different particle sizes manufactured by wet-media milling, see Table 1.

Table 1. Naproxen suspensions manufactured for UES method development with particle sizes determined by laser light diffraction (LLD) and dynamic light scattering (DLS).

Batch (applied offline characterization technique)	x_{10} / µm	x_{50} / µm	x_{90} / µm
Suspension 2.5 µm (LLD)	0.82	2.45	5.52
Suspension 1.4 µm (LLD)	0.56	1.42	3.47
Suspension 0.23 µm (DLS)	0.14	0.23	0.39
Suspension 0.18 µm (DLS)	0.10	0.18	0.31

3 Results

A method sensitivity analysis was performed considering frequency range and gap width of the UES equipment, Naproxen suspensions and continuous

aqueous media with 3% w/w Copovidone and 0.05% w/w Sodium Laurylsulfate for background measurement. The operational settings of frequency and gap width were developed to obtain optimal method sensitivity, resolution and repetition. The obtained extinction normalized by the related gap width is shown vs frequency for all Naproxen suspensions in Figure 1.

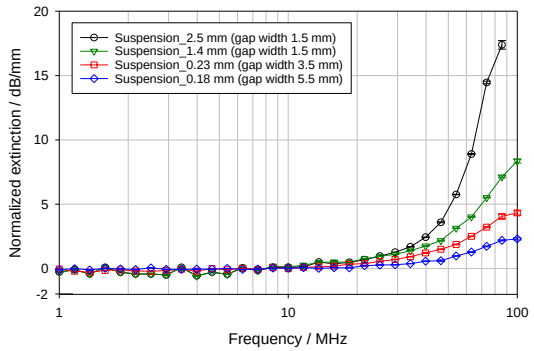

Fig. 1. Normalized extinction against frequency for Naproxen suspensions obtained with developed method (n=6).

The impact of process parameters suspension flow rate and temperature on the normalized extinction of the UES method were identified as negligible within the investigate range (data not shown).

A proof-of-concept experiment was performed by introducing the UES equipment and a sampling valve inline into the wet-media mill process, see Figure 2.

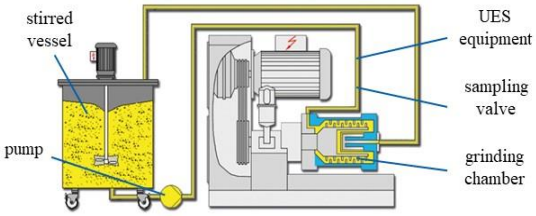

Fig. 2. Experimental set-up for the inline particle size determination by UES during wet-media milling.

The normalized extinction for selected frequencies of the UES method determined during wet-media milling of the Naproxen suspension is shown in Figure 3. The process was started with a gap width of 1.5 mm, and increased to 3.5 and 5.5 mm at predefined normalized extinction levels for an optimal sensitivity of the UES method as shown in Figure 1.

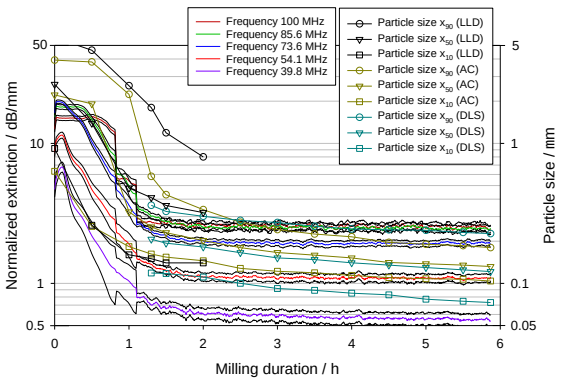

Fig. 3. Normalized extinction including mean squared error for selected frequencies determined by UES during wet-media milling in comparison with particle sizes determined offline by laser light diffraction (LLD), analytical centrifugation (AC) and dynamic light scattering (DLS).

The evolution of Naproxen particle size is well correlated with the evolution of the normalized extinction from the beginning of the process until the major size reduction of the Naproxen particles has taken place. Limitations on the measurement of fine particles by laser light diffraction (LLD) and of coarse particles by dynamic light scattering (DLS) are in good agreement with the general understanding on both methods. Interestingly, the UES method showed limitations on the sensitivity of particle sizes below about 0.2 µm, in comparison with dynamic light scattering (DLS) results.

4 Conclusions

Ultrasonic extinction spectroscopy was successfully applied for the inline determination of the evolution of particle size during wet-media milling of Naproxen suspension. The normalized extinction of the applied inline method showed a good correlation with particle sizes determined by offline methods. The inline method showed good sensitivity down to about 0.2 µm.

References

Bonacucina, G., Perinelli, D. R., Cespi, M., Casettari, L., Cossi, R., Blasi, P., and Palmieri, G. F. (2016). Acoustic spectroscopy: A powerful analytical method for the pharmaceutical field? *International Journal of Pharmaceutics*, 503, 174-195.

Geers, H., and Witt, W., (2003). Ultrasonic extinction for in-line measurement of particle size and concentration of suspensions and emulsions. In: *Particulate Systems Analysis*, Harrogate, UK.

Hess, W. F., Pankewitz, A., and Steigerwald, S., (2003). In-line particle size measurement by means of ultrasonic extinction for control of a stirred-ball-mill process. *Powder Handling and Processing*, 15, 238-245.

Li., M., Azad, M., Davé, R., and Bilgili, E., (2016). Nanomilling of drugs for bioavailability enhancement: A holistic formulation-process perspective. *Pharmaceutics*, 6, 17.

Merisko-Liversidge, E., and Liversidge, G. G., (2011). Nanosizing for oral and parenteral drug delivery: A perspective on formulating poorly-water soluble compounds using wet media milling technology. *Advanced Drug Delivery Reviews*, 63, 427-440.

Pankewitz, A., Behrens, C., Geng, J., and Smith, A., (2010). Ultrasonic extinction for high resolution particle size and concentration analysis. In: *XXV International Mineral Processing Congress*, Brisbane, Australia, 2989-2996.

Scott, D. M., (2006). On-line ultrasonic spectroscopy. In: *Advances in Process Measurements for the Ceramic Industry*. Jillavenkatesa, A., Onoda, G. Y., (editors). American Ceramic Society, 223-236.

ID36 - Development of a Deflector Wheel Classifier for Fine Classification

Daniel-Christian Karhoff*, *Fabian* Mertens, and *Marc* Giersemehl

NEUMAN & ESSER Process Technology GmbH, Übach-Palenberg, Germany

Summary. A novel design for a deflector wheel classifier is shown. The main idea behind the design is to achieve efficient classification by significant improvement of both the particle routing and the air flow into the classification zone. Computational Fluid Dynamics (CFD) were used to a great extent in the design process. Preliminary tests have shown good agreement between the predicted and measured performance parameters on the one hand as well as a high classification efficiency on the other hand.

1 Introduction

A new deflector wheel classifier for in-line air classifying (see Figure 5) has been developed.

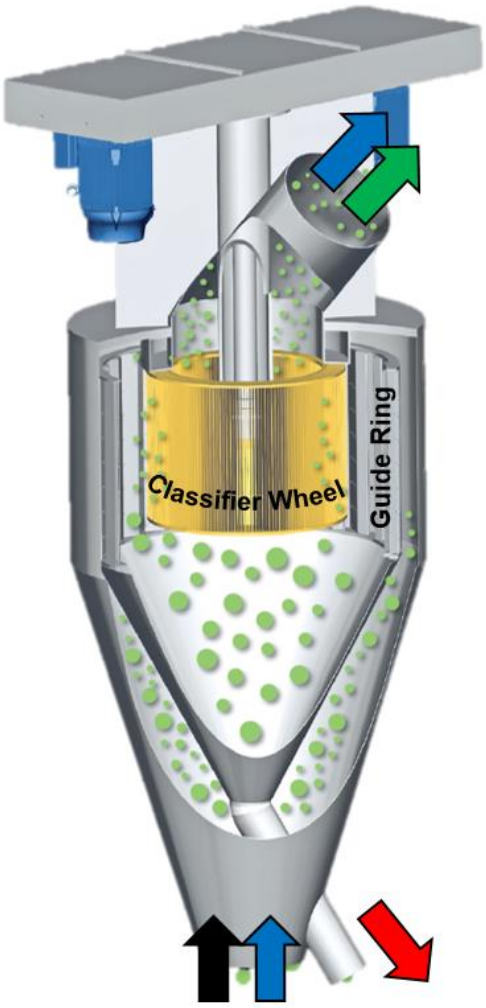

Figure 5 : Deflector Classifier Extra

The overall goal was to design an external classifier with a classifier wheel diameter of up to 3,000 mm for top cuts between 8 µm and 50 µm which can be utilized after grinding systems such as ball mills, roller mills, impact mills etc. Depending on the size, the capacity is between 0.5 and 50 t/h, at a volumetric flow rate of air between 3,000 m³/h and 60,000 m³/h with installed classifier drive powers between 15 and 300 kW. Since this classifier has been designed for fine grinding processes, it is called Deflector Classifier Extra (DCX) by NEUMAN & ESSER Process Technology GmbH.

The operating principle is depicted in Figure 5: The ground product (black arrow) from an upstream grinding system is transported pneumatically by the process gas (air, blue arrow) into the classifier housing. Once the gas and the product stream arrive at the guide ring, they either pass *through* the orifices in the guide ring or *over* the guide ring. The orifices are designed as channels with a rectangular cross section. The product is then classified at the classifier wheel into the coarse and the fine fraction. The coarse fraction is transported gravimetrically out of the classifier (red arrow). The fine fractions is being transported pneumatically through the classifier outlet (green arrow).

2 Design Approach

The fact that both the process gas and the product pass through the guide ring offers the possibility to control both of these streams to a certain extent. For good classification results, both the radial and tangential velocity component of the process gas have to correspond to the desired cut condition at the outer circumference of the classifier wheel. The efficiency of the classification process is strongly dependent on the flow situation in the classification zone, i.e., in the immediate vicinity of the outer circumference of the dynamic classifier wheel [1] [2] [3] [4] [5].

The guide ring was designed to achieve this favorable flow condition in combination with a classifier wheel designed for superfine cuts. The design principle of both the classifier wheel and the guide ring correspond

to the design of the NEA PMX [6], and the NEA GRC [7].

The design process was conducted using Computational Fluid Dynamics (CFD). A first design concept was used as input geometry, which was then analyzed and improved with focus on flow guidance and energy efficiency.

3 Results, Conclusion, and Outlook

Results from lab scale tests show good agreement with the predicted performance. A production-size DCX with a classifier wheel diameter of 1500 mm has been in operation for three years. The material to be classified is bentonite with a particle density of approx. 2,500 kg/m³ [8], achieving a top cut (d_{97}) of 9 µm with a specific energy consumption of 30 kWh/t.
The presentation will show the development and design process as well as detailed results. The utilization of the same principle of the classification process and design of the classifier unit as a mill-internal classifier in a pendulum roller mill is also shown.

References

[1] J. Galk, Feinsttrennung in Abweiseradsichtern, Köln: Botermann und Botermann, 1996.

[2] J. Galk, W. Peukert and J. Krahnen, "Industrial classification in a new impeller wheel classifier," *Powder Technology,* vol. 105, no. 1-3, pp. 189-189, 1999.

[3] K. Leschonski, "Classification of particles in gases," IFPRI-Report, Clausthal, 1981.

[4] K. Leschonski, "Das Klassieren disperser Feststoffe in gasförmigen Medien," *Chemie Ingenieur Technik 49 (9),* vol. 49, no. 9, pp. 708-719, 1977.

[5] H. Rumpf and K. Leschonski, "Prinzipien und neuere Verfahren der Windsichtung," *Chemie-Ingenieur-Technik 39,* vol. 39, no. 21, p. 1231–1241, 1967.

[6] D.-C. Karhoff, F. Mertens and M. Giersemehl, "Feinmahlung und –klassierung in einer Pendelrollenmühle," in *Jahrestreffen der ProcessNet-Fachgruppen Zerkleinern und Klassieren, Kristallisation und Grenzflächenbestimmte Systeme und Prozesse,* Bamberg, 2019.

[7] D.-C. Karhoff, F. Mertens and M. Giersemehl, "Entwicklung eines Leitringsichters," in *Freiberger Symposium für Aufbereitungstechnik*, Freiberg, 2019.

[8] S. Kaufhold, Bentonites – from mine to application. – Geologisches Jahrbuch B 107, ISBN 978-3-510-96859-6: Schweizerbart, 2019.

ID37 - On the identifiability of population balance model for air jet mills

Satyajeet Bhonsale[1,2], *Bard* Stokbroekx[2], and *Jan* Van Impe[1,*]

[1]BioTeC+, Department of Chemical Engineering, KU Leuven, Ghent, Belgium
[2]Crystalization Technology Unit, Janssen Pharmaceutica, Beerse, Belgium

Summary. Air jet mills are common breakage devices used in the pharmaceutical industry. Their popularity arises due to its self-classifying nature. In many cases, the comminution is modelled using the population balance approach. The parameters in such a semi-empirical model are estimated through experimental data. In many cases the data available is insufficient or of bad quality to guarantee the estimation of unique parameters. In this study, we analyse the identifiability of the population balance model developed for the jet mill. It is shown that out of the four parameters atleast one parameter is practically unidentifiable.

1 Introduction

Air jet mill is one of the most common comminution devices used to micronize active pharmaceutical ingredients. The popularity of jet milling arises from the fact that it is a mom-degrading, non-contaminating self-classifying mill. The primary mode of breakage in impact due inter-particle collisions which occurs when particles are fed to a high-pressure air vortex created within a cylindrical milling chamber. As the particles break, the centrifugal forces decay more rapidly ($\sim x^3$) than the radial forces ($\sim x^3$), leading the smaller particles to be dragged towards the centre, until a point where it exits the mill.

2 Mathematical Model

Particulate processes have been traditionally modelled using population balance models (PBMs). The model uses the concept of breakage rate and breakage distribution proposed by Epstien [1]. The breakage rate (S_i) is defined as the fraction of material in a class i selected to break. The breakage distribution function (B_{ij}) describes the probability that the particle in size class j, will break into a particle of size class i. As we empirically know larger particles break easier than smaller particles, the breakage rate is commonly described as

$$S_i = \alpha \left(\frac{x_i}{x_0}\right)^{\gamma}$$

For breakage processes with small time scales like the jet mill, breakage distribution can be approximated by as a direct function of the breakage rate [2]. The jet mill is a (semi) continuous mill with particles below a particular size exiting the mill. To simulate such a classification, we define a classification curve that assumes a log-normal distribution as follows:

$$P_i = 1 - \frac{1}{2}\left[1 + \text{erf}\left(\frac{\log x_i - \mu}{\sqrt{2\sigma}}\right)\right]$$

For the primary analysis, the model contains only four parameters: the two breakage parameters: α and γ, and two classification parameters μ and σ.

2.1 Parameter Estimation

The identifiability of the model structure is studied by generating in-silico data using the above model. The data obtained is the particle size measurement at the exit of the mill. This setup mimics the practical assembly available in our lab. The data is then used for parameter estimation using the nonlinear least square method. For nonlinear parameter estimation, the error between the 'experimental' data and model is minimized using an optimization algorithm. The objective function for the optimization is given by

$$\chi^2(\theta) = \sum_j \sum_i \left(y_{ij}^* - y_{ij}^m(\theta)\right)$$

where, i is the size class, j is the experiment number, and θ is the parameter vector containing the parameters discussed above.

3 Parameter Identifiability

Parameter identifiability refers to the ability to estimate unique parameters for a model based on a given set of data. A parameter can be structurally unidentifiable, practically unidentifiable, or identifiable. Structural unidentifiability arises from excessive parameterization of the model and insufficient mapping of the internal states to the measurable output. The only way to resolve such an unidentifiability is to reparametrize the model. A structurally identifiable model can be practically unidentifiable if the quality, and/or quantity of

experimental data is insufficient to be able to estimate unique parameters. Such unidentifiability can be overcome by obtaining better quality of data, or trying to get more measurements. A confidence interval of the parameter estimate that signifies to a level β, the true value of the parameter is located in the interval. For identifiable parameters, the confidence interval should be finite.

3.1 Raue Identifiability

In this study, we use the Raue identifiability criterion [] which is based on the concept of profile likelihood. A profile likelihood is calculated for each parameter as

$$\chi^2_{PL}(\theta_k) = \min_{\theta \neq \theta_k}[\chi^2(\theta)]$$

i.e. the objective function of parameter estimation is re-optimized by keeping parameter θ_k constant. A structurally unidentifiable parameter is characterized by a completely flat profile likelihood. A profile likelihood of a practically unidentifiable parameter has a visible minimum, but the likelihood does not cross a threshold Δ_β for decreasing or increasing values. The threshold is defined by the likelihood based confidence interval and is the β quantile of the χ^2- distribution. The profile likelihood for an identifiable parameter crosses this threshold line for both increasing and decreasing parameter values.

4 Results

Using the in-situ data, we used the Raue approach to study the identifiability of the PBM for the jet mill. Figure 1 shows the profile likelihood of the four parameters.

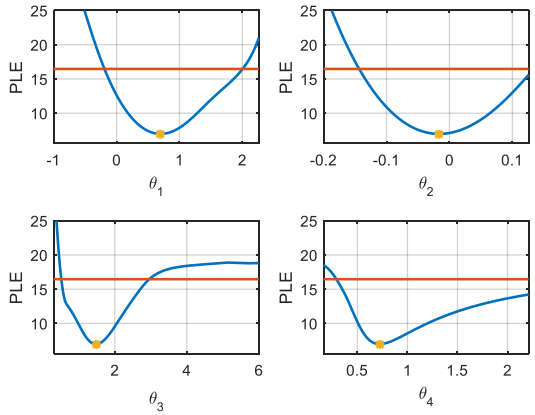

Figure 6. Profile likelihood for the four parameters. The red line shows the threshold value.

The results confirm that the model is structurally identifiable. But one parameter is practically unidentifiable. The unidentifiable parameter θ_4 refers to the deviation parameter in the classification curve. As the dynamics of the mill become faster, i.e., the pressure is increased (leading to a higher α for in-silico experiments), the unidentifiability becomes stronger in this parameter.

In the jet mill, breakage and classification occur in the same chamber and the same input variable that affect the breakage, influence the classification. In other terms, the breakage and classification function are correlated. This might be the reason why one of the classification function parameters is practically unidentifiable. Fixing either of the parameter pairs (breakage or classification) results in the remaining two parameters being identifiable. Moreover, adding number of measurements also improves the identifiability of the parameters. The number of measurements is increased by a finer discretization of the size. However, in this case the practical identifiability was not completely removed. Finally, it was assumed that measurements inside the mill were available. Adding these measurements to the parameter estimation led to a fully identifiable system.

5 Conclusions

If a model is going to be used for predictive purposes, the parameters of the model should be unique and have a very small confidence interval. Assessing the identifiability of a semi-empirical model is an important step in design of experiments for data collection. In this study, we tried to asses the identifiability of the PBM for jet mill. Based on the Raue identifiability test, it was shown that the PBM is practically unidentifiable because of the correlation between breakage and classification in the mill chamber. The only way to remove the unidentifiability is to obtain internal measurement of the particle size distribution. This is however very impractical, as the only way to obtaining this is to crash the mill assembly through the use of ‘emergency stop’. Another approach would be to be able to fix the parameter pairs. At the moment, we are working towards building a CFD-based model to determine the classification curve which once fixed can be used to estimate the breakage parameters.

Acknowledgements

This work was supported by Project G0863.18 of the Fund for Scientific Research-Flanders. SB holds an IWT-Baekeland grant [IWT150715].

References

[1] B Epstein (1947), The mathematical description of certain breakage mechanisms leading to the logarithmic -normal distribution, Journal of The Franklin Institute 244(6), p471.

[2] H Berthiaux, C Varinot, J Dodds (1996) Approximate calculation of breakage parameters from batch grinding tests. Chemical Engineering Science. (51)19, p 4509-4516.

[3] A. Raue, C. Kreutz, T. Maiwald, J. Bachmann, M. Schilling, U. Klingmüller, J. Timmer (2009), Structural and practical identifiability analysis of partially observed dynamical models by exploiting the profile likelihood, Bioinformatics, (25) 15, p1923–1929

ID41 - Impact of Stress Conditions on Wet Grinding of Material Mixtures within a Stirred Media Mill

Markus Nöske[1,*], *Sandra* Breitung-Faes[1], and *Arno* Kwade[1]

[1]Institute for Particle Technology, Technische Universität Braunschweig, Braunschweig, DE

Summary. A selective particle size analysis was applied for the differentiation of component specific particle size distributions in order to investigate mixture samples of a fine grinding process. Within this process, on the formulation side the solids mass proportion of the limestone and quartz mixture as well as the particle stabilisation was varied. Process effects were induced by the variation of the maximum stress energy, which was adjusted by different stirrer tip speeds. An energy split factor approach was chosen for the calculation of a component specific energy utilized to grind a component in mixture. The correlation between particle size and component specific energy stays consistent for nearly all mixture ratios at higher stress energy compared to the results of the single component grinding experiments. The requirements for this grinding behaviour seem to be that the grinding of the harder component is ensured by a sufficient stress energy and its proportion in the mixture is not too high. In contrast, the grinding of the harder component is highly inefficient at low stress energy and even the grinding of the softer component is limited. In this case the quartz particles act as spacers during grinding media contacts. Thus, less stress energy is transferred to grind the softer limestone leading to a reduced grinding efficiency of the limestone compared to the single component grinding experiment. This effect seems to appear already at relatively small amounts of the harder quartz particles of rel. 20 wt.% and increases with higher proportions.

1 Introduction

Grinding of mixed materials is relevant for a variety of industries. In the field of mineral processing or recycling multi component ores or composites have always been omnipresent. Besides, material mixtures play an important role in grinding processes of very hard and abrasive materials because of the significant amount of wear which occurs and is found in the product. Furthermore, the area of multi component formulations is rising recently.

Fine grinding of pure materials in wet operated stirred media mills has been examined in the past, which leads to a good understanding of this process nowadays. However, systematically investigations regarding breakage behaviour of material mixtures in fine grinding processes, especially in the sub-micron particle size range, are still missing. Moreover, analysis methods for the characterization of these material systems with regard to particle size are not commercially available. Thus, the latter challenge was focused at the beginning of the project. An aim of the method establishment was a selective particle size analysis of at least two dispersed solids in a suspension. Therefore, a selective dissolution method was established and used in combination with laser diffraction to characterize the particle size distributions separately.

Employing this characterization method limestone/quartz ($CaCO_3$/SiO_2) mixtures were milled and the impact of different formulation parameters like component mixing ratio and stabilisation as well as processing parameters on the breakage behaviour of each component was investigated. Due to the differentiated analysis of obtained particle size distributions general conclusions on the comminution behaviour of material mixtures during stirred media milling can be outlined. In future these investigations could help to develop optimization strategies to reach defined product fines by reduced specific energy requirement and wear formation.

2 Particle Stabilisation

Figure 1 shows the impact of the adjusted pH value in the aqueous single component suspensions of SiO_2 and $CaCO_3$ on the measured zeta potential. Zeta potentials with an absolute value of more than 30 mV indicate colloidal stability. The SiO_2 suspensions show a good stability in a pH range of 4 to 10. In contrast, for the $CaCO_3$ particles the pH value adjustment doesn't lead to the formation of high zeta potentials. Due to the addition of Sodium polyacrylic acid (NaPAS), an electrosteric stabilisation of these particles is succeeded at pH 10. This pH value was suitable for quartz as well, thus it was chosen for all grinding experiments.

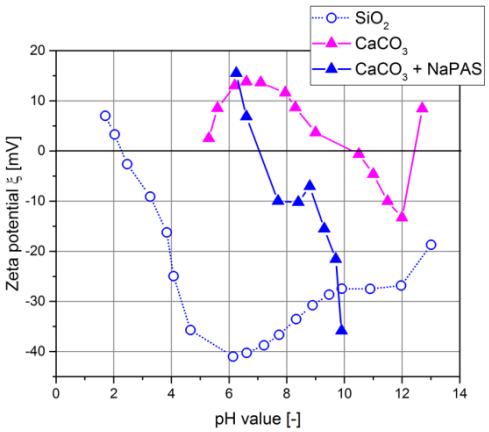

Fig. 1. Zeta potential of SiO_2 and $CaCO_3$ particles dependent on pH value and additive addition

2 Selective Particle Size Analyses

For characterization of the grinding result a selective particle size analysis method was established. In consideration of nearly equal refractive indices of both solid materials, a particle size distribution of the mixture can be analysed by laser diffraction (see Figure 2).

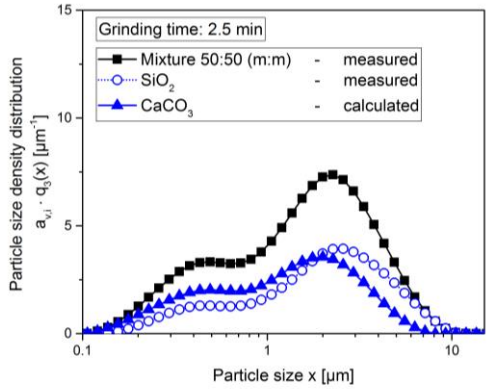

Fig. 2. Particle size density distributions of measured mixture sample, as well as the measured SiO_2 content and calculated $CaCO_3$ content of the same sample

Due to a dissolution step with hydrochloric acid the $CaCO_3$ particles are washed out of the sample. After a re-dispersing step and renewed pH value adjustment for stabilisation of the particles, the SiO_2 particle size distribution can be measured.

$$q_{CaCO3}(x) = \frac{q_{Mix}(x) - a_{v,SiO2} \cdot q_{SiO2}(x)}{a_{v,CaCO3}} \quad (1)$$

For the calculation of the $CaCO_3$ particle size distribution equation 1, which was adapted from particle classification examinations [1], is used with regard to the volume content $a_{v,j}$ of each component j in the mixture.

3 Grinding Regimes in Mixtures

Grinding experiments were first carried out in a way that grinding of the harder component SiO_2 was in an optimal stress energy range according to the model of Kwade [2]. In figure 3 two different grinding regimes are shown for a grinding result of a 50:50 (w:w) mixture.

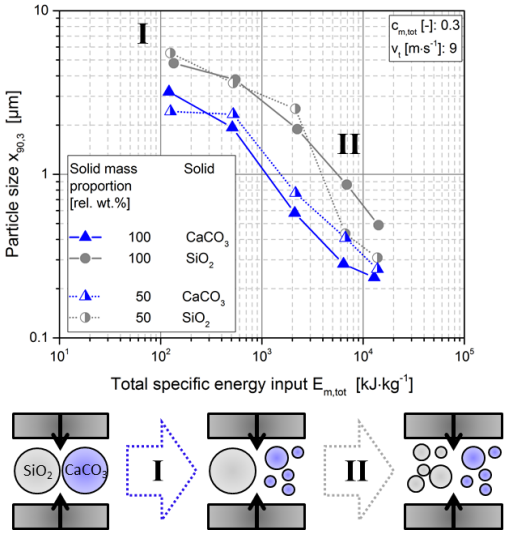

Fig. 3. Grinding regimes dependent on particle size ratios of $CaCO_3$ and SiO_2 particles during mixture grinding

At the beginning of grinding the breakage of the softer $CaCO_3$ particles is more dominant with regard to equal feed particle sizes (regime I). In the following regime II the particle ratios of SiO_2 and $CaCO_3$ influence the grinding efficiency of each component in a way that the breakage of coarser SiO_2 particles becomes more pronounced (II). After both particle species have reached similar sizes, the breakage behaviour of the harder SiO_2 particles shows the biggest impact on the further grinding progress.

Hence, the energy input can be divided for each component not only by their mass proportion, but also by an energy split factor, which was adapted from a model by Fuerstenau [3]. This theoretical value can be used for a better interpretation of grinding results with different component mixing ratios, stabilisation strategies for the components and operating parameters of the mill.

We kindly acknowledge the Deutsche Forschungsgemeinschaft DFG for the financial support.

References

1. M. Stieß, Mechanische Verfahrenstechnik 1. Berlin, Heidelberg: Springer Berlin Heidelberg, 1995.
2. A. Kwade, "A Stressing Model for the Description and Optimization of Grinding Processes," Chem. Eng. Technol., vol. 26, no. 2, pp. 199–205, 2003.
3. D. W. Fuerstenau, A.-Z.M. Abouzeid, and P. C. Kapur, "Energy split and kinetics of ball mill grinding of mixture feeds in heterogeneous environment," Powder Technology, vol. 72, no. 2, pp. 105–111, 1992.

ID42 - Texture, liberation and separation modelling of complex ores

Marko Hilden[1,*] and *Mohsen* Yahyaei[1]

[1]Sustainable Minerals Institute, University of Queensland, Brisbane, Australia

Summary. Many of the existing liberation models combine a model of texture that describes the intact ore structure with a model of particle production. The Geometric Texture Model (GTM) proposed by the authors calculates particle compositions for describing multi-mineral liberation distributions, but these can also be used to generate particles with representative composition distributions to feed particle-based models of various unit processes. In this paper, a model of a meso-texture from the George Fisher deposit is used in combination with a particle-based model that responds to surface composition of particles to predict the overall flotation response of the ore.

1 Introduction

Gaudin (1939) described liberation using a simple thought-experiment, portraying mineral grains as a grid of equi-spaced mono-sized cubes and overlaying a randomly offset grid to produce particles of a range of compositions. As a mathematical model, this is considered overly simplistic leading many researchers to extend the concept in an effort to describe the texture and liberation process in a more realistic manner (Wiegel and Li, 1967, Gay, 2004).

The Geometrical Texture Model developed by the author (Hilden, 2014; Hilden and Powell, 2107) has extended texture modelling to include multiple mineral phases, realistic grain size distributions, preferential mineral associations and non-random spatial distributions of grains. The model describes these textural features mathematically to define the texture using a small set of parameters. The approach eliminates some of the more glaring oversimplifications of geometrical mineral texture models. Nevertheless, the resulting model does model mineral grains and particles as simple geometric shapes (cubes or spheres), and random breakage is assumed.

Other ways of modelling liberation of multi-mineral particles include:

- image tessellation (van der Wielen and Rollinson, 2016) which produces 2D particles;
- numerical simulation of fracture, which is slow, especially in 3D; and
- particle tracking using automated liberation analysis (Lamberg and Vianna, 2007) which requires mineralogy data and to assume that 2D properties are equivalent to 3D properties.

This paper describes how texture and liberation modelling can be combined with the simulation of multi-mineral separations of particles following comminution. The liberation model is extended by calculating the properties of the particles produced and applying a particle-based model to each particle generated. By evaluating a large number of particles of different sizes, the particle composition in each size class can be estimated for the different products of the separation device.

2 Modelling intact ore texture

The procedure outlined in Hilden and Powell (2017) was used to fit the texture model to Bojcevski's (2004) mineralogy data for the George Fisher deposit in Queensland, Australia. The banded sphalerite meso-texture contains sphalerite (21.76%), iron and other sulphides (15.47%) and galena (3.41%) with the balance being non-sulphide gangue. Figure 1 shows the modelled parent texture and typical particles derived by randomly sampling the parent texture. The parent texture consists of a continuous phase representing the dominant gangue minerals interspersed with grains of minerals of interest. As expected, larger particles sampled from the parent texture are poorly liberated, while smaller particles are mostly liberated.

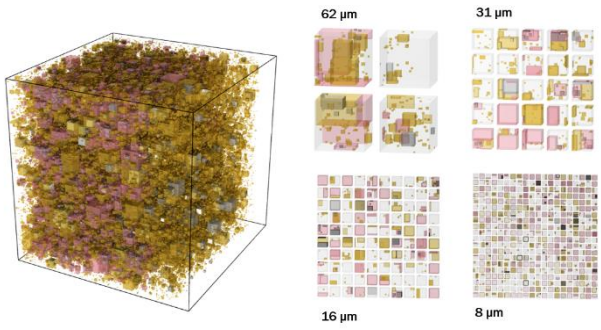

Fig. 1. Banded Sphalerite mesotexture and particles derived by random sampling (sphalerite = pink; pyrite = ochre; galena = grey; NSG = no colour).

Properties calculated for each particle include its density and composition by volume, cross-section area, surface area, perimeter and linear intercept.

3 Particle-based separation

Outputs from a liberation model such as in the form of a liberation distribution are often used as inputs to separation models thus decoupling the liberation and separation models. While feasible for binary ores, this approach fails with complex multi-mineral ores as the number of particle property classes expands rapidly for each mineral phase and mineral property.

In this study, the properties of each particle generated is passed individually to a separation model to calculate the probability of that particle reporting to either concentrate or tailings. When repeated for thousands of particles of each size class, the cumulative compositions of the separator products can be determined. This approach avoids the problems with binning particles or defining archetypal particles. Also, relatively simple models can suffice. For example, a simple partition curve can be applied to calculate the probability of a particle with a given size and density reporting to the floats or sinks stream in a dense medium separation device. For evaluating flotation separations, an empirical model fit to data from Wightman et al. (2010) relating particle composition to recoverability was developed.

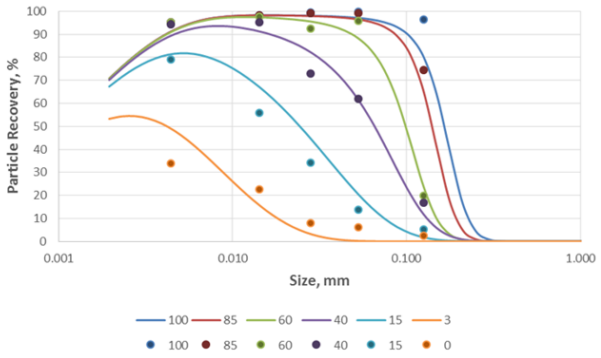

Fig. 2. Flotation as a function of particle composition after Wightman et al. (2010).

The particles produced by sampling the intact texture in Figure 1 were fed to the flotation recovery function above yielding a mass distribution of particles in the concentrate stream. These results are summarised by the locking characteristic shown in Figure 3 alongside the measured locking data from Bojcevski (2004).

4 Conclusions

The methodology described in this paper provides a promising method for predicting the separation outcomes following comminution of a complex multi-mineral ore. Similarly, the effect of changing grind size can also be simulated, for example to predict the optimum grind size for an ore sample.

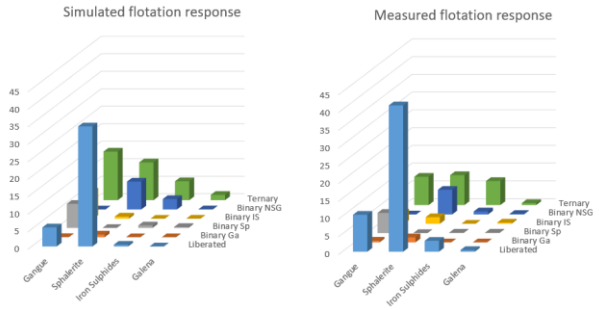

Fig. 3. Simulated Zn rougher concentrate locking distributions calculated (left) vs measured (right).

References

Bojcevski, D., 2004. Metallurgical characterisation of George Fisher Mesotextures and Microtextures, MSc Thesis, University of Queensland.

Gaudin, A. M., (1939). Principles of Mineral Dressing, New York, McGraw-Hill, pp. 70-91.

Gay S.L., (2004). Simple texture based liberation modelling of ores, *Minerals Engineering*, 17: 1209-1216.

Hilden, M.M., 2014. Simulating the effect of mineral association using a multi-mineral rock texture and liberation model. In *Proc. IMPC 2014*, Santiago, Chile, (210-218). 20-24 October 2014.

Hilden, M. M. and Powell, M.S. (2017). A geometrical texture model for multi-mineral liberation prediction. *Minerals Engineering,* 111, 57-69.

Lamberg, P. and Vianna, S. (2007). A technique for tracking multiphase mineral particles in flotation circuits. In *VII Meeting of the Southern Hemisphere on Mineral Technology*. Ouro Preto, Brasil, 195–202.

van der Wielen, K.P. and Rollinson G. (2016). Texture-based analysis of liberation behaviour using Voronoi tessellations, *Minerals Engineering*, 89, 93-107

Wiegel, R. L. and Li, K. (1967). A random model for mineral liberation by size reduction, AIME Transactions, 238, 179-189.

Wightman, E., Evans, C., Bradshaw, D. and Manlapig, E. (2010). Predicting flotation response from liberation information. In Proc. *IMPC 2010,* Brisbane, Australia.

ID43 - Analysis of particle dynamics due to the influence of hold-up in a spiral jet mill using CFD-DEM

Lewis Scott [1]*, *Antonia* Borissova [1], *Alan* Burns [1], *Ian* Gabbott [2], *Catherine* Hallam [2] and *Mojtaba* Ghadiri [1]
[1] School of Chemical and Process Engineering, University of Leeds, Leeds, UK
[2] AstraZeneca, Charter Way, Macclesfield, UK

Summary. Within a spiral jet mill, both breakage and classification occur in the same chamber. The result is a complex fluid flow field, which is difficult to study through traditional experimental techniques. Within this study, Discrete Element Method (DEM) coupled with Computational Fluid Dynamics (CFD) is used to model the effect the hold-up has on both the fluid flow field and solid particle phase within the mill. It was found that with an increase in the hold-up, the average particle velocity, as well as the span of its distribution decreased. As a result, the energy associated with an average collision also decreased. Without breakage present, it was found that the bed has little influence over the air velocity surrounding the classifier. As a result, was no particles exited the mill, as too few were able to cause significant damping to the velocity.

1. Introduction

The spiral jet mill is the equipment of choice for particle size reduction within the pharmaceutical industry. Such mills have no moving parts, providing low maintenance and significantly little contamination of the product. Breakage in the mill is the result of inter-particle and particle-wall collisions.

The simulation of the mill used in this study is based on the AS-50 spiral jet mill manufactured by Hosokawa Micron (Runcorn, UK). The mill has four jets that are placed around the circumference of the main chamber at an angle. Once the material is added into the mill, a moving bed of particles forms along the outer wall due to the centrifugal forces. The bed is sheared by the high-velocity jets, resulting in particle size reduction primarily by abrasion. When the particles pass in front of the jets, they are ejected out of the bed and are subjected to collisions. In this case, particle size reduction now occurs either by chipping or fragmentation. As the particle size is gradually reduced, the radial component of the drag force becomes greater than the centrifugal force. As a result, the particles are carried towards the exit located at the centre of the chamber.

The hold-up of material in the mill plays a crucial role in particle size reduction; as it affects the dynamics of the particle motion and collisions. However, predicting the two-phase velocity has not always been possible, as the high number of particles entrained within the gas significantly alters the velocity of both the particles and the gas (Müller et al., 1996; Rodnianski et al., 2013; MacDonald et al., 2016).

CFD-DEM, though over twenty years old (Tsuji et al., 1992), is still limited by computational power. This power requirement has limited what is feasible when modelling a spiral jet mill, due to the high count of small particles (Dogbe, 2017). However, with the continuing rise of higher processing power, larger simulations that allow the user to model scales larger with the technique are becoming possible.

In this study, the effect of the hold-up in the mill is analysed using coupled CFD-DEM. Its effect on the fluid field, as well as inter-particle and particle-wall collisions energies, are all analysed.

2. Method

The main chamber and feed section of the AS-50 spiral jet mill was used to create a to-scale model. EDEM^{tm} (DEM Solutions, UK) is used to model the particulate solids, treated as spheres. Fluent 18.1 (ANSYS, USA) is used to model the fluid phase, with the k-ε model implemented as the turbulence closure model and air as the chosen gas. Throughout all of the simulation, the particle properties are kept constant.

3. Results and Discussion

3.1. Fluid observation

It was found that as the loading of material increased, the greater the disparity in the velocity between the fluid in the bed and that in the free vortex becomes.

Increasing the mill loading results in little change to the air velocity that directly surrounds the classifier wall within the main chamber. Without breakage present in the simulation, few particles reached the centre. As a result, damping of the gas velocity surrounding the classifier was negligible. Additionally, the decrease in the static pressure near the classifier gave rise to a further increase in the gas velocity. Though unrealistic, as breakage would naturally be present, the results show that the material bed exerts

little influence over the gas velocity surrounding the classifier at low mass loadings.

3.2. Particle observations

No particles in each of the simulation were able to leave, due to the excessive centrifugal speeds experienced near the chamber exit.

At the lowest loading case (0.4g), the material was uniformly distributed over the chamber wall and maintained a flat bed throughout the simulation. However, it was observed that as material loading increased, the profile of the beds surface became uneven. The sudden change in direction, as particles pass in front of the jet, causes subsequent particles to build up behind, as their own path becomes impeded. Due to the material becoming ejected from the bed by the jets, the bed height is lowered directly following this event and further enhances the unevenness of the bed profile.

However, at no point during any of the simulations, did the loading of the bed cause vortex instability. Instead, the bed is held closer to the wall and its movement is a result of the shearing layers.

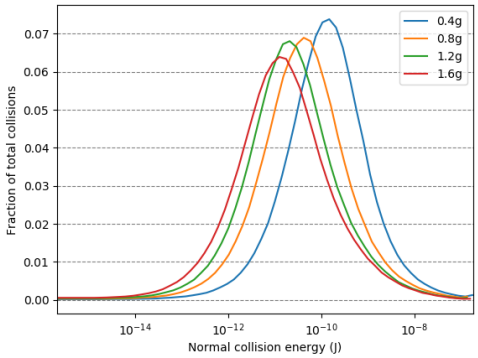

Fig 7. Normal collision energy distribution.

The increase in the material present in the mill results in a decrease in the average velocity of the particles present. Additionally, there is also a decrease in the span of the particle velocity distribution, as the particle loading is increased. Both of these findings are consistent with Dogbe et al. (2017) who reported a decrease in the average particle velocity and the span of the velocity distribution with increased particle number, due to higher dissipation of energy from the fluid.

The overall decrease in the particle velocity also leads a to an average decrease in the energy dissipated per collision; which can be seen in Figure 1. However, due to the increased particle number, the total power associated with collision energy also begins to decrease after the second-lowest loading (0.8g). The decrease in energy associated with a collision may also alter the breakage rate.

4. Conclusions

Particle and fluid dynamics were analysed using CFD-DEM simulations. A number of different mass loadings were introduced into a model of the AS-50 spiral jet mill main chamber. It was found that as the particle loading is increased, the overall bed velocity decreased, as more momentum was transferred to particles from the air. This lowered the overall energy transfer rate due to collisions, as the average particle velocity was lower, even though collisions became more frequent.
It was also shown that at low loading of material within the mill, the bed had little influence on the fluid velocity directly next to the classifier.

The authors; especially the lead author, would like to thank the EPSRC and AstraZeneca for funding this PhD project.

References

Dogbe, S., Ghadiri, M., Hassanpour, A., Hare, C., Wilson, D., Storey, R. and Crosley, I. 2017. Fluid-particle energy transfer in spiral jet milling. *EPJ Web of Conferences*. [Online]. **140**, pp.7–10.

Dogbe, S.C. 2017. *Predictive Milling of Active Pharmaceutical Ingredients and Excipients*. The University of Leeds.

MacDonald, R., Rowe, D., Martin, E. and Gorringe, L. 2016. The spiral jet mill cut size equation. *Powder Technology*. [Online]. **299**, pp.26–40.

Müller, F., Polke, R. and Schädel, G. 1996. Spiral jet mills: hold up and scale up. *International Journal of Mineral Processing*. **44**–**45**, pp.315–326.

Rodnianski, V., Krakauer, N., Darwesh, K., Levy, A., Kalman, H., Peyron, I. and Ricard, F. 2013. Aerodynamic classification in a spiral jet mill. *Powder Technology*. [Online]. **243**, pp.110–119.

Tsuji, Y., Tanaka, T. and Ishida, T. 1992. Lagrangian numerical simulation of plug flow of cohesionless particles in a horizontal pipe. *Powder Technology*. [Online]. **71**(3), pp.239–250.

ID45 - Evaluation of separation and segregation in dynamic air classifiers

Markus Buchmann[1,*] and *Thomas* Mütze[1]

[1]Institute of Mechanical Process Engineering and Mineral Processing, TU Bergakademie Freiberg, Freiberg, Germany

Summary. Dynamic air classifiers separate particles in a gas flow due to their different trajectories. The characteristic property of separation is the settling velocity of the particles which is influenced by their size, shape, and density. The present contribution takes a close look at the separation behaviour of heterogeneous feeds, in which valuables and gangue minerals show significant differences in density. A new concept of multi-dimensional characterization of a separation process is presented and compared to the classical approach of the evaluation by partition curves (split factor, cut size, separation efficiency etc.) The new concept utilises the complex information from an automated mineral liberation analysis (MLA) and provides information of the enrichment and segregation of individual mineral phases in the products.

1 Introduction

Dynamic air classifiers separate particles in a gas flow due to the different trajectories of the particles. The result of such a separation process depends on the gas throughput of the classifier, the dimensions, design and rotational speed of the deflector wheel, as well as the state of dispersion and thus the geometry of as well as the turbulence and interparticle interactions in the separation zone. Air classification of moist feed materials can be divided into several sub-process [1, 2]:

- dosage of the feed material,
- dispersing the solid feed material into a gas stream,
- feeding the dispersed material into the classification zone by pneumatic conveying,
- drying of moist particles during pneumatic conveying,
- separation of coarse and fine particles, and
- separation of fine particles from gas.

The characteristic property of particles in this kind of separation is their settling velocity v_s (eq. 1). This velocity depends on the size x of the particle, its solid's density ρ_p and shape. Shape as well as flow regime and the density ρ_f of the fluid influence the coefficient of drag c_D.

$$v_s^2 = \frac{4}{3}\frac{g \cdot x \cdot (\rho_p - \rho_f)}{c_D \rho_f} \qquad \textbf{(1)}$$

The present contribution takes a closer look at the separation behaviour of heterogeneous mixtures, in which valuables and gangue minerals show significant differences in density.

2 Material and Methods

One iron ore sample was used and characterized in terms of mineralogy, grain size distribution, and particle size distribution. The material was ground by an HPGR and sieved at 315 µm. Representative samples for analysis and air classification tests were prepared by thoroughly mixing and the use of riffle sampler and rotary sample splitter. The material was classified in a dynamic laboratory air classifier at a cut size of 45 µm and feed moisture between 0 and 6 wt.-%.

The quality of classification was assessed by split factor, cut size, and separation efficiency. Additionally the moisture of both products was measured as well as the yield of fines as product fraction in a corresponding processing plant. An automated mineral liberation analysis (MLA) provided information of the enrichment and segregation of individual mineral phases in the products.

Further the data from MLA was utilized for a multidimensional characterization of the separation process via particle size (x_P), particle density (ρ_P) and mineral content. For the generated partition maps (*T*-maps) the separation behavior, selectivity and data reliability is evaluated.

Therefore, the *T*-map is calculated as a function of two particle properties (x_P and ρ_P). For the generation of these maps the kernel density estimation, which is a non-parametric way to smooth the discrete particle data, is applied. The reliability for significant areas of these generated *T*-maps is derived via the coefficient of variation (*CV*) based on virtually generated samples by bootstrap resampling. The selectivity is assessed by calculating the information entropy (*H*) for such a two-output process based on the generated *T*-maps.

3 Results

Classic approach: Evaluation via partition curves

Classically the evaluation of classification processes is based on the measurement of particle size distributions which are made e.g. by analytical sieving, laser diffraction or image analytical methods like MLA [3]. Its result is an evaluation of a single specific equivalent diameter which is taken into account for all particles or eventually for only a single species of particles. The cut size, separation efficiency and split factor of all particles as well as the parameters specifically for the Magnetite containing particles are summarized for one example in Table 2. The example used a feed of 6 % moisture and process parameter for a theoretical cut size of 45 µm.

Table 2. Classification parameters for all particles (measured by laser diffraction) compared to the parameters of only the Magnetite containing particles (measured by MLA).

Data base	Cut size x_T in µm	Separation efficiency κ	Split factor T_0 in %
all particles (laser diffraction)	26.4	0.17	32.8
all particles (MLA)	31.1	0.65	4.8
Magnetite containing particles (MLA)	12.5	0.13	19.7

The classic approach of evaluation by the particle size is not able to characterize the process behaviour of individual components. This approach leads to the design of inefficient grinding circuits. Automated mineralogical analyses like MLA appear to be a promising tool for developing more efficient process strategies. In the shown case a overgrinding of the value containing Magnetite particles can be avoided by increasing the cut size to an optimized value.

New approach: Multi-dimensional evaluation via partition maps

A typical air classification process is not only a function of the particle size, but is also e.g. depending on particle density and shape. The data from MLA allows for a multidimensional evaluation as various properties are assigned to each single particle. Based on partition curves for a single property with such data it is possible to calculate *T*-maps as a function of more than one particle property.

The T-map for the described classification process is shown for an example with a feed moisture of 0 % as a function of size x and particle density ρ_P in Fig. 4. Here the color scale illustrates the enrichment of the particles with a certain property combination in the coarse product. The yellow color indicated a high probability to be enriched in the coarse product, whereas the purple color shows a low probability of enrichment in the coarse product. The dashed line (cut function) is following the approach of the cut size in the one dimensional case. The cut function ($T = 50$ %) marks the range between high and low probability for a particle to be found in the coarse product according to its property combination.

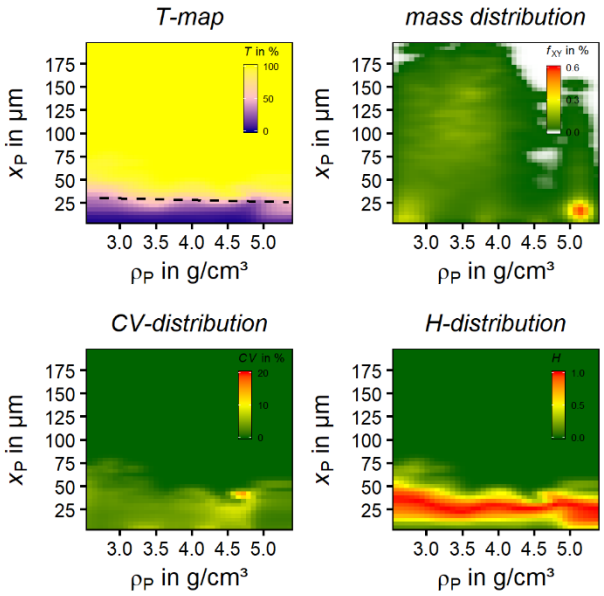

Fig. 4: T-map, mass distribution, CV-distribution and *H*-distribution as a function of x_P and ρ_P for the classification process of the sample with 0 % moisture.

The shown *T*-map indicates a strong dependency on the size of the particles. Above a certain size value all particle will be enriched in the coarse product. There is also a slight dependency on ρ_P visible: The cut size is lowered with increasing ρ_P. The mass distribution indicates the distribution of the mass in the feed material as a function of the investigated particle properties. The distribution of the values for *CV* indicates the error based on the virtual samples from bootstrap resampling (N=1000). The selectivity is assessed with the help of the associated *H*-distribution, where high values (maximum=1) indicate low selectivity (red) in Fig. 4.

The presented multidimensional approach of evaluation of separation quality is not only limited to MLA data but is extendable to other techniques measuring particle properties. A promising field of application will be computer-tomography, where three dimensional data is available.

References

[1] K. Leschonski: Das Klassieren disperser Feststoffe in gasförmigen Medien. Chemie Ingenieur Technik **49** (1977) 9, 708-719

[2] T. Mütze et al.: Influence of feed moisture on the efficiency of dynamic air classifiers. XXVIII IMPC, Quebec, 2016

[3] T. Mütze et al.: Segregation of minerals in dynamic air classifiers. XXIX IMPC, Moscow, 2018

ID46 - Optimization of dolomite processing for shaft kilns

Tony Fraszczak[1], *Urs A.* Peuker[1], *Bernd* Lychatz[2], *Olaf* Ortlepp[3] and *Thomas* Mütze[1*]

[1]Institute of Mechanical Process Engineering and Mineral Processing, TU Bergakademie Freiberg, Freiberg, Germany

[2]Institute of Iron and Steel Technology, TU Bergakademie Freiberg, Freiberg, Germany

[3]Wünschendorfer Dolomitwerk GmbH, Wünschendorf/Elster, Germany

Summary. For the production of burnt dolomite the Wünschendorfer Dolomitwerk GmbH is currently changing the extraction process from open pit to underground mining. Among other things, a change in rock morphology was expected as well as higher extraction costs. Therefore the existing crusher circuit had to be optimized with respect to the yield of an intermediate product for a calcination in shaft kilns. In addition to an analysis of the existing plant it was predicted from basic investigations that there might be an increase of the yield possible by more than 10 %.

1 Introduction

Dolomite is a carbonate rock that belongs to the group of sedimentary rocks. This material is formed by deposition processes and can be found all around the world in a wide range of modifications, such as chalk, limestone, dolomite and marble. It has variety of applications [1]. Dolomite is used as an aggregate for road building and in concrete production, is the main constituent in the production of mineral wool and industrial glasses, and it is used as a fertilizer in agriculture.

In its burnt state dolomite is used in water treatment and as flux in the production of pig iron and steel [2]. Burnt dolomite is produced at Wünschendorfer Dolomitwerk GmbH in shaft kilns for which a specific "kiln stone" is required to achieve a sufficient flow of gas through the moving dolomite bed. The kiln stones are usually of sizes from 25 to 63 mm.

Because of the impending exhaustion of the open-cast deposit the Wünschendorfer Dolomitwerk is changing to underground mining for the extraction of the raw dolomite. With the change of extraction a changing rock morphology was to be expected, among other things. The change in extraction was initiated in 2013 with the driving of the Martina tunnel in Caaschwitz. The comminution characteristics of the dolomite from the newly opened "Lerchenberg Underground Mine" deposit were investigated. Also the existing crusher circuit were optimized with respect to the yield of the kiln stone fraction [3].

2 Material and Methods

Initially the quality of the mined material was evaluated in order to give an accurate assessment of the existing processing plant and to be able to draw up recommendations for further use of the raw material. The mining is carried out by the pillar-and-chamber method and blasting, which produces about 300 t raw dolomite per blast and 2,400 t per day.

2.1 Size distribution of the blasted rock

The size analysis of the blasted rock was carried out on two samples from different blasting locations in the deposit. The sample were taken with a wheeled front-end loader and corresponded to a rock weight of about 20 t. After they had been weighed the sample were tipped out and spread so that coarse pieces (> 200 mm) could be picked out by hand. This step was necessary to determine the upper limit of the feed and to get a representative sample for analytical sieving (≤ 200 mm).

The size distribution of the bigger pieces of the sample were determined by manual sorting and square-hole screens. The finer material was screened using HAVER EML 400 digital T analysis screening machine from Haver & Boecker following the procedure described in DIN 66165 [4].

2.2 Analysis of the actual processing plant

Two industrial-scale comminution tests were carried out in order to determine the performance of the components, for which the routine operation was interrupted and the processing plant was cleaned.

- Test 1: existing plant
- Test 2: existing plant with simulated pre-screening

Based on the size distribution of the blasted rock and the industrial-scale performance tests a Lokotrack St2.8 mobile screening plant from Metso was tested in order to validate the recommendations to extend and optimize the processing plant. Finally a Warrior 2400 mobile

screening plant from Christophel was integrated and the new processing performance evaluated.

- Test 3: existing plant with large scale pre-screening (Lokotrack)
- Test 4: final processing plant (Warrior)

3 Results

The cumulative distribution $Q_3(x)$ obtained from size analysis of the blasted rock and the tests with the industrial-scale-closed-circuit with and without pre-screening are shown in Fig. 1.

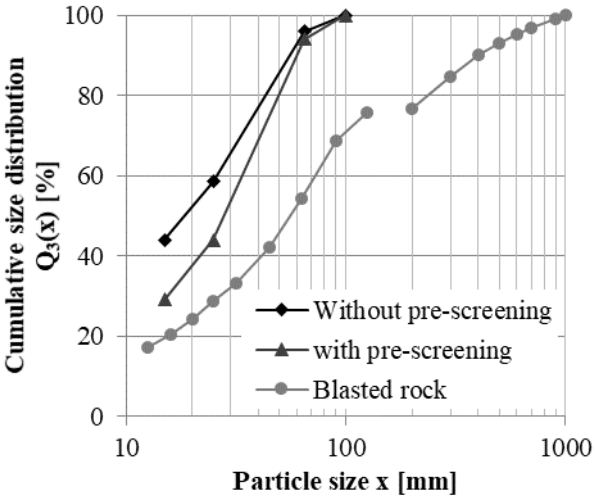

Fig. 8 : Size distribution of the blasted rock and the products of the industrial-scale-closed-circuit (existing plant without and with pre-screening)

Since the sizes for the blasted rock were determined by two different methods of analysis (manual sorting and sieve analysis) the curves of the cumulative size distribution are not joined to one another. The yield of the kiln stone fraction (25 to 63 mm) was about 25.7 % after extraction. The material smaller 25 mm was about 28.7 % and the fraction of coarse material (> 63 mm) was about 45.6 %. The combined amount of the kiln stone and the fine fraction after blasting came to 54.4 %. Therefore and in contrast to the existing plant, pre-screening at about 63 mm before crushing was considered necessary.

The simulated pre-screening resulted in a significant reduction in the fine fraction (< 25 mm) by about 14 %. Within the accuracy of the method of measurement described here the percentage of coarse material was the same in both cases. As a result, the yield of the kiln stone fraction with one-off return of the coarse material (x > 63 mm) rose by about 13 % to a mass yield of about 50 %. For a daily production of 2400 t this increase corresponds to a mass of about 310 t additional kiln stones or one whole blast of raw dolomite in the extraction step. This result confirmed the need for pre-screening as a possible way of optimizing the existing process.

The results of the industrial screening (test 3) are summarized in Tab. 1. The result showed that the simulated pre-screening and characterization techniques used gave a representative approximation of the size distribution of the extracted feed material and proved a suitable method for design and optimization of the processing plant.

Table 3 : Comparison of the mass fractions from analytical screening and industrial-scale screening (test 3)

Fraction in mm	Amount in analytical screening in %	Amount in industrial-scale screening in %
< 28	30.9	23
28 to 70	27.4	24
> 70	41.7	53

The processing result of the final plant is shown in Tab. 2. It was possible to increase the yield of the kiln stone fraction by 14 basis points to 49 % which is close to the simulated intermediate steps. This result could even be increased by circulating the coarse fraction (>63 mm) back to the crusher if necessary.

Table 4 : Product fractions of the final processing plant

Fraction in mm	Amount in final processing plant in %
< 25	37
25 to 65	49
> 65	14

References

[1] Markl, G. and Marks, M. (2008). Minerale und Gesteine. Minerale – Petrographie – Geochemie. 2. Neu bearb. und stark erweiterte Auflage. Spektrum Akademischer Verlag. Heidelberg.

[2] Gorenjski, T. (1998). Mineralien und Edelsteine. Neuer Kaiser Verlag. Klagenfurt.

[3] Fraszczak, T. et al. (2016). Optimizing an existing dolomite processing plant. Cement International 14/5.

[4] DIN 66165. (1987). Siebanalyse – Grundlagen, Durchführung. Beuth Verlag. Berlin.

ID47 - Experimental investigation and DEM modelling of the breakage behaviour of bicomponent agglomerates

Philipp Grohn[1,*], *Maksym* Dosta[2], and *Sergiy* Antonyuk[1]

[1]Institute of Particle Process Engineering, Technische Universität Kaiserslautern, Kaiserslautern, Germany
[2]Institute of Solids Process Engineering and Particle Technology, Hamburg University of Technology, Hamburg, Germany

Summary. In this study, the deformation and breakage behaviour of agglomerates consisting of two different materials bonded with a solid binder was investigated experimentally and simulated using DEM with a bonded particle model. The agglomerates were produced by mixing two fractions of particles with different material properties (hard and soft) and bonded by a polymeric binder which mechanical behaviour were varied. The modulus of elasticity, yield limit, stiffness and strength of agglomerates have been measured by single particle compression tests depending on the composition. The DEM simulations were performed on virtual microstructures generated by a stochastic agglomerate model.

1 Introduction

In chemical and pharmaceutical industries, the compaction of particles with a binding agent to produce robust agglomerates e.g. tablets and pellets is an important production step. During handling and transportation, the agglomerates are subjected to a lot of mechanical stressing that can lead to their breakage. Therefore, the knowledge about relationships between breakage mechanisms and microstructure is important for the optimisation of these processes. One aim of this work is to describe the force-displacement behaviour of dry cylindrical agglomerates obtained by compression tests and to determine their mechanical properties. The second objective is to quantify the relationship between the microstructure of agglomerates and their macroscopic breakage behaviour by simulation.

2 Methods

2.1 Experimental investigation

The agglomerates were prepared with a well measured mixture of hard and soft particles and with a binding agent by compaction in a die (Fig. 1**)** and drying at 80°C. The binding agent was prepared as a solution of a polymer and mixed with the particles in a mixer. In order to investigate the influence of the composition of the agglomerates, the number ratio of hard and soft particles was varied. Moreover, the polymer concentration in the solution was varied resulting in different mechanical behaviour of the binder. Single uniaxial compression tests were conducted with the agglomerates by using a Texture Analyser®.

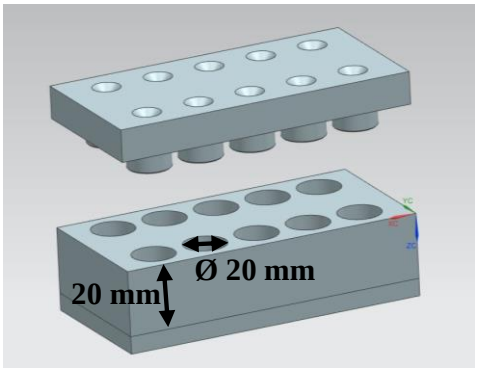

Fig. 5 : CAD model of the used die for the agglomerate preparation

2.1 DEM simulation

To gain better understanding of the influence of agglomerate microstructure and composition on the mechanical behaviour and breakage dynamics a numerical study with the discrete element method (DEM) was performed. For the simulations, the MUSEN framework [1, 2] was applied, which used a bonded particle model (BPM) to simulate the time-resolved behaviour of an agglomerate under compressive load.
The considered agglomerates were created in two stages. In the first stage, a packing of primary particles was generated in the cylindrical volume using a stochastic model. The mixing ratio of soft and hard particles, their material parameters and size, as well as the packing density correspond to the experimental produced agglomerates. In the second stage, the cylindrical bonds between the primary particles are generated. Fig. 2 shows the simulation setup for the quasi-static compression test in MUSEN.

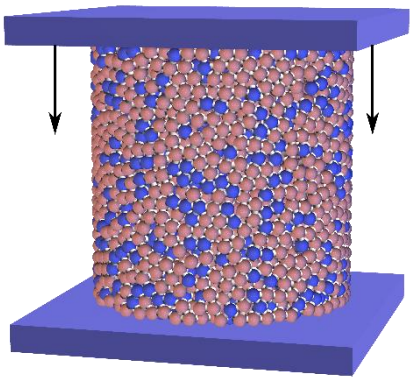

Fig. 6: Simulation setup for the compression test of generated agglomerates

3 Results and discussion

In this work, the experimental results of uni-axial quasi-static compression tests with bicomponent agglomerates were compared with the numeric calculations achieved by simulations with BPM. The obtained results show that the microstructure and composition of bicomponent aggregates have a significant influence on their mechanical properties such as stiffness or strength. The relationships of these micro-macro interactions were described.

References

[1] Dosta, M., Dale, S., Antonyuk, S., Wassgren, C., Heinrich, S. and J. D. Litster: Numerical and experimental analysis of influence of granule microstructure on its compression breakage, Powder Technology 299 (2016) 87-97.

[2] Spettl, A., Dosta, M., Antonyuk, S., Heinrich, S., Schmidt, V.: Statistical investigation of agglomerate breakage based on combined stochastic microstructure modeling and DEM simulations, Advanced Powder Technology 26 (2015), 1021-1030.

ID48 - The influence of particle size distribution on compaction and comminution of cement clinker in high-pressure grinding

Lieven Schützenmeister[1,*], *Evi* Schulze[1], *Thomas* Mütze[1] and *Guido* Kache[2]

[1]Institut of Mechanical Process Engineering and Mineral Processing, Technische Universität Bergakademie Freiberg, Freiberg, DE
[2]thyssenkrupp Industrial Solutions AG, Beckum, DE

Summary. To investigate the impact of the particle size distribution $Q_3(x)$ on compaction and comminution, different cement clinker fractions with defined $Q_3(x)$ have been stressed in a hydraulic press and the compaction and breakage behaviour have been analysed. The contribution presents a model to describe the compaction behaviour of cement clinker and analyses the influence of $Q_3(x)$ on the model parameters. Finally, the applicability of the model to the compaction in high-pressure grinding rollers will be discussed.

1 Introduction

Over the last decades, High-Pressure Grinding Rolls (HPGR) have been integrated into cement grinding circuits worldwide, but still require attention in research. One main purpose is the development of a reliable model, which describes the function of HPGR as accurately as possible. Such model would simplify the design, enable simulation of HPGR in grinding circuits and, at best, predict malfunctions caused by e.g. high proportions of fines and high circumferential speeds of the rollers.

Existing approaches from the literature usually focus only on the prediction of the grinding results and are so far insufficient for some practical applications (Rashidi 2017). In order to obtain a more precise view into the process, the compaction as well as the associated deaeration have to be addressed.

The compression of brittle mineral materials can be described with the model of Mütze (Mütze 2012):

$$\theta = \theta^* \ln\left(1+\frac{p}{p^*}\right) \tag{1}$$

with

$$\theta(p) = \frac{\rho_b(p) - \rho_{b,0}}{\rho_s - \rho_{b,0}} \tag{2}$$

Where θ stands for the normalized compaction, p for the applied pressure, $\rho_{b,0}$ and $\rho_b(p)$ for the initial bulk density and the bulk density at pressure p and ρ_s for the solid density. The reference compaction θ^* and reference pressure p^* are empirical model parameters.

A comparison of different models showed that modelling according to Mütze achieved the best results for the stressing of cement clinker (Makowlew 2018). While previous investigations have mostly been limited to the stressing of monodisperse or bimodal particle systems (e.g. Mütze 2015), here broadly distributed $Q_3(x)$ of different shapes are examined.

2 Experimental setup

The broadness b of $Q_3(x)$ can be defined as the ratio of upper to lower sieve mash size. Sieve fractions of the R10 series were mixed to logarithmically equally distributed fractions in order to investigate the influence of the broadness (see Figure 1). To consider the shape influence of the $Q_3(x)$, mixtures with constant broadness but varying median sizes were additionally prepared in accordance with classifications of the cement industry.

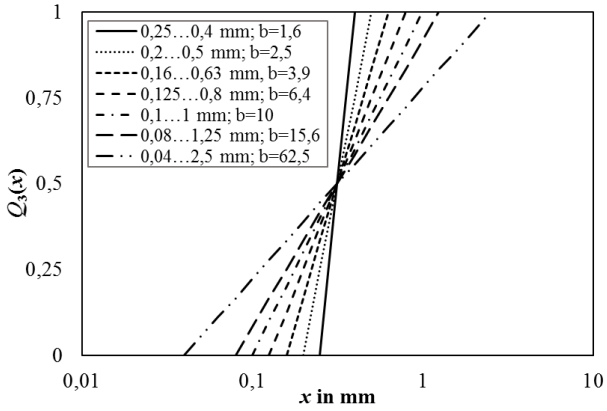

Fig. 1. Influence of broadness of $Q_3(x)$ on bulk density ρ_b and porosity ε

All fractions have been stressed in a hydraulic press with 57 mm piston diameter at an average stressing velocity of 0.01 mm/s to maximum pressure of 175 MPa. To guarantee the independence of the compaction behaviour from the dimensions of the particle bed, the requirements of an ideal particle bed are met (Mütze 2011).

3 Compaction results

The increase in initial bulk density $\rho_{b,0}$ with increasing broadness can be well described with a power function (Figure 2). Due to the denser initial packing, the friction losses increase for broader distributions, leading to higher energy absorptions and lower final compaction. The reference pressure p^*, describing the resistance to compaction, increases accordingly (Figure 3). The reference compaction θ^* can be regarded as independent of the broadness of distribution.

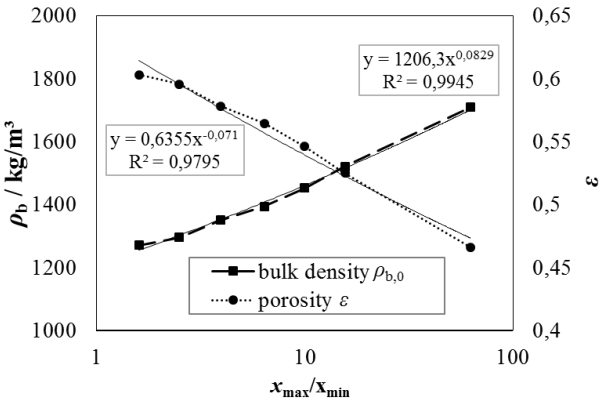

Fig. 2. Influence of broadness of $Q_3(x)$ on initial bulk density $\rho_{b,0}$ and porosity ε

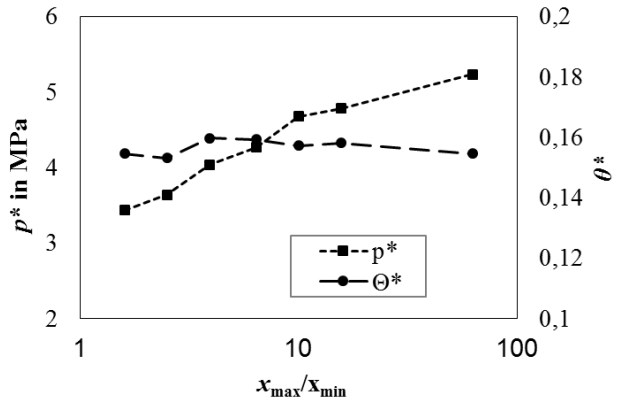

Fig. 3. Influence of broadness of $Q_3(x)$ on bulk density ρ_b and porosity ε

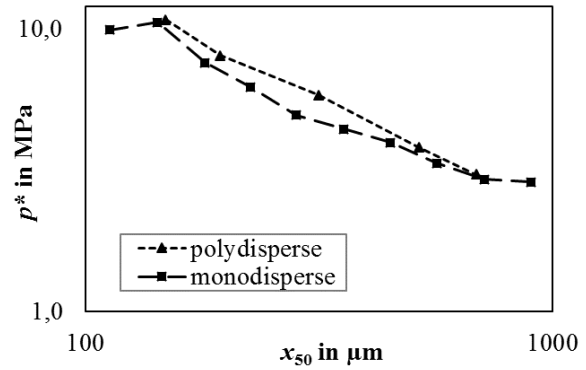

Fig. 4. Course of reference pressure of polydisperse clinker fractions of constant broadness over median size x_{50} and comparison to monodisperse classes.

The resistance against compaction increases with decreasing median value, which in turn can be explained by increasing friction losses due to increasing adhesive forces (Figure 4). In polydisperse classes, the influence of the median value is superimposed by the broadness, so that the reference pressure is higher than for monodisperse classes.

4 Comminution results

If the energy absorption E_m of polydisperse fractions is compared to monodisperse ones (Figure 5), a minimum can been seen instead of a steady decrease with increasing particle size. This can be explained by the protection of the largest grains by fine ones (Fuerstenau 1991): The coarsest fraction is crushed to a higher amount and as a result the energy absorption increases.

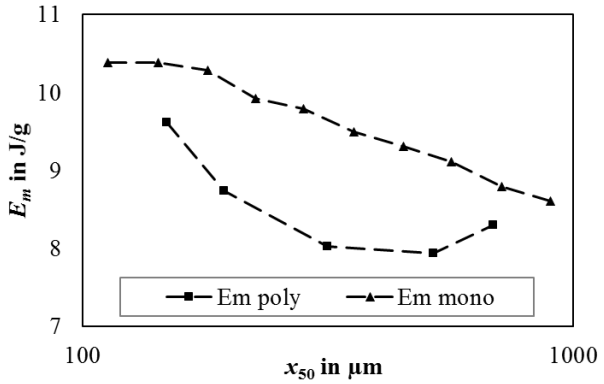

Fig. 5. Comparison of energy absorption E_m over median size for mono- and polydisperse fractions

References

Fuerstenau, D., W., (1991). Energy consumption and product size distributions in choke-fed, high-compression roll mills. *International Journal of Mineral Processing* 32: 59-79.

Makowlew, D., Schützenmeister, L., Mütze, T., and Kache, G., (2018). Modelling the compaction behaviour of cement clinker. *9th International Conference on Conveying and Handling of Particulate Solids*, London.

Mütze, T., (2011). Das Ideale Gutbett. *Chemie Ingenieur Technik* 83 (5): 720-724.

Mütze, T., (2012). Modelling and parameter study of the elastic–plastic deformation. *7th International Conference on Conveying and Handling of Particulate Solids*, Friedrichshafen.

Mütze, T., (2015). Energy dissipation in particle bed comminution. *International Journal of Mineral Processing* 136: 15-19.

Rashidi, S., Rajamani, R., K., and Fuerstenau, D., W., (2017). A Review of the Modelling of High Pressure Grinding Rolls. *KONA Powders and Particles Journal* 34: 125-140.

ID49 - Fine particle breakage testing with a two-roll mill

Ann-Christin Böttcher[1,*], *Christoph* Thon[1], *Greta* Fragnière[1], *Carsten* Schilde[1], and *Arno* Kwade[1]

[1]Institute of Particle Technology, Technische Universität Braunschweig, Braunschweig, Germany

Summary. Breakage characteristics of materials such as energy-size relationship and breakage distribution function are used to simulate grinding processes. In stirred media mills it is estimated that for a wide range of typical operational states fine particles are mainly stressed as individual particle by compression between two surfaces. However, there is yet no simple method available to efficiently measure breakage characteristics of fine particles by compression testing. Here, a rigidly-mounted two roll mill is presented that allows for gap-sizes down to 5 µm. The mill is fed continuously and the torque and line load on the rolls are measured over time. On the basis of test runs with glass particles the device is characterized to describe the influence of the operation parameter on the particle size distribution. It could be shown that the feeding velocity and roller speed influence the breakage of particles. Moreover, new results for different particle sizes and gap widths will be integrated into the presentation.

1 Introduction

Single particle breakage characteristics are increasingly used in advanced modeling and simulation of milling processes. However, it is a challenge to efficiently measure breakage characteristics of particles in the micrometer range. For impact testing of fine particles, for example Meier et al. (2008) and Bonakdar et al. (2016) presented air jet particle impactors and Yu et al. (2019) described a drop weight testing method of a monolayer. Furthermore, Ghadiri et al. (2002) used Indentation fracture mechanics to analyse the propagation of cracks through aggregates. Single particle slow compression testing has been carried out for particles down to a few micrometre and even below with great insight into the deformation and breakage process (e.g. Romeis et al. 2015, Ribas et al. 2014). However, it is a very tedious and slow process and the breakage distribution function cannot be obtained with statistical significance.

Compression testing in a rigidly-mounted two roll mill allows testing a stream of narrow sieved particles. By measuring the torque on the rolls over time the energy-size relationships can be derived, while the progeny particle size distribution gives the breakage function of the feeding fraction for a certain reduction ratio (Kapur et al 1990, Fuerstenau et al. 1990).We are seeking to apply a rigidly mounted two roll mill for compression testing of fine particles. For the adjacent size range, smaller a few hundred micrometer, we are presenting a rigidly-mounted two roll mill with gap sizes down to 5 µm.

In this work we present results on operational parameter studies such as roll speed, reduction ratio (i.e. ratio of particle size to gap size), and particle feeding velocity.

2 Material and methods

2.1 Construction details

The breakage tester is based on the three roll mill of Exakt (Germany), the E-line Plus, which has the capability to precisely set the gap size from 180 µm down to 5 µm. The gearbox was modified in order to achieve equal tangential velocity of the rolls. Only two of the three rolls are used for the two roll tester. The rolls have a diameter of 80 mm and the surface material is aluminium oxide. With an internal force and an external torque measurement, the lineload and the consumed power input can be detected during the stress events. The particle feed is set to a rate at which the particles are stressed in a monolayer and therefore, on the whole length of the roll. Additionally, the vibrating conveyor is modified via an attached fan-type feeding device to distribute the particles along the roll length. The particles fall directly through the funnel above the rolls. This way, it is possible to reduce dusting and product loss of fine particles. The material is removed from the rolls and collected for subsequent particle size analysis. The removal unit consists of scrapers resting directly on the roll surfaces.

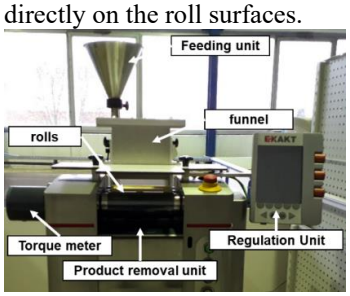

Fig. 7 : The design of the breakage tester

2.2 Experimental Set-Up

In order to test the device, soda-lime-glass particles were tested on the breakage tester. Since the particles had a defined surface with almost ideal sphericity (0.89 x_{min}/x_{max}), all fragments detected can be clearly assigned to the stress applied by the tester itself. With a hardness of over 6 Mohs, the material is widely used in literature. The $x_{3,50}$ of the feed particle size approximates to 79 µm. The particle sizes were analysed by dynamic light scattering (Helos, Sympatec). The dry samples were tested with the Rodos unit that is available for the device. In total, there are two different sets of parameters to vary, the operation parameters and product parameters. On the operational side, the roller speed, gap size, feeding velocity and falling height were varied. To fully determine the breakage function of the material, the particle size was investigated as well. The results of the parameter variations should lead to a best practice to determine the breakage function of different materials featuring different behaviour.

3 Results and discussion

For reasons of continuity, the first parameters changed were the operation parameters, such as feeding velocity and roller speed. The feeding velocity was set to a constant value of 0.15 g/s to prevent the formation of a particle bed and to achieve a better distribution of the particles across the rolls. Figure 2 also shows that the resulting particle size is smaller when using a slower feeding velocity.

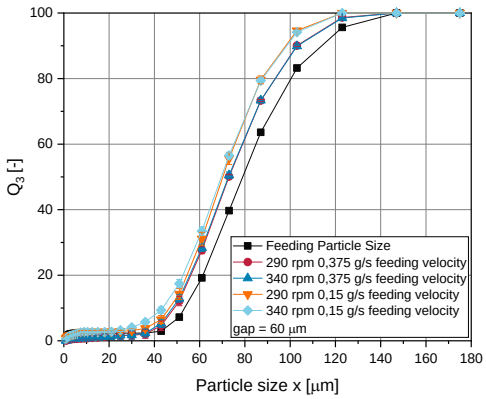

Fig. 8 : Product particle size distribution at different feeding velocities

However, for a gap size of 60 µm, the particle size reduction totals only about 10 µm, if the particles have a feed particle size of 79 µm. During these first tests, the roller speed was set to the tangential velocity of 72.8 m/s. Additionally, a higher velocity of 85.45 m/s was tested. Since the breakage of the tested silica particles is observed to result in long fragments, the product particle size is hard to describe by dynamic light scattering. The ratio of tangential velocity, therefore the falling height, to roll speed was found to considerably effect the breakage behaviour, since primary particle breakage was only found at the same tangential velocity and roller speed. Slower velocities have proven to result in less efficient or non-existent breakage of particles. It is possible to observe an abrasion at the top and bottom surface of the particles but the energy appears to be too low, to actually crack the whole particle itself. In literature, there are basically these two types of comminution stated, compressive stress resulting in disintegrative fracture and attrition/abrasion leaving the parent particle mainly unaffected. [Tavares, 2007] Faster velocities of the rolls caused a deformation of the particles (Fig.3). At higher velocities of the rolls, the shear is enhanced resulting in deformation for most of the particles. In the moment, further tests are fulfilled with different particles sizes and gap widths which will also be involved into the presentation.

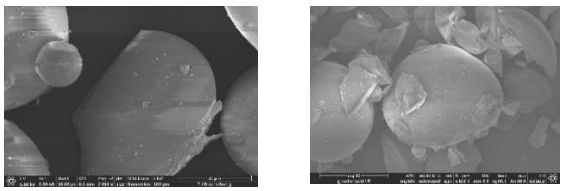

Fig. 9 : Particle fragments at 190 rpm (left) and 600 rpm (right)

References

Bonakdar, T. et al. (2016), A method for grindability testing using the Scirocco disperser. *Int. J. Pharm.* 501 (1-2), 65-74.

Fuerstenau, D. W. et al. (1990). *Comparison of energy consumption in the breakage of single particles in a rigidly mounted roll mill with ball mill grinding. Int. J. Miner. Process.* 28, 109-125.

Ghadiri, M. et al. (2002) *Impact attrition of particulate solids. Part : A theoretical model of chipping. Chemical Engineering Science.* 57, 3659-3669.

Meier,M. et al. (2008*). Characterization of the grinding behaviour in a single particle impact device: studies on pharmaceutical powders. Eur. J. Pharm. Sci.* 34 (1), 45-55.

Kapur, P. C. et al. (1990). *Energy-size relationship for breakage of single particles in a rigidly mounted roll mill. Int. J. Miner. Process.* 29, 221–233.

Ribas, L. et al. (2014). *Measuring the strength of irregularly-shaped fine particles in a microcompression tester. Min. Eng.*, 65, 149–155.

Romeis, S. et al. (2015). *In Situ Deformation and Breakage of Silica Particles Inside a SEM. Proc. Eng.* 102, 201–210.

Tavares, L. M., (2007). *Breakage of Single Particles : Quasi-Static. Handbook of Powder Technology,* 12, 4.

Yu, P et al. (2019). *Applying Fréchet distance to evaluate the discrepancy of product size distribution between single particle and monolayer multi-particle breakage. Pow. Tech.* 344, S. 647–653.

ID50 - Understanding the flow of calcium carbonate in stirred media mills

Sophie Rimmer[1, 2,*], *Andrew* Ingram[1], *Federico* Alberini[1], and *Richard* Tamblyn[2]

[1]School of Chemical Engineering, University of Birmingham, Birmingham, UK
[2]Imerys, Par Moor Centre, Par Moor Road, Par, PL24 2SQ

Summary. Finely ground calcium carbonate has many applications, including in the paint and paper industries. However, the fine grinding process is very energy inefficient due to energy dissipation. Flow patterns within stirred media mills can be analysed to determine which regions of the mill have the most grinding occurring. Knowledge gained from understanding the motion of the slurry and grinding media can be used to determine which operating parameters or design aspects could be changed to give a better milling efficiency. Particle image velocimetry (PIV) has been commonly used to look at flow patterns in a range of engineering equipment such as stirred tanks, but has had very limited application to mills due to the requirement for a fully transparent set-up. Transparent fluids and grinding media may be of different viscosity and density to calcium carbonate slurries and ceramic grinding media. This work looks at developing a transparent system, determining how representative it is of calcium carbonate grinding in a batch stirred media mill and using PIV to analyse flow patterns.

1 Introduction

Stirred media mills are used extensively in industry for the fine grinding of minerals such as calcium carbonate. For use in products such as paints and papers, calcium carbonate with a d_{80} of around 2 μm is required. However, fine grinding has a low energy efficiency due to energy dissipation as heat, noise or vibrational energy. Hence, there is potential for a lot of improvements to be made by making changes to the design or operating parameters. One way of determining which parameters to change is the investigation of flow patterns within the vessel. Knowledge of the motion of grinding media and calcium carbonate particles in different zones of the mill can be indicative of the grinding intensity in each zone.

2 Recent research areas

Numerical models, where the forces between particles or particles and fluids are assessed, can be useful for predicting the motion pathways of the slurry and grinding media. Commonly used models include DEM [1-2], which negates the impact of the fluid, or coupled CFD/DEM, which incorporates the fluid motion into the model [3-4].

Flow patterns in stirred media mills have previously been visualised using positron emission particle tracking (PEPT). A grinding media bead is irradiated and added to a batch vessel [5-6]. However, usually only one grinding media bead is tracked, which means that experimental run times are long and an average occupancy plot or velocity distribution is obtained. Additionally, only the grinding media is tracked, so there is no information about the motion or shear rates of the calcium carbonate slurry.

3 Alternative approach

This research looks at the potential use of particle image velocimetry (PIV) in stirred media mills to overcome the disadvantages of PEPT and provide higher resolution flow patterns. Using PIV, it is possible to look at the flow of either the grinding media or smaller seeding particles which follow the flow of the mimic fluid.

The main challenge of using PIV is the requirement for a completely transparent set-up. A Perspex vessel has been produced, several mimic fluids have been tested for use in place of the calcium carbonate slurry and glass beads have been used in place of the ceramic grinding media. If the refractive index of the mimic fluid matches that of the grinding media, the grinding media are not seen in PIV experiments, enabling high quality images to be obtained.

Clove oil and cedarwood oil are Newtonian fluids with refractive indices matching that of glass beads. Additionally, their viscosities are very different (0.01 and 1.2 Pa s respectively) and so an investigation of the impact of slurry viscosity on flow patterns can be conducted.

Differences between the transparent and actual milling set-ups may lead to PIV data being invalid for real mills. The main differences in the set-ups are the

density of the grinding media and the density and viscosity of the slurry. Both clove oil and cedarwood oil have significantly lower densities than calcium carbonate slurries and cedarwood oil is of higher viscosity. The glass grinding media are of similar density to Carbolite ceramic grinding media. The effect of these parameters on the power draw of the mill have been investigated. The changes to the power draw caused by density can be predicted using the power number, as shown in equation 1.

$$P = Po\rho N^3 D^5 \quad (1)$$

However, this equation is valid for turbulent flow where viscosity does not have a significant effect. It is unlikely that flow is turbulent in a stirred media mill. By using glycerol-water solutions of varying concentration in place of the calcium carbonate slurries, it is possible to test fluids of vastly different viscosities but similar densities. From this, it was shown that viscosity does have a large effect on the power draw of the mill and will hence have an impact on flow patterns.

To determine the extent to which the selected mimic fluids are representative of a calcium carbonate slurry, the viscosity of calcium carbonate slurries and how it changes during grinding has been investigated. Slurry viscosity is of high importance in grinding processes since it affects the amount of viscous energy dissipation occurring during grinding media collisions. Due to the reduction in particle size, viscosity changes throughout grinding, meaning that flow patterns also change.

Calcium carbonate slurries for use in the paint and paper industries have a very high solids content (typically >70 wt%) and so viscosity has been measured using a vane rheometer, since this is an effective way of eliminating wall slip [7]. Additionally, the shear rate in the mill is unknown and varies throughout the mill, so the viscosity was measured over a range of shear rates.

The viscosity of calcium carbonate slurries with 72 wt% solids has been measured using the vane rheometer, as is shown in figure 1. Since viscosity increases during milling as particle size decreases, the viscosity was measured after various amounts of energy had been consumed. The measurements were made at the temperature that the mill had reached when the sample was taken.

The viscosity of 72 wt% slurries during milling ranges from 0.01 Pa s to 0.4 Pa s. By using a selection of transparent mimic fluids with different viscosities, the development of flow patterns over the course of a batch grind could be determined.

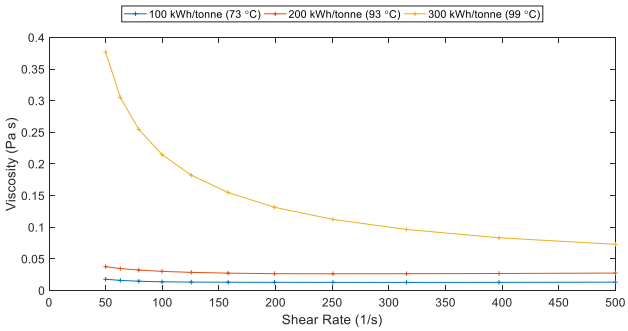

Fig. 1. Viscosity of calcium carbonate slurries after energy input by milling (energy input is per tonne of calcium carbonate being ground)

5 Conclusions

By using transparent mimic fluids with a refractive index matching that of glass beads, PIV can be used to experimentally determine flow patterns of grinding beads or slurry particles within stirred media mills. However, the differences between the density and viscosity of the fluids and grinding media used in the transparent and actual milling set-ups must be considered.

References

1. Sinnott M, Cleary PW, Morrison R. (2006) Analysis of stirred mill performance using DEM simulation: Part 1- Media motion, energy consumption and collisional environment. Minerals Engineering. 19(15), 1537–1550.
2. Jayasundara CT, Yang RY, Guo BY, Yu AB, Rubenstein J. (2009) Effect of slurry properties on particle motion in IsaMills. Minerals Engineering 22(11), 886–892.
3. Zhao J, Shan T. (2013) Coupled CFD-DEM simulation of fluid-particle interaction in geomechanics. Powder Technology, 239, 248–258.
4. Beinert S, Fragnière G, Schilde C, Kwade A. (2018) Multiscale simulation of fine grinding and dispersing processes: Stressing probability, stressing energy and resultant breakage rate. Adv Powder Technology, 29(3), 573–583
5. Barley RW, Conway-Baker J, Pascoe RD, Kostuch J, McLoughlin B, Parker DJ. (2002) Measurement of the motion of grinding media in a vertically stirred mill using positron emission particle tracking (PEPT). Minerals Engineering, 15, 53–59.
6. Van Der Westhuizen AP, Govender I, Mainza AN, Rubenstein J. (2011) Tracking the motion of media particles inside an IsaMill™ using PEPT. Minerals Engineering, 24(3–4), 195–204.
7. Pierre, A. Perrot, A. Histace, S. Gharsalli, E.H. Kadri, A. (2017) Study on the Limitations of a Vane Rheometer for Mineral Suspensions Using Image Processing, Rheologica Acta, 556, 351-367

ID53 - Charge-based agglomeration of submicron particles with potential for selective separation in grinding processes

Christoph Peppersack[1*], *Arno* Kwade[1] and *Sandra* Breitung-Faes[1]

[1]Institute for Particle Technology, Technical University of Braunschweig, Braunschweig, GER

Summary. Products which are produced by wet fine grinding in stirred media mills often suffer a considerable loss of quality because the mill components wear out due to mechanical stress and the suspensions are thus contaminated. Here, a promising method to selectively agglomerating the wear components is presented. The attained knowledge about an efficient, selective agglomeration can be used to remove the wear components from the product suspension in a suitable separation process. Hereby, this ensures that wear-free, submicron suspensions can be produced using a top-down process.

1 Introduction

In the field of pharmaceutical and life science products as well as for optical applications, suspensions with particle sizes in the submicron/nanometer range with the highest quality standards are required. Within the top-down synthesis in stirred media mills, wear (abrasion) of the mill components, primarily the grinding media, is a major challenge. Due to an increasing contamination of suspensions with wear particles during the grinding process, the products suffer a loss of quality and can often only be used to a limited extent. A direct mechanical separation of the wear particles during/after the grinding process cannot be accomplished easily, as these usually have particle sizes similar to the product components.

The (hetero)agglomeration of submicron particle suspensions, induced by electrostatic particle-particle interactions, is a known process in literature. On the contrary, a selective agglomeration of certain components from a mixture of different materials has not been studied extensively yet. In this context, the principle of electrostatically induced agglomeration of submicron particles was investigated in a first step using zirconium dioxide suspensions as an exemplary wear component, since it is one of the most frequently used grinding media material. This study compares different agglomeration mechanisms with regard to their kinetics, agglomerate size and strength as well as the yield of agglomerated particles. The results are related to analytical-theoretical observations of particle-particle interactions using DLVO theory. Subsequently, selective agglomeration of zirconium dioxide particles in a binary mixture with either an organic or inorganic material was evaluated. Here, this will be briefly described in its feasibility for anthraquinone as the organic material example.

2 Experimental

For the data shown here, anthraquinone (product component) and zirconium dioxide (wear component) were chosen as materials. Using a stirred media mill (PML 2, Bühler AG), these substances were first ground in water to a defined particle size. The most relevant properties of the suspensions obtained are summarized in Table 1.

Table 1. Properties of suspensions

	anthraquinone	zirconium dioxide
density of raw material	1.31 g/cm^3	5.68 g/cm^3
particle size $x_{50,3}$	0.3 µm	0.2 µm
mass concentration	5 %-w/w	5 %-w/w
pH value	5.5	5.5
type of stabilisation	electro-steric	electro-static
ζ-potential	- 35 mV	+ 60 mV

To induce selective agglomeration of zirconium dioxide particles, the anthrachinone suspension was first mixed with deionized water and a certain amount of agglomeration additive under magnetic stirring. Subsequently, the zirconium dioxide suspension was added in order to imitate the generation of wear - also under stirring magnetic stirring for a time of 5 minutes. The quantities of the individual components were selected so that the final suspension had a mass concentration of anthraquinone equal to 4 %-w/w and of zirconium dioxide equal to 0.2 %-w/w. The resulting solids mass ratio of 0.05 g/g was adjusted to prevent

destabilisation of the suspension due to heteroagglomeration caused by interaction of the oppositely charged particle surfaces.

To analyse the success of selective agglomeration, samples of the suspensions were centrifuged for 5 minutes at different RCF values. Then, a defined volume was taken from the supernatants, which was first dried at 110 °C and then burnt out in a muffle furnace at 600 °C to decompose the organic material. After each heating step, samples were gravimetrically analysed in order to obtain both the loss of anthraquinone (product) and the loss of zirconium dioxide due to centrifugation.

3 Results and discussion

Figure 1 shows the percentage losses of anthraquinone (product) and zirconium dioxide in the supernatant obtained by centrifugation due to different RCF values with and without agglomeration additive. If the curves without additive are considered first, it can be seen that the zirconium dioxide particles can only be separated by higher centrifugal forces in larger quantities. However, this is associated with an undesired product loss, since anthraquinone particles are also centrifuged with the corresponding centrifugal forces. This effect would be enhanced if the centrifugal forces were increased or the centrifugation time extended. Separation by filtration would also not be possible in this case due to the similar particle sizes of 0.2 and 0.3 µm (see Table 1.).

In comparison, the curves with agglomeration additive show that a considerably higher proportion of zirconium dioxide could be separated from the suspension at significantly lower centrifugal forces (approx. 50 %-w/w at RCF = 380). This also ensures that almost the entire product material remains in the suspension because the centrifugal forces are too low to cause sedimentation of the anthraquinone particles. For this reason, it can be assumed from the results that the addition of the agglomeration ingredient resulted in selective agglomeration of the zirconium dioxide particles. This assumption can be supported by particle size analyses and SEM/EDX images (not shown).

The fact that the separation of zirconium dioxide due to the agglomeration additive cannot be significantly increased above a value of approx. 50 % w/w, even with an increase in centrifugal forces, indicates a limitation on the yield of selectively agglomerated zirconium dioxide particles. It should be noted, that the volume-specific concentration of anthraquinone is 90 times higher in the suspension due to its mass concentration and much lower density (see Table 1.). It is therefore easy to imagine that the yield of the selective agglomeration depends on a multiple number of parameters, e.g. additive concentration, structure and type of additive, concentration and particle size of the zirconium dioxide particles, ionic strength, surface potential or the conditions under which the additive is given. Such parameters as well as their possible combinations are still under investigation. The ultimate goal is to identify the most appropriate set of parameters which can guarantee the complete adsorption of the additive selectively at the interface of zirconium dioxide particles and their entire capture in agglomerates.

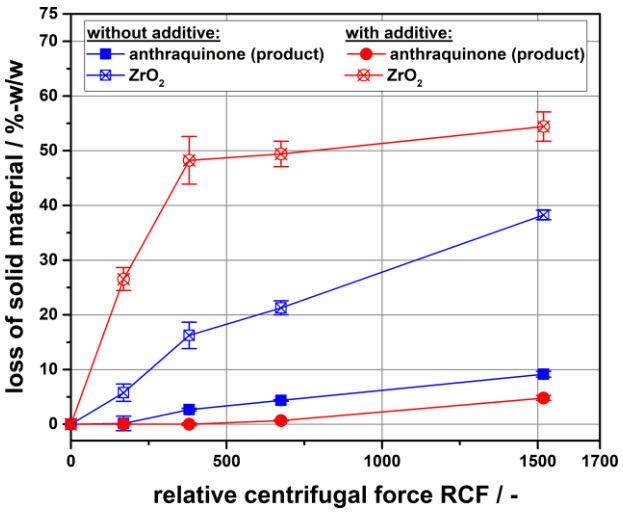

Fig. 1. Gravimetrical analysis of selective agglomeration / separation

The German Research Foundation (DFG) is gratefully acknowledged for funding this research work.

References

Breitung-Faes, S. and Kwade, A., (2011). Production of transparent suspensions by real grinding of fused corundum, *Powder Technology*, 212(3), 383-389.

Flach, F. et al., (2016). Impact of formulation and operating parameters on particle size and grinding media wear in wet media milling of organic compounds – A case study for pyrene, *Advanced Powder Technology*, 27(6), 2507-2519.

Flach, F., Breitung-Faes, S. and Kwade, A., (2017). Grinding media wear induced agglomeration of electrosteric stabilized particles, *Colloids and Surfaces A: Physicochem. Eng. Aspects*, 522, 140-151.

Lin,W. et al., (2006), Heteroaggregation in Binary Mixtures of Oppositely Charged Colloidal Particles, *Langmuir*, 22, 1038-1047.

ID57 - Experimental determination of the disc wear behaviour of a M4 IsaMill™ in dependence on the axial grinding media distribution

David Sterling[1,*], *Didier* Schons[2], *Sandra* Breitung-Faes[1] and *Arno* Kwade[1]

[1]Institute for Particle Technology, Technical University of Braunschweig, Braunschweig, DE
[2]Glatt Integrated Process Solutions, Weimar, DE

Summary. Stirred media mills are commonly used process units for wet fine grinding and dispersing. During wet grinding operations in horizontal stirred media mills, the grinding media and material can cause wear to the process unit. The IsaMill™ with its internal classifier holds the grinding media off from the discharge and implies a counteracting current force to the drag forces which are caused by the product flow. The disc wear was investigated with regard to the axial grinding media distribution in dependence of different process parameters. Thereby, the disc wear was measured by special designed aluminium discs which shows a fast abrasion. To correlate the process parameters to the disc wear for each set of parameters or rather the stress energies (SE) the disc set was changed. In order to measure the axial grinding media filling ratio along the M4 IsaMill™, a radiometric densitometer was installed. This method enables the determination of the local filling ratio by correlating it with the attenuation of gamma radiation of a Cs^{137} nuclide. The experiments showed that the disc wear per energy input increases with rising SE. In relation to the axial grinding media distribution, higher wear rates were observed in the areas of increased filling ratios and grinding media packing. As a result of this, it can be stated that a homogeneous grinding media distribution leads to a longer system operating time and thus, lower maintenance costs due to the homogenous wear rates along the disc.

1 Introduction

Fine grinding is an important process step not only in the chemical or pharmaceutical industries, but also in mineral processing and ceramics industries. Stirred media mills are commonly used process units for wet fine grinding and dispersing. During wet grinding operations in horizontal stirred media mills the grinding media and product material can cause wear to the process unit. Due to high throughputs, the grinding media tend to be pushed towards the product discharge. This grinding media displacement may lead to hydraulic packing which has negative consequences for the grinding process. The IsaMill™ with its internal classifier keeps the grinding media away from the discharge and implies a counteracting current to the drag forces which are caused by the product flow. In fact, *Anymadu* has shown that about 50 % of the operating costs of an M10.000 IsaMill™ are related to maintenance. Focussing on stirred media mills, the agitator is the component most affected by wear. Within this context, *Rule* has shown that the wear is caused by the contact of the stirrer, the grinding media and the material. To understand this behaviour, present study investigated the relation between the disc wear and the axial grinding media distribution. Thereby, the disc wear was measured by stressing specially designed aluminium discs with constant parameter sets and monitoring the weight reduction and the disc deformation. In order to measure the axial grinding media filling ratio lengthwise to the M4 IsaMill™, a radiometric densitometer was installed.

2 Setup and radiometric densitometry

Figure 1 shows the M4 IsaMill™ setup including the suspension flow, classification wheel, different grinding compartments of the grinding chamber (C0 to C6) between the discs and the radiometric densitometer. To determine the disc wear by weight difference, the original polyurethane (PU) discs were replaced by extra designed aluminium discs.

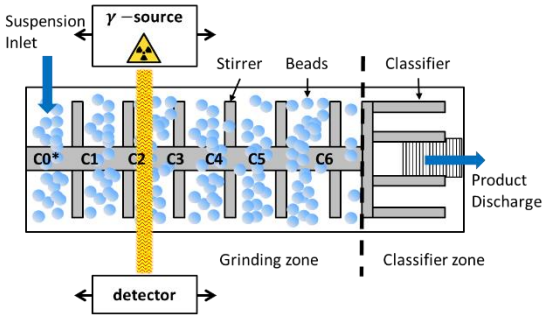

Fig. 1. M4 IsaMill™ and radiometric densitometer setup

The axial grinding media filling ratio lengthwise to the M4 IsaMill™ was measured by a radiometric densitometer. This method enabled the determination of the local filling ratio by correlating it with the attenuation of gamma radiation. Thereby a Cs^{137} radio nuclide was used as photon emission (gamma rays). This technique exploits the attenuation of gamma radiation as it interacts with materials. Therefore, the transmitted beam was detected at the opposite side of the grinding chamber with a scintillator. In the case of mono energetic gamma radiation passing through a homogeneous material, the resulting exponential loss of intensity can be described according to Lambert-Beer's law (see equation 1). Equation 2 shows the correlation transferred to the local grinding media fill ratio (φ_i), where N_0 represents the initial count rate, N_i the count rate attenuated by the grinding chamber, k_{liquid} the attenuation by the liquid, ε the porosity of the grinding media and k_{GM} the attenuation by the grinding media.

$$I = I_0 \exp(-\rho\mu x) \quad (1)$$

$$\varphi_i = (\ln(N_i/N_0)+k_{liquid})/((1-\varepsilon)(k_{liquid}-k_{GM}))+100 \quad (2)$$

3 Results and Discussion

Each aluminium disc set was subjected to a certain stress energy (SE, see equation 3) to investigate the wear impact of different loadings on the disc. The relative mass loss of each disc set was determined in relation to the energy input over the SE, as shown in Figure 2. A linear correlation was established, from which the wear rate k as a function of the SE was obtained (see equation 4). Hence, the wear per energy increases with higher SE (see equation 5).

Diverse grinding media distributions occurred due to different values of SE resulting from various grinding bead sizes and densities per disc set. As a result of the flow, the grinding media were unevenly distributed in the individual cells of the grinding chamber, which led to different local grinding media fill degrees ϕ_i. This caused different wear rates k_ϕ depending on the local grinding media filling degrees at the individual discs. Fig. 3 shows the wear rates on single discs k_ϕ normalized to the overall filling ratio of 70 % as a function of the local grinding media fill degree ϕ_i. Increased wear rates were observed in the area of higher filling ratios and in the area of grinding media packing. Finally, it can be stated that a homogeneous grinding media distribution leads to a longer system operating time and thus, to lower maintenance costs. This can be achieved by adjusting the operating parameters.

$$SE \propto d_{GM}^3 \rho_{GM} v_t^2 \quad (3)$$

$$k(SE) \cong 0{,}1\ SE + 1{,}65 \quad (4)$$

$$\Delta m/m = k(SE) \cdot E \quad (5)$$

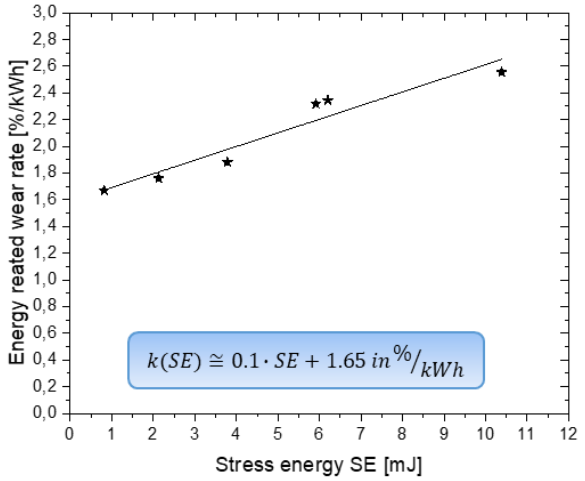

Fig. 2. Energy related wear rate with regard to the stress energy

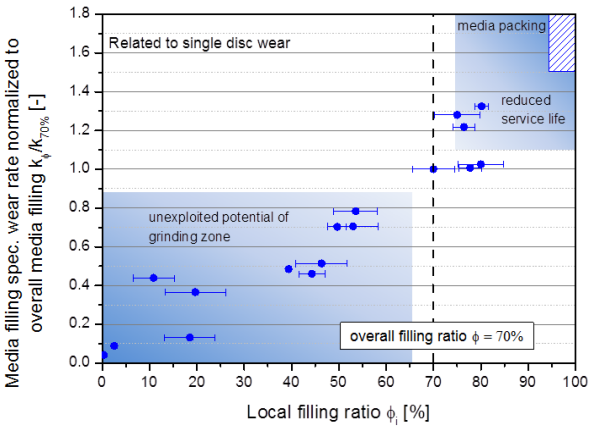

Fig. 3. Normalized media specific wear rate related to the local filling ratio

References

Anymadu, A.K., Rule, C.M., Konopjes, L., (2006). The development of ultra-fine grinding at Anglo Platinum, South African Institute of Mining.

Rule, C., Waal, H., (2011). IsaMill™ Design Improvements and Operational Performance at Anglo Platinum.

Schons, D., Kwade, A. (2019), Determination of the axial grinding media distribution in the IsaMill™ using radiometric densitometry. *Minerals Engineering*, 130, 110-116.

ID58 - Classification of de-dusting residues

Christof Lanzerstorfer[1,*]

[1]School of Engineering, University of Applied Sciences Upper Austria, WELS, Austria

Summary. In steel mill as well as in cement mills large amounts of dust are generated and separated from the off-gas by dust separators. The resulting residues are fine grained and enriched in components volatile under the process conditions like zinc, lead and alkali chlorides. The concentration of the re-condensed matter is higher in fine particles. Since these components are often problematic in the recycling of the residues, the removal of the finest size fraction from the residues can improve recycling possibilities. In some cases, the enriched fine fraction could also be used for the recovery of the volatile components as products. For the separation of the finest size fraction of de-dusting residue air classification would be appropriate because of the required cut size of the classification of few micrometre.

1 Introduction

Large amounts of dust are generated in steel mills as well as in cement mills. The residues from de-dusting of the off-gases are fine granular materials, which either have to be used in some way or disposed of in landfill sites. The residues are enriched in components volatile under the process conditions, especially with Zn, Pb and alkali chlorides. Once vaporized in the process, the vapour condenses on existing particles when the temperature in the off-gas decreases. The smaller the dust particles contained in the off-gas the higher is their specific surface area. Thus, the concentration of re-condensed matter is higher in finer particles. In the recycling of the dusts the volatile components are usually unwanted. Due to the size dependence of the concentration of volatile components classification is a feasible process to reduce such components in the bulk of the residue by separating off the finest fractions. The treatment of the sludge from wet off-gas cleaning of blast furnaces (BFs) by hydro-cyclones is a well-established process (Lajtonyi, 2006; Butterworth et al., 1996 ; Großpietsch et al., 2001). Thereby, the fine fraction enriched in Zn is separated from the coarser fraction of the sludge.
This paper discusses possible applications of air classification for the treatment of residues from dry de-dusting systems in steel mills and cement mills.

2 De-dusting residues

2.1 Particle size

The de-dusting residues are fine grained, the size of the dust particles ranges from submicron to several hundreds of micrometre. Typical particle size distributions of dusts separated from the off-gas of various processes are shown in Fig. 1.

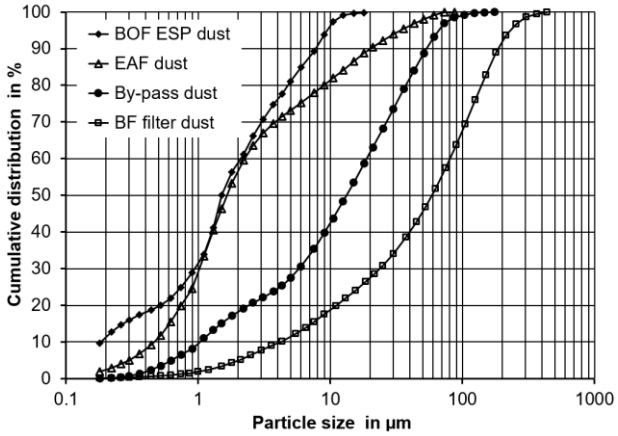

Figure 1. Typical size distribution of de-dusting residues

Due to the required small cut size of the classification process in the range of approximately 1 to 30 µm depending on the dust treated, air classification would be appropriate.

2.1 Up-cycling of volatile components

The volatility of the components depends on the temperature in the process, on the gas composition (O_2, CO, HCl, ...), and on the composition of the solids remaining in the process (slag, ash, …). Components which are typically volatilized in steel mills and cement mills are Zn and Pb, some other heavy metals (Cd, Hg, As, …) and the alkali chlorides NaCl and KCl.
The de-dusting residues from steel mills and cement mills should preferably be recycled in one of the process steps of the mill, since they mainly consist of material processed in the mill. Alternatives to internal recycling are the extraction of valuable substances from the dusts in external processes (for example, extraction of zinc from steel mill dust) or the dumping of dusts.
A frequent problem in recycling applications is the up-cycling of volatile stable components e.g. Zn in the

steel mill or alkali chlorides in the cement mill. In such cases, the residue could be treated to reduce the content of the volatile components. This can be achieved in leaching processes. However, such wet processes usually generate waste water, which is not desired in most mills.
Air classification of the dusts would be an alternative treatment method. In the classification process the dust is split into two size fractions: the coarse fraction and the fine fraction. The coarse fraction is depleted in the volatile components and, therefore, can be recycled much easier. The fine fraction has to be discharged to an external treatment or to landfill because it is enriched in the volatile components. After air classification, the recovery of the volatile components might be more feasible because of the higher concentrations.

3 Application of air classification

3.1 Cement kiln by-pass dust

Cement kiln by-pass dust (CKBD) is usually enriched in chlorides. Reported chloride contents of CKBD are in the range of 7.5% to 17% (Heikal et al., 2002; Suzuki et al., 2002). Therefore, the CKBD often cannot be recycled into the process. In some plants, CKBD is used as a source for the production of KCl for fertilizers (Sturm & Galichet, 2012; Suzuki et al., 2002). Laboratory experiments have shown that by the use of air classification the KCl concentration in the fine fraction can be increased significantly, while at the same time the coarse fraction is depleted in chloride (Lanzerstorfer, 2016). This can improve the profitability of the leaching process as well as the recycling of the chloride depleted coarse fraction.

3.2 Steelmaking dust

The dusts from an electric arc furnace (EAF) or from a basic oxygen furnace (BOF) are enriched in Zn, which enters the steelmaking process with the scrap. Internal recycling of the dusts into the furnace leads to an up-cycling of the Zn concentration. This has to be limited because of the increased energy consumption of the furnace for the volatilization of the Zn. For the optimization of in-plant dust recycling air classification could be applied. The size dependence of the Zn concentration has been demonstrated in laboratory experiments (Lanzerstorfer, 2018, 2019). The increased Zn content of the fine fraction is an additional benefit when the Zn from the dust is recovered in external plants.

3.3 Blast furnace dust

The Zn separation in blast furnace (BF) dust by air classification has been demonstrated in pilot tests by Murai et al. (1986). In a recent study by Lanzerstorfer and Kröppl (2014) the Zn concentration in the coarse fraction consisting of 70% of the mass of the dust was reduced by approximately 40%.

4 Conclusions

Air classification shows a potential for the use in processing residues from off-gas de-dusting for increased utilization by recycling. This is on the one hand, due to the reduced concentration of the volatile components in the coarse size fraction which supports recycling of the dusts and on the other hand because of the increased concentrations in the fine fractions if the volatile components are recovered as products (KCl, Zn) in external processes.

References

Butterworth, P., Linsley, K. & Aumonier, J., (1996). Hydrocyclone treatment of blast furnace slurry within British Steel. *La Revue de Metallurgie CIT*, 93 (6) : 807-815.

Großpietsch, K.-H., Lüngen, H.B. & Theobald W., (2001). BAT an Hochöfen – eine Bestandsaufnahme zum derzeitigen Umweltschutz an Hochöfen. *Stahl und Eisen*, 121 (5): 51-57.

Heikal, M., Aiad, I. & Helmy, I.M., (2002). Portland cement clinker, granulated slag and by-pass cement dust composites. *Cement and Concrete Research*, 32, 1805-1812.

Lajtonyi, A., (2006). Blast furnaces gas cleaning systems *Millenium Steel*, 2006, 57-65.

Lanzerstorfer, C., (2016). Residue from the chloride bypass de-dusting of cement kilns: Reduction of the chloride content by air classification for improved utilization. *Process Safety and Environmental Protection* 104: 444-450.

Lanzerstorfer, C., (2018). Electric arc furnace (EAF) dust: application of air classification for improved zinc enrichment in in-plant recycling. *Journal of Cleaner Production* 174: 1-6.

Lanzerstorfer, C., (2019). Zinc Enrichment in In-Plant Electrostatic Precipitator Dust Recycling by Air Classification in Converter Steelmaking. *Steel Research International* 90(2): 1800377, 1-7.

Lanzerstorfer, C. & Kröppl, M., (2014). Air classification of blast furnace dust collected in a fabric filter for recycling to the sinter process. *Resources, Conservation and Recycling*, 86: 132-137.

Murai, T., Kometani, A., Ono, Y. & Hashimoto T., (1986). Blast furnace gas dry cleaning system and dry removal system of zinc in dry dust. *The Sumitomo Search,* 1986 (32) : 1-7.

Sturm, G. & Galichet, B., 2012. The ReduDust Project – an innovative solution for treatment of bypass dust. *Cement International*, 10(1), 60-65.

Suzuki, T., Saunders, J., Tamura, N. & Saito, S., (2002). Recovering Potassium Salt for Fertilizer Use from Chlorine Bypass Dust. *Taiheiyo Cement Kenkyu Hokoku* 162, 37-42.

ID59 - Investigation on the kinetic of a Diels-Alder reaction carried out in a vibratory ball mill

Lori Gonnet[1,2,*], *Alain* Chamayou[1], *Brigitte* Guidetti[2], *Christiane* André-Barrès[2], *Michel* Baron[1], *Michel* Baltas[2] and *Rachel* Calvet[1]

[1]Université de Toulouse, IMT Mines Albi, UMR CNRS 5302, Centre RAPSODEE, Campus Jarlard, Albi cedex 09 F-81013, France
[2]LSPCMIB, CNRS UMR 5068, Paul Sabatier University, Toulouse, France

Summary. The Diels-Alder reaction between maleimide and diphenylfulvene was carried out using mechanochemistry in a vibratory ball-mill. The influence of different grinding parameters on reaction kinetic was examined: effects of temperature, ball weight or diameter. Moreover, the solid-state mechanochemical reaction was compared with the classical synthesis in toluene.

1 Introduction

The awareness of environmental problems led scientists to imagine new processes environmentally friendly to reduce waste generation and limit solvent use. With this perspective, mechanochemistry appears as a strong emerging field to conduct organic reaction in the absence of solvent.
The Diels-Alder reaction (reaction between a diene and an alkene, also called dienophile) is widely used for the synthesis of cyclic compounds. This reaction is known as a concerted pericyclic reaction, without reaction intermediates. In this work, the Diels-Alder reaction between maleimide and diphenylfulvene (**Fig. 1.**) is carried out in solid state using a vibratory ball mill.

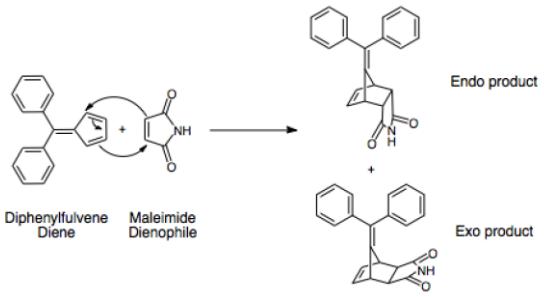

Fig. 1. The Diels-Alder reaction between diphenylfulvene and maleimide.

The influence of several process parameters on reactions kinetic was investigated: temperature, ball diameter and ball weight.

2 Experimental conditions

A vibratory ball mill, called Pulverisette 0 (P0) provided by Fritsch company (**Fig. 2**) was modified adding a heating/cooling coil around the vessel in order to obtain a better thermal control. The syntheses were performed in a stainless steel jar (9.5 cm of diameter) with a single stainless steel ball. The plate vibrates with a frequency of 50 Hz and amplitude of 1.5 mm. A mixture of diphenylfulvene (2 g, 1 mol eq) and maleimide (0.843 g, 1 mol eq) were ground.

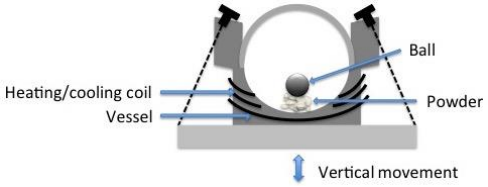

Fig. 2. Scheme of the modified Pulverisette 0

3 Results and discussion

The mechanical reaction is very selective leading to a very small amount of exo product (less than 3 %) whatever the operating conditions.

3.1 Effect of temperature

The reaction between maleimide and diphenylfulvene using P0 was studied under different temperatures. **Fig. 3** shows clearly significant conversion ratios and the reaction rate increase with the temperature.

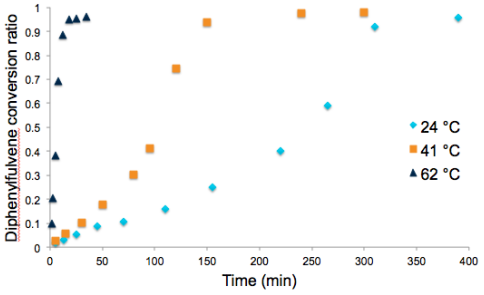

Fig. 3. Diphenylfulvene conversion ratio over time at different temperatures

3.2 Effect of ball weight

The ball-to-powder weight ratio is an important parameter (Oliveira et al., 2016; Suryanarayana, 2001). To evaluate its influence, two 50 mm stainless steel balls of respectively 507 g and 109 g were used and the vessel temperature was fixed at 41 °C. **Fig. 4.** shows an increase of the reaction rate for a heavier ball in particular after 1 h grinding time.

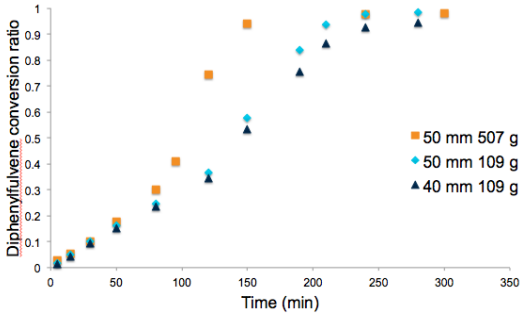

Fig. 4. Effect of ball weight and ball diameter

3.3 Effect of ball diameter

The ball diameter can also play an important role (McKissic et al., 2014) and its influence was studied. Two stainless steel balls of 109 g with 50 mm and 40 mm diameter and a vessel temperature of 41 °C were used. **Fig. 4.** shows a faster reaction with the ball of 50 mm diameter. This result may be explained by the powder amount affected in each impact that is higher with the biggest ball.

3.4 Comparison of solid-state and liquid-state reactions

The Diels-Alder reaction was studied in solution to compare with the mechanochemical one. The synthesis is less selective (exo product reaches 10 % in toluene and 3 % using mechanochemistry) in solution than in mechanochemistry and not quantitative (20 % of diphenylfulvene remaining at 450 min) (**Fig. 5.** a). Moreover, the comparison between mechanochemical and classical reaction (**Fig. 5.** b) shows a faster reaction in toluene until 100 min, but after mechanochemistry enables to reach a better diphenylfulvene conversion ratio until total conversion at 240 min.

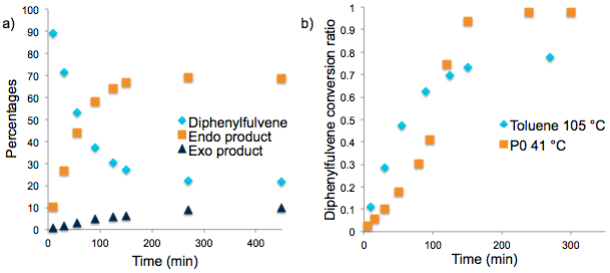

Fig. 5. a) Diels-Alder reaction in toluene at 105 °C b) Diels-Alder reaction comparison between mechanochemistry at 41 °C and toluene at 105 °C

3.5 Reaction progression after grinding

The Diels-Alder reaction continues after grinding. Two experiments were performed at 24 °C with 15 min and 1 h of co-grinding. **Fig. 6.** shows the reaction progression after stopping the grinding step at the same temperature. A greater reaction rate is observed for a longer grinding time. Further studies should be interesting to optimize the ratio between grinding time and aging time in order to reduce the energy consumption.

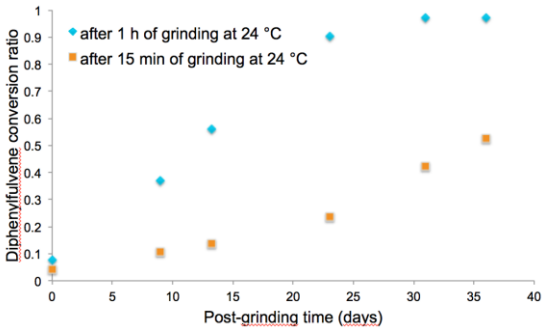

Fig. 6. Monitoring the post-grinding reaction

4 Conclusion

The Diels-Alder reaction using mechanochemistry is quicker and more selective compared to the liquid-state reaction. To improve the synthesis, several process parameters can be changed. The experiments show that an increase in the reaction rate is accomplished with the help of a bigger and heavier ball. Finally, the synthesis continues after grinding until a complete reaction. This method can be a good way to conduct organic reactions considering the 12 Green Chemistry Principles (Anastas and Warner, 2000), with a reduced energy consumption and without solvent.

References

Anastas, P.T., Warner, J.C., (2000). Green Chemistry, Theory and Practice. *Oxford University Press.*

McKissic, K.S., Caruso, J.T., Blair, R.G., Mack, J., (2014). Comparison of shaking versus baking: further understanding the energetics of a mechanochemical reaction. *Green Chemistry.* 16, 1628–1632.

Oliveira, P.F.M., Baron, M., Chamayou, A., Baltas, M., Guidetti, B., Haruta, N., Tanaka, K., Sato, T., (2016). Lowering the Activation Energy under Mechanochemical Conditions: The Case of 2,3-diphenylquinoxaline. *ChemistrySelect,* 5, 984–988.

Suryanarayana, C., (2001). Mechanical alloying and milling. *Progress in Materials Science,* 46, 1–184.

ID62 - Development of a laboratory test to quantify the size segregation in stockpiles

Ziming Ye[1], *Mohsen* Yahyaei[1*], *Marko* Hilden[1] and *Malcolm* Powell[1]

[1]Julius Kruttschnitt Mineral Research Centre, University of Queensland, Brisbane, Australia

Summary. Large coarse ore stockpiles are very common in mine sites. The uniform output from the stockpile is essential for stable operation in the downstream equipment and the whole comminution circuit. However, due to size segregation in stockpiles which is inevitable, the particle size distribution of stockpile product can vary significantly. Therefore, it is important to understand size segregation in materials handling and storage units. However, it is very difficult to quantify size segregation of an industrial stockpile due to the size of the stockpile. Therefore, this research has focused on developing a laboratory experiment which allows quantifying the size segregation of stockpiles and extends the results to industrial scale. The result of preliminary lab tests indicated that it is possible to quantify size segregation in a laboratory and to scale up the results.

1 Introduction

Stockpiles and bins are very common in mine sites and their design can play a significant role in circuit performance. However, in general neither at the plant design stage nor during the process optimisation, they do not receive as much attention as comminution and classification units. For example, segregation of coarse and fine particles which is a common phenomenon in most storage facilities and transfer-points could have severe impact on performance of comminution and classification units (Yahyaei & Powell, 2018). The term segregation in bulk handling and storage means uneven distribution of materials due to difference in their properties such as size, shape, density, etc (Skorych, Dosta, Hartge, & Heinrich, 2017). In mining processes, the segregation occurs throughout the whole process from the load and haul to waste disposal. However, this issue has a significant impact when it occurs in bins and stockpiles, in particular, during the filling and discharging process(Shinohara & Golman, 2002).The size segregation will result in uneven distribution of material to parallel units or uneven feed to a unit which consequently results in poor performance of process units. For example, the different feeders placed at different location of a stockpile will receive different size particles over the time because of the size segregation. This phenomenon will introduce surges to the downstream process and might cause fluctuations in performance of the comminution and classification units.

In a mine site, stockpiles contain hundreds or thousands of tons material ranging from few microns up to a meter. Therefore, practically it is impossible to quantify size segregation of an industrial stockpile. Therefore, development of a small scale test to quantify size segregation in stockpiles will be beneficial. This research presents a laboratory test which is designed for quantifying size segregation which can be utilised for quantification of size segregation in full scale as well as validation of numerical modelling. The proposed laboratory scale test is based on the assumption that if the shape of the particle size distribution of a material is the same for different top size, it will result in a same size segregation behaviour and it will give the same size segregation index.

2 Method and Materials

2.1 Materials and sample preparation

To validate the hypothesis behind the laboratory scale test for qualifying size segregation, a typical particle size distribution from primary crushing of a coper/gold ore is used to create three sample with top sizes 42.5mm, 22.5mm, and 11.2mm. All three groups have identical shape of particle size distribution as it is presented in Fig 1 but their top sizes are different. The sample used in this research is a copper/gold ore sourced from a mine in Australia.

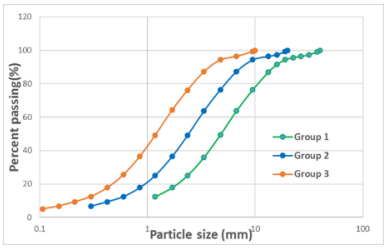

Figure 9 Particle size distribution of three groups

* Corresponding author: info@escc2019.com

Two sets of size segregation test were conducted with all three groups. The first set was conducted with materials of only five selected size fractions from each group (marked with * in table 1). The second set was conducted with the full size distribution for each group. Conducting test with only five size fractions for each group is very convenient and it will make it possible to use coloured rocks to test possibility of utilising image processing for automatic quantification of size segregation. Whereas, including all size classes in the experiment is to validate that results of five size fraction is consistent with the results of full particle size distribution.

Table 1. Size classes of three group used for lab scale size segregation test

Group 1	Group 2	Group 3
-42.5+37.5mm*	-22.5+19mm*	-11.2+9.5mm*
-37.5+31.5mm	-19+16mm	-9.5+6.7mm
-31.5+26.5mm	-16+13.2mm	-6.7+4.75mm
-26.5+22.5mm*	-13.2+9.5mm*	-4.75+3.35mm*
-22.5+19mm	-9.5+6.7mm	-3.35+2.36mm
-19+16mm	-6.7+4.75mm	-2.36+1.7mm
-16+13.2mm*	-4.75+3.35mm*	-1.7+1.18mm*
-13.2+9.5mm	-3.35+2.36mm	-1.18+0.85mm
-9.5+6.7mm	-2.36+1.7mm	-0.85+0.6mm
-6.7+4.75mm*	-1.7+1.18mm*	-0.6+0.425mm*
-4.75+3.35mm	-1.18+0.85mm	-0.425+0.3mm
-3.35+2.36mm*	-0.85+0.6mm*	-0.3+0.212mm*
-2.36+1.7mm	-0.6+0.425mm	-0.212+0.15mm
-1.7mm	-0.425mm	-0.15mm

2.2 Size segregation quantification test

To conduct the size segregation test, feed from each group is divided into 8 subsamples with equal mass to be fed to stockpile in sequence. This practice was done to reduce the size segregation during the feeding process. Feed passed through a funnel which was placed at the designed height to create stockpile.

The scoping experiments were conducted with positioning the funnel at three different heights for each group. Two different overall mass was also tested for Group 2 and Group 3. The scoping tests were conducted with the objective to identify if the drop height and size of the stockpile will results in a different size segregation. However, the results proved that the drop height and size of the stockpile do not play a role in size segregation.

Once the stockpile is formed, each stockpile was divided into 5 circular sections which is positions at the same relative distance from the centre of stockpile using a special cutter presented in Fig. 2.

Figure 2 The sample cutter used for Group 2

Materials collected from each section were then sized to measure the size distribution of each section and compare against the feed size distribution. The size distribution of materials of equivalent sections from each group were compared against each other to validate the underlying assumption of the lab scale size segregation test.

3 Results and Discussion

The data from 5 sections are combined to form two sections: inside and outside for convenience in presenting the results in this paper.

Comparing the size segregation results for three group is presented in Fig 3.

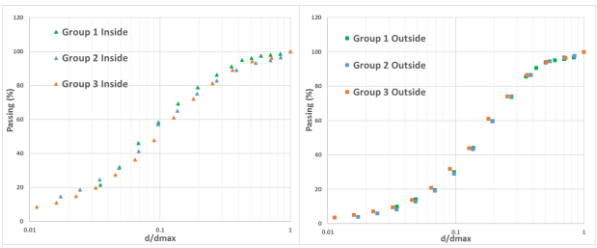

Figure 3 Normalized data for inside and outside for the three groups

The result shows that the underlying assumption for the lab scale test holds within the range this experiment is conducted. The research aims at collecting data from larger stockpile from industry to extend the range of sizes tested and further validate the hypothesis.

References

Shinohara, K., & Golman, B. (2002). Segregation indices of multi-sized particle mixtures during the filling of a two-dimensional hopper. Advanced Powder Technology, 13(1), 93-107.

Skorych, V., Dosta, M., Hartge, E.-U., & Heinrich, S. (2017). Novel system for dynamic flowsheet simulation of solids processes. Powder Technology, 314(Supplement C), 665-679.

Yahyaei, M., & Powell, M. (2018). Production improvement opportunities in comminution circuits. Paper presented at the Mill Operators conference, Brisbane, Australia.

ID63 - A New Impact Breakage Assessment Tool for Acicular Particles

Wei Pin Goh, *Saba* Saifoori, *Muzammil* Ali and *Mojtaba* Ghadiri

Faculty of Engineering, University of Leeds, Leeds, UK

Summary. Acicular particles are frequently encountered in pharmaceutical and fine chemical industries. Their breakage is influenced not only by their mechanical properties (hardness, stiffness and toughness), but also by their aspect ratio, as the bending moment can induce high tensile stresses. It is therefore important to develop a method to investigate their breakage quickly and using small amounts of such materials. An experimental work has been carried out for investigation of the breakage of acicular particles in Morphologi G3 at various pressures, as it uses the smallest quantity of powder sample for analysis. The impact velocity of the particles during dispersion in G3 at different pressures is estimated by CFD calculations. The breakage mechanism of the acicular particles is investigated by means of the morphological information of the broken products provided by the in-built image analysis suite. By comparing the size distributions of the feed and broken particles, the resulting extent of breakage is determined. Three different materials, namely β-glutamic acid, benzothiazine and potassium phosphate are used as the model test materials. The breakage data are then analysed using a modified impact breakage model, and the results will be presented

1 Introduction

Acicular crystals are a norm in the pharmaceutical industry. Very often, the size distribution of the end product after crystallisation does not possess the desired characteristics that are essential for further downstream processing. Hence, intentional comminution processes such as milling and grinding is normally used to reduce the particle size down and to a narrow distribution to improve the bioavailability of the drug, compactability and tabletability, etc (Rowe, 2006). The focus of this paper is on developing a new method to assess the breakage of acicular particles under impact loading. Being able to assess the processability issues prior to mass production is of great interest of the pharmaceutical industry, especially when the formulation is still in clinical trial stage, and the available quantity of the material is scarce. Predicting the milling behaviour of new active pharmaceutical ingredients remains a challenge as its grindability is unknown and its milling performance is untested before. Though there exists a wide range of assessment techniques (both quasi-static and dynamic conditions) in the literature, those testing devices are often not commercially available. The demand of having a grindability assessment tool commercially available has led to the work of Bonakdar et al. (2016) in which they develop a method based on Ghadiri and Zhang (2002) model to assess the grindability of materials using the dry dispersion unit of a commercial particle size analyser, the Scirocco disperser of Mastersizer 2000. The breakage propensity is expressed in the shift of specific surface area, which can be easily calculated from the size distribution measured by laser diffraction technique. This new assessment technique has proven to agree very well with the results obtained from the single particle impact tester. However, a huge fraction of pharmaceutical materials is highly acicular in shape and laser diffraction is known to give false representation of the particle size of high aspect ratio particles, hence using this technique for acicular particles is inadequate. For acicular particles, a better technique to measure their size distribution would be by optical image analysis, where the actual particle size and shape are measured directly and not inferred from laser light scattering data. In this paper, Morphologi G3 of Malvern Panalytical, a particle size analyser based on static optical imaging analysis technique is used to assess the breakage of carbamazepine dihydrate crystals under impact loading. The source of impact comes from the dry dispersion unit of the device, where a pulse of pressurised air is released, by which the particles in the sample well are dispersed and impact on to the internal wall of the spool before settling down onto a glass slide for subsequent size and shape analysis. In this study, a modified Ghadiri and Zhang (2002) model is used to analyse the breakage data of acicular particles. The impact velocity of particles in the sample dispersion spool is calculated using CFD modelling. The same approach as of the work of Ali & Ghadiri (2017) is adopted using a Lagrangian method of calculation of particle velocity, but with Ganser (1993) shape-dependent correlation to account for the drag on non-spherical particles. The shift in the particle size distribution is then used following the approach of Bonakdar et al. (2016) to estimate the breakability of the acicular particles.

2 Methodology

A small amount of sample (~5 mm^3) is first placed into the dispersion spool of the dry dispersion unit of

Morphologi G3. A pulse of pressurised air is then applied to disperse the particles, as a result of which they impact against the internal walls of the spool and possibly break before they exit the disperser and settle down onto the glass slide inside the collection chamber. The individual particle morphological properties are then analysed using the built-in image analysis suite.

The extent of breakage, R^* gives a measure of the amount of debris produced after a breakage event, normally expressed on gravimetric basis, given by Eq. 1. This gravimetric ratio can be converted to volumetric ratio as the density is the same for all the particles.

$$R^* = \frac{M_d}{M_f} = \frac{V_d \times \rho}{V_f \times \rho} = \frac{V_d}{V_f} \quad (1)$$

where M_d is the mass of debris, M_f is the mass of feed, V_d and V_f are the cumulative particle volumes (not the bulk volume) of debris, and the feed, respectively and ρ is the density of the particles. This relationship can further be simplified and expressed as a ratio of projected areas if the thickness term is considered constant for all sizes:

$$R^* = \frac{M_d}{M_f} = \frac{V_d}{V_f} = \frac{A_d \times h}{A_f \times h} = \frac{A_d}{A_f} \quad (2)$$

where h is the thickness of the particles, A_d the projected area of debris and A_f the projected area of feed particles. can be obtained by subtracting the reference PSD (subjected to the lowest dispersion, 0.5 barg) from the PSD of interest. The integral of the positive difference as illustrated in Fig. 10 can be calculated using Eq. 3 and Eq. 4.

$$S_i = B_i - B_{ref,i} \quad (3)$$

$$R^* = \sum_{i=1}^{n} S_i \left[S_i > 0 \right] \quad (4)$$

where S_i is the difference between the area percentage of the reference PSD, $B_{ref,i}$ and the PSD of interest, B_i of the particle size bin number i and R^* the sum of the positive differences between the two PSDs up to bin number n (the particle size is segmented into 1001 bins in the Morphologi G3, maximum particle size being 2 mm).

4 Conclusions

A new breakability assessment technique has been used to study the extent of impact breakage of acicular particles. The shift of particle size, length, width and aspect ratio are analysed, assessing the tendency of breakage along their largest dimension, due to bending arising from the geometric effect of the high aspect ratio Nevertheless, breakage along the crystallographic cleavage plane of weakness is also observed to a minor extent. These observations suggest that the breakage is dominated by both fracturing perpendicular and cleaving parallel to the particle length. A full particle size distribution is used in the test due to difficulty of classifying the crystals in narrow size ranges. The breakability index is determined by plotting the graph of R^* versus $\sum \rho dV^2$, where a non-linear relationship is noted (Figure 1). There exists a transition point at which the rate of change the particle size is reduced, corresponding to a switch in the breakage mode. The first breakability index is higher than the second one and corresponds to the snapping of the particles along their length, while the latter smaller one is associated with chipping. This work demonstrates that by using a combination of image analysis and modified impact breakage model, the role of crystal structure properties, particularly the existence of cleavage planes, together with the physical geometric properties on the breakage behaviour of crystals can be isolated and studied individually.

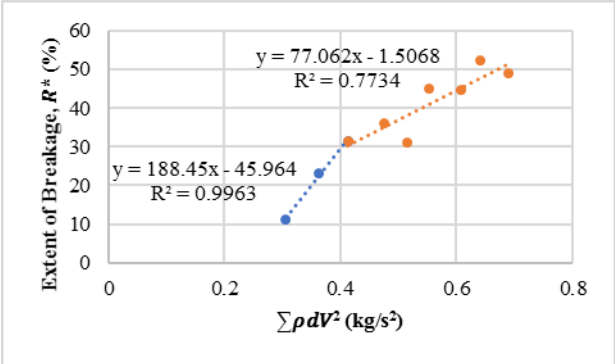

Fig. 1. Breakability of β L-glutamic acid

References

Ali, M., & Ghadiri, M. (2017). Analysis of triboelectric charging of particles due to aerodynamic dispersion by a pulse of pressurised air jet. *Advanced Powder Technology*, *28*(10), 2735–2740.

Bonakdar, T., Ali, M., Dogbe, S., Ghadiri, M., & Tinke, A. (2016). A method for grindability testing using the Scirocco disperser. *International Journal of Pharmaceutics*, *501*(1–2), 65–74.

Ganser, G. H. (1993). A rational approach to drag prediction of spherical and nonspherical particles. *Powder Technology*, *77*(2), 143–152.

Ghadiri, M., & Zhang, Z. (2002). Impact attrition of particulate solids. Part 1: A theoretical model of chipping. *Chemical Engineering Science*, *57*(17), 3659–3669.

Rowe, R. (2006). *Handbook of pharmaceutical excipients*. London Greyslake, IL Washington, DC: Pharmaceutical Press American Pharmacists Association.

ID64 - Modelling iron ore desliming in hydroclones

Luciana P. Alves[1], *Juliana* Salazar-Segura[1], *Henrique D.G.* Turrer[2], *Aubrey N.* Mainza[3], *Luís Marcelo* Tavares[1,*]

[1]Department of Metallurgical and Materials Engineering, COPPE-UFRJ, Universidade Federal do Rio de Janeiro, Rio de Janeiro, Brazil
[2]Anglo American, Minas Rio, Conceição do Mato Dentro, Minas Gerais, Brazil
[3]Centre for Minerals Research, University of Cape Town, Cape Town, Republic of South Africa

Summary. With the progressive impoverishment of run-of-mine iron ore head grades, upgrading by flotation has become widespread in the iron ore industry in Brazil. Successful reverse flotation of these ores requires removal of the ultrafine (slime) fraction, which is carried out in hydrocyclones. Given the fine cut sizes involved in this operation, small-diameter hydrocyclones have become favoured. The work investigates the performance of 4" and 2.5" hydrocyclones in desliming of iron ore from the Minas Rio mine in Brazil, through experiments conducted both in pilot plant and in industry. Data have then been fitted to Narasimha-Mainza hydrocyclone model, which has demonstrated good ability to represent the performance of the hydrocyclones under a range of operating conditions.

1 Introduction

With the progressive reduction in iron contents in the run-of-mine ores in the main production region in Brazil, located in the state of Minas Gerais, upgrading through concentration has become a necessity. The leading process that has been used in their concentration is flotation, carried out by floating the gangue minerals, mainly quartz, and depressing the iron minerals. Removal of excessively fine material (slimes) from the feed of flotation is a requirement for the success of this operation, given the potential competition of slimes for the collection (amine) (Araujo et al., 2005).

Desliming in this industry is carried out in hydrocyclones, which often operate in multiple stages. Given the fine cut sizes involved, in the order of 10 μm, small diameter hydrocyclones, typically as small as 4", have been used. Unfortunately, the literature lacks auditable data in this task and the suitability of mathematical models currently used to simulate it has not been investigated systematically.

The work presents results from experiments conducted both in industrial and pilot-plants on 4" and 2.5" hydrocyclones, investigating the effect of several operating variables and fitting the mathematical model by Narasimha-Mainza.

2 Experimental

Experiments have been carried out both in continuous mode in the industrial Minas Rio circuit, located in Conceição do Mato Dentro (MG), as well as in classification test rigs, in which cyclones were operated in closed loop (Fig. 1). In the pilot-plant experiments have been carried out with both the industrial 4" (106 mm) hydrocyclones and with 2.5" (64 mm) diameter hydrocyclones. Variables studied included the percent of solids in the feed, the inlet pressure, the apex and vortex finder diameters and the feed size distributions.

Fig 1. Comparison between the modelled and simulated t_4 values for drop weight tests of 5.5 mm particles for different impact energies

Size analyzes have been carried out by laser scattering in Malvern Mastersizer 2000. Data from the tests, namely size analyzes, percent solids and feed and product flowrates, were reconciled using the JKSimMet software (Grimes and Keenan, 2015).

3 Results

Data from a total of 26 experiments have been validated and used as the basis for modelling feed flowrate, water split to the underflow stream, corrected d_{50} and sharpness of separation. Parameters of the Narasimha-Mainza models have been estimated and a summary is given in Table 1. In the case of the model for the corrected cutpoint, only a marginal fit of the model to the data has been observed.

Table 1. Summary of values of Narasimha-Mainza parameters for desliming of iron ore

Model	Value	Number of data sets
Capacity – K_{Q0}	0.074	26
Water split – K_{W0}	5.008	20
d50c – K_{D0}	0.00079	24

The sharpness of separation has been estimated by superimposing data from the tests in a normalized curve (Fig. 2). It shows that a reasonable fit could be reached with a value of alpha of about 1.2 in the Lynch model, which characterizes poor separation performance.

Finally, evidence existed of the fishhook phenomenon for particles with sizes smaller than about 10 microns, but this was not incorporated in the model at this time.

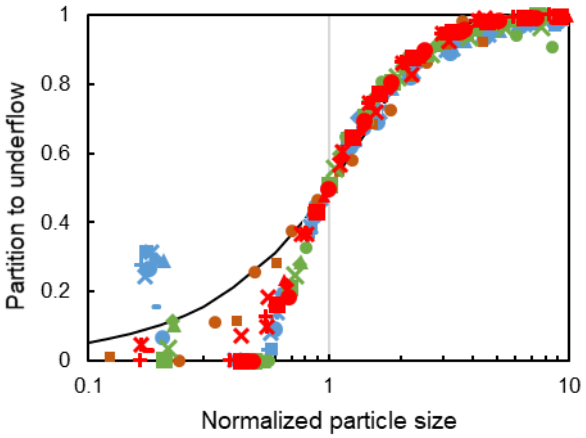

Fig 2. Normalized and corrected partition curves for the various datasets (the solid line represents the fit to the Lynch model).

4 Conclusions

Data from the industrial surveys as well as pilot-plant tests in a closed-circuit test rig could be well described using the Narasimha-Mainza models for capacity and water split. Data on the corrected d_{50} demonstrated to respond only marginally to the operating and design conditions, resulting in less confidence of this part of the model. Finally, the sharpness of separation demonstrated to be relatively independent of operating conditions, equal to a value of 1.2.

ID65 - Qualitative evaluation of the grinding efficiency of a gravity induced stirred mill using the size specific energy approach

Priscila Esteves[1,*], *Douglas* Mazzinghy[1], *Marko* Hilden[2], *Mohsen* Yahyaei[2], *Malcolm* Powell[2] and *Roberto* Galery[1]

[1]PPGEM, Federal University of Minas Gerais, Brazil
[2]JKMRC, University of Queensland, Australia

Comminution is the most energy intensive process in mining industry, due to its low efficiency. Comminution efficiency decreases with particle size, providing a great incentive for the optimisation of fine grinding applications. Related to this issue, the Size Specific Energy (SSE) approach is a technique that provides a better evaluation of comminution efficiency, once it takes in account the generation of fines and it is less dependent on particle shape. Based on this, the SSE can be used as a benchmarking for fine grinding evaluation. The aim of this paper is to apply the SSE approach to the evaluation of grinding efficiency of gravity induced stirred mills. Batch grinding experiments were conducted in a laboratory gravity induced stirred mill using an iron ore sample with a top size of 0,180mm.

1 Introduction

Comminution is the most energy intensive process in mining industry, due to its low efficiency (Napier-Munn, 2015). Comminution efficiency decreases with particle size, providing a great incentive for the optimisation of fine grinding applications.

At the same time, the gradual depletion of the mineral resources and lower ore grades increase the importance and need for fine grinding operations. For the specific case of iron ore, the availability of high-grade iron ore coarse material presents a continuous depletion and for this reason, there is an increasing need for fine grinding of iron ores that liberate at smaller sizes and present greater proportions of silica grades (Eswaraiah and Venkat, 2015).

Due to the increasing need for fine grinding applications and to the reduced energy efficiency of the comminution of fine materials, it is very important to focus on process optimizations. The first stage of optimization is the establishment of a benchmarking for energy efficiency of those processes (Ballantyne, 2018). Related to this issue, the Size Specific Energy (SSE) approach is a technique that provides a better evaluation of comminution efficiency, once it takes in account the generation of fines and is less dependent on particle shape (Ballantyne, 2018).

2 Methodology

A batch gravity induced stirred mill of approximately 25L was used to conduct test work using an Itabirite iron ore sample with a top size of 0,180mm and 15mm high chrome steel balls as grinding media. Solids percentage was fixed at 65%, balls filling as 80% and torque and speed were measured at a 10 Hz sampling frequency.

Speed selection was based on equipment database presented by Mazzinghy et al. (2017) for the relation between screw speed and screw diameter, as shown in Figure 1.

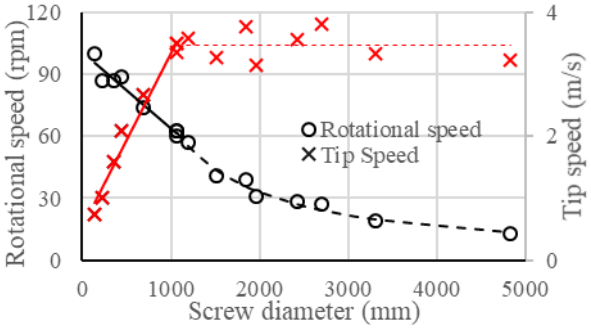

Fig. 1. Relation between screw diameter and rotational speed for gravity induced stirred mills. Adapted from Mazzinghy et al. (2017)

For screw diameters greater than one meter, the trend seems to follow a fixed tip speed relationship. However, for smaller diameters tip speed is approximately proportional to diameter. Based on the equipment dataset, the following model is considered:

$$\omega = -0.037d + 101.35 \quad d < 1000$$
$$\omega = 66.08\left(\frac{d}{1000}\right)^{-1} \quad d > 1000 \qquad (1)$$

$$v = 0.0028d + 0.5392 \quad d < 1000$$
$$v = 3.46 \quad d > 1000 \qquad (2)$$

ω = rotational speed (rpm)

v = tip speed (m/s)

d = screw diameter (mm)

Samples were obtained during different grinding times and a Cilas laser was used for obtaining the particle size distribution (PSD). A 0,038mm marker size was selected for evaluation of Size Specific Energy.

The SSE is calculated as shown in Equation 1:

$$SSE_{38}\left(\frac{kWh}{t}\right) = \frac{SE}{\%-38\mu m\ generated} \quad (1)$$

3 Results

Figure 2 shows the obtained results for the batch grinding test. It can be seen that the data is modelled with two different lines, inferring that the material consists of two breakage components. As hematite mineral is considerably softer than quartz mineral, the steepest slope confirms that hematite mineral breaks faster than quartz mineral. Quartz mineral needs more impacts to break in the same grinding environment, and this means more time to break when compared to hematite mineral. Consequently, the quartz mineral breakage occurs later as it is a harder material.

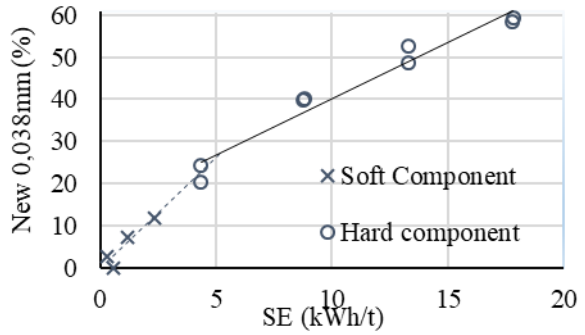

Fig. 2. Relationship between cumulative 0.038mm production and energy input.

In addition, torque and speed were measured for different balls filling running the mill with only balls and water. The results for net power are shown in Figure 3. Net power for industrial equipment were obtained by Esteves (2016) under similar conditions and are shown together for comparison purposes. Despite the scale difference, it is possible to note that both curves present similar behaviour, with a quadratic relation between balls filling and power.

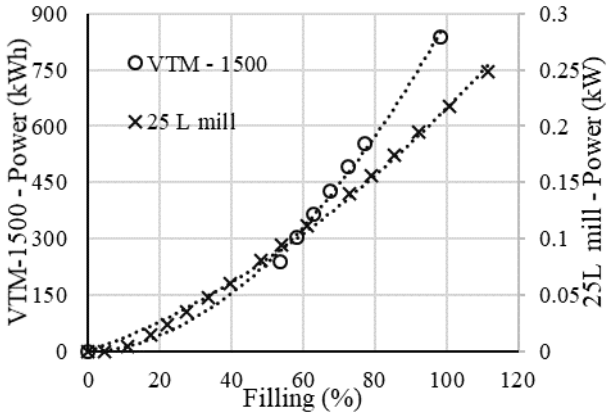

Fig. 3. Relation between balls filling and net power for a 25L laboratory mill and an industrial VTM-1500

4 Conclusions

The paper proposes the use of SSE approach for the evaluation of energy efficiency of fine grinding processes. Test work was conducted with a laboratory gravity induced stirred mill for grinding of an iron ore sample. The SSE approach indicated that the material contains two different breakage components, due to hardness differences between Hematite and Quartz minerals present in the investigated iron ore.

The results indicate that SSE is a valid methodology for the energy efficiency analysis of fine grinding applications and can be used for the evaluation of equipment performance.

Speed selection was made based on an existing equipment database set, and for this speed, the relation between filling and power was similar to industrial measurements.

Acknowledgments

This work was conducted during a scholarship financed by CAPES at the University of Queensland. The authors would like to thank CAPES for the financial support and the JKMRC-SMI and PPGEM-UFMG for the collaborative support.

References

Ballantyne, G., 2019. Assessing comminution energy efficiency with the Size Specific Energy (SSE) approach, 16th *European Symposium on Comminution & Classification (ESCC 2019)*, 2-4 September 2019, Leeds, UK

Esteves, P., Stopa, M., Galery, R., Mazzinghy, D., & Russo, J. (2016). Relation between electrical power and media filling for vertical mills. *Tecnologia em Metalurgia, Materiais e Mineração*, pp. 288-294. (In portuguese)

Eswaraiah, C., & Venkat, N. (2015). Modeling of Vertical Stirred Mill using an objective experimental design. *56th Annual Technical Session*, (pp. 102 - 111). India.

Mazzinghy, D., Carvalho, R., Rodriguez, V., Tavares, M., Teixeira , C., & Galéry, R. (2017). Numerical analysis of vertical stirred mills scale-up using discrete element method. *Computational Modelling '17* , (pp. 1-14). Falmouth.

Napier-Munn, T. (2014). Is progress in energy-efficient comminution doomed? *Minerals Engineering*, 73, pp. 1-6.

ID66 - Versatile crusher control and cloud computing process monitoring

Gauti Asbjörnsson[1], *Anton* Bolander[2], *Erik* Hulthén[1] and *Magnus* Evertsson[1,*]

[1]Department of Industrial and Materials Science, Rock Processing Systems, Chalmers University of Technology, Göteborg, Sweden
[2]Roctim AB, Hugo Grauers gata 11, 411 33, Göteborg, Sweden

Summary. The main task of a crusher control system is to keep production on a desired level and to protect the crusher from overload and fatigue failure. A stable production can be achieved through control of the crusher's closed side setting (CSS), which implies compensation of the wear of the crusher liners. A further objective is to provide with the possibility to optimize operational performance and utilization. For an efficient system the sampling rate needs to be sufficiently high and the control and optimization algorithms need to be robust. In addition and equally important, configuration of the electrical cabinet and wiring must be able to withstand the harsh environment. Modelling and simulation of cone crushers have been on-going at Chalmers University of Technology during the last 25 years. Over time the research has expanded to include several different aspects of cone crusher operation, design optimisation, real-time control and product yield optimization. As a consequence a strong need for dedicated control possibilities of cone crushers have risen. The requirement for precise control led to the development of a new system for crusher control which was named Crusher Control Unit or CCU. The system have been further developed by Roctim to provide an independent, modular and flexible development platform for different crusher types. A unique feature is that the CCU can be retrofitted to both Hydrocone type of cone crushers as well as to Symons type independent of brand or age of the crusher.

1 Introduction

An essential part of minerals processing is the liberation of elements from the ore. This is achieved through particle size reduction, either with crushers and/or mills. The performance of a crushing unit or a plant determines the system efficiency. The crushing performance depends on the design and configuration of each individual process unit, the configuration of the plant, the design of the control system and physical properties of the incoming feed (Evertsson, 2000), (Hulthén, 2010) & (Asbjörnsson, 2015).

Compressive crushing, such as utilized in cone crusher, is energy efficient because of the utilized crushing principle and the imposed stress-state on the particles (Schönert, 1972). Crushing units do however not operate under ideal conditions and as a result the electrical and hydraulic system will experience an uneven load during operation. Also, the compressive pressure and thus the internal loads and stresses in a crusher can vary significantly during operation because of the mechanical design and material properties.

Local control units are installed with the main function of protecting the crusher from overload. Secondary functions include load control and CSS control depending on the mechanical design and the setup of the process. OEMs such as S****** and M**** supply those units with their crushers, A** for S****** and I* for M****. However not much is published regarding the functionality of those units for obvious reasons.

This paper aims to describe the work done at Chalmers Rock Processing Systems and Roctim in the development of the Crusher Control Unit (CCU) which is a versatile control development platform for crusher and process control.

2 Materials and methods

The CCU is a PLC based control unit developed for harsh conditions and flexible application. The first initial generation was developed for Hydrocone type of crushers only. This was both installed as a standalone unit as well as an embedded version in a plant control system. The next (current) generation provides more possibilities in of integration and improved adaptation. The focus was to provide a modular design which could be applied to Hydrocone type crushers (top supported main shaft, hydraulically adjustment of CSS), as the first generation, but also to Symons type crushers (normally threaded bowl adjustment of CSS) and incorporating integrated feeder control.
In order to meet modern requirements for flexibility, customization, easy installation and high customer value a modular system architecture was chosen, shown in Fig. 1. The core of the CCU control system is the

CCU Base unit. All other modules are optional depending on the user needs. The CCU can be connected to the existing plant control system and/or to a cloud dedicated for crusher monitoring which is a significant advantage. The cloud based system structure is illustrated in Fig 2. The CCU has been installed on several cone crushers and one example is the Metso Nordberg HP4 depicted in Fig. 3.

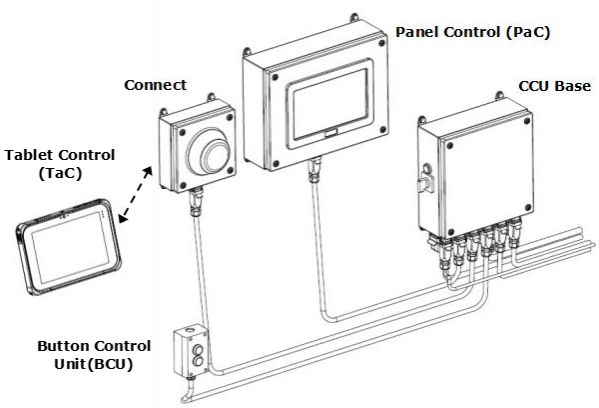

Fig. 1. Modular design of the second generation of the Crusher Control Unit (CCU).

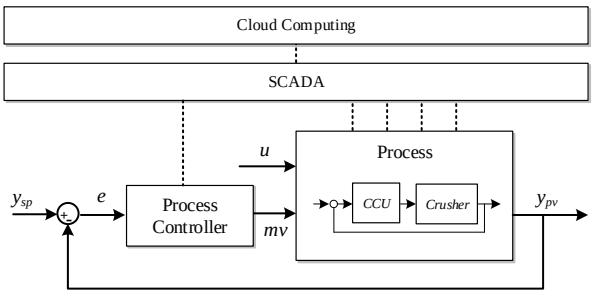

Fig. 2. System architecture for the Cloud plant wide controller and local control loop with a CCU.

Fig. 3. The CCU is installed on a Metso Nordberg HP4.

3 Results and discussion

The two crusher types act totally different to change CSS. The Symons type crusher needs to run empty before the CSS is changed, this usually causes operators not to adjust the CSS enough frequently. However, by automating this sequence with the CCU the time each adjustment takes can be minimized as seen in Fig 4.

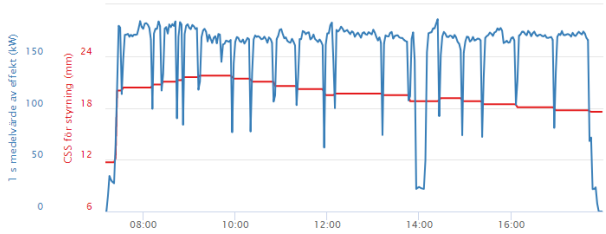

Fig. 4. Power draw and CSS during a day of operation for a Symons type crusher (HP4).

Hydrocone type crusher on the other hand can be adjusted during operation as depicted in Fig 5.

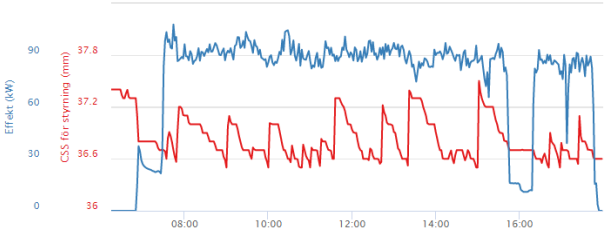

Fig. 5. Power draw and CSS during a day of operation for a Hydrocone type crusher.

4 Conclusion

Crusher control provides protection of the equipment from overload while providing improved process performance across multiple suppliers. With connection to a cloud the process performance is not only distributed within the local control system but the data is assessable anywhere.

References

Evertsson, M., (2000), Cone Crusher Performance. PhD Thesis from Chalmers University of Technology

Hulthén, E., (2010), Real-time optimization of crushing plants. PhD Thesis from Chalmers University of Technology

Asbjörnsson, G., (2015), Crushing Plant Dynamics. PhD Thesis from Chalmers University of Technology

Asbjörnsson, G., (2010), Crusher Control Unit. MSc Thesis from Chalmers university of Technology

ID68 - Numerical simulation of the Bond grindability test using a mechanistic ball mill model

Victor A. Rodriguez[1], *Renan C.* Calmon[1], *Rodrigo M. de* Carvalho[1], *Luís Marcelo* Tavares[1,*]

[1]Department of Metallurgical and Materials Engineering, COPPE-UFRJ, Universidade Federal do Rio de Janeiro, Rio de Janeiro, Brazil

Summary. A great deal of effort has been put on recent years on mechanistic models as an alternative to both empirical and phenomenological approaches to ball mill modeling. Recognizing the complexities associated with the description of material transport and internal classification in continuous mill operation, an attempt is here made to further validate it in prediction of locked-cycle grinding tests. The popular Bond ball mill grindability test emulates continuous operation by using a sequence of batch grinding and classification steps in a standardized locked-cycle test. From this it is possible to determine the ore grindability, which, in turn, is used to estimate the Bond ball mill work index. The paper simulates this locked-cycle test with the aid of a combination of batch grinding test predictions using the UFRJ mechanistic model and predictions of classification carried out with the aid of laboratory sieves. First, the collision energy spectrum for the standard Bond ball mill as well as detailed data on material breakage characterization for selected materials is presented. Predictions of batch grinding tests are then compared to experiments and a simple model is proposed to classification by dry screening that follows each grinding cycle.

Keywords: Ball mill, Bond test, impact, modeling

1. Introduction

Closed-circuit grinding involving ball mills for fine size reduction and cyclones for classification is the usual circuit configuration utilized in the mineral industry to prepare an ore for further downstream processing (Fuerstenau et al., 1984). Locked-cycle grinding tests are widely used for assessing the grindability of industrial minerals and ores for design and scale-up of grinding mills (Rowland and Kjos, 1980) and also for studying the probable behavior of industrial grinding circuits under different operating conditions. These tests simulate on the laboratory scale a tumbling mill operating under plug flow conditions in closed-circuit with a perfect classifier (Kapur and Fuerstenau, 1989).

A good practice in the pursuit to validate a model is comparing its predictions with established procedures, as the Bond index test. Tavares and Carvalho (2009) proposed a mechanistic model, which can be tested in Bond ball mill conditions. For instance, in the experimental test, the product is screened on a prescribed mesh-of-grind after a certain number of rotations in the mill. The oversize, that is, the material retained on the screen is combined with new make-up feed and the grinding cycle is repeated. This evaluates different assumptions about the mechanistic model, since the breakage energy of the particles is modeled as a probability distribution (Tavares & King 1998) and this distribution changes due to damage caused by unsuccessful repeated impacts (Tavares & King 2002). Besides that, the experiment is done with a low filling level, what gives an excellent opportunity to apply the effective collision model proposed by Rodriguez *et al.* (2018). On the other hand, the Bond ball mill does not contain lifters, which limited the raise of the charge and the frequency of high energy collisions.

The latest improvements that have been incorporated in the UFRJ mechanistic model are hereby used to predict the Bond work index (Wi) of different ores and rocks. Rather than proposing a new method to estimate Wi, the work aims to demonstrate that a mechanistic model may be used to predict technical tests, such as Bond´s grindability test.

2. Experimental

The UFRJ model could be dividing into two main parts. The first part is related with the energetic environment provide by the equipment, which is described using simulations in the discrete element (DEM) (Weerasekara et al. 2013). The second part has to do with the ore breakage characteristics, which are estimated in standardized experimental tests.

The DEM simulations were carried out using the EDEM software version 2018 by DEM Solutions (Edinburgh, UK). The selected as a contact model the

no-slip Hertz-Mindlin, which require estimation of its contact parameters. This was carried out by fitting the Bond mill with an acrylic lid which made it possible to observe the charge motion inside the mill. A Nikon D3200 with 24.2 MP and 60 fps was used. The experimental power was measured with the aid of a torque sensor (DR-3000 manufactured by Lorenz Messtechnik GmbH) placed in the shaft of the mill. The DEM simulated power was calculated by two methods: the mass center of the charge and the integrations of the energy loss values.

The parameters to feed the sub-models describing the breakage behavior of the ore material were taken from a previous work (Carvalho & Tavares 2013). The materials selected were granulite, two iron ores and two limestones. A simple partition curve model, fitted to experimental data, was used to describe product classification between the cycles.

Bond ball mill tests were conducted with different closing sieves in order to assess the ability of the mechanistic model to capture such variations.

3 Results

An example of the charge movement registered in the experimental results is presented in **Error! Reference source not found.**1. In the figure, the mill is charged with steel balls distribution and ore particles of granulite rock contained in the range of 3.35-0.6 mm size. In spite of the absence of lifters in the Bond mill, it is evident that balls are able to cataract, generating significant collision energies. These energies can explain the existence of body breakage and not only surface breakage (abrasion) in the Bond test. In Fig. 1 results from DEM simulation are also presented, showing ball velocities of up to 0.8 m/s. The spectra collected from these simulations were used to feed the mechanistic model.

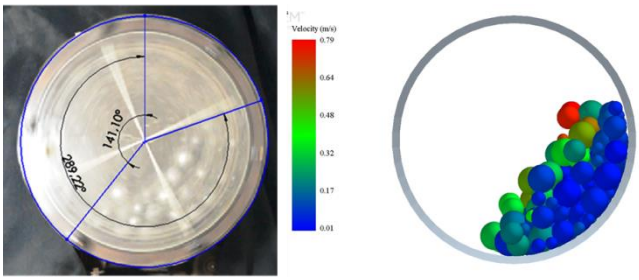

Fig. 1. Charge motion inside the Bond mill (30x30cm), with granulite rock, contained in size range 3.5-0.6 mm. Experimental (left) and simulated (right). Coefficient of rolling and static friction 0.45 and 0.15. Restitution coefficient of 0.4.

Fig 2 is presented a comparison between experimental and simulated results. It demonstrates the good agreement of the UFRJ mechanistic model to data, as well as its ability to predict with confidence the Wi of ores with widely different grindability.

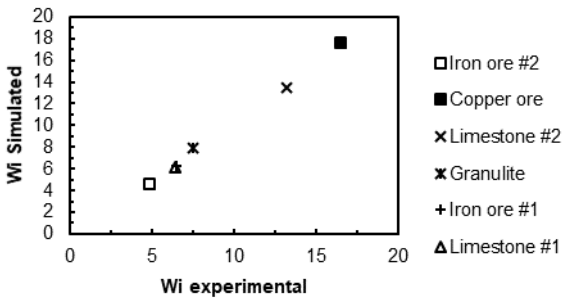

Fig. 2. Comparison between the experimental Wi and the prediction of the mechanistic UFRJ model.

4 Conclusion

DEM simulations were used as an effective tool to study the charge behavior and the energy transfer conditions inside the Bond test mill. The UFRJ model presents good ability to predict the Bond ball mill work index, demonstrating to be an excellent alternative to describe ball milling operations.

5 acknowledgements

The authors would like to thank the financial support from the Brazilian research agencies CNPq and CAPES, as well as from AMIRA, through the P9Q project. The authors also thank DEM Solutions for the use of the EDEM Academic Software under the EDEM Academic Partner Program (EAPP).

6. References

Carvalho, R.M. & Tavares, L.M., 2013. *Miner Eng*. 43-44, 91-101.

Fuerstenau et al., 1984. In: J.A. Herbst (Ed.), Control '84 Mineral Metallurgical Processing, AIME, New York, N.Y (1984), pp. 49-53

Rodriguez, V.A., de Carvalho, R.M. & Tavares, L.M., 2018. *Miner. Eng.* 127, 48–60.

Rowland, C.A., Kjos, D.M., 1980. In: Mular, A.L., Bhappu, R.B. (Eds.). American Institute of Mining, Metallurgical and Petroleum Engineers, Inc., Baltimore, pp. 239–278.

Tavares, L.M. & Carvalho, R.M., 2009. *Miner. Eng.* 22, 650-659.

Tavares, L.M. & King, R., 1998. *Int. J. Miner. Process.* 54(1), 1–28.

Tavares, L.M. & King, R.P., 2002. *Powder Technol.* 123, 138–146.

Weerasekara, N.S., Powell, M.S., Cleary, P.S., Tavares, L.M., Evertsson, M., Quist, J., Carvalho, R.M.., 2013. *Powder Technol.* 248, 3–24.

ID70 - Milling batch parameters of corundum powder milled in a water medium

Jaroslav Vlasak [1], *Nikola* Sulekova [1], *Ritva* Tuunila [2], *Teemu* Kinnarinen [2], *Tomas* Sverak[1,*], and *Antti* Häkkinen [2]

[1]Faculty of Chemistry, Brno University of Technology, Brno, Czechia
[2]Lappeenranta University of Technology, Lappeenranta, Finland

Summary. The paper presents results of corundum powder milling in a planetary laboratory mill in the wet process. The results show in interrelations, how the entire spectrum of milling batch parameters is changing in conformity with the milling time and thus, most importantly, with the fineness of milled material. The paper suggests that, for continual checking of the fineness of the milled particles during the corundum powder milling process in a water medium, it is possible to use, apart from the constant measurement of viscosity, also the measurement of turbidity.

1Introduction

Due to the broad applicability of corundum in the form of ultra-down to nano-fine powder material, the milling processes of this material have been meeting with great interest. See [Eisermann], [Toraman], [Breitung-Faes], [Shin], [Sverak], [Schilde], [Patel], [Damm]…

2 Experimental

2.1 Milling system

- milling device: the Fritsch planetary mill with ceramic mill-vessels of 323 ml in volume;
- milling beads: Zircon–Silica–Aluminium–Oxide, Type ZSA-3.8, SiLibeads (Art.No. 9135);
- milling stock: synthetic white corundum powder (A99 F1000, Abranova company) and water in the dosing ratio 1:5 (mass);
- corundum dosing: 20 g of corundum powder for each batch;
- volumetric filling of mill: milling beads/milling vessel volume - 25% in terms of volume;
- stabilization of milling process: TEA (triethanolamin) in 0,1 % concentration (mass in proportion to the milled corundum powder);

2.2 The process parameters recorded

Milling time, particle-size of milled material, specific energy passed in the mill, suspension-viscosity values, ζ-potential values and turbidity values.

3 Results and discussion

3.1 Milling process stabilization

Using triethanolamine (TEA) as a milling stabilization agent showed that the TEA function requires a particular time for its effective distribution. In the wet corundum-milling, after 16 hours of milling, with TEA present, the median of particle-sizes decreased from the initial 5,94 μm to 2,11 μm whereas, without an activator, under identical milling-parameters, the particle size reached 1,61 μm. However, after 32 hours of milling with TEA, the measurement showed the value 1.33 μm, which is the smallest particle-size that we managed to achieve in these milling-tests.

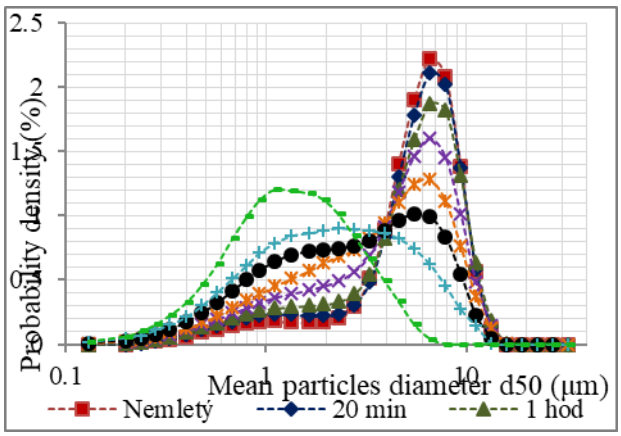

Fig. 1. The course of the milling process.

3.2 The Zeta potential

The ζ potential of all samples ranges from -30 to 30 mV, so these suspensions can be over labelled as unstable systems possessing a higher probability of aggregation because the individual particles do not display a charge high enough to cause their mutual repulsion. In the course of milling, the initially negative ζ potential, having got over the isoelectric point, reached the area of positive values. On the other hand, after 8 hours of milling, no marked changes in the ζ potential occurred.

The use of TEA did not cause any considerable decrease in the ζ potential or development of stable suspensions. In milling without TEA, the isoelectric point arises somewhat later than that originating in milling without the activator. This fact may imply that using TEA promotes, in the initial hours, the system´s partial stabilization. Over the isoelectric point, the ζ potential values are higher than those achieved in milling without the activator.

3.3 Viscosity

Viscosity measurements suggest that all suspensions display pseudoplastic behaviour. The initial decrease in measured viscosity may be related to the occurrence of aggregates of particles which, by the action of tension, release the immobilized liquid contained in the aggregates. While the particle sizes were decreasing, the viscosity values were on the increase. This relation results from the growing intensity of the particle-particle interactions and, on the other hand, from the increase of the effective concentration of solid stuff in the volume of the liquid. Another considerable change of viscosity also occurred in regimes with increasing contents of the finest particles; this again is the only aspect that displays a visible difference in milling either with or without a stabilizer of milling. In suspensions with TEA, in low shear-velocities, the viscosity was markedly higher, and its decrease with growing shear-velocities arose later than these phenomena arrived in milling without the activator. In the scope of high shear-velocities, no difference between the TEA and the non-TEA milling became evident. Apparently, in TEA-suspensions there are aggregates which possess higher strength and therefore remain in the suspension intact in higher shear velocities than it goes on in suspensions without activators.

3.4 Turbidity

The dependence of turbidity on milling time is linear, on particle-sizes non-linear. Consequently, it is not only the fineness of the product that determines turbidity, but also the presence of aggregates and the product contamination by abrasion of the milling vessel and milling beads.

4 Conclusions

The ultrafine corundum-milling processes require enormous quantities of specific energy. Very long milling times which are natural to these processes, see Fig. 1, emphasize the careful choice of stabilizing chemical ingredients and, moreover, need a continuous control of the batch product grain sizing.

The results of measurements, especially those of milling batch viscosity and turbidity, offer an opportunity of using easy-to-measure parameters of milled-material suspension to check the current fineness of the milled material and its overall quality for further product processing.

References

Eisermann, C., Mallembakam, M. R., Damm, C., Peukert, W. S., Breitung-Faes., and A. Kwade. (2012). Polymeric stabilization of fused corundum during nanogrinding in stirred media mills. *Powder Technology* 217, 315-324.

Toraman, O.Y., Çayirli, S. and Uçurum, M. (2016). The grinding-aids effect of moisture, triethanolamine (TEA) and ethylene glycol (EG) on grinding performance and product quality of calcite. *International Journal of Engineering Research & Science (IJOER)* Vol-2, Issue12, 121-128.

Breitung-Faes, S. and Kwade, A. (2011). Production of transparent suspensions by real grinding of fused corundum. *Powder Technology* 212(3), 383-389.

Shin, Y.J, Su, Ch.Ch. and Shen, Y.H. (2006). Dispersion of aqueous nano-sized alumina suspensions using cationic polyelectrolyte. *Materials Research Bulletin* 41(10), 1964-1971.

Sverak, T.S., Baker, C.G.J. and Kozdas, O. (2013). Efficiency of grinding stabilizers in cement clinker processing. *Minerals Engineering* 43-44, 52-57.

Schilde, C., Breitung-Faes, S., Kampen, I. and Kwade, A. (2013). Grinding kinetics of nano-sized particles for different electrostatic stabilizing acids in a stirred media mill. *Powder Technology* 235(4), 1008-1016.

Patel, Ch. M., Chakraborty, M. and Murthy, Z.V.P. (2014). Influence of pH on the Stability of Alumina and Silica Nanosuspension Produced by Wet Grinding. *Particulate Science and Technology* 33(3), 240-245.

Damm, C., Peukert, W., Jakob, P., Peukert, W., Breitung-Faes, S., and Kwade, A. (2011). Mechano-chemical radical formation and polymerization initiation during wet grinding of alumina: Opportunities and Limits. *Journal of Colloid and Interface Science* 363(1), 386-392.

ID73 - Study on the particle interaction in a hydrocyclone classifier with multicomponent feed blend

Mandakini Padhi *and Narasimha* Mangadodd[1*], , *A.N.* Mainza[2]

[1]*Department of Chemical Engineering, IIT Hyderabad, Kandi (V), Sangareddy (M), Medak, 502285, India.*
[2]*Centre for Minerals Research, Chemical Engineering, University of Cape Town, Rondebosch, 7701, Cape Town, South Africa*

Abstract. In mineral processing circuits, the feed to hydrocyclone consists of a heterogeneous mixture having varied degrees of liberation and sizes leading to the multi-component particle system. The presence of multicomponent particles exhibits a significant change in the classification performance parameters. The interaction of the particles at higher solid percentage slurry system seems profound due to the enhanced hindered settling phenomenon in a hydrocyclone classifier. In this work, the settling experiments, rheological studies and classification experiments for the pure components and the mixture of magnetite and silica particles at various proportions are conducted systematically. The performance of the classifier is tested with the dual-component system, i.e. artificial mixture of magnetite and silica. Suspension with the solids concentration of 10 to 30 percent by weight is considered. The slurry mixture is prepared at 50:50 proportions, compared with the pure components at various operating, and design parameters in the laboratory 3inch hydrocyclone. The classification experiments are conducted using central composite design (CCD) at three levels of cone force ratio and three levels of feed pressures. The classification performance curve is constructed based on individual component mass recovery to underflow using standard mass-balancing approach. A model for relative component interaction parameter is proposed statistically, which represents the size separation based on the size, density and solid fraction in the feed blend. The influence of the heavier component (magnetite) on the lighter density component (silica) particles is observed to be significant and increases with the magnetite content in the feed mixture. The estimated interaction parameter for the components is discussed in the light of its use towards developing a mathematical model for multi-component classification.

ID74 - Evaluation of the micro and macro processes in dry operated stirred media mills

Paul Przwara[1,*], *Sandra* Breitung-Faes[1], and *Arno* Kwade[1]

[1]Institute for Particle Technology, Technische Universität Braunschweig, Braunschweig, Germany

Summary. Dry stirred media mills are a promising option for efficient dry fine grinding processes due to their high energy densities, high stress frequencies and variable process parameters. Within this study, the most important sub-processes in such mills at both micro and macro levels were investigated in order to gain a better understanding of this emerging mill type. The relation between process parameters and powder flow behaviour was evaluated with special regard to the grinding efficiency by systematic batch experiments. In addition to that, the motion of the grinding beads was investigated by means of DEM simulation to identify collision energies and frequencies. Also, the particle capturing between approaching grinding tools was evaluated using a modified drop-weight test. Finally, continuously operated grinding experiments were carried out to identify overlapping influences of the product transport inside such mills.

1 Introduction

Since the demand on fine minerals is still increasing, new methods for improving the common production ways are needed. The different approaches for increasing the energy efficiency of dry fine grinding processes can roughly be divided into three groups: (1) further development of mills and mill equipment, (2) improving classifiers as well as grinding-classifying-circuits and (3) enhancing the process behaviour of the ground material [1]. The use of stirred media mills is a promising option for efficient dry fine grinding due to their high stress intensity, high stress frequency as well as better energy efficiency compared to tumbling ball mills [2,3]. However, because of the difficult process control of fine grinding processes in dry stirred media mills, this development is still in an early to intermediate stage. Also, the individual sub-processes at both micro (e.g. particle behaviour between the grinding beads) and macro scale (e.g. media motion, material transport or residence times) are not understood yet for this mill type.
Within this study, fine grinding of limestone is investigated using different dry operated stirred mills. A lab-scale batch mill is used to evaluate the stressing mechanisms inside such mills. These grinding experiments are accompanied by DEM simulations and further tests to evaluate the impact of the powder behaviour. In a second step, continuous grinding is considered using a pilot-scale mill. Thereby, the grinding performance is investigated as a function of different grinding aids as well as process parameters. It is shown how far the grinding aids affect the product quality, product throughput and specific energy consumption. The results are further correlated with the bulk and flow properties of the product, which – in turn – strongly depend on the applied grinding aid. For an even more comprehensive understanding of the pilot plant, the material transport is also investigated.

2 Methods

2.1 Grinding experiments

2.1.1 Batch-wise stirred media milling

A dry operated vertical stirred media mill with a chamber volume of 1.6 L was used for the laboratory batch experiments. Within this study, the product formulation (especially by applying grinding aids) as well as the most important process parameters were changed systematically in order to identify the impacts of the powder flow behaviour and the stress energies of the beads on the stressing conditions inside the mill. Particle sizes were analyzed by wet laser diffraction measurements (Helos, Sympatec). The powder flowability is characterized by the ff_c-values which were obtained by ring shear tests (ring shear tester RST-XS, Schulze).

2.1.2 Continuously operated stirred media milling

A pilot scale mill-classifier circuit was used for the grinding experiments. The grinding plant consists of a 6.6 L dry operated horizontal stirred media mill with pin stirrer as well as a deflector wheel air classifier (ATP100, Hosokawa Alpine, Germany). The power draw of the mill is measured via torque meter and is used for determining the specific grinding energy consumption. For the grinding experiments, alumina grinding beads (Microbit Leonardo, Bitossi) as well as

* Corresponding author: p.przwara@tu-bs.de

varying stirrer tip speeds in the range of 2-4 m/s were investigated. Furthermore, the circumferential speed of the classifier was varied in order to obtain different product finenesses in the range of $x_{50} < 4$ µm. In addition to that, residence time distributions were measured for both grinding in passage mode as well as in closed circuit operation. Thereby, the impact of grinding aids and process parameters on the macro-processes inside the grinding plant, such as the material transport through the mill or the material recirculation, was investigated.

2.2 Investigation of the particle capturing

A drop-weight tester was used to quantify the capturing of fine product particles between approaching grinding beads or balls. Within an idealized test set-up, the influences of several parameters, such as process-related settings (e.g. the impact velocity of the ball on the powder bed or the ball size) as well as product-related characteristics (e.g. particle size distribution, powder bed thickness or the powder flowability), were investigated.

2.3 DEM simulation of the grinding media motion

In a first instance, a combination of experimental tests and basic DEM simulations was carried out to determine the restitution and friction coefficients for different product formulations. Afterwards, the obtained calibration parameters were used for simulating the grinding bead motion inside the dry and batch-wise operated vertical stirred media mill (software EDEM 2.7 on Intel Xeon CPU ES-2690 with 2.60 GHz and 8 cores). Thereby, the single grinding beads were considered as spheres. The contact frequency of the grinding beads, their contact energy distribution as well as the torque of the stirring unit were used as the main information from the simulation. Additionally, the simulation results were compared and validated with the experimental data, especially regarding the resulting power draw of the stirring unit.

3 Results

The batch grinding study revealed that the grinding efficiency in dry operated stirred media mills is determined essentially by the combination of the flow behaviour of the product powder and the used process parameters. This finding can mainly be attributed to the fact that the actual stress intensities inside the mill are not only influenced by the contact energies of the beads, and thus, the combination of process parameters such as bead size, bead density and stirrer tip speed. In addition to that, a similar influence can be attributed to the mass of particles, which is captured and stressed between the beads at each collision event. Therefore, the powder flow behaviour and the product formulation (e.g. by applying grinding aids) have a strong impact on the stress conditions inside the mill.

The results from the drop-weight tester confirmed that the particle capturing is influenced significantly by the powder flow behaviour, and thus, the product formulation. It is also revealed that the capturing behaviour changes with the particle size distribution of the feed material. Furthermore, the mass of captured particles increases for both, coarser grinding beads/balls as well as higher impact velocities. The DEM simulations indicate that the bead motion inside dry stirred mills is also influenced by the product formulation. This is not surprising since the powder flow behaviour generally affects the friction properties of the mill load. However, the impacts of the product formulation on the stress frequencies and energies are marginal in comparison to the influence of the process parameters. Regarding this, it becomes clear that the media motion is significantly different compared to the bead motion in wet operated mills. Also, the extent of the single process parameters regarding the magnitude of the contact energy of the beads varies for the dry mode. It is further shown that the calculation of the actual stress intensity by considering both, the stress energies from the DEM simulation as well as the particle capturing from the drop-weight test gives a good approximation of the optimum processing conditions.

The continuous grinding experiments revealed that the stress mechanisms between the beads are strongly overlapped by the axial transport behaviour of the product powder through the mill. Especially grinding aids, which lead to different powder flowabilities, may lead to crucial changes of the material transport, and thus, the grinding efficiency. This can be attributed to different effects: On the one hand, the residence times of the particles inside the mill change as a consequence of the powder flowability. On the other hand, an internal grinding bead deflector wheel, which is installed in front of the mill exit to hold back grinding beads, may also lead to a disadvantageous accumulation of coarse particles inside the mill. In closed-circuits, the product formulation further determines the material recirculation within the circuit, which influences the stress conditions, e.g. by changing the powder-to-ball-ratio inside the mill.

References

Scheibe, W., B. Hoffmann, and H. Dombrowe, Der Einsatz von Mahlhilfsmitteln als eine Möglichkeit zur Verbesserung von trockenen Feinmahlprozessen. Freiberger Forschungshefte A, 1978. 602: p. 61-70.

Jankovic, A., W. Valery, and E. Davis, Cement Grinding Optimisation. Minerals Engineering, 2004. 17(11-12): p. 1075-1081.

Shi, F., et al., Comparison of energy efficiency between ball mills and stirred mills in coarse grinding. Minerals Engineering, 2009. 22(7-8): p. 673-680.

ID75 - Particle scale modelling of wet SAG and ball mills

Paul W. Cleary[1], *Matt* D. Sinnott[1], and *Rob* D. Morrison[2]

[1]CSIRO Data61, Clayton, Australia
[2]JKMRC, retired, Brisbane, Australia

Summary. A particle scale model based on full 2-way coupling of the DEM and SPH methods is used to predict charge and slurry behaviour in tumbling mills. Motion of resolved coarser particles within the mills is predicted by the DEM component. Fine particles combine with water to form slurry which is well represented using the SPH component. The slurry size distribution is discretised allowing the transport and dispersion of fine material to be tracked by solving coupled advection-diffusion equations in the SPH part of the model. Grinding of the slurry particles due to the collisions and shear of the coarser particles (rocks and grinding media) is performed by solving a local population balance model for each SPH particle. This allows, at least in principle, the prediction of the breakage and transport of the finer material within the grinding and pulp chambers of a SAG mill including discharge performance of the mill. It also allows prediction of slurry transport and grinding in ball mills. The operation of this particle scale model to predict performance (meaning throughput, product size distribution, resident particle size distribution, net power draw, wear) will be demonstrated for three mill scenarios.

1 Introduction

In this paper, we use a previously developed fully coupled DEM+SPH method (Cleary, 2004, 2015) and Cleary et al (2018, 2019) and include open grates and feed of both slurry and coarse rock via a feed chute in the model. This enables prediction of the axial flow of both rock and slurry phases within the grinding chamber, flow through the grates and within the pulp chamber and finally discharge from the mill. The inclusion of axial flow allows residence time and slurry flow paths to be investigated and the degree to which feed slurry is exposed to grinding by the solid charge. The model is applied to a Hardinge pilot mill and to a 36 ft industrial scale mill that is generated predominantly by scaling up the pilot scale mill design. It is also used to examine charge and slurry motion in an industrial scale 6.0 m x 10 m overflow ball mill. These will be discussed in the talk.

2 Computational Method

A computational particle scale model framework (termed the Virtual Comminution Machine by Morrison and Cleary (2008)) was developed previously for predicting some aspects of SAG milling. Cleary et al. (2015) coupled the Discrete Element Method (DEM) and Smoothed Particle Hydrodynamics (SPH) method to produce a 2-way coupled DEM+SPH multiphase model for predicting charge and slurry behaviour in a mill. This consisted of:

1. Prediction of the collisional environment of the mill and the flow of resolved particles (media and ore) in the charge represented by DEM.
2. Prediction of the mechanical strength of the charge by reasonable representation of non-round particle shapes to represent the rocks.
3. Prediction of the free surface flow of the slurry phase represented by SPH

The VCM model was extended by Cleary et al. (2018) to incorporate explicit breakage of the resolved solids in the mill using an incremental damage model and the generation of resolved fragments from these breakage events. Fine unresolved progeny were incorporated locally into the SPH slurry phase. Further extensions to this model reported in Cleary et al. (2019) include the use of an energy formulated population balance model (PBM) for each SPH particle allowing prediction of slurry phase grinding and tracking of the spatial distribution of fines and interstitial water. The slurry rheology was updated based on local solids fraction and size distribution of the unresolved fines. Granular dispersion of unresolved fines in the slurry along their spatially varying concentration gradients was also considered.

3 Multiphase flow in a SAG mill

Figure 1 shows the flow of solid charge and slurry in a 1.8 m diameter pilot mill. Figure 1a shows the solid charge as brown particles and the slurry as light blue. The slurry shoulder is below the solid charge shoulder

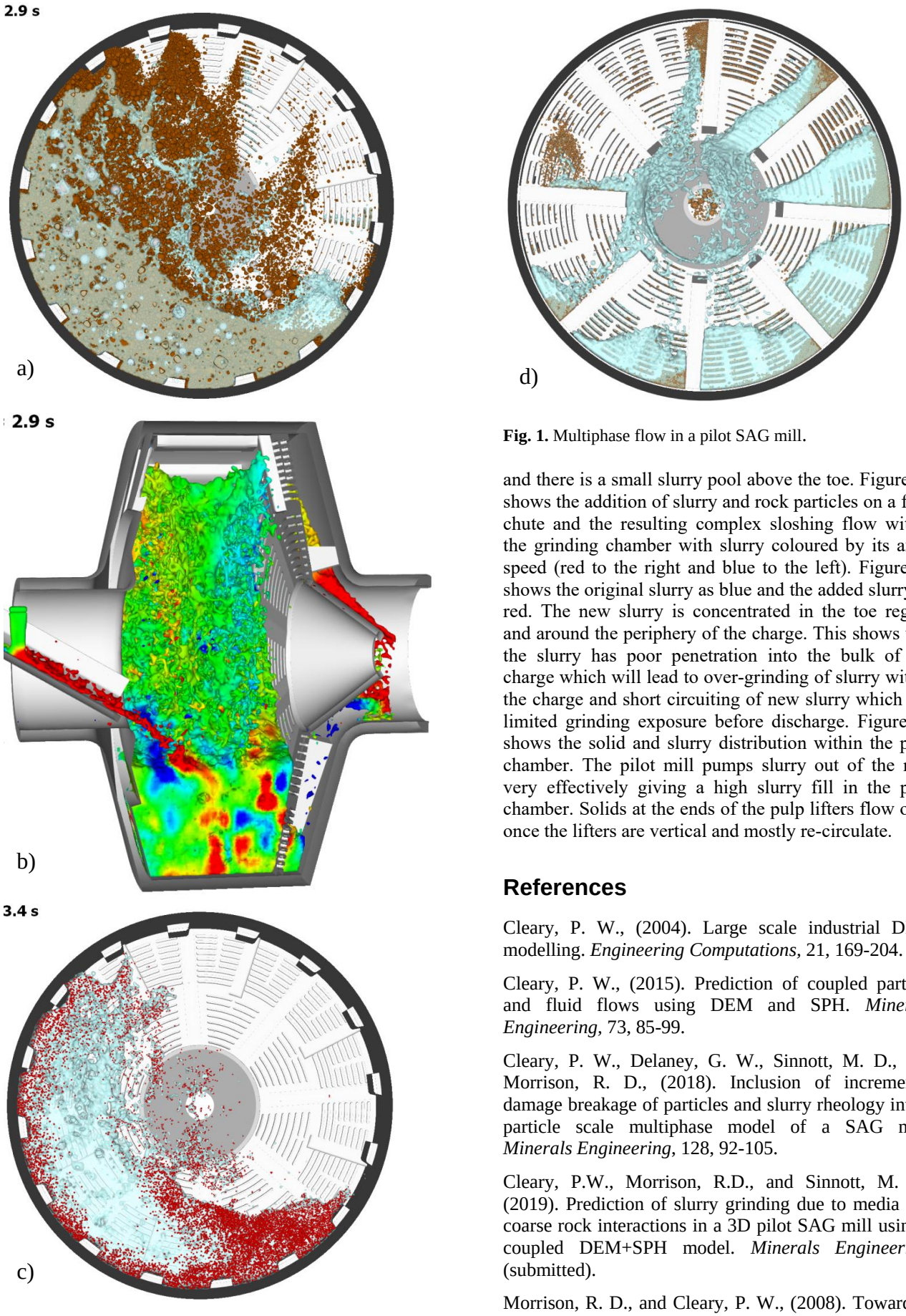

Fig. 1. Multiphase flow in a pilot SAG mill.

and there is a small slurry pool above the toe. Figure 1b shows the addition of slurry and rock particles on a feed chute and the resulting complex sloshing flow within the grinding chamber with slurry coloured by its axial speed (red to the right and blue to the left). Figure 1c shows the original slurry as blue and the added slurry as red. The new slurry is concentrated in the toe region and around the periphery of the charge. This shows that the slurry has poor penetration into the bulk of the charge which will lead to over-grinding of slurry within the charge and short circuiting of new slurry which has limited grinding exposure before discharge. Figure 1d shows the solid and slurry distribution within the pulp chamber. The pilot mill pumps slurry out of the mill very effectively giving a high slurry fill in the pulp chamber. Solids at the ends of the pulp lifters flow only once the lifters are vertical and mostly re-circulate.

References

Cleary, P. W., (2004). Large scale industrial DEM modelling. *Engineering Computations*, 21, 169-204.

Cleary, P. W., (2015). Prediction of coupled particle and fluid flows using DEM and SPH. *Minerals Engineering*, 73, 85-99.

Cleary, P. W., Delaney, G. W., Sinnott, M. D., and Morrison, R. D., (2018). Inclusion of incremental damage breakage of particles and slurry rheology into a particle scale multiphase model of a SAG mill. *Minerals Engineering*, 128, 92-105.

Cleary, P.W., Morrison, R.D., and Sinnott, M. D., (2019). Prediction of slurry grinding due to media and coarse rock interactions in a 3D pilot SAG mill using a coupled DEM+SPH model. *Minerals Engineering*, (submitted).

Morrison, R. D., and Cleary, P. W., (2008). Towards a Virtual Comminution Machine. *Minerals Engineering*, 21, 770-781.

ID76 - Vacuum comminuting of gold-bearing clay rocks

I V Yarygin, V G Prikhodko, S A Novopashin

Kutateladze Institute of Thermophysics, Novosibirsk, Russiam Federation, sanov@itp.nsc.ru

Summary The first experimental results of vacuum technology to increase the extraction of fine gold from clay rocks are presented. The depth of vacuum, the exposure time under vacuum of the geometry of the clay samples and the frequency of the vacuum action were studied. Under optimal conditions, with enrichment of the rock by centrifugal technology, an increase in the extraction of fine gold from 12% (without vacuum processing) to 30% was achieved.

* Corresponding author: p.prziwara@tu-bs.de

ID77 - Characterisation and degradation of polyphosphate dispersant interactions with aluminium-doped titania nanoparticles during milling

Laura N. Elliott[1,2], *Richard A.* Bourne[1,2], *Ali* Hassanpour[1], *John L.* Edwards[3], *Stephen* Sutcliffe[3], *and Timothy* N. Hunter[1,*]

[1]Faculty of Engineering, University of Leeds, Leeds, UK
[2]Institute of Process Research and Development, School of Chemistry, University of Leeds, Leeds, UK
[3]Venator, Titanium House, Hanzard Drive, Wynyard Park, Stockton-on-Tees, TS22 5FD, UK

Summary. Investigated is the characterisation of industrially produced alumina-doped pigment particles, milled for different periods of time in the presence of sodium hexametaphosphate (SHMP). Transmission electron microscopy (TEM) showed that prolonged milling times led to titania particle fines in the order of 10 nm electrostatically attracted to particles, and no change in the crystal structure was observed. The TiO_2 was found to have an isoelectric point (iep) in the range of pH 3 to 4.5, with an increase in milling time leading to a lower pH_{iep}, indicative of an increase in SHMP coverage. X-ray photoelectron spectroscopy (XPS) scans in the P_{2p} region showed broadening in the peak with increased milling time. XPS suggests that extended milling times cause hydrolysis or other structural changes within the SHMP dispersant.

1 Introduction

Polyphosphate salts are widely used as dispersants in mineral and material processing industries, due to their ability to adsorb onto metal-oxides and clay-particle surfaces. Sodium hexametaphosphate (SHMP), also known as Calgon or described as a polyphosphate salt, is used during pigment TiO_2 processing to reduce suspension viscosity and aid in the milling of particle agglomerates. Farrokhpay *et al.* (2012) have investigated the stability of polyphosphate dispersants on titania pigment particles. They found that acidic (pH 3.5 – 5.5), high calcium ion concentrations and elevated temperatures all decreased the polyphosphate dispersion properties of titanium pigment particles. Recent reviews by Cini (2014) and Rashchi (2000) report the stability of aqueous polyphosphate solutions which start to degrade at elevated temperatures (above 120 °C), under acidic pH conditions, and in other work, Rulliere (2012), in the presence of some metal ions.

Although efforts have been made to understand the influence of dispersants on slurry rheology during milling (see review by He *et al.* (2004)), there appears to be limited published research studying polyphosphates despite their wide use in industrial processing. Even with the widely accessible literature showing aqueous polyphosphate degradation, the influence of milling time on the structure and density of polyphosphate dispersants on the surface of titania pigment particles has not yet been explored. The authors aim to address this by exploring the change in polyphosphate structure of SHMP by X-ray photoelectron spectroscopy (XPS) with changes in milling time, RPM and other processing conditions such as temperature and ion concentration.

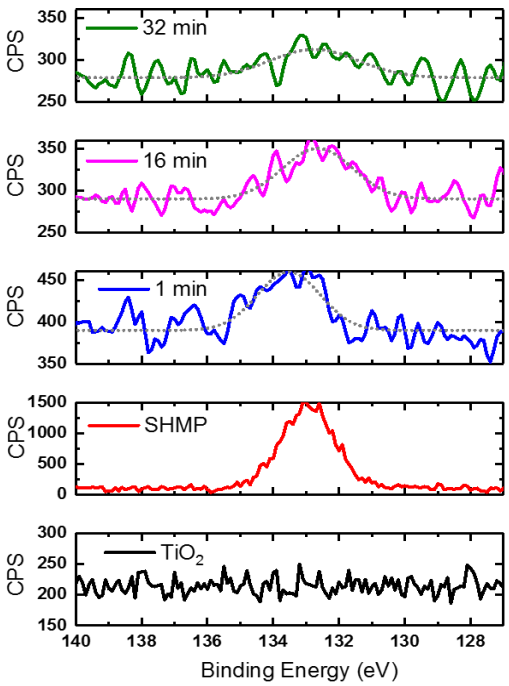

Fig. 1. XPS data of the P(2p) region for unmilled TiO_2 (aluminium doped TiO_2 without SHMP) (black), SHMP (pure i.e. no pigment attached) (red) and TiO_2 milled samples (1, 16

and 32 minutes) with SHMP adsorbed (blue, pink and green, respectively).

2 Materials and Methods

The industrially produced rutile pigment samples (aluminium doped TiO_2, Al-TiO_2) were firstly adjusted to pH 10-10.5 with NaOH and sodium hexametaphosphate (SHMP) was added prior to milling at 0.14% w/w as P_2O_5 on TiO_2. Suspensions were milled at concentrations of 400 g/L in a stirred wet mill using a rotor speed of 12,000 RPM. The milling media used was grade 8 ballotini with a mean size of 500 µm. Aliquots of TiO_2 were removed after 1, 2, 4, 8, 16 and 32 minutes of milling and dried in an oven at 105 °C. XPS spectra in the range of 0-1400 eV was collected with a monochromatic Al Kα source at hv = 1486 eV. The constituent elements which are important in the system studied were: Al, Ti, O, P, Ca, Na. Of most interest is the P(2p) region in which phosphate degradation can be observed. All binding energies were referenced to the C1s peak at 284.4 eV. Peak fitting was performed manually using Casa XPS.

3 Results and Discussion

Transmission electron microscopy (TEM) images were obtained for TiO_2 particles in order to understand the primary particle size and morphology changes within the two extreme milling times (after 1 minute and 32 minutes). The primary particle size measured by TEM and dynamic light scattering (DLS) were in good agreement (~250 nm), however, samples which were milled for prolonged times (32 minutes) showed signs of particle fracturing. Particle fines of 10-20 nm were observed in the TiO_2 sample milled for 32 minutes, importantly, no change in the crystal structure was observed through d-spacing analysis or bulk x-ray diffraction (XRD) measurements. Previous works by Sen *et al.* (2011) and Gajovic *et al.* have reported nanoparticle fines ~10 to 50 nm in size after ball milling TiO_2, however, milling times in the order of 10 to 100 hours were required. Furthermore, particle fracturing was observed for the anatase polymorph and these studies reported the formation of the uncommon metastable TiO_2-II phase. This is the first time to the authors knowledge that particle fines in the order of ~10 nm have been observed for the more stable rutile nanoparticles after ball milling for ~0.5 hours.

X-ray photoelectron spectroscopy (XPS) has been performed on a TiO_2 reference material, consisting of Al-TiO_2 which is unmilled without the polyphosphate attached. Also investigated was the spectral pattern of SHMP without pigment particles. Further, XPS data has been obtained for milled samples (at 1, 16 and 32 minutes) with SHMP adsorbed. It was observed from the survey scan that aluminium is present in all pigment samples as expected, and additionally, the adsorption of the SHMP can be seen in the P region as shown in Figure 1. Interestingly, Figure 1 shows that degradation of SHMP is occurring with milling time when attached to the pigment surface, this is supported by the broadening of the peak in the P region (for the 16- and 32-minute milled sample) and also a reduction in the intensity of the peak. The broadening of a peak can indicate a change in the number of chemical bonds contributing to that peak, which could suggest some hydrolysis or other chemical changes have occurred for the 32-minute milled sample. Currently the mechanism of degradation is unknown, and it may indeed be that certain processing conditions effect the polyphosphate degradation rate such as, milling time or energy (RPM). It is known in the literature that aqueous polyphosphates can be degraded with elevated temperatures (120 °C), ca^{2+} ions and extreme pH conditions. Thus, investigating the influence of these conditions may aid in the understanding of the polyphosphate-pigment degradation process and this is an area of ongoing research.

The authors would like to thank the Engineering and Physical Sciences Research Council (EPSRC, UK) (EP/L015285/1) and Venator, for funding this research, as part of the Centre for Doctoral Training in Complex Particulate Products and Processes (CP3 CDT). Elizabeth Willneff is thanked for her help collecting XPS data.

References

Farrokhpay, S., Morris, GE., and Britcher LG., (2012). Stability of sodium polyphosphate dispersants in mineral processing applications. *Minerals Engineering*, 39, 39-44.

Cini, N. and Ball, V., (2014). Polyphosphates as inorganic polyelectrolytes interacting with oppositely charged ions, polymers and deposited on surfaces: fundamentals and applications. *Advances in Colloid and Interface Science*, 209, 84-97.

Rashchi, F. and Finch, JA., (2000). Polyphosphates: A review their chemistry and application with particular reference to mineral processing. *Minerals Engineering*, 13 (10): 1019-1035.

Rulliere, C., Perenes, L., Senocq, D., Dodi, A. and Marchesseau, S., (2012). Heat treatment effect on polyphosphate chain length in aqueous and calcium solutions. *Food Chemistry*, 134 (2): 712-716.

He, M., Wang, Y. and Forssberg, E., (2004). Slurry rheology in wet ultrafine grinding of industrial minerals: a review. *Powder Technology*, 147 (1): 94-112.

Sen, S., Ram, ML., Roy, S. and Sarkar, BK., (2011). The structural transformation of anatase TiO_2 by high-energy vibrational ball milling. *Journal of Materials Research*, 14 (3): 841-848.

Gajovic, A., Furic, K. and Music, S., Ball-Milling of TiO_2 and ZrO_2. *Rudjer Boskovic Institute, Bijenicka*.54, 10000.

ID78 - Effect of VRM on a polymetallic sulfide ore and the flotation response as compared to conventional wet and dry rod milling

Hebert Simbarashe Nyakunuhwa[1,*], *Markus* Stapelmann[2], *Aubrey* Mainza[1],*Carsten* Gerold[2], *Kirsten* Corin[1],and *Megan* Becker[1]

[1]Centre of Minerals Research, Department of Chemical Engineering, University of Cape Town, Cape Town, South Africa
[2]Loesche GmbH, Dusseldorf, Germany

Comminution is an energy intensive process which consumes up to 50% of concentrator energy consumption. Conventional methods use mainly a combination of crushers and tumbling mills in comminution circuits and energy consumption has been found to be relatively high. To reduce the energy requirements, compression grinding equipment, Vertical Roller Mills (VRMs) and High-Pressure Grinding Rolls (HPGRs) have been identified as potential solutions, and they have been adopted in the cement industry. Unlike in the cement industry, comminution equipment in mineral processing circuits are also required to produce particles that can be recovered in downstream processes. The present study was aimed at assessing the specific energy consumptions and the flotation response from material comminuted using the VRM and comparing it to conventional dry and wet rod milling products ground to the same specifications and floated under the same batch flotation conditions. A coarse-grained ore containing chalcopyrite, galena and sphalerite as main value minerals was used. Specific energy consumption was 54 % lower after VRM milling. The flotation response for the various minerals contained in the ore showed that the same flotation performance can be achieved with the VRM for the coarse-grained ore tested.

1 Introduction

Comminution is an energy intensive, size reduction and mineral dressing process which consumes up to 50% of concentrator energy consumption (Cohen, 1983). Where the downstream processes are flotation or leaching, comminution aims to liberate the value minerals from the unwanted gangue while producing particle sizes required for the downstream process. As ore become more finely grained, the demand for finer comminuted products has seen the increase in energy requirements for comminution (Norgate and Jahanshahi, 2011). High compression grinding equipment, tabled as potential solutions to reducing energy requirements for comminution, has been widely adopted in the cement and coal industry (Schaefer, 2001). The Vertical Roller Mill (VRM) is a high compression grinding mill which incorporates comminution and classification in a single unit operation. The grinding section of the VRM consists of conical grinding rollers positioned on a grinding track of rotating circular table. As material falls off the rotating grinding table, it is pneumatically transported to the dynamic classifiers situated above the grinding table. The coarse material is recirculated to the grinding table for further grinding.

Reference to the downstream process requirements, wet grinding has traditionally been preferred to dry grinding as no dust control systems are involved. During wet grinding, galvanic interactions occur in the presence of water, oxygen, steel medium and sulfide minerals resulting in the precipitation of sulfur-oxy and metal hydroxides on sulfide mineral surfaces (Koleini et al., 2012). These hydroxides coat the sulfide mineral surface and negatively impact on collector action and recovery. VRM operations are mostly autogenous, hence steel-ore interactions are minimised (van Drunick et al., 2010). Progeny particles from dry grinding have rough surfaces with microstructural defects, which has been reported to increase collector adsorption during flotation and improve recoveries at the expense of selectivity. On the other hand, wet grinding products are smoother and cleaner, which was observed to improve selectivity (Feng and Aldrich, 2000).

As studies have indicated that VRM operations have dust control systems and are more energy efficient, one would become curious to understand whether efficiencies can be maintained in the downstream flotation unit operations? The aim of the present study was to compare the specific comminution energy consumption and the flotation response when material was comminuted using the VRM and rod mill and floated under batch conditions.

2 Experimental

Swartberg ore, a polymetallic sulfide ore, sourced from Black Mountain Mine in Aggeneys, Northern Cape, South Africa was used for the study. The ore had a top size of 14 mm. It contained chalcopyrite (1.3 %), sphalerite (1.8 %) and galena (2.4 %) as value bearing minerals. Magnetite (68.0 %), quartz (15.7 %),

pyroxmangite (5.5 %) and pyrite (2.3 %) were the dominant gangue minerals.

The Loesche VRM (LM3.6/2) and the Eriez Magnetics MASCLAB stainless steel laboratory scale rod mill were used for comminution. Prior to rod milling, the ore was crushed to minus 2 mm. For wet milling tests, standard synthetic plant water (SPW) was added to the rod mill to make up the 67% solids required for comminution. SPW was prepared using the standard UCT procedure (Wiese et al., 2005). Milling curves were used to determine the time required to achieve the target grind for wet and dry rod milling. Ore was ground for 16 minutes to achieve the grind for both wet and dry rod milling.

Milled products were transferred to the 3 L Barker flotation cell and SPW water added to the 2 cm froth height mark, achieving 33 wt.% solids of the pulp. The slurry was kept in suspension using an impeller (1250 rpm). Before adding any reagents, a feed sample was collected. Copper sulfate activator was added at 160 g/t and allowed to condition for 1 minute. A mixed collector, SEX at 80 g/t and Senkol 700 at 10 g/t was then added and conditioned for 2 minutes. A frother, MIBC (25 g/t) was added and conditioned for 1 minute. Air was then introduced at a constant rate of 7.5 L/min. Froth was scraped every 15 seconds from the cell and was collected into pre-weighed concentrate trays. C1, C2, C3 and C4 were the concentrates collected after 2, 4, 6 and 8 minutes of scrapping respectively. Froth height was maintained at 2 cm using SPW water. Each flotation test was done in duplicate to measure repeatability and level of confidence in the observations.

3 Results

The concentrate grade-recovery relationship is presented in Figure 10. The valuable mineral recoveries are summarised in Table 5.

Table 5: Mass pull and achieved elemental recoveries

Grinding Mechanism	Mass pull (%)	Cu Rec (%)	Pb Rec (%)	Zn Rec (%)
VRM	11.2	96.7	94.3	96.6
RD	13.9	96.3	94.3	97.4
RW	10.1	96.7	92.9	97.4

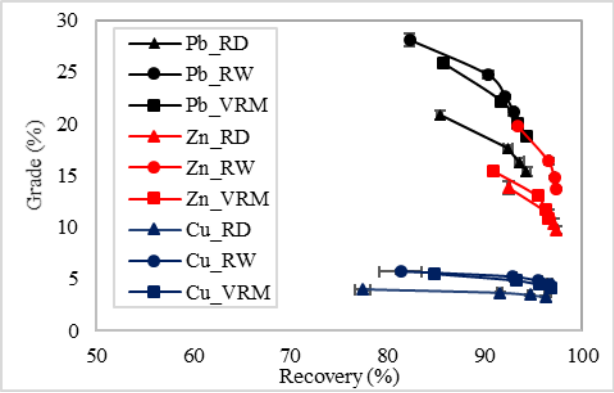

Figure 10: Concentrate grade vs. recovery relationship

The VRM specific grinding energy consumption was 5.7 kWh/t, 54.3 % lower than the specific grinding energy consumption for the traditional rod mill-ball mill comminution circuit (12.5 kWh/t).

4 Discussion

The resultant PSDs were similar. As the milling times for dry and wet rod milling to achieve the required grind were the same, specific comminution energy consumptions for the two comminution procedures are the same. Specific grinding energy consumption was 54.3 % lower for the VRM as compared to the conventional comminution circuit. Using ANOVA and the 95 % confidence limit, the differences in recovery were statistically insignificant: chalcopyrite (72 % confidence of a difference), galena (63 % confidence of a difference) and sphalerite (18 % confidence of a difference). As the recoveries were similar, the higher mass pull observed resulted in lower concentrate grade.

5 Conclusion

Mineral recoveries were similar after floating the coarse-grained, polymetallic Swartberg sulfide ore comminuted using the VRM, dry and wet rod milling. Specific grinding energy consumption for the VRM was 54 % lower. The VRM can be retrofitted into existing plant installations as it is more energy efficient and the flotation performance was similar when using the flotation procedure tailored for tumbling mill-flotation systems.

References

Cohen, H.E., (1983). Energy usage in mineral processing. *Institution of Mining and Metallurgy Transactions*. (92): C160-164.

van Drunick, W., Gerold, C. & Palm, N., (2010). Implementation of an energy efficient dry grinding technology into an Anglo American zinc beneficiation process. *International Mineral Processing Congress*. (September):1333–1341.

Feng, D. & Aldrich, C., (2000). A comparison of the flotation of ore from the Merensky Reef after wet and dry grinding. *International Journal of Mineral Processing* 60(2):115–129.

Koleini, S.M.J., Abdollahy, M. & Soltani, F., (2012). Wet and dry grinding methods effect on the flotation of Taknar Cu-Zn sulphide ore using a mixed collector. *XXVI International Mineral Processing Congress (IMPC)*. (603):5113–5119.

Norgate, T. & Jahanshahi, S., (2011). Reducing the greenhouse gas footprint of primary metal production: Where should the focus be? *Minerals Engineering* 24(14):1563–1570.

Schaefer, H.U., (2001). LOESCHE vertical roller mills for the comminution of ores and minerals. *Minerals Engineering* 14(10):1155–1160.

Wiese, J., Harris, P. & Bradshaw, D., (2005). The influence of the reagent suite on the flotation of ores from the Merensky reef. *Minerals Engineering* 18(2):189–198.

ID80 - Factors influencing triboelectric separation of fine organic powders

Johann Landauer*, and *Petra* Foerst

Chair of Process Systems Engineering, School of Life Sciences Weihenstephan, Technical University of Munich

Summary. Triboelectic separation is valuable tool to separate powder of different chemical composition without reference to particle size and density. Triboelectric charging occurs when two surfaces come into contact and are separated subsequently. To improve the separation process, influence factors on the charging process have to be validated. Particle-wall and particle-particle interaction are interaction possibilities of particles conveyed in a turbulent flow. Experiments showed a subordinate role of particle-wall interaction on the separation selectivity. Also the influence of the empirical triboelectric series might be questioned. On the contrary, a clear dependence of particle-particle contact number estimated according Saffman and Turner was demonstrated. Higher contact numbers lead to an increase in protein content to 80 wt.% on the cathode. Therefore, particle-particle interaction is proposed to be the relevant charging mechanism.

1 Introduction

Triboelectric charging occurs when two surfaces come into contact and are separated subsequently. This occurs always in powder handling. Thus, triboelectric charging is principally an undesirable effect because highly cumulated charge in plant can lead to durst explosion. Furthermore, charged pharmaceutical powders show reduced flow properties (Ghori et al. 2014). On the contrary, triboelectric charging can be used to separate powders (Landauer and Foerst 2018; Landauer et al. 2019; Wang et al. 2016). The separation feature is the triboelectric chargeability. For conductive particles the charging is described by the work function of the different materials. Insulating materials have a huge band gap which is insuperable at normal conditions and thus several factors like humidity, chemical composition of the particles, crystallinity of the particle surfaces, etc. are used to describe triboelectric charging but a complete physical understanding still does not exist.

However, lots of studies show the feasibility of triboelectric separation as a powerful tool to separate particles of different chemical composition within the same size range (Wang et al. 2015; Tabtabaei et al. 2016). To make triboelectric separation available for industrial processes the main influencing factors of triboelectric charging with regard to plant design has to be evaluated. The hypothesis of this study is how can particle interaction be influenced to enlarge separation selectivity.

2 Material and Methods

Whey protein powder with a men particle size of 10 µm and barley starch powder with a mean particle size of 20 µm is used for all experiments. Particles are dispersed in a nitrogen stream (3 m^3/h) using a Venturi nozzle and conveyed through a tube with an inner diameter of 10 mm. The charging tube is made of different plastics (PTFE, PE, POM, PVC, PMMA). Further, a boundary layer control setup including a porous tube with a perpendicular gas flow (2.5% and 5% of the main flow rate) is used to inhibit particle-wall interaction. At the end of the charging tube a rectangular separation chamber with an electrical field (109 kv/m) is applied to separate charged particles.

3 Results and Discussion

3.1 Influence of wall materials

Derived from the work function of conductive materials, a so call triboelectric series is proposed for insulating materials. In the charging tube both particle-particle and particle wall interaction occur. If the particle wall interaction plays a decisive role, different charging tube materials should promote or impair separation selectivity. A powder composed of 15 wt.% whey protein and 85 wt.% barley starch was used. The separation selectivity of all different charging tubes was identical. Furthermore, no increase or decrease of separation selectivity along the empirical triboelectric series was determined. Thus, the influence of the wall material in the charging step can be neglected but the influence of the particle wall interaction is not answerd yet.

To prevent particle-wall interaction, the charging tube is replaced by a porous tube with a perpendicular

flow rate. This boundary layer control setup enables a particle-particle interaction without particle-wall interaction. Separation experiments show a slight decile in separation selectivity. This slight decline in the separation selectivity is probably provoked by a decrease in turbulence eddy dissipation rate which is an important parameter in the calculation particle interaction (Saffman and Turner 1956). In conclusion, the particle-wall interaction plays only a subordinate role in triboelectric charging and separation.

3.2 Influence of particle-particle interaction

As the particle wall interaction plays a subordinate role in triboelectric separation, particle-particle interaction might be an appropriate control parameter. Therefore, contact numbers of starch and protein are varied. The contact number for two particles in a turbulent flow as suggested by Saffman and Turner depends on the particle size of the contacting particles, the Kolmogorov time scale, and the concentration of protein and starch (Saffman and Turner 1956). Different mixing ratios of protein and starch and different turbulence eddy dissipation rates due to boundary layer control enable a variation in the contact numbers.

Fig. 1 shows a huge increase of the protein content on the cathode (closed symbols) by increasing the contact number of particles. On the anode also a slight increase in protein content is visible. Thus, particle-particle interaction might play a decisive role in triboelectric charging. Even a single contact is sufficient to generate surface charge (Horn and Smith 1992). However, it is unlikely that every contact of two particles can transfer surface charge, but if only 1 percent of the contacts succeeds, a large number of charge remain. This different interaction parameters might be a hint to multimodal charge distributions (Landauer et al.)

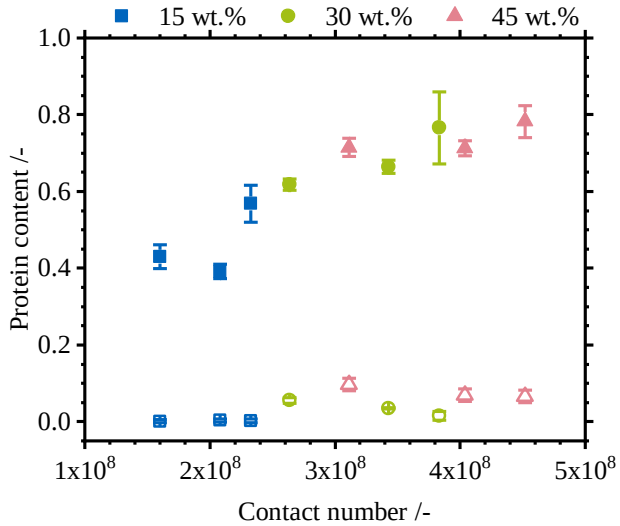

Fig. 1. Protein content on the cathode (closed symbols) and on the anode (open symbols) at different contact numbers. An increase in contact numbers leads to higher protein contents on the cathode.

4 Conclusion

Triboelectric separation is a suitable tool to separate fine powders (20 µm mean particle size) with approximately the same true density. Thus, the separation feature is independent form particle size and density. Results show that different wall materials along the empirical so called “triboelectric series” neither promote nor impair separation selectivity indicated by the protein content. Further experiments show the subordinate role of particle-wall interaction on triboelectric separation of particles conveyed in a turbulent flow.

On the contrary, particle-particle interaction characterised by the contact number shows a huge impact on the protein content and thus on the separation selectivity. The protein contact on the cathode increases by an increase in the contact number. Therefore, particle-particle interaction is proposed to be one of the relevant process variables in triboelectric separation. This knowledge can help to promote triboelectric separation as an industrial process in separation technology.

References

Ghori, M. U.; Supuk, E.; Conway, B. R. (2014): Triboelectric charging and adhesion of cellulose ethers and their mixtures with flurbiprofen. *European journal of pharmaceutical sciences* 65, 1–8.

Horn, R. G.; Smith, D. T. (1992): Contact electrification and adhesion between dissimilar materials. *Science (New York, N.Y.)* 256 (5055), 362–364.

Landauer, J.; Aigner, F.; Kuhn, M.; Först, P. (2019): Effect of particle-wall interaction on triboelectric separation of fine particles in a turbulent flow. *Advanced Powder Technology* in pres.

Landauer, J.; Foerst, P. (2018): Triboelectric separation of a starch-protein mixture – Impact of electric field strength and flow rate. *Advanced Powder Technology* 29 (1), 117–123.

Landauer, J.; Tauwald, S. M.; Foerst, P.: A simple µ-PTV setup to the measure single-particle charge of triboelectic charged particles. *Frontiers Chemistry - Chemical Engineering*, accepted.

Saffman, P. G.; Turner, J. S. (1956): On the collision of drops in turbulent clouds. *J. Fluid Mech.* 1 (01), p. 16.

Tabtabaei, S.; Jafari, M.; Rajabzadeh, A. R.; Legge, R. L. (2016): Development and optimization of a triboelectrification bioseparation process for dry fractionation of legume flours. *Separation and Purification Technology* 163, 48–58.

Wang, J.; Suo, G.; Wit, M. de; Boom, R. M.; Schutyser, M. A.I. (2016): Dietary fibre enrichment from defatted rice bran by dry fractionation. *Journal of Food Engineering* 186, 50–57.

Wang, J.; Wit, M. de; Boom, R. M.; Schutyser, M. A.I. (2015): Charging and separation behavior of gluten–starch mixtures assessed with a custom-built electrostatic separator. *Separation and Purification Technology* 152, 164–171.

ID81 - DEM Modelling of Ribbon Milling: a Comparison of Modelling Approaches

Colin Hare[1,*], *Chuan-Yu Wu*[1], and *Mojtaba Ghadiri*[1]

[1]Department of Chemical and Process Engineering, University of Surrey, Guildford, UK
[2]School of Chemical and Process Engineering, University of Leeds, Leeds, UK

Summary. Two DEM-PBM methods for predicting ribbon milling breakage data are assessed. The methods differ both by the representation of primary particle bonds in the ribbon, and by the determination of size distribution. Both methods give a reasonable estimate of the magnitude of breakage in the mills, but do not accurately estimate the full size distribution.

1 Introduction

Roller compaction followed by milling is a common process route for transforming very fine powders into larger granulates that are more suitable for further processing, such as in tabletting processes. In the employed rotary mills, ribbons experience breakage due to impacts with rotating bars/impellers and the screen mesh at the base, and due to be sheared against the mesh at the base. There is often only limited or no understanding of the effect of milling parameters, such as rotational speed, on the milling efficiency of ribbons. The Discrete Element Method (DEM) can be used to better understand the influence of material and process parameters on particle processing operations. Here we contrast two methods for predicting ribbon milling performance based on DEM coupled with Population Balance Modelling (PBM).

2 Methods

The first DEM approach, reported by Hare *et al.* (2016), uses the rigid bonding model developed by Brown *et al.* (2014) to represent the ribbons in the DEM, whilst the second approach, reported by Loreti *et al.* (2016), uses the JKR-Thornton auto-adhesive particle model (Thornton & Yin, 1991).

2.1 Rigid bonding model (method A)

The bonds are characterised by the following properties: bond radius, Young's modulus, Poisson's ratio and compressive, tensile and shear strengths, and their distributions. A 3-point bend test of the ribbons was carried out experimentally and by simulation, with the bond properties varied to mimic the experimental breakage force. The ribbons are created using a collection of monodisperse 1.8 mm diameter spheres in a single layer, square packing arrangement. Ten ribbons fall successively into the simulated mill. The ribbons first impact against the base or bar of the mill, and are then stressed and broken due to the shearing actions of the rotating bars against the mesh. The stresses experienced by the ribbons are estimated by considering the force acting on each individual bar and the number of primary particles in contact with the bar. The shear strain is determined based on the duration of the shearing event. The influence of mill speed and initial ribbon length is assessed.

The breakage occurring in the mill is predicted by experimentally impacting a sample of ribbons against a rigid surface of the same material as the mill, at the impact velocities identified by the DEM. The ribbon fragments are then arranged in a single layer in an Ajax attrition shear cell and sheared under the stress and strain conditions identified by the DEM. The sheared material is passed through a 3.35 mm aperture sieve, representing the outlet of the mill. Fragments retained on the sieve are sheared again, to represent subsequent bar passes. This process is repeated until the entire mass passes through the sieve, after which sieve analysis is carried out.

2.2 Auto-adhesive bonding model (method B)

An agglomerate of 1460 polydisperse spheres (77 – 312 μm), with the properties of Mannitol Perlitol SD 200, is created by generating the spheres in a parellelpiped geometry, following which the confining walls move inwards to consolidate the spheres to a solid fraction of 0.74. A surface energy (γ) of 200 J/m^2 is then applied to each contact. The surface energy is gradually reduced whilst the confinement of the walls is relaxed. The created ribbons have length, width and height of 3 and

1.2 and 0.8 mm, respectively. Ribbons with surface energies of 0.03 – 2 J/m^2 are created.

The ribbon breakage due to impact against a rigid plate is explored, with the size distribution of breakage products determined in each case. A population balance model following the approach of Reynolds (2010) is applied to the breakage data, which accounts for the bimodal product size distribution. This approach assumes that fragments smaller than the screen size exit the mill, whilst fragment size distribution is described by five independent parameters: the geometric mean and standard deviation of a log-normal fit to the PSD, the volume fraction of the small mode, the volume fraction of fines per breakage event and the number of large fragments per breakage event. The size distribution of mill products is predicted by assuming that each breakage event occurs at a fixed velocity. The influence of screen size is investigated.

3 Results and discussion

Figures 1 and 2 show the predicted and measured breakage data for methods A and B, respectively.

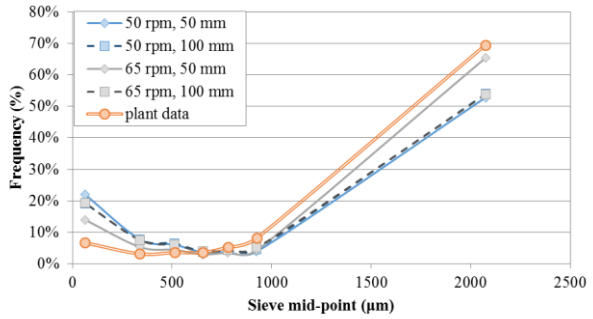

Fig. 1. Predicted and actual mill product size distribution (method A).

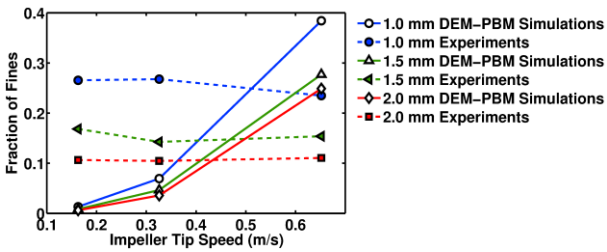

Fig. 2. Predicted granule fraction of fines with γ = 0.12 J/m^2 and measured ribbon milling data (method B).

For method A the plant data corresponds to a mill speed similar to that of the DEM, with ribbon lengths of approximately 50 – 100 mm fed into the mill. The prediction captures the general shape of the product size distribution, though overestimates the fraction of fines generated. This may be due to the gripping surface used in the shear cell differing from that in the mill; providing more effective shearing and potentially also scraping the ribbons. Also, in the actual mill fines are free to exit the mill soon after being generated, once they percolate through the sheared material, whereas in the shear cell all fines remain in the shearing zone for the duration of the shearing event, and as such may experience further breakage that would otherwise not occur in the mill.

For method B the influence of mesh size on the fraction of fines generated is correctly predicted, though the fraction of fines is predicted to increase with mill speed, which is not the case for the measured mill data. This may be due to the prediction method being driven by impact velocity alone, with breakage due to shearing against the mesh not being accounted for.

Both the rigid bonding model and the auto-adhesive model appear capable of representing ribbon breakage. Whichever method is used, the breakage behaviour of the material of interest must be robustly captured by the model. Experimentally assessing the breakage under representative stressing events is a suitable approach, though high fidelity of the actual mill conditions must be captured. By relying on the surface energy of the bonded primary particles in the ribbon to capture the real breakage behaviour, it may be necessary to include the full distribution of this property. Greater accuracy is expected by including a larger number of primary particles, the full primary particle PSD and the actual shape distribution, to represent the ribbon.

4 Conclusions

Both DEM-PBM methods provide a reasonable prediction of particle size distribution of the milled products compared with experimental data, however neither approach fully accounts for the breakage behaviour experienced in the mill and the influence of milling conditions.

References

Brown, N.J., Chen, J-F., Ooi, and J.Y., (2014). A bond model for DEM simulation of cementitious materials and deformable structures. *Granular Matter*, 16(3), 299-311.

Hare, C., Ghadiri, M., Guillard, N., Bosworth, T. and Egan, G. (2016). Analysis of Milling of Dry Compacted Ribbons by Distinct Element Method. *Chemical Engineering Science* 149, 204-214.

Loreti, S., Wu, C.Y., Reynolds, G., Mirtič, A. and Seville, J. (2016). DEM-PBM modelling of impact dominated ribbon milling. *AIChE Journal* 63(9), 3692-3705.

Reynolds, G. (2010). Modelling of pharmaceutical granule size reduction in a conical screen mill. *Chemical Engineering Journal* 164, 383-392.

Thornton, C. and Yin, K.K. (1991). Impact of elastic spheres with and without adhesion. *Powder Technology* 65, 153-166.

ID82 - Validating the Lubrication approximation in Rotating Drums

David N. de Klerk[1,2,*], *Aubrey N.* Mainza[2], and *Indresan* Govender[3]

[1]Department of Physics, University of Cape Town, Rondebosch, South Africa
[2]Centre for Minerals Research, University of Cape Town, Rondebosch, South Africa
[3]School of Engineering, University of KwaZulu-Natal, Glenwood, South Africa

Summary. Simulations of granular material have become common place. Some recent studies incorporate viscous effects of an interstitial fluid by adding a lubrication force between particles that are close together. This study compares results of a wet granular material in a rotating drum between Positron Emission Particle Tracking (PEPT) and Discrete Element Method (DEM). A 10 mm glass beads and water/glycerol mixtures were used in the experimental study. In the numerical study, a lubrication approximation was used to capture the viscous effect of the fluid. The Stokes number and velocity profiles in the flowing layer are compared and good agreement between simulation and experiment is observed for both quantities.

Recent investigations (cf. Trulsson et. al. (2012), Seto et. al. (2013)) of dense granular suspensions used a a range of forces acting on DEM particles to account for the effect of an interstitial fluid. These fluid forces where applied in addition to the usual Hertzian or Hookian contact forces that simulate particle collisions. The effect of a thin fluid film between nearby particles is simulated using a lubrication force. In addition, a drag force and Archimedes force were applied. However, Ness and Sun (2015, 2016) found that energy dissipation due to the fluid forces was dominated by the lubrication force and neglected other forces in their simulations. The lubrication force between two particles labelled *i* and *j* is given by

$$F_{ij} = F_n(\eta_f, v_i - v_j, h_{ij})\, \boldsymbol{n}_{ij} + F_t(\eta_f, v_i - v_j, h_{ij})\, \boldsymbol{t}_{ij}, \quad (1)$$

where η_f is the fluid viscosity, v is the particle velocity and h_{ij} is the separation between the particles. Previous studies used a simple shearing configuration and in particular, its use in the context of rotating drums has not been demonstrated.

In this study, DEM simulations where carried out with a rotating drum (inner radius R = 0.2 m and length L = 0.2 m) filled with 15000 spheres of diameter d = 10 mm, ρ = 2400 kg/m^3, Young's modulus $Y = 5 \times 10^6$ kg/m/s^2, Poisson ratio ν = 0.45, coefficient of restitution e = 0.5 and coefficient of friction μ = 0.5. Inter-particle contacts were simulated using the Hertz-Mindlin model and the lubrication approximation mentioned earlier. Four different rates of rotation were used (0.3:0.1:0.6 $\omega_c = \sqrt{g/R}$) and three different values for the viscosity parameter {0.01, 0.03, 0.22} Pa s.

Positron Emission Particle Tracking (PEPT) experiments of a rotating drum with inner radius R = 0.23 m and length L = 0.2 m was performed at the PEPT Cape Town facility. The drum was filled to 50 % of its volume with glass beads of d = 10 mm. The fluid was a water/glycerol mixture. Three different ratios, (60%, 75% and 90% w/w) of glycerol to water was used, which corresponded with fluid viscosities of {0.011 ± 0.001, 0.038 ± 0.005, 0.25 ± 0.04} Pa s. Drum speeds where varied between (0.3:0.05:0.6of $\omega_c = \sqrt{g/R}$).

Particle level information, such as position and velocity were coarse-grained using the method described by Artoni and Richard (2015). The average density, velocity and velocity gradient of the bulk material for each of DEM and PEPT data sets where calculated. Using the average quantities, the Stokes number and velocity profiles perpendicular to the free surface can be calculated.

Scaling relations for velocity profiles can be derived from their constitutive equation (Jop et al. (2005)). Their method involves performing a force balance on a volume element in the flowing layer. The $\tau/P = \mu(I)$ constitutive relationship is used to obtain a model for the shear rate as a function of the depth (y) of the flowing layer, which is then integrated to solve for the scaled velocity as a function of the scaled depth $(v_t/gd)^{1/2}$. The same procedure for deriving their scaling relation can be applied to other constitutive equations and it is therefore reasonable to expect that the same constitutive equation holds in both cases, if the same scaling relation is observed in simulations and experiments.

The Stokes number, St, plays an important role in determining the flow regime of dense granular suspensions. For low Stokes number, St << 1, the drag forces dominate particle dynamics and such systems can be simulated using only fluid dynamics. When St >> 1, particle momentum dominates fluid dynamics and

simulations only need to account for particle interactions and the most important fluid effects. The Stokes number is given by

$$St = \frac{\rho_p d^2 \dot{\gamma}}{\eta_f}, \quad (2)$$

where ρ_p is the particle density, d the particle diameter, $\dot{\gamma}$ the shear rate and η_f the fluid viscosity, can be calculated for both DEM simulations and PEPT experiments. It is possible to determine whether the lubrication approximation and DEM contact model sufficiently captures the dynamics of dense granular materials in rotating drums, by comparing the Stokes number between simulation and experiment.

Simulations have two important advantages over experiments. They are cheaper to perform and provide direct access to all particle properties including forces between interacting particles. Despite these advantages, simulations cannot be performed in isolation. To have confidence that simulation results represent what happens in a physical system, validation of the simulation is required. It is reasonable to conclude that the lubrication approximation is sufficient to model the effect of a granular material and interstitial fluid in a rotating drum configuration. Both velocity profiles and the range of Stokes number show good agreement between PEPT experiments and DEM simulations.

There are several advantages to using the DEM lubrication approximation over experimental methods or coupled simulations. It is much cheaper (in terms of equipment cost, time, lab space and human resources) to run simulations than experiments. Simulations also provide opportunities to study more configurations and design ideas than experiments. It is easier to run DEM simulations with the lubrication approximation than coupled simulations. Other approaches to simulate dense suspensions include coupling DEM with Computational Fluid Dynamics (CFD) or Smooth Particle Hydrodynamics (SPH). However, both these solutions require substantially more computing resources: SPH requires additional particles that represent the fluid to be simulated and CFD coupled simulations requires the fluid to be simulated in a separate software package. In addition, DEM-CFD coupled simulations needs a software layer to communicate between the solid and fluid simulation. The lubrication approximation can be incorporated into open source DEM software packages and the simulations can be executed in a single step.

References

Artoni, R. and Richard, P., (2015). Average balance equations, scale dependence, and energy cascade for granular materials. *Physical Review E* 91, 032202.

Jop, P., Forterre, Y. and Pouliquen, O., (2005). Crucial role of sidewalls in granular surface flows: consequences for the rheology. *Journal of Fluid Mechanics* 541, 167.

Ness, C. and Sun, J., (2015). Flow regime transitions in dense non-Brownian suspensions: Rheology, microstructural characterization, and constitutive modeling. *Physical Review E* 91 12201.

Ness, C. and Sun, J., (2016). Shear thickening regimes of dense non-Brownian suspensions. *Soft Matter* 12, 914–924.

Seto, R., Mari, R., Morris, J. F. and Denn, M. M., (2013) Discontinuous shear thickening of frictional hard-sphere suspensions. *Physical Review Letters* 111, 218301.

Trulsson, M., Andreotti, B. and Claudin, P., (2012). Transition from the viscous to inertial regime in dense suspensions. *Physical Review Letters* 109, 118305.

ID83 - Simulation of the Influence of Different Modes of Selective Liberation on Metallurgical Performance

van der Wielen, Klaas Peter[1*]

[1] Grinding Solutions, Truro, Cornwall, UK

Summary. Selective liberation has often been considered the ultimate goal for grinding technologies used in the mining industry. Several technologies, such as high voltage pulse comminution, microwave-assisted breakage, the VeRo liberator and high pressure grinding rolls have been shown to liberate, at least to some degree, selectively. However, conclusively proving that selective liberation from these technologies resulted in improved metallurgical performance has often been problematic.

Different modes of liberation were simulated using Voronoi tessellations. Results of samples with the same composition and particle size distribution, were assessed in terms of grade/recovery performance. As well as comparing 'static' theoretical grade-recovery curves, performance was also simulated under dynamic conditions by assigning a probability of recovery to ore and gangue particles. The theoretical grade-recovery curves showed a clear benefit to selective liberation, but results from the Monte Carlo simulations showed there may be a detriment to recovery in particular compared to non-selective liberation. This is attributed to the generation of overly coarse or fine particles, as well as a very poorly liberated fraction depending on the mode of liberation, all of which have a low probability of recovery. The results are specific to both the recovery method and ore texture but they do demonstrate that, in order to benefit from selective liberation, these two factors need careful consideration.

1 Methods

1.1 Liberation Simulation

Liberation was simulated with Voronoi tessellations as outlined by van der Wielen and Rollinson (2016). Five sizes with P_{80}s between 390 and 30µm were simulated, and patterns were re-used for all tests. Selectivity was controlled by overlaying different grain boundary-based patterns and all simulations were performed in ImageJ. The original image (~20 x 30mm) is of a Western African granodiorite with gold hosted in well-defined pyrite crystals. This material was chosen as the relatively euhedral nature of the pyrite crystals, given its comparatively low degree of intergrowth with gangue minerals, was considered to be a good candidate for liberation with a high degree of selectivity Six modes of liberation were simulated to broadly represent the different liberation modes that may be encountered:

- Non-selective liberation
- Selective liberation near the grain boundary
- Selective liberation inside the grain boundary
- Selective liberation outside the grain boundary
- Selective internal fragmentation
- Maximum selectivity fragmentation

1.2 Assessment of Metallurgical performance

Key metrics for metallurgical performance were calculated based on particle-by-particle data available from the Voronoi simulations. Of particular interest were the following:

- Pyrite grade in the 'concentrate'
- Pyrite recovery to the 'concentrate'
- Particle size distribution of pyrite after simulated fragmentation

These numbers are often used in a 'static' manner, without consideration for concentrate dilution by entrained gangue, as well as losses of concentrate particles to tailings. Both can have a significant effect on final grades and recoveries. To incorporate an indication of these factors, Monte Carlo simulations were conducted, assigning probabilities of recovery based on mineralogy and particle size distribution.

From simulated fragmentation products at various sizes a 'typical' mill product particle size distribution (PSD) with a P_{80} of 70µm was reconstructed. As a result of the PSD adjustment the composition of the resultant sample showed a minor variation in pyrite content in the 4.2 – 4.5% range. Probability distributions were set up to resemble performance of a 'typical' rougher bulk sulphide flotation cell based on operational experience and data available for several base metal ores. The key characteristics of the recovery probability distribution were an increasing probability of recovery towards higher liberation values and a peak in probability of recovery in the 25 – 106µm size range, tailing off to 50% in the <25µm range and 15% in the >106µm range. The Monte Carlo simulation involved 1000 individual simulations per sample.

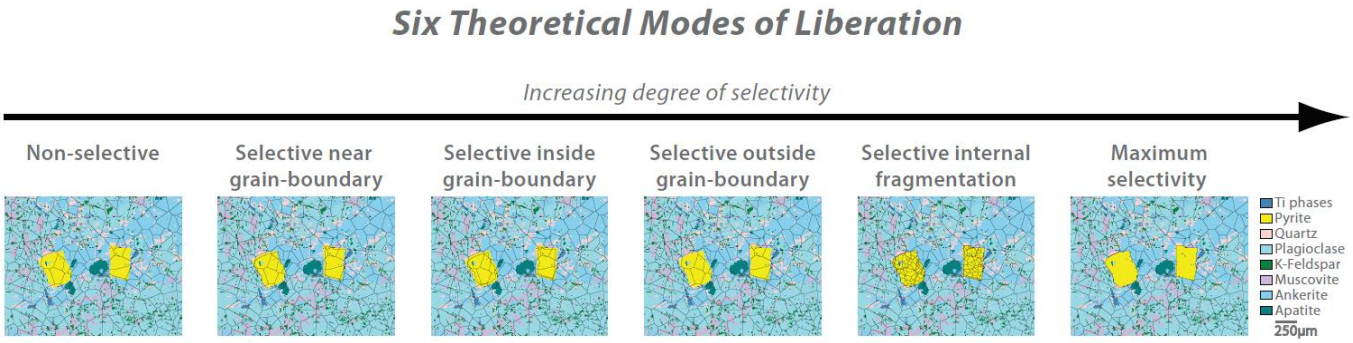

Figure 1 – Effect of theoretical mode of liberation on grade-recovery performance and suggested target grind size

3 Results and Discussion

Figure 1 shows the various modes of liberation ranging from completely non-selective liberation to purely selective liberation. Figure 2 compares 'static' grade-recovery curves for these six modes of liberation, showing a very clear benefit to selective liberation, especially the 'selective internal' and 'maximum selectivity' modes. To achieve a target 85% pyrite grade/80% recovery concentrate, the calculated grind size increases from 61µm for the a-selective sample to >400µm for the 'selective internal' and 'maximum selectivity' samples. This suggests that there could be considerable energy savings at equal metallurgical performance, but as noted in the summary this 'static' assessment does not account for the more dynamic environment of a flotation cell.

Figure 3 shows simulated grade-recovery performance, thought give a more realistic indication of the performance of a bulk sulphide flotation step given the differences in liberation and ore particle size distribution. There are stark differences between the 'static' and simulated grade-recovery response. Firstly, by taking into account losses and entrainment the grade and recovery are both lower than the 'ideal' theoretical grade-recovery curve. Secondly, non-selective fragmentation performs significantly better, providing amongst the best recovery without much detriment to grade. Selective fragmentation outside the grain boundary also performed comparatively well in terms of grade and recovery is whilst selective fragmentation inside the grain boundary provides the best grade, but at a reduced recovery. Grade-recovery curves typically show a decrease in grade with a decrease in recovery, which is not evident from the simulated samples. No explanation is currently available for this unexpected behaviour.

The difference in performance for the theoretical and simulated grade-recovery performance is attributed to the following factors:

- Lower probability of recovery of the very fine and very coarse particles, particularly impacting on metallurgical performance of the selective internal and maximum selectivity modes of liberation
- Selective fragmentation inside the grain boundary creating a proportionally high number of particles with a low percentage of mineral, reducing the likelihood of recovery of these particles.

These results demonstrate that, contrary to common assumption, selective liberation does not automatically result in better metallurgical performance. The probability distribution of recovery/entrainment is a key factor in this, and this will vary strongly across ore textures and recovery techniques. For instance, the probability distribution can be expected to be vastly different between a gravity separation device and a flotation device. Therefore, if consistent selective liberation is found to be achievable with a given comminution technology, careful consideration should still be given as to which ore textures are suitable, as well as the means of recovery after comminution.

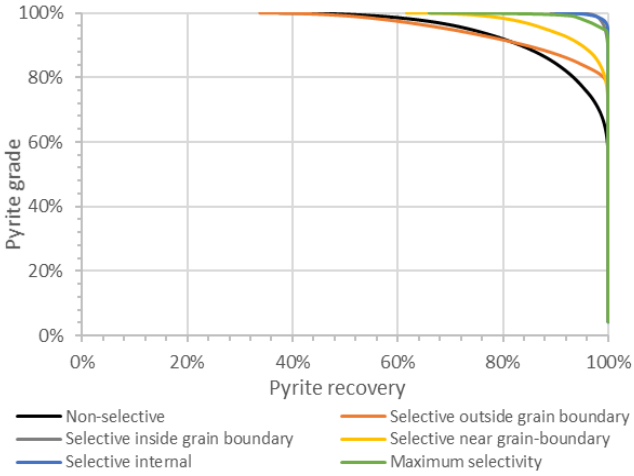

Figure 2 – Theoretical grade recovery curves for the various selective liberation modes

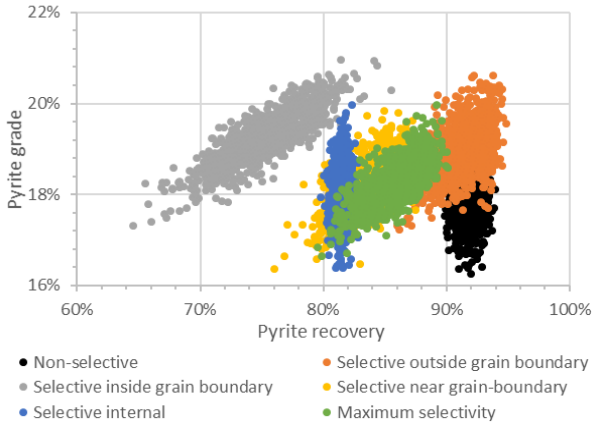

Figure 3 – Simulated dynamic grade and recovery for the various selective liberation modes

4 Conclusions

Various modes of selective liberation were simulated and compared in terms of theoretical as well as simulated 'dynamic' grade-recovery performance. Comparing theoretical grade-recovery curves showed selective liberation to consistently outperform non-

selective liberation. However, when comparing simulated grade-recovery performance accounting for the probability of gangue entrainment and/or concentrate particle loss, non-selective liberation is amongst the best performers in terms of recovery, with little reduction in grade. This conclusion is specific to this ore texture and entrainment/recovery probability distribution. Nonetheless, it has a general relevance in that it demonstrates that selective liberation does not automatically translate to improved metallurgical performance. Consequently, ore textures and recovery methods should be carefully considered when attempting to benefit from selective liberation.

5 References

van der Wielen, K.P and Rollinson, G.K. 2016. Texture-based analysis of liberation behaviour using Voronoi tessellations. Minerals Engineering 89, 93 – 107

ID84 - Mechanistic simulation of dry grinding processes

Anderson Chagas[1,*], *Sandra* Breitung-Faes[1], and *Arno* Kwade[1]

[1]Institute for Particle Technology, Technische Universität Braunschweig, Braunschweig, DE

Summary. Mechanistic modelling approach to grinding operations presents itself was very flexible and capable tool since aims to describe the effect and contribution of the individual interactions and breakage modes between particles. This work assesses the predictive capability of the UFRJ mechanistic model in batch ball milling of Cement Clinker and Limestone, in operational conditions in the limits of its originally intended, in order to evaluate possible improvements and propose future studies in inter-particle interaction models.

1 Introduction

The mechanistic modelling approach to grinding operations presents itself was very flexible and capable tool since aims to describe the effect and contribution of the individual interactions and breakage modes between product particles. In the especial case of dry fine grinding, the relevance of particle-particle interactions rises with decreasing product size. In high energy-intensive operations such dry ball milling and dry stirred media milling, poor description of fine particles interactions may lead to inefficient size reduction and high energy conversion into heat.

Carvalho and Tavares [1] proposed a batch grinding Ball mill model with input from the Discrete Element Method (DEM), called UFRJ mechanistic model. This approach account for the contribution of some microscale particle interactions, namely catastrophic (body) breakage, surface breakage (abrasion/chipping) and loss of resistance to breakage (weakening). DEM simulations were used to describe the mechanical environment in the mill. The model was capable of describing the effects of several design and operating variables in batch ball milling [2] with good product size predictions for coarser particles (bigger than 1 mm), without parameter fitting from milling experiments. In the current formulation, it does not account for the interaction of particles of different sizes captured between the grinding media, in spite of evidences that this is relevant to account the collision energy dampening caused by fine particles [1]. The model also does not directly consider the adhesive forces and agglomeration tendency related with to ultra-fine particles, making its application to dry stirred media mills limited, since those phenomena affect the specific power consumption and product size [4].

The present work assesses the predictive capability of the UFRJ mechanistic model [1] in batch ball milling of Cement Clinker and Limestone. The model is applied to conditions in the limits of its originally intended milling operation in order to evaluate possible improvements and propose future studies in inter-particle interaction models.

2 Materials and methods

Due to the spatial constrains for this paper, details on the adopted model formulation can be found at cited references [1-2].

2.1 Experimental set-up

For the grinding experiments, Cement Clinker and Limestone with median particle size of x50 ≈ 1.34 and 1.06 mm, respectively, was used. In previous experiments, the selected Limestone have presented high tendency of agglomeration for sizes below 300 µm, unlike the selected Cement Clinker. This difference is advantageous in the sense of comparing the model response for both materials once such phenomena is not included on its formulation. The material parameters required by the model were characterized for both materials, based on literature referenced at [1-2]. The particle size of the product samples was measured by laser diffraction using a Mastersizer 3000 instrument (Malvern Panalytical).

The grinding experiments were conducted on a 400 mm diameter by 500 mm length batch mill, fitted with ten 10x10 mm squared lifters. Both mill and lifters were made of steel. All the tests were conducted at dry mode, using 30 mm diameter steel balls as grinding media.

2.2 Discrete Element Method simulations

The UFRJ mechanistic model requires as one of the inputs the distribution of dissipated energy for

collisions between grinding media and mill geometry. These distributions were estimated using the DEM simulations, with the software package EDEM 2018 (DEM Solutions).

It must be mentioned that DEM simulations have included only grinding media and mill geometry due to computational impossibility of including the immense number of product particles. The DEM contact parameters were calibrated by using small scale experiments with grinding media and product together. Simulations using only grinding media were compared to experiments with grinding media + product. As such, it is assumed that the registered collisions during simulation would represent ball-ball contacts with product particles captured between them. This assumption was also adopted by other authors [2, 5].

3 Results and Conclusions

Figure 1 presents a comparison between grinding experimental results and model predictions. Both batch ball grinding tests were done at 70% of the critical speed, with 30% ball filling and 100% product void filling. The grinding time was of 20 minutes. As can be seen in Figure 1, the model presented relative good agreement with Cement Clinker grinding, although, the results begin to deviate for sizes below around 20 µm, with model overestimating generation of fine particles. On possible explanation is that DEM simulation, without product particle, assumes constant collision energy transfer, independently of product median size. However, during batch grinding, the product size in the mill is constantly getting finer. The grinding efficiency and transfer of energy from balls to product might be reduced by dampening as the product becomes finer.

In the case of the Limestone grinding, the current state of the model was less capable of predicting grinding results. With the model again overestimating breakage for sizes below 100 µm. Considering that the used Limestone presents particle agglomeration for such sizes and this behaviour is not considered in the model, this discrepancy was expected. During milling, finer size classes, with higher surface area, tends to agglomerate back to bigger sizes. Those agglomerates are easier to break than original particles. However, some amount of energy is being expended in the desagglomeration process. This process reduces considerable the grinding efficiency, and might explain the model disagreement.

In conclusion, the evaluated UFRJ mechanistic model presents has a versatile formulation and good predictive capacity in a certain region of application. However, improvements are required. The model is formulated as the traditional population balance model (PBM) applied to microscale size reduction processes, describing the rates of changes in mass contained in sizes classes. One way of including the agglomeration phenomena into the model is by adding to the PBM a size dependent particle growth function. This function might also take into account the effect of operational conditions. Naturally, the product would have to be separated in to classes of material, since the agglomerates are weaker than original particles. This alternative is current being studied by the authors of this paper.

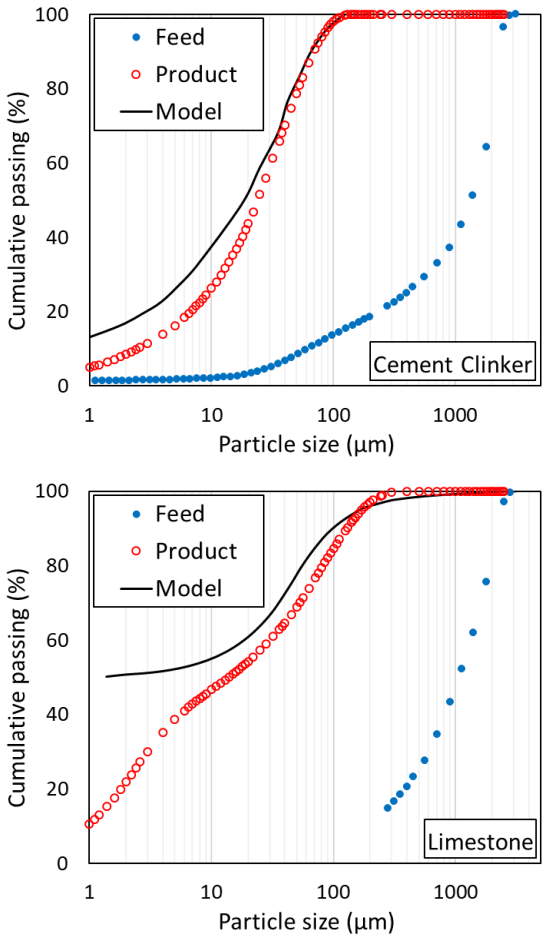

Fig. 1. Comparison between experimental and model results.

References

[1] Carvalho, R.M. and Tavares, L.M., (2010). A mechanistic model of batch grinding in Ball mills. *XXV International Mineral Processing Congress*. vol. 1 AUSIMM, Brisbane, pp. 1287-1297.

[2] Carvalho, R.M., Tavares, L.M. (2013). Predicting the effect of operating and design variables on breakage rates using the mechanistic ball mill model. *Minerals Engineering* 43-44, pp. 91-101.

[4] Prziwara, P., Hamilton, L.D., Breitung-Faes, S., Kwade, A. (2018). Impact of grinding aids and process parameters on dry stirred media milling. *Powder Technology* 335, pp. 114-123.

[5] Burmeister, C., Titscher, L., Breitung-Faes, S. and Kwade, A., (2018). Dry grinding in Planetary ball mills: Evaluation of stressing model. *Advanced Powder Technology* 29, pp. 191.201

ID85 - Development of a single particle breakage model incorporating oblique impact

Li Ge Wang[1,2*], *John P.* Morrissey[3], and *Jin Y.* Ooi[3*]

[1]Department of Chemical and Biological Engineering, University of Sheffield, Sheffield, UK
[2]Process System Enterprise, London, UK
[3]Institue for Infrastructure and Environment, University of Edinburgh, Edinburgh, UK

Summary. This paper presents a mechanistic study of particle breakage subject to impact loading. A simple breakage model based on indentation fracture mechanics is presented assuming that lateral crack accounts for the mass loss of particle in a chipping regime. Addressing the omission of tangential velocity in existing models, the effect of oblique impact angle is incorporated in the breakage model by introducing an equivalent velocity in the light of friction mobilisation. The developed breakage model is assessed with literature data under both normal and oblique impact loading. DEM simulation of particle breakage is carried out to overcome the limitation of impact velocity in the experiments. A bonded contact model based on Timoshenko beam theory is used and the breakage behaviour of chipping and fragmentation are investigated under varying impact velocities and beyond the experimental scope. The concept of equivalent velocity under oblique impact in DEM simulation is examined and discussed. The proposed breakage model provides a basis to evaluate breakage propensity when particle breakage occurs under normal and oblique impact.

1 Introduction

Milling is an essential processing step in many industrial sectors to achieve a desired particle size reduction. Considerable theoretical work has been carried out to elucidate the mechanism of particle breakage subject to stressing events such as impact loading. However, all existing models have their limitations. For example, the majority of breakage models are empirical and fall short of providing a robust mechanistic understanding of the particle breakage. Also, only normal impact velocity is considered whereas the effect of tangential velocity is often omitted. This paper presents a simple breakage model where the effect of oblique impact is considered, based on an indentation fracture mechanism. The new developed analytical model is examined with an experimental dataset under both normal and oblique impact. DEM simulation of particle breakage is further carried out to investigate the breakage beyond the impact velocity limitation in the experiments. A bonded DEM model is used based on the Timoshenko beam theory, which can be used to study cementitious granular materials.

2 Impact breakage pattern

The particle breakage pattern under impact loading can be categorized by two types: chipping and fragmentation. Figure 1 shows the schematic illustration of the two breakage patterns, which are distinguished by the particle size distribution after impact [1].

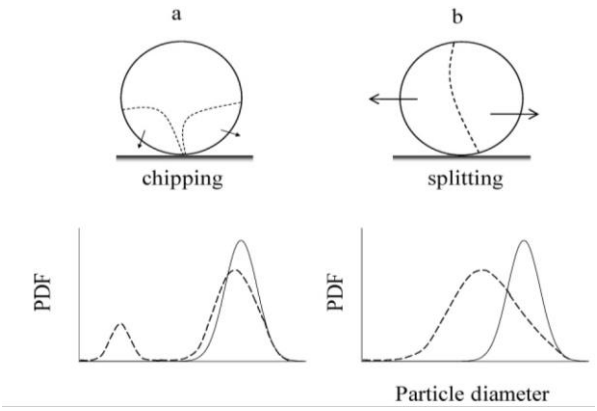

Fig. 1. Schematic outline of two breakage patterns (a) chipping and (b) fragmentation

3 Theoretical breakage model

3.1 Normal impact

The fractional loss on impact under the chipping regime is assumed to arise from the lateral cracking. The breakage probability ε on the basis of indentation fracture mechanism gives:

$$\varepsilon \propto \frac{\rho^{1/4} R^2 H^{1/2}}{k_c^{5/2}} v^{9/2} \quad (1)$$

where ρ and R are the particle density and radius; H and k_c are the hardness and fracture toughness; v is the impact velocity.

3.2 Oblique impact

Breakage models in the literature usually ignores the tangential velocity although the effect of oblique impact has been reported by several studies[1]. It is proposed to give an equivalent velocity v_{en} by mobilizing the dynamic friction coefficient. The impact velocity in Eq. (1) is replaced with the equivalent velocity:

$$v_{en} = v\sqrt{sin^2\theta + \xi^2 sin^2\theta cos^2\theta} \quad (2)$$

where θ is the impact angle and $\xi = \alpha\mu$ is a coefficient including the friction coefficient μ and the mobilisation coefficient α.

3.3 Breakage model prediction

Figure 2 compares the predictions from the proposed breakage model with the measured breakage data from the impact loading tests [1], indicating the effectiveness of equivalent velocity in capturing the influence of oblique impact.

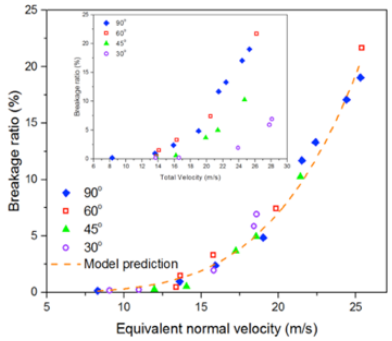

Fig. 2. Breakage model fitting vs. particle breakage data

4 DEM modelling of particle impact breakage

4.1 Bonded DEM contact model and contact evolution

A novel bonded contact model based on Timoshenko beam theory was used to simulate the particle impact breakage[2]. Material damage is represented by the number of broken bonds and more details of this bonded model can be found in [2]. The contact evolution of particle breakage subject to normal impact velocity of 10 m/s and 30 m/s is shown in Figure 3. It can be clearly seen with the chipping under 10 m/s and fragmentation under 30 m/s. Note that the red colour is the intact bond and the blue colour is the broken bond.

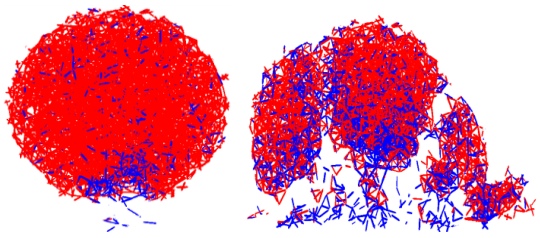

(a) (b)

Fig. 3. Breakage pattern of (a) chipping at 10 m/s impact and (b) fragmentation at 30 m/s

4.2 Validated model of zeolite particle impact

Figure 4(a) shows the damage ratio of zeolite particle in the bonded contact model and Figure 4(b) shows the validated numerical results compared to experimental dataset[1].

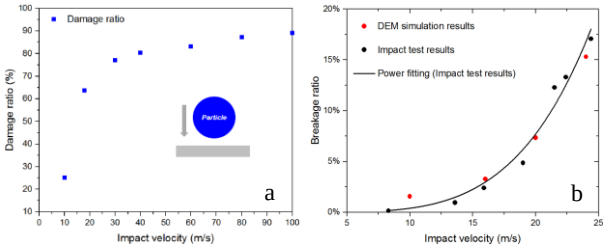

Fig. 4. Breakage evaluation of zeolite particle by (a) damage ratio and (b) breakage probability

5 Conclusion

This paper presents a mechanistic study of particle breakage subject to impact loading. The breakage pattern is first reviewed and a simple breakage model was developed based on an indentation fracture mechanism. The effect of oblique impact was incorporated by proposing an equivalent velocity concept. The DEM simulation of particle breakage using a bonded contact model was deployed to investigate the breakage beyond the impact velocity limitation. The proposed breakage model provides a basis to evaluate the breakage propensity, in particular under oblique impact.

The authors gratefully acknowledge the financial support from International Fine Particle Research Institute (IFPRI). We would like to thank Prof. Mojtaba Ghadiri and Dr. Colin Hare for the courtesy of impact tester and many useful discussions.

References

1. Wang, L.G.: Particle Breakage Mechanics in Milling Operation, (2016)
2. Brown, N.J., Chen, J.F., Ooi, J.Y.: A bond model for DEM simulation of cementitious materials and deformable structures. Granul. Matter. 16, 299–311 (2014)

ID87 - Predictive simulation of impact milling using DEM-PBM multiscale model

Xizhong Chen[1], *John P.* Morrissey[1*], *Li Ge* Wang[2,3], and *Jin Y.* Ooi[1]

[1]Institute for Infrastructure and Environment, University of Edinburgh, Edinburgh, UK
[2]Department of Chemical and Biological Engineering, University of Sheffield, Sheffield, UK
[3]Process System Enterprise, London, UK

Summary. This paper presents a hybrid multiscale modelling framework to predict the milling performance in an impact pin mill by coupling the discrete element method (DEM) and population balance model (PBM). The DEM-PBM coupling framework is established using the commercial DEM code of EDEM[1] and the commercial PBM code in gFORMULATE [2]. DEM simulations at particle level is first carried out to characterize the particle dynamics and the stressing events inside the impact pin mill. The particle scale information such as the impact velocity and impact frequency from DEM is upscaled to inform the selection function in PBM at the process scale. The developed hybrid DEM-PBM coupling framework is shown to provide a good agreement of product size distribution with the experimental results, which serves as a model driven design approach to optimize the design and operation of the impact pin mill, with potential application to many other types of mill.

1 Introduction

Milling is widely used as a size reduction process for particulate materials in many industries, which is notoriously known to be energy intensive and highly inefficient. Hence, more scientific understanding of particle breakage in the milling process is required in light of the overwhelming empiricism of the design and operation of a milling process. To that end, this paper develops a hybrid multiscale modelling using the discrete element method (DEM) and the population balance model (PBM) to predict the milling performance in an impact pin mill. DEM simulation is carried out to provide particle-scale physics and inform the breakage kernel in the PBM at process level. The coupling interface between DEM and PBM are built upon the commercial DEM software EDEM[1] and the commercial PBM software gFORMULATE[2]. The parameters in the DEM-PBM coupling model are calibrated with the experimental data from the impact pin mill. The coupling model with calibrated parameter is then used to predict the other dataset, where the predictive capacity of the model is quantified.

2 DEM-PBM coupling framework

A generic DEM-PBM coupling framework is depicted in Figure 1. The model inputs consist of the material-dependent parameters, i.e. the initial particle size distribution and material properties, and the geometry-dependent parameter, i.e. operational conditions. The multiscale model provides the data exchange mechanism between DEM and PBM. The DEM is carried out to provide the collision velocity distribution to PBM and in turn with such information, PBM is able to predict the product size distribution subject to varying operational conditions.

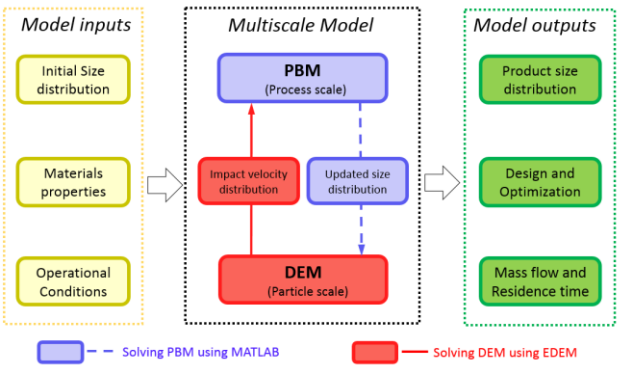

Fig. 1. Multiscale modelling framework of DEM-PBM coupling for milling process

3 DEM modelling of impact pin mill

3.1 DEM geometry of impact pin mill

The impact pin mill of Hosokawa UPZ100 is chosen and its full scale 3D geometry is shown in Figure 2. It can be seen that the mill consists of eight rings of pins. Among

these rings, four rings of pins are fixed to the static plate (shown as red colour) whilst another four rings of pins with blue colour are fixed to the rotary plate which rotate at a given speed. Particles are fed into the mill chamber through the central inlet.

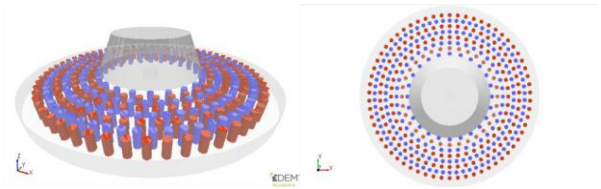

Fig. 2. Schematics of the impact pin mill UPZ100

3.2 DEM geometry of impact pin mill

DEM employs an explicit numerical method to track all particle interactions in a domain with a defined physical law upon contact. The Hertz-Mindlin (no slip) contact model was chosen to resolve the particle and geometry contact interaction, where the normal contact force is based on the Hertzian contact theory and tangential force is based on Mindlin-Deresiewicz's theory.

3.3 Particle dynamics analysis

Figure 3 shows the cumulative density distribution of collision velocity for the pin mill at different rotary speeds. It shows that the average particle collision velocity increases considerably with the increase of rotary speed. Other impact statistics such as the impact frequency, the residence time distribution has also been computed.

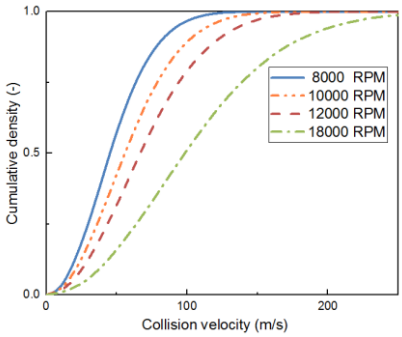

Fig. 3. Cumulative distribution of particle collision velocity

4 PBM modelling of impact pin mill

The mass-based breakage equation in PBM can be expressed as:

$$\frac{dm_i(t)}{dt} = \sum_{j=1}^{i-1} S_j m_j(t) b_{ij} - S_i m_i(t) \quad (1)$$

where i, j are the integers of particle size intervals, $m_i(t)$ is the mass of particle in size interval i, S is the breakage rate and b_{ij} is the mass fraction between i and j.
The breakage rate function S in this study is chosen from the model proposed by Vogel and Peukert[3] whereas the mass fragment size distribution is adopted from Vogel and Peukert[4].

5 DEM-PBM coupling predictions

Figure 4(a) shows the fitted results of particle size distribution of impact pin mill under 12000 RPM with calibrated parameters. With the impact velocity and impact frequency predicted from DEM, the product size distribution subject to three other rotary speeds, i.e. 8000, 10000 and 18000 RPMs is shown in Figure 4(b). The comparison between the hybrid multiscale model and the experiments shows a very good agreement. This indicates a promising application of the developed coupling framework to milling operations.

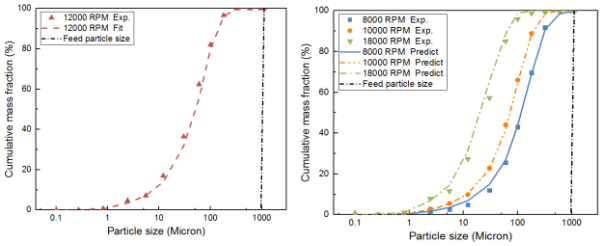

(a) (b)

Fig. 4. DEM-PBM coupling modelling of (a) calibrated 12000 RPM and (b) validated results in 8000, 10000 and 18000 RPMs

6 Conclusion

This paper presents a development of the hybrid multiscale modelling of DEM and PBM to predict the milling behaviour of particles in an impact pin mill. The DEM simulations were carried out to characterise the particle dynamics and the information relevant to the PBM function was used to predict the product size distribution. As compared to the experimental results of the impact pin mill, the developed coupling framework demonstrates a strong predictive capacity with good agreement reached from the numerical results. The proposed multiscale model can also be applied to other types of milling operation to improve the understanding of breakage mechanism and to optimize the design and operation of milling processes.

The authors gratefully acknowledge the financial support from International Fine Particle Research Institute (IFPRI). We would also like to thank useful discussions with staff from Hosokawa, DEM Solutions and Process System Enterprise.

References

1. DEM Solutions Ltd.: EDEM 2017, https://www.edemsimulation.com/, (2017)
2. gPROMS® 4.1 Release Notes, https://www.psenterprise.com/, (2016)
3. Vogel, L., Peukert, W.: Determination of material properties relevant to grinding by practicable labscale milling tests. Int. J. Miner. Process. 74, 329–338 (2004)
4. Vogel, L., Peukert, W.: From single particle impact behaviour to modelling of impact mills. Chem. Eng. Sci. 60, 5164–5176 (2005)

ID89 - A study of Particle Attrition in a (Circulating) Fluidised Bed

Fabio Fulchini[1,2,*], *Antonia* Borissova [1], *Benjamin* Amblard[2], *Stephane* Bertholin[2] , *Ann* Cloupet[2], *Mahdi* Yazdanpanah[3], *Mojtaba* Ghadiri [1]

[1]Faculty of Engineering, University of Leeds, Leeds, UK
[2]IFP Energies Nouvelles, Solaize, France
[3]TOTAL Research & Technology Gonfreville, Le Havre, France

Summary Particle attrition in fluidised beds and circulating fluidised beds is a major issue. It strongly affects the particle size distribution (PSD) of the bed inventory as particles tend to wear out and generate small fines, a part of which can be elutriated, leading to undesired mass loss, variation in the operating behaviour and performances of the process. The evolution with time of the PSD in a fluidised bed and a circulating fluidised bed is addressed by means of a Population Balance Model (PBM), developed in-house, using discretised size classes. Particle attrition is assumed to be caused by three different sources: the gas jets, the bubbling bed and the cyclone for which attrition correlations have been developed experimentally for fresh and equilibrium MnO particles intended to be used as oxygen carriers for the Chemical Looping Combustion. The single particle breakability index of the same particles is determined by impact tests and used to normalise the three attrition correlations. The main assumption of the PBM is that each attrition event will generate a smaller mother particle and one or more debris particles, i.e. no fragmentation. The PBM is then used to simulate particle attrition in a fluidised bed and a circulating fluidised bed, where the recirculation is provided by a high efficiency cyclone and a return leg. The analysis focuses on the strong interplay between the attrition rate and the loss rate at steady state as well as on the PSD evolution of the bed inventory, cyclone and recycle with time as a function of different operating conditions and single particle breakability index.

1 Introduction

Particle attrition in fluidised beds and circulating fluidised beds is a major issue. It strongly affects the particle size distribution (PSD) of the bed inventory as particles tend to wear out and generate small fines, a part of which is elutriated, leading to undesired mass loss, variation in the operating behaviour and performance of the process. Thus, particle attrition is often quantified in terms of mass loss but by itself it does not give any information about the shrinking of the so-called mother particles and consequently on the change in PSD. For this purpose the method of population balance is used in order to unravel the mass transfer between different size classes of particles, with particle size evolving as a result of attrition (Yang, 2003). With the basic assumption that attrition only occurs by surface abrasion, several mathematical models have been formulated in the past. This assumption simplifies the resolution allowing to treat the attrition mass as it would be completely lost (Levenspiel et al., 1968) or collected in the last size class (Hansen and Ottino, 1997) (Ray et al., 1987) (Werther and Hartge, 2004)(Klett et al., 2007) (Redemann et al., 2009). The latter approach always brings along another main assumption: the material collected in the last size class is no longer subjected to attrition and as a result the upper limit of the lowest size class becomes the minimum mother particle size.

In numerous cases, the PSD of real circulating fluidised bed processes is successfully compared with that given by the population balance (Hartge et al., 2007) (Redemann et al., 2009) confirming its validity and reliability into predicting what occurs to the bed inventory.

Moreover, Werther and Hartge (2004) showed the strong interrelation between attrition and efficiency of the solids recovery cyclone, which is able to hold and recycle the majority of particles back but, at the same time, produces fines due to attrition. Cyclone attrition would indeed increase with its efficiency.

Ray et al. (1987) and Werther and Hartge (2004) confirmed that the material loss rate from the bed is directly linked to the attrition rate. The latter is the rate-controlling step at steady state because the amount of fines inside the bed does not change considerably as they are continuously produced by attrition and promptly elutriated.

* Corresponding author: pmwpg@leeds.ac.uk

Accordingly, this work aims to study the effect of particle attrition in a fluidised and circulating fluidised bed by means of a population balance model, where attrition is caused by three main sources: the gas jets at the distributor, the bubbling bed and the cyclone. Each source of attrition, in the population balance, is represented by a mathematical correlation that returns the fractional mass loss per unit time.

The solids recirculation in the circulating fluidised bed is provided by a high efficiency cyclone and a return leg.

The study focuses on the evolution of the PSD as a function of time and on the interplay between attrition rate and loss rate.

2 Materials and Methods

The test materials are a fresh and an equilibrium MnO, Geldart group B, powder intended to be used as oxygen carrier for the chemical looping combustion. Initially, the single particle breakability upon impact is evaluated using two different items of equipment: the single particle impact test (Ahmadian and Ghadiri, 2007; Kwan et al., 2004) and the Scirocco impact test (Bonakdar et al., 2016; Ali et al., 2015). The experimental data, obtained as a function of different impact velocities and sizes, are reported in terms of fractional mass loss. The model of Ghadiri and Zhang (2002) of chipping of semi brittle material is used to fit the experimental data. It is then used to calculate the minimum. mother particle size for the population balance.

The attrition correlation for the gas jets/bubbling bed and the cyclone are empirical based on experimental data for the two test materials. In particular, the gas jets/bubbling bed attrition is characterised as the steady state mass loss rate using a fluidised bed of 0.1 m diameter and 1 m high while the cyclone induced attrition is characterised as the fractional mass loss per cycle using a high efficiency Stairmand cyclone of 0.04 m diameter and 0.16 m high.

The main assumption of the population balance is that one mother particle produces one or more debris particles. The mass of the debris produced by attrition from each mother particle, on each time step, is compared with the mass produced by the same mother particle upon the critical impact velocity mentioned above. If the former is larger than the latter, then the number of debris becomes equal to the ratio of the two masses. The integration time step accounts for the solids circulation rate and the attrition rate, as it should not be greater than 1% of the average recirculation time of the solids and at the same time, it should not allow debris particles larger than 80 μm.

The mass transfer between discretised size classes occurs then for both mother and debris particles.

The Population Balance Model is developed and solved in Matlab.

References

Ahmadian, H. and Ghadiri, M. 2007. Analysis of enzyme dust formation in detergent manufacturing plants. *Advanced Powder Technology*. **18**(1),pp.53–67.

Ali, M., Bonakdar, T., Ghadiri, M. and Tinke, A. 2015. Particle Breakage in a Scirocco Disperser. *Powder Technology*. **285**,pp.138–145.

Bonakdar, T., Ali, M., Dogbe, S., Ghadiri, M. and Tinke, A. 2016. A method for grindability testing using the Scirocco disperser. *International Journal of Pharmaceutics*. **501**(1),pp.65–74.

Ghadiri, M. and Zhang, Z. 2002. Impact attrition of particulate solids. Part 1: A theoretical model of chipping. *Chemical Engineering Science*. **57**(17),pp.3659–3669.

Hansen, S. and Ottino, J.M. 1997. Fragmentation with abrasion and cleavage: analytical results. *Powder Technology*. **93**,pp.177–184.

Hartge, E.-U., Klett, C. and Werther, J. 2007. Dynamic simulation of the particle size distribution in a circulating fluidized bed combustor. *Chemical Engineering Science*. **62**(1–2),pp.281–293.

Klett, C., Hartge, E.-U. and Werther, J. 2007. Time-Dependent Behavior of a Catalyst in a Fluidized Bed/Cyclone Circulation System. *IFAC Proceedings Volumes (IFAC-PapersOnline)*. **53**,pp.769–779.

Kwan, C.C., Chen, Y.Q., Ding, Y.L., Papadopoulos, D.G., Bentham, A.C. and Ghadiri, M. 2004. Development of a novel approach towards predicting the milling behaviour of pharmaceutical powders. *European Journal of Pharmaceutical Sciences*. **23**(4–5),pp.327–336.

Levenspiel, O., Kunii, D. and Fitzgerald, T. 1968. The Processing of Solids of Changing Size in Bubbling Fluidized Beds. *Powder Technology*. **2**,pp.87–96.

Ray, Y.C., Jiang, T.S. and Jiang, T.L. 1987. Particle Population Model for a Fluidized Bed with Attrition. *Powder Technology*. **52**,pp.35–48.

Redemann, K., Hartge, E.U. and Werther, J. 2009. A particle population balancing model for a circulating fluidized bed combustion system. *Powder Technology*. **191**(1–2),pp.78–90.

Werther, J. and Hartge, E.U. 2004. A population balance model of the particle inventory in a fluidized-bed reactor/regenerator system. *Powder Technology*. **148**(2-3 SPEC. ISS.),pp.113–122.

Yang, W.-C. 2003. *Handbook of Fluidization and Fluid-Particle Systems*.

ID91-Investigation of Phase Transformations of Omeprazole Magnesium during Milling

Hanane Abouhakim[1], *Ali* Hassanpour[1], *Frans* Muller[1], *Sven* Schroeder[1], *Mike* Quayle[2]

[1] School of Chemical and Process Engineering, University of Leeds, Leeds LS2 9JT, UK
[2] AstraZeneca, Pharmaceutical Technology & Development, Pepparedsleden 1, SE-431 83 Mölndal, Sweden

Introduction

Pharmaceutical processes such as milling induce different levels of disorder to the crystalline solid API (Newman & Zografi, 2014). Phase transformation of drugs remains unanticipated and it causes potential costs to the pharmaceutical industry due to the lack of research and any work is heavily depending on trial and error (Savjani *et al.*, 2012; Halme *et al.*, 2019). The aim of this work is to design a new approach that allows anticipating and controlling the phase transformation based on a novel route called quality by design approach which relates the critical attributes (material properties) to the critical parameters (process conditions) (Storey & Ymen, 2011; Halme *et al.*, 2019; Hossain Shariare *et al.*, 2012). For this purpose, Omeprazole magnesium a pharmaceutical API used to treat stomach acid reflux was milled in planetary ball mill at different milling time (from 1 min to 300 min). Moreover, key material properties including crystal structure, slip planes and mechanical properties were predicted using molecular modelling approaches. Experimentally, various analytical techniques were employed to investigate the impact of milling on the crystalline structure of Omeprazole magnesium including XRD, TGA and FTIR.

Results and Discussion

The milling of Omeprazole magnesium leads to the formation of amorphous form after 30 min milling as shown in Figure 11.

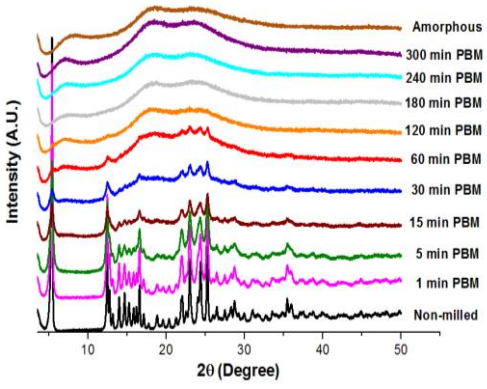

Figure 11. XRD of Omeprazole magnesium before milling and after milling with Planetary Ball Mill from 1 min to 300min

Where sharp peaks represent the crystalline form of Omeprazole magnesium and broad peaks represent the amorphous form. The mechanism of this phase transformation is related to the shear and impact from the planetary ball mill (Chauruka *et al.*, 2015) which lead to the distortion of crystalline structure of the Omeprazole magnesium. The thermal analysis of Omeprazole magnesium revealed two mass losses (Figure 12) which are equivalent to the loss of four water molecules holding the crystalline structure of Omeprazole magnesium. The mass losses appear to occur during two consecutive events which indicate the different bonding nature of these water molecules. Moreover, the heat generated from milling is thought to facilitate the movement of water molecules which evaporate and lead to further distortion of the crystalline order. An additional factor can be related to the presence of slip planes which can further enhances the plastic deformation as a result of the movement of dislocation within the crystalline structure (Olusanmi *et al.*, 2011).

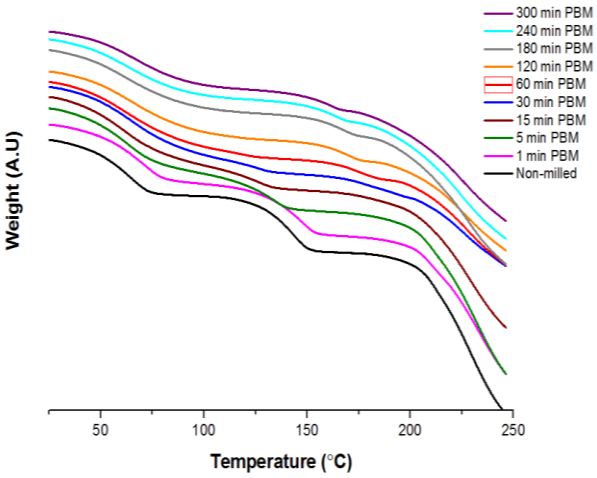

Figure 12: TGA Profile of Omeprazole magnesium for the non-milled and milled at Planetary Ball Mill.

Conclusion

Phase transformation of Omeprazole magnesium is suggested to occur as a result of the loss of water molecules, distortion of the hydrogen bonds holding the crystal lattice, and the movement of dislocation as a result of the shear and impact stresses generated inside the planetary ball mill. The main

underlying critical attributes responsible for this change include the crystalline and mechanical properties of Omeprazole magnesium, and the main critical parameters attributing to this phase transformation are the prevailing shear and impact from the mill in addition to the milling time.

References

Chauruka, S. R., Hassanpour, A., Brydson, R., Roberts, K. J., Ghadiri, M. & Stitt, H. (2015). *Chem. Eng. Sci.* **134**, 774–783.

Halme, A., Quayle, M. J., Nilsson Lill, S. O., Pettersen, A., Fransson, M. & Boissier, C. (2019). *Cryst. Growth Des.* **19**, 3670–3680.

Hossain Shariare, M., J Leusen, F. J., de Matas, M., York, P. & Anwar, J. (2012). *Pharma Res*. **29**, 319–331.

Newman, A. & Zografi, G. (2014). *J. Pharm. Sci.* **103**, 2595–2604.

Olusanmi, D., Roberts, K. J., Ghadiri, M. & Ding, Y. (2011). *Int. J. Pharm.* **411**, 49–63.

Savjani, K. T., Gajjar, A. K. & Savjani, J. K. (2012). *ISRN Pharm.* **2012**, 1–10.

Storey, R. A. & Ymen, I. (2011). Solid state characterization of pharmaceuticals John Wiley & Sons.

ID92 - Analysis of Pin Milling of Pharmaceutical Materials by Discrete Element Method

Wei Pin Goh, *Tina* Bonakdar and *Mojtaba* Ghadiri

School of Chemical and Process Engineering, University of Leeds, Leeds, LS2 9JT, UK

Summary. Milling is an important process for tailoring the particle size distribution for enhanced dissolution, content uniformity, tableting, etc., especially for active pharmaceutical ingredients and excipient in pharmaceutical industries. Milling performance of particulate solids depends on the equipment operating conditions (geometry, process conditions and input energy etc.) as well as material properties (particle size, shape, and mechanical properties, such as Young's modulus, hardness and fracture toughness). A novel approach has been developed to assess the breakability of pharmaceutical materials using an aerodynamic dispersion method. In this work, we combine this approach with the Discrete Element Method (DEM) to simulate the dynamic behaviour of a number of pharmaceutical materials in a pin mill. A sensitivity analysis is carried out addressing the effect of the milling condition (rotational speed of the mill and feed particle flow rate) and feed properties on the quality of the milled products in terms of the shift in the specific surface area of the milled particles. The outcome of the work is used as a method to predict the breakage of the particles for the milling conditions where chipping takes place.

1 Introduction

Milling is commonly used in a wide range of manufacturing operations to tailor desired product specifications and quality attributes (Rowe, 2006). The milling performance of particulates is dictated by the mechanical properties of the material (hardness, fracture toughness and Young's modulus) and, the operating conditions of the chosen mill such as the geometry, process conditions, input energy, etc. The use of pin mill is ubiquitous as it has a small footprint, is versatile, able to mill a wide range of solids and has a relatively reasonable energy consumption. Pin mill is essentially a disc mill that consists of two steel plates with a number of sets of concentric pins that can be configured to: (i) have one of the discs rotating while the other stays stationary or (ii) have both of the discs rotating in the opposing direction to achieve higher energy milling. The working principle of a pin mill is similar to that of a hammer mill where the size reduction is due to the impacts between the particles and the pins but generally at higher tip speed configuration.

At the early stages of product and process development, adequate test material is not generally available. Therefore, a methodology is required to predict the milling behaviour based on the properties of the test material. For materials that exhibit semi-brittle behaviour, their breakage propensity can be described as a function of their mechanical and physical properties and incident impact energy (Ghadiri and Zhang, 2002). Several experimental approaches have been developed to obtain the material breakage kernel using various equipment, concerning single particle impact. The earliest one being the single particle impact tester developed by Yüregir et al. (1986), where the size analysis is gravimetric based. However, the device is not available commercially and therefore generally not accessible. Bonakdar et al. (2016) proposed a new approach where the extent of particle breakage can be determined experimentally in a commercially-available particle size analyser. For brittle failure mode, the model of Vogel and Peukert (2003), based on Weibull's model (1951) is also widely used.

During pin milling, particles undergo a series of impacts at varying degree of impact velocities before they exit the milling chamber. The complex interaction between the particles and the pins is an important factor that decides the particle size distribution of the milled product. In this work, we analysed the particle dynamics and breakage behaviour of crystalline materials in a commercially available pin mill, PicoPlex using the Discrete Element Method (DEM). The particles are modelled as polyhedra, which remain as a single element until the load applied exceeds the minimum required energy for the particle to break. The impact breakage model of Bonakdar et al. (2016) is adopted to obtain the impact breakage kernel of materials. The effect of the process conditions such as the feed rate and rotation speed of the pins on the size of the milled materials, expressed as the shift of specific surface area, is investigated.

2 Methodology

The PicoPlex pin mill of Hosokawa Micron (Fig. 1 (a)) is simulated using Rocky DEM software package (ESSS Co., Florianópolis, Brazil). For simulation, the material properties are based on paracetamol crystals. 327, 388 and 461 µm mono-sized particles corresponding to the geometric mean of sieve cuts of 300-355, 355-425 and 425-500 µm (BS410) are used. The shape of the particle is assumed as polyhedron of 26 faces as shown in Fig. 1 (b). The geometry of the pin mill is simplified to remove features that would otherwise slow down the simulation (Fig. 1 (c)). The material properties and interactions used in the simulation are shown in Table 1. Feed rates of 0.1, 0.2 and 0.4 g/s are investigated as well as the rotational speeds (3000, 6000, 10000 and 30000 RPM) of the mill.

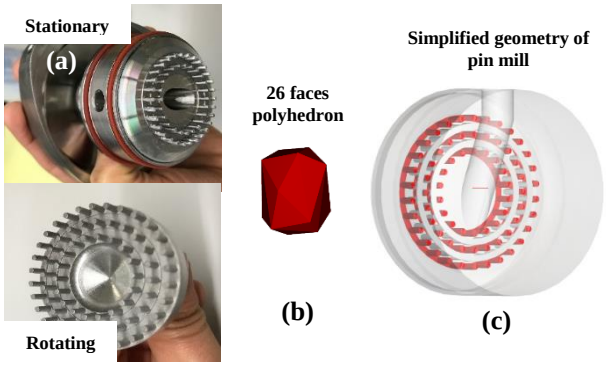

Fig. 1. PicoPlex pin mill of Hosokawa Micron comprising a stationary and a rotating part (a); particle modelled as 26 faces polyhedron (b) and simplified geometry of pin mill (c).

Table 1. Material properties and interactions

MATERIAL PROPERTIES		
	GEOMETRY	PARTICLE
DENSITY, *P* (KG/M^3)	7800	1290
YOUNG'S MODULUS, *E* (N/M^2)	2 x 10^{11}	5.7 x 10^7
MATERIAL INTERACTIONS		
	GEOMETRY-PARTICLE	PARTICLE-PARTICLE
STATIC FRICTION (-)	0.3	0.25
DYNAMIC FRICTION (-)	0.3	0.25
COEFFICIENT OF RESTITUTION (-)	0.3	0.25

4 Discussion and Conclusion

Increasing the rotational speed reduces the particle residence time in the mill. The higher the feed rate, the shorter the particle residence time (Fig. 2 (a)). The average number of collisions between the particles and the outer most ring increases slightly as the rotational speed increases from 3000 to 10000 RPM. There is a substantial increase in the average number of collisions when the RPM is increased from 10000 to 30000 RPM (Fig. 2 (b)). Though experiencing the lowest average number of collisions, at the outermost ring, highest collision energy is recorded. However, most of the collision energy is dissipated on the middle ring of the pin mill (Fig. 2 (c)).

The above information, when combined with the breakage kernel of a given material, would provide predictive capability of size reduction in pin mills.

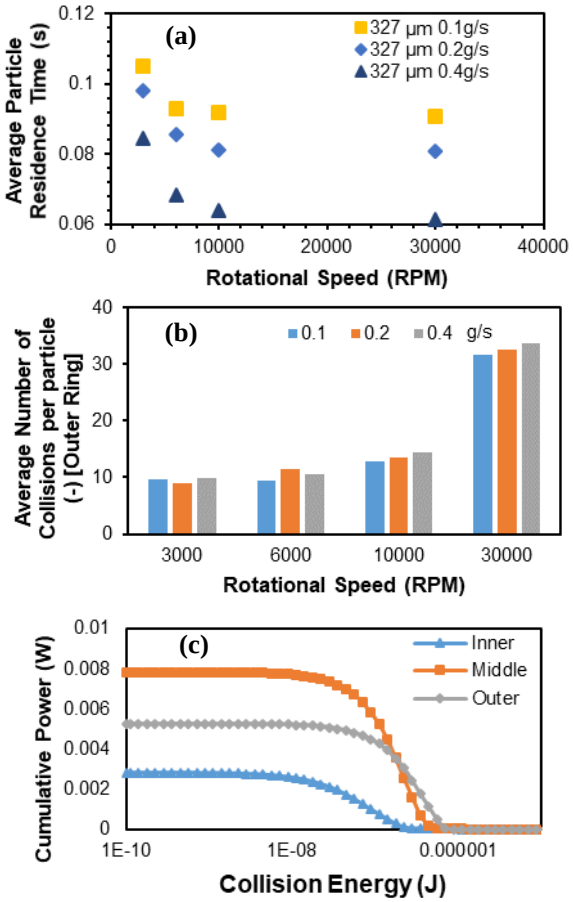

Fig. 2. Average particle residence time vs RPM (a); Average number of collision per particle vs RPM (b); Cumulative power vs collision energy (c)

References

Bonakdar, T., Ali, M., Dogbe, S., Ghadiri, M. and Tinke, A. 2016. A method for grindability testing using the Scirocco disperser. *International Journal of Pharmaceutics*. **501**(1–2),pp.65–74.

Ghadiri, M. and Zhang, Z. 2002. Impact attrition of particulate solids. Part 1: A theoretical model of chipping. *Chemical Engineering Science*. **57**(17),pp.3659–3669.

Rowe, R. 2006. *Handbook of pharmaceutical excipients*. London Greyslake, IL Washington, DC: Pharmaceutical Press American Pharmacists Association.

Vogel, L. and Peukert, W. 2003. Breakage behaviour of different materials - Construction of a mastercurve for the breakage probability. *Powder Technology*. **129**(1–3),pp.101–110.

Weibull, W. 1951. A statistical distribution function of wide applicability. *Journal of applied mechanics*. **18**,pp.293–297.

Yüregir, K.R., Ghadiri, M. and Clift, R. 1986. Observations on impact attrition of granular solids. *Powder Technology*. **49**(1),pp.53–57.

ID93 - Investigating the Effect of Particle Characteristics on Iron Ore Separation using X-ray Micro Tomography

Mehdi Safari[1,*], *Sadegh* Nadimi[2], *David* Deglon[1], *Laurindo* Filho[3] and *Thiago* Souza[4]

[1]Centre for Mineral Research, University of Cape Town, Cape Town, South Africa
[2]School of Engineering, Newcastle University, Newcastle upon Tyne, UK, NE1 7RU
[3]University of São Paulo, Polytechnic Engineering School, Mining and Petroleum Department 2373 Prof. Mello Moraes Av., 05508-900 São Paulo, SP, Brazil, Vale
[4]Vale Institute of Technology, Juscelino Kubitschek , Av., 31 – Bauxita, Ouro Preto, MG 35.400-000, Brazil

Summary. This study provides a simple, meaningful and quantitative approach for particle characterisation that is suitable for mineral particles. The effect of particle characteristics (shape, size and liberation) on particle mineral floatability is investigated which can contribute towards the better understanding of flotation process.

1 Introduction

Flotation is a separation method used for the beneficiation of a considerable portion of the world's mineral ores. Global resource companies are currently operating under very challenging economic and regulatory conditions. Historically, research in minerals processing has been carried out without access to detailed particle characterisation information. The assessment of comminution performance was (and in many cases still is) based on size reduction, and the assessment of separation processes such as flotation was based on elemental recoveries. The need to characterise and understand mineral behaviour during minerals processing is increasingly being recognised for both optimisation and design, as it is liberation and particle properties which to a large extent controls the process.
Particle size distribution has a strong impact on flotation performance. A relatively narrow distribution is preferable to avoid loss of coarse composites or ultra-fines. However, different flotation conditions are optimal for different particle size distributions. Recovery and flotation rate are closely linked to liberation. Flotation is affected by many physical and chemical factors, such as particle shape, size and surface hydrophobicity. It is acknowledged that problems of shape and morphology are 3D problems, and advances in X-ray micro Computed Tomography (μCT) are increasing the feasibility of 3D morphological analysis.
This paper investigates the effect of particle physical properties on the reverse flotation of iron ore. Flotation is affected by both physical and chemical factors. The focus of this paper is on the physical properties including particle morphology.

2 Experiment

This work has been carried out using the case study of Iron ore (Hematite and Quartz). The study uses results from the flotation of Timbopeba iron ore (Brazil, Vale) in a laboratory batch mechanical flotation cell. The effect of particle morphology on the recovery of coarse quartz and hematite (+150 μm) are investigated.
To determine the effect of particle properties on recovery of coarse quartz and hematite particles, flotation experiment were performed at a fixed impeller speed, froth height, flotation time and reagent dosage (collector, depressant and frother). The results are shown in Fig. 1. The recovery of quartz particles for different particle sizes shows that maximum peaks for the particle size of 25 μm can be attributed to the entrainment phenomena. Furthermore, maximum peaks for particle size of 100 μm can be due to increasing attachment efficiency detachment efficiency in this particle size fraction. The increase in the particle size led to a more decrease in the coarse particle recovery rather than the decrease in the fine particle recovery. The increase of bubble drainages causes the detachment of coarse quartz particles with higher density that has less chance to be transported to the concentrate and settled more quickly and drop back to the pulp phase.
The water recovery is a carrying medium to transfer the fine particles of hematite into the concentrate by entrainment. The increase in the particle size led to a more decrease in the coarse hematite recovery with entrainment rather than the decrease in the fine hematite recovery. The comparison of plant results and lab results shows that the coarse quartz particles in plant were not recovered properly; however they were recovered easily in the lab.

The results show that the increasing of superficial gas velocity has a more significant effect on the hematite recovery than the quartz recovery.

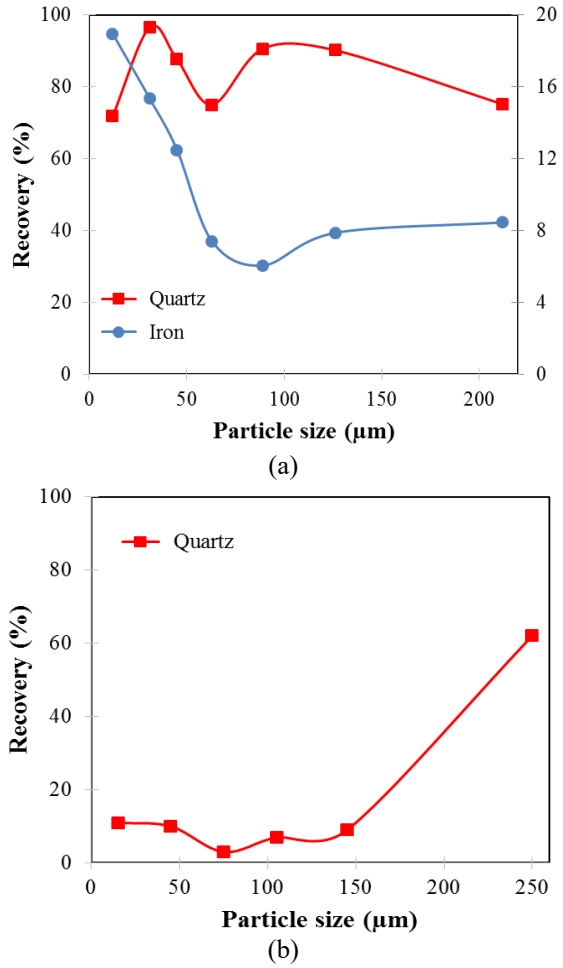

Fig. 1. Recovery of quartz and hematite (a) Recovery in concentrate, Lab scale (b) Recovery in tail, Industry scale

3 X-ray micro computed tomography

µCT was performed using a North Star Imaging X5000 CT scanning system. The 3D images obtained are maps of X-ray attenuation based on composition and density of the material. Therefore, each pixel in the image has an intensity value (or colour) associated with the material it represents. A total of 1440 images were captured on a pixel size of 6.4µm using a 160 kV accelerating voltage. Figure 2a,b shows a cross section of tail and concentrate samples. The white particles shows hematite and the grey particles are quartz. It can be seen that most of the fine quartz particle have been recovered and they are in concentrate. While the coarse quartz remained in the tail (it is important to note that the process is reverse flotation in which the main ore remains in the tail).

Figure 3a shows the 3D volume of the concentrate sample. In order to perform the shape characterisation, the images are segmented using watershed algorithm (Nadimi & Fonseca, 2019) and the particle sphericity, angularity, convexity and etc. are reported. Figure 3a presents the coarse quartz and hematite particles in the tail sample. Figure 3b presents the coarse hematite particles in the concentrate which mainly is quartz.

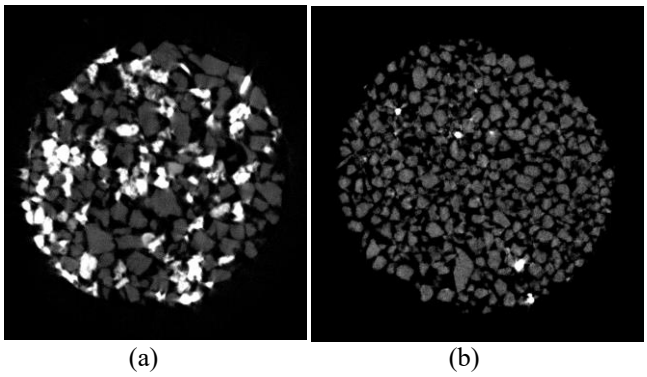

Fig. 2. Cross-section through the sample (a) Tail (b) Concentrate

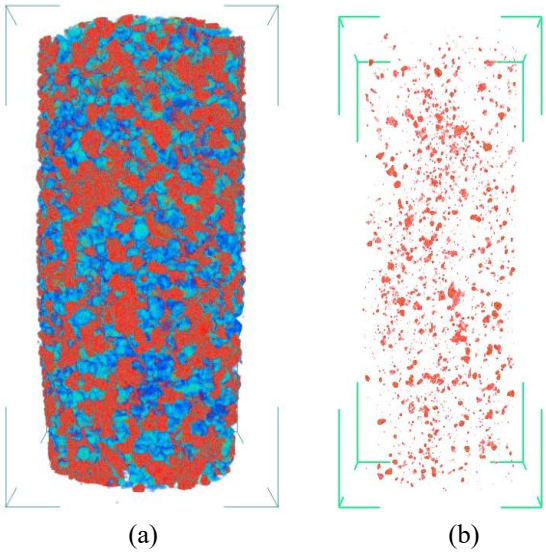

Fig. 3. 3D visualisation of (a) concentrate (b) tail samples (hematite is presented in red and quartz in blue).

This study applies a new technique, i.e. µCT, to better understand the separation of minerals.

Acknowledgment

This study was supported by the Royal Academy of Engineering under the Industry Academia Partnership Programme - 17/18 scheme (Ref: IAPP1\100146: Characterisation Advances in Particle Engineering). The authors would also like to thank Mr. Guy Tolley of North Star Imaging UK for his assistance with running CT scans.

References

Nadimi, S. and Fonseca, J., 2019. Image based simulation of one-dimensional compression tests on carbonate sand. *Meccanica*, 54(4-5), pp.697-706.

ID94 - Influence of Mechanical Properties on Milling of Amorphous and Crystalline Silica-Based Solids

Siwarote Siriluck[1], *Umair* Zafar[1], *Colin* Hare[1i], *Ali* Hassanpour[1], *Martin J.* Murtagh[1,2], *Nadja T.* Lönnroth[2ii], *Navin* Venugopal[2], *Mojtaba* Ghadiri[1]

[1]*School of Chemical and Process Engineering, University of Leeds, LS2 9JT, UK*
[2]*Corning Incorporated, Corning, NY, United States*[1]Faculty of Engineering, University of Leeds, Leeds, UK

Summary. Milling is an important and energy-intensive stage in manufacturing processes for preparing particulate solids to required product specifications in many industrial sectors. It has been studied extensively over the last few decades in order to improve the rate of milling, energy utilisation and control of milling operations. With development of new inorganic materials and application of new milling systems, understanding the underlying science of milling is highly desirable for efficient and predictable size reduction processes. In the glass industry, grades of silicate glasses have been developed with special properties such as high hardness, durability, transparency, low density, high bendability and high scratch resistance, which enable their use in specialised applications. However, knowledge of these glasses for the process of particle size reduction is still limited and poses challenges in the manufacturing process. In this work, breakability and grindability of such silicate materials are investigated and correlations for their milling performance and energy utilisation as a function of material properties are developed. This involves detailed physical and mechanical characterisation of the selected materials along with the analysis of milling rate in a single ball mill to develop a better understanding and control of milling behaviour which can be used for process optimisation.

1 Introduction

Silicates have special properties which have been explored by many manufacturing industries, in particular the glass industry. However, evaluation of milling technology and method for newly developed glasses is challenging due to their high hardness, toughness and stiffness, which require considerable energy to reduce their size. Therefore, it is of great interest to establish the most efficient size reduction method for both amorphous and crystalline structures of such materials.

The milling process for glass materials has been studied extensively with the aim of improving the rate of milling, energy utilization and control of the milling process. These milling characteristics have been linked with the material physical and mechanical properties by Förch et al., 2009; Chen et al.,2010; Glover and Ball, 2014, Gross and Tomozawa, 2008; Kjeldsen et al., 2013. Nevertheless, the ability to predict milling performance of new and specialty glasses, such as lithium silicate and sodium aluminium silicate, is still limited due to the complex nature of these materials. Therefore, in this work an attempt is made to understand the underlying science of milling for these materials, and to correlate the milling rate and energy utilisation to the physical and mechanical properties as proposed by Ghadiri and Zhang (2002).

2 Material

Three sets of model material in two forms, amorphous and crystalline, were chosen and assessed for their milling. Fused silica and quartzite constituted one set and pairs of lithium silicate and sodium aluminium silicate (prepared in amorphous and crystalline forms) were the other two sets. All samples were cut into 7.5 mm cubes and supplied by Corning Inc., USA. Fused silica was obtained by melting and fast cooling of quartz sand. The crystalline quartzite was obtained from natural stones from Squaw Peak on Monument Mountain located in Great Barrington, Massachusetts, U.S.A. The silicate samples were produced at different cooling rates in order to create the amorphous and crystalline structures. The list of these model materials and their compositions are given in Table 1. They have been characterised for their physical and mechanical properties relevant to the size reduction.

Table 1: List of model materials used in the milling work

Pair	Amorphous	Crystalline
1	Fused Silica SiO_2	Quartzite α-SiO_2
2	Lithium silicate 33.3 Li_2O-66.6 SiO_2	Lithium silicate $Li_2Si_2O_5$
3	Sodium aluminium silicate 25 Na_2O-25 Al_2O_3-50 SiO_2	Sodium aluminium silicate $NaAl(SiO_4)$

3 Milling Results and Discussion

The milling of the six silicate materials was carried out using a Retsch MM200 single ball mill and the milling behaviour and breakage mechanism in terms of fracture, micro cracks, chipping and fragmentation were analysed.

The milling performance was assessed on single cubes of each test material using a single ball mill at different relative humidity values. It was found that relative humidity had no notable influence on the milling rate. The amorphous form of the test materials underwent chipping by conchoidal fracture initially, followed by propagation of cracks into the body of the specimens. In contrast, the crystalline forms initially failed by crystallite grain boundary failure, followed by the fracture of crystallite grains themselves. A first order milling rate described the size reduction of the amorphous forms, whilst the crystallite forms showed a more complex breakage rate, which was approximated by two sequential first order rate processes. The milling rate constant corresponding to tests at 44 % RH was used in the analysis for relating the milling rate to the mechanical properties as the latter was measured under similar conditions. For both amorphous and crystalline forms, sodium aluminium silicate has the largest milling rate constant, albeit by different mechanisms for crack initiation and propagation.

The breakability index as described by H/K_c^2 was used to explore the dependence of the milling rate constant on the mechanical properties. As intuitively expected, the amorphous forms does not show a strong dependence on H/K_c^2 as the failure mode is brittle for which pre-existing flaws are responsible. In contrast the crystalline forms show strong correlations for both inter-crystallite grain boundary as well as crystallite milling, implicitly suggesting that they both undergo semi-brittle failure; the milling rate constant increases with the breakability index. However, whilst H/K_c^2 describes the milling rate consistently for all the three materials within each set of material failure system, i.e. amorphous, inter-crystallite grain and crystallite milling, the quantitative trend for each material on its own for amorphous and crystalline milling does not follow the expected trends. For example for sodium aluminium silicate H/K_c^2 is nearly the same for both amorphous and inter-crystallite grain (around 4.3 m^2/kJ), but the milling rate constant of amorphous form is about half of the inter-crystallite breakage rate. Similarly the crystallite form of the same material has a large value of 9.93 m^2/kJ for H/K_c^2 but the milling rate constant is 0.13, i.e. roughly a third of the other two breakage forms. Similar trend is also seen for SiO_2 and lithium silicate. So clearly the brittleness index alone cannot describe the changes in the intermolecular structure as the silicates transform from amorphous to crystalline, and for the latter the differences in the bulk ensemble of bonded crystallites and individual crystallites. However within each set of structures the milling rate constant is described well by the breakability index.

This work was supported by a scholarship for the first author by the Royal Thai Government and sponsorship of the project by Corning, USA.

References

Chen, X., M. A. Rickard, J. W. Hull Jr, C. Zheng, A. Leugers and P. Simoncic. 2010. Raman spectroscopic investigation of tetraethylammonium polybromides. *Inorganic chemistry*, 49(19), pp.8684-8689.

Förch, R., H. Schönherr and A. T. A. Jenkins. 2009. *Surface design: Applications in bioscience and nanotechnology*. John Wiley & Sons.

Ghadiri, M. and Z. Zhang. 2002. Impact attrition of particulate solids. Part 1: a theoretical model of chipping. *Chemical Engineering Science*, 57(17), pp.3659-3669.

Glover, G. and A. Ball. 1979. The Deformation and Fracture of Quartz. *In: Engineering Applications of Fracture Analysis: Proceedings of the First National Conference on Fracture Held in Johannesburg, South Africa*, Elsevier, pp.419-428.

Gross, T. and M. Tomozawa. 2008. Indentation-induced microhardness changes in glasses: Possible fictive temperature increase caused by plastic deformation. *Journal of Non-Crystalline Solids*, 354(34), pp.4056-4062.

Kjeldsen, J., M. M. Smedskjaer, J. C. Mauro, R. E. Youngman, L. Huang and Y. Yue. 2013. Mixed alkaline earth effect in sodium aluminosilicate glasses. *Journal of Non-Crystalline Solids*, 369, pp.61-68.

[i] Current address: Department of Chemical and Process Engineering, University of Surrey, Guildford, Surrey, GU2 7XH

[ii] Current Address: Helsinki R&D Center, Huawei Technologies Finland Oy Co. Ltd, Helsinki, Finland

UNIVERSITY OF LEEDS